SOME ASPECTS OF MAGNETOHYDRODYNAMICS

by

J.C.R.HUNT,
Trinity College.

A dissertation submitted for the Ph.D. degree at the University of Cambridge.

January 1967.

Summary

This thesis is an account of various phenomena caused by the interaction of the motion of electrically conducting fluids with magnetic fields. Such phenomena, the study of which is usually known as Magnetohydrodynamics (MHD), occur on a galactic, planetary or laboratory length scale; however in this thesis we concentrate on those phenomena which can be reproduced in the laboratory.

In chapter 2 we study the laminar flow of uniformly conducting, incompressible fluids in rectangular ducts under the action of transverse magnetic fields. We begin by proving that when the duct has a constant cross-section the solution is unique and then we analyse theoretically some of the curious effects on the flow of the duct's walls being electrically conducting. We find close agreement between the results of these theories and the experiments of Alty (1966) and Baylis (1966). We then analyse the flow in ducts with varying cross-sections.

In chapter 3 we analyse some of the curious flows and current streamline patterns produced by placing electrodes on the non-conducting walls of a container, filled with a conducting fluid, and passing electric currents between the electrodes in the presence of a strong magnetic field.

In chapter 4 we analyse some of the theoretical limitations on the use of Pitot tubes and electric potential (e.p.) probes in MHD flows, and provide some estimates of the errors to be expected.

In chapter 5 we analyse the stability of parallel flows in parallel magnetic fields and also some aspects of the stability of the flows analysed in chapters 2 and 3.

In chapters 6, 7 and 8 we describe our experimental apparatus, the experiments to investigate directly some of the flows analysed theoretically in chapters 2 and 3 by means of Pitot and e.p. probes, and experiments to measure the MHD errors inherent in the use of these probes. We concluded that the curious phenomena predicted actually exist. We also learnt much about the use of Pitot and e.p. probes, especially as some of the experimental results were as predicted in chapter 4.

CONTENTS

Index of figures.

Tables.

Preface

The work described in this thesis begun at the Department of Engineering of Cambridge University during the academic year 1963-4, was mainly done at the School of Engineering Science of the University of Warwick from September 1964 to December 1966. During this time I have been given a generous salary by the Central Electricity Generating Board. The Board also enabled me to make two visits to France and one to Salzburg in order to attend conferences and meet other research workers. Furthermore, by means of a contract with the University of Warwick, the Board helped towards the costs of the experimental work at Coventry. I should like to express my thanks to the Board for this support and, in particular, to Mr.H.J.Lowe, Mr.L.Young and Mr.D.J.W. Richards of the Central Electricity Research Laboratories at Leatherhead for the help they have given me and for the interest they have shown in my work. I should also like to record my thanks to Professor J.A. Shercliff for being such an excellent supervisor in providing judicious quantities of both encouragement and criticism, and to Dr.H.K.Moffatt and Professor K.Stewartson for many interesting discussions on the theoretical aspects of MHD. As regards the experiments, I must first of all thank Mr.A.E.Webb for his excellent work in the construction of the apparatus, his patience with the endless modifications, and, perhaps most important of all, his advice in the design of the apparatus. (The design of the 66" duct was as much his as mine). I should also like to thank Dr.C.J.N.Alty for sharing with us the benefit of his experience with MHD duct flows. Mr.E.P.Sutton and the Cambridge University Aeronautical Department advised us in the design of small Pitot tubes, for which we are very grateful. Finally, I must thank my wife for doing most of the drawings and filling in the mathematics between the typing.

The work described in this thesis is original except where references are given to the work of others. In particular, the introductory chapters 1 and 2 are not original except for §2.3.1. and 2.3.2. all the subsequent chapters being substantially original.

None of the thesis has been submitted at any other university, although some parts have been published or have been submitted for publication in scientific journals. Chapters 2, 3, 5 and 7 were submitted as a Fellowship dissertation at Trinity College, Cambridge.

J.R. Hunt

5. i. 67.

University of Warwick.

1. Introduction.

1.1. What magnetohydrodynamics is all about.

This thesis is an examination into various aspects of the dynamics of electrically conducting fluids under the action of magnetic fields, a subject usually known as Magnetohydrodynamics (MHD). Before describing the new work presented in this thesis we first briefly discuss the general principles of the subject and then mention a few of the reasons for its study.

MHD is a combination of the two subjects, classical electromagnetism, i.e. the study of the interaction of electric currents, electric fields, and magnetic fields, and fluid mechanics, i.e. the study of the interaction of forces and motion of liquids and gases, the principles of which are basically Newtonian. Normally, the motion of a fluid is examined without considering any electromagnetic effects; however, when the fluid is electrically conducting and in the presence of electric and magnetic fields, the mechanical and electromagnetic effects become interdependent because the electric currents are changed by the fluid's motion through the magnetic field and the forces on the fluid are altered by the electric currents and magnetic fields. The aim of MHD is to study the phenomena created by these combined effects. The method of the study is similar to those of fluid and solid mechanics, in that the phenomena are examined with a view to explaining them in terms of the basic principles of the subject, namely classical electromagnetism and fluid mechanics, and the physical properties of the fluid, e.g. its electrical conductivity and viscosity; the phenomena are not studied, as in plasma physics, with a view to explaining them in terms of atoms and electrons.

There are three main classes of reason for studying MHD, the first being that MHD is a comparatively unexplored and intrinsically fascinating branch of classical physics and applied mathematics, the second being that MHD effects are often believed to exert a controlling influence on many geo- and astro- physical phenomena, and the third being that many MHD phenomena can be used for practical purposes e.g. measuring the flow of liquids and accelerating, controlling, or generating electrical power from, streams of high temperature gases.

1.2. The aspects of MHD considered here.

In this thesis we concentrate on those MHD phenomena which can be reproduced in the laboratory as opposed to those phenomena which can only occur with very large magnetic fields or on planetary length scales. Also we confined ourselves to examining situations which have some similarity with those found in practical MHD devices, though the conclusions we draw from these studies have some considerably wider significance. The third limitation of our study was that we only consider situations which are simple enough to be analysed theoretically as well as experimentally.

Since the four main aspects of MHD examined in this thesis form a rather motley collection, a word of introduction is necessary to explain the actual reasons for choosing to study these particular aspects. (Formal introductions to each aspect of the thesis with a review of the previous work and a summary of the main results are given at the beginnning of each chapter).

At the time of my joining the Cambridge University Engineering Laboratory MHD group under Professor J.A.Shercliff in October 1963, Messrs. C.J.N.Alty and J.A.Baylis were engaged in experiments to investigate the MHD flow of mercury through rectangular ducts of constant cross-section whose walls are electrically conducting. At the time the theory of such flows was very incomplete, but most of all we lacked a physical insight into the processes involved. Consequently, with the encouragement of Professor Shercliff, I began work on extending the existing theory of such flows which had been developed by Chang & Lundgren (1961) and Shercliff (1953), concentrating on the interesting physical effects which occur when the magnetic field strongly affects the flow. As a result of this theoretical work it became clear that the presence of electrically conducting walls radically alters the flow when the magnetic field is strong. This conclusion was justified by the experiments results of Alty (1965) and Baylis (1966) whose results agreed well with the theory developed by myself (Hunt, 1965) and that developed in collaboration with Professor K.Stewartson (Hunt & Stewartson, 1965). See also chapter 2.

The other interesting result of this work was that it showed that in some circumstances a magnetic field can make flow in a duct less stable, contrary to all previous evidence. This conclusion stimulated my interest in the problem of how a magnetic field affects the stability of a flow and some results of this study have been published (Hunt, 1966a) and others are mentioned in chapter 5.

Further work on MHD duct flows has been concentrated on the more important practical problem of flow in ducts whose cross-sections vary along their length (§2.7). This work has recently been extended to the study of compressible flows (Hunt, 1966b).

In parallel with the work on MHD duct flow, at the instigation of Professor Shercliff, I studied the theory of some of the interesting effects found in electrically driven flows in MHD i.e. those caused by current sources and sinks being placed round the boundary of a fluid placed in a strong magnetic field. (This problem may not be altogether academic since the walls of an MHD generator are divided into conducting and non-conducting strips which are like some of the situations considered in the analysis of chapter 3).

Since at the University of Warwick it was possible to obtain an electromagnet with a 3" gap, and therefore to have a duct with an internal dimension of $2\frac{1}{2}$", I decided to concentrate on investigating some MHD flows internally, by using pressure and electric potential probes rather than investigating such flows by external measurements as performed by Alty and Baylis. Although some pioneering work on the use of such probes had been begun by East (1964), Lecocq (1964), and Moreau (1965), we have been involved in a considerable amount of trial and error in the design of a suitable duct and apparatus for moving the probes and there is still a lot more development which needs doing. We also extended the theory of the measurement of MHD flows by pressure and electric potential probes (chapter 4).

The experiments which have been performed have confirmed directly many of the phenomena predicted in the theory of MHD duct flows and electrically driven flows, as well as indicating the kind of errors to be expected in the use of pressure and electric potential probes.

Although these internal measurements have not been anything like as accurate as the external ones normally made, e.g. static pressure and electric potential on the boundaries, they show that such measurements can certainly indicate the nature of the flow quite satisfactorily when no theoretical model exists and therefore should be of use in studying turbulent flows.

2. Magnetohydrodynamic flow in rectangular ducts

2.1. Introduction to chapter 2.

2.2.1. Aims.

In this chapter we examine the theory of the flow in rectangular ducts of electrically conducting fluids under the action of a transverse magnetic field, confining ourselves to the study of steady, laminar flow of incompressible fluids whose conductivity, viscosity, and density are assumed to be constant. There are two main aims of the study.

The first aim is to examine how the flow through a rectangular duct is affected by the electrical conductivity of the walls of the duct and the external electrical connections made to them. To do this we make some further simplifying restrictions to our study; we only study flows which are fully developed, that is to say the velocity in the duct does not vary in the streamwise direction; we only consider uniform magnetic field which are perpendicular to two of the walls of the duct, and we only consider ducts whose walls have uniform conductivity, though the conductivity of different walls may vary. Although flows in rectangular ducts, subject to the same restrictions, have been studied before the only type of duct studied at all completely is that with non-conducting walls, the work on flows in ducts with conducting walls being very incomplete. For this type of duct there has been no attempt to understand the physical implications of the mathematics nor to compare the solutions for various types of ducts. Our aim is to use the mathematical solutions to the problem in order to obtain a sound physical understanding of the flow in different types of duct with various electrical connections, and to obtain useful formulae for volume flow rate through a duct, electric potential difference across the duct etc, which can readily be tested experimentally.

The second aim is to examine the flow in ducts whose cross-section varies in the streamwise direction, when the transverse magnetic field is very strong. In this case the restrictions we make are: only the dimension of the duct in the direction of the magnetic field varies, we can ignore the variation of the flow in the direction perpendicular to the streamwise and magnetic field

directions, the magnetic Reynolds number, R_m, is low enough for induced magnetic fields to be ignored, and the magnetic field is uniform. These approximations and restrictions lead to a great simplification in the otherwise very complicated problem of calculating the flow over a body placed in a transverse magnetic field. We find that these same approximations also lead to great simplifcations in calculating internal flows and our aim is to use and develop the existing mathematical solutions to provide a physical understanding of this problem and to provide formulae which can be tested in the laboratory.

2.1.2. Reasons

There are two main reasons for studying the incompressible flow of fluids with uniform properties through rectangular ducts under the action of a uniform transverse magnetic field (MHD duct flow for short).

Firstly there are practical reasons. The first practical use of MHD was in flow measurement and this affected most of the original work on MHD duct flow, as reviewed by Shercliff (1962). To find the flow rate through a duct when a transverse magnetic field is applied, the voltage between two electrodes in the walls of the duct is measured by drawing a very small current through the electrodes which has a negligible effect on the flow or the current in the duct. Most of such measurements are made in ducts whose walls have low or zero conductivity in order that the voltage should not be short circuited. Therefore much of the early work was on ducts whose walls were of low or zero conductivity and on flows not affected by external electrical circuits (e.g. Shercliff 1953). However, with the growing interest in using magnetohydrodynamic means to pump liquid metals, accelerate ionized gases and generate electricity from moving streams of ionized gas, it is now important to study the interaction of duct flows with external circuits when appreciable electric currents circulate between them. Also in order to minimise the electrical losses, the ducts must have highly conducting walls and the effects of such walls should also be studied. The analysis of the flow in these applications is extremely complicated, since the flows are usually turbulent and the fluids highly non-uniform, as well as being compressible in most cases. In order to make any

progress in our understanding, various simplications are necessary: for example the flow velocity is assumed to be uniform across the duct with laminar boundary layers formed on the walls (Kemebrock 1961, Hale and Kemebrock 1964), or to be inviscid and two-dimensional (Sutton and Carlson 1961), or the approximations of one-dimensional gas dynamics are used (Resler and Sears 1958). The simplification considered in this dissertation that the flow is laminar and incompressible and that the fluids' properties are uniform is merely one amongst many. Each of the simplifications enable certain aspects of the flow to be studied and taken together an understanding of the overall process may emerge. The aspect of the flow which our simplification chiefly reveals is the interaction of the electro-magnetic and viscous forces in the boundary layers on the walls, an effect which becomes increasingly important as the size of the device and the strength of the magnetic field are increased.

The second reason for our examining MHD duct flows is that they are one of the few instances in MHD whereby the theory may be critically tested by experiment. Most theoretical and experimental work ~~is concentrated~~ in MHD is concentrated on compressible flows because of the greater practical and astrophysical interest in such flows, and in such flows it is very rare indeed for the experiments to be accurate or repeatable enough for the theory to be tested at all critically. On the other hand, using liquid metals experimentalists have been able to achieve accuracies of 1 or 2%, and such experiments provide real tests for the theory. Since the whole structure of MHD theory must be judged by the accuracy with which its predictions agree with those of experiment, the theoretical and experimental study of MHD duct flows is crucially necessary for the further understanding of MHD.

2.1.3. Contents

§2.2. We state the equations and boundary conditions of MHD for the incompressible flow of fluids with uniform properties, making some observations on the approximations in the equations.

§2.3. We present a novel derivation of the equations and boundary conditions for fully developed flow in ducts of constant cross-sectional

area under the action of a uniform magnetic field, first formulated by Shercliff (1953). The essential feature of this derivation is a uniqueness theorem (a generalisation of one deduced by Moffatt (1964) for electrically driven flows), which proves conclusively that the assumptions made in deducing Shercliff's equations are justified.

§2.4. We analyse the fully developed flow in rectangular ducts under the action of a transverse magnetic field, concentrating on the effects of the duct having electrically conducting walls. To do this we generalise the mathematical solutions of Chang and Lundgren (1961) and Uflyand (1961), and Shercliff (1953), to cover flow in two main types of duct:

(i) The walls perpendicular to the field (~~AA~~ BB) perfectly conducting and the walls parallel to the field (~~BB~~ AA) of arbitrary conductivity.

(ii) Walls AA non-conducting and walls ~~BB~~ BB of arbitrary conductivity.

We then concentrate on the flow when the Hartmann number, $M, = B_o a(\sigma/\tilde{\eta})^{\frac{1}{2}}$ is large, where B_o is the imposed magnetic field, a half the duct width, σ the conductivity and $\tilde{\eta}$ the viscosity of the fluid. Various interesting physical effects are found in the boundary layers on the walls parallel to the magnetic field (~~BB~~ AA) as the conductivities of the walls are altered. The most interesting and unexpected effect occurs when the walls of the duct perpendicular to the magnetic field are highly conducting and the walls parallel to the magnetic field are non-conducting; then when $M \gg 1$, large positive and negative velocities of order MV_c are induced in the boundary layers on the wall ~~BB~~ AA, where V_c is the uniform velocity in the centre of the duct, usually known as the core velocity. It is therefore likely that, in contrast to all previous evidence, the magnetic field may in some situations have a destabilizing effect on flow in ducts. (Rather than copy out the author's paper (Hunt, 1965), we refer the reader to the paper which is attached to this thesis).

Finally in this section we show that the experimental results of Alty (1966) agree remarkably closely with the theoretical predicted values and also that these results conclusively bear out the hypothesis

that the magnetic field destablizes the flow.

§2.5. We continue the analysis of the effects of conducting walls, this time investigating the flow in a duct whose walls AA are non-conducting and walls BB are perfectly conducting. We also examine the effects of an external electrical circuit. Finally we compare the flows in rectangular ducts with all combinations of conducting and non-conducting walls. (In this section we refer to the paper Hunt & Stewartson (1965)).

§2.6. We apply the results of §2.5 to flow in a rectangular annulus which is driven by an electric current with an applied magnetic field parallel to the axis of the annulus. Then we compare the theoretically predicted values with those found by Baylis (1966) to find reasonable agreement between them.

§2.7. We analyse the steady, incompressible, two-dimensional flow of conducting fluids through ducts of arbitrarily varying cross-section when a strong, uniform, magnetic field is imposed. The direction of the magnetic field is perpendicular to the flow and parallel to the direction in which the ducts diverge. It is assumed that the interaction parameter, $N(=M^2/Re) \gg 1$, where M is the Hartmann number and R_e is the Reynolds number, and also that $M \gg 1$ and $R_m \ll 1$ where $R_m (=\mu\sigma\bar{U}l)$ is the magnetic Reynolds number, μ is the magnetic permeability, σ the conductivity, $\bar{U}$ a typical velocity and l a characteristic length of the flow.

We examine the flow in three separate regions:

(i) The 'core' region in which the pressure gradient is balanced by electro-magnetic forces.

(ii) Hartmann boundary layers where electromagnetic forces are balanced by viscous forces.

(iii) Thin layers parallel to the magnetic field in which electro-magnetic forces, inertial forces, and the pressure gradient balance each other. These layers which have thickness $O(N^{-1/3})$ occur where the slope of the duct wall changes abruptly.

By expanding the solution as a series in descending powers of N we calculate the velocity distribution in regions (i) and (ii) for finite values of N attainable in the laboratory.

2.2. Equations and boundary conditions for incompressible magnetohydrodynamic flows.

2.2.1. The governing equations

The equations governing the flow of incompressible fluids with uniform electrical conductivity, viscosity and density have been derived in many text books e.g. Shercliff (1965). These equations describe the behaviour of liquid metals very accurately and in some circumstances may describe the flow of conducting gases if their velocity is low enough. They are:-

the momentum equation,

$$\rho\left\{\frac{\partial \underset{\sim}{v}}{\partial t} + (\underset{\sim}{v}\cdot\nabla)\underset{\sim}{v}\right\} = -\nabla p + \underset{\sim}{j}\times\underset{\sim}{B} + \tilde{\eta}\nabla^2\underset{\sim}{v}, \qquad 2.2.1.$$

the equation of continuity,

$$\nabla\cdot\underset{\sim}{v} = 0, \qquad 2.2.2.$$

Ohm's Law,

$$\underset{\sim}{j} = \sigma\left(\underset{\sim}{E} + \underset{\sim}{v}\times\underset{\sim}{B}\right), \qquad 2.2.3.$$

Maxwell's Equations,

$$\nabla\times\underset{\sim}{E} = -\partial\underset{\sim}{B}/\partial t, \qquad 2.2.4.$$

$$\nabla\cdot\underset{\sim}{B} = 0, \qquad 2.2.5.$$

$$\underset{\sim}{j} = \nabla\times\underset{\sim}{H}, \qquad 2.2.6.$$

where ρ is the density, $\underset{\sim}{v}$ the velocity, p the pressure, η the viscosity, $\underset{\sim}{j}$ the current density, $\underset{\sim}{B}$ the magnetic flux density, σ the electrical conductivity, $\underset{\sim}{E}$ the electric field strenght, and $\underset{\sim}{H}$ the magnetic field. Since we will only be considering materials, whose permeability, μ_0 is that of a vacuum

$$\underset{\sim}{B} = \mu_0\underset{\sim}{H}. \qquad 2.2.7.$$

Hence, using (2.2.5) and (2.2.6) we have:

$$\nabla\cdot\underset{\sim}{j} = 0 \qquad 2.2.8.$$

Hereafter we will use the suffices x, y, z to refer to the components of vector quantities e.g. v_x, v_y, v_z refer to the compoenents of $\underset{\sim}{v}$.

2.2.1. Approximations made in the equations.

In these equations certain effects are ignored which we now state along with the conditions in which these effects are truly negligible. For further justification of the equations see, for example, Shercliff's book.

(1) Compressibility. The velocities must be sufficiently low compared to the speed of sound in the fluid.

(2) Variation in fluid properties due to heating by electric currents and viscous dissipation. This effect is negligible in most experimental situations with liquid metals, but it is an important effect with gases.

(3) Hall effect and 'ion slip'. These effects which alter the relation between the electric current and the electric field, equation (2.2.3) are appreciable in gases, but may be ignored in liquid metals, unless the magnetic field is exceptionally high by laboratory standards. (i.e. greater than 10^5 gauss).

(4) 'Displacement Current'. This effect, which produces a modification in the relation between current and magnetic flux density (equation (2.2.6)), is only significant for very high frequency electromagnetic oscillations and is quite negligible in laboratory MHD experiments.

(5) Charge concentration. It may be shown that although charge concentrations exist (i.e. $\nabla \cdot \underset{\sim}{E} \neq 0$), the forces on the fluid due to $\underset{\sim}{E}$ and q, the charge density, are negligible in all practical or experimental situations.

2.2.3. Boundary conditions at a rigid surface.

For future reference we state here the boundary conditions at an interface between a solid and fluid with finite viscosity, both of which have finite conductivity:

$\underset{\sim}{v} = 0$, since there is no slip at the wall 2.2.9.

$[\underset{\sim}{j} \cdot \underset{\sim}{n}] = 0$, since $\nabla \cdot \underset{\sim}{j} = 0$ 2.2.10.

$[\underset{\sim}{E} \times \underset{\sim}{n}] = 0$, since $\nabla \times \underset{\sim}{E} = -\partial \underset{\sim}{B} / \partial t$ 2.2.11.

$$[\underset{\sim}{B}\cdot\underset{\sim}{n}]=0 \quad , \text{since} \quad \nabla\cdot\underset{\sim}{B}=0 \qquad 2.2.12.$$

$$[\underset{\sim}{H}\times\underset{\sim}{n}]=0 \quad , \text{since} \quad \underset{\sim}{j}=\nabla\times\underset{\sim}{H} \qquad 2.2.13.$$

The brackets $[\ ]$ refers to the change across the boundary and $\underset{\sim}{n}$ is the vector normal to the boundary. For detailed derivation of these conditions see Shercliff (1965). Note that in steady flow, since $\nabla\times E=0$, we can write $\underset{\sim}{E}=\nabla\phi$, where ϕ is the scalar, electric potential. Then (2.2.11) becomes:

$$[\nabla\phi\times\underset{\sim}{n}] = 0. \qquad 2.2.14.$$

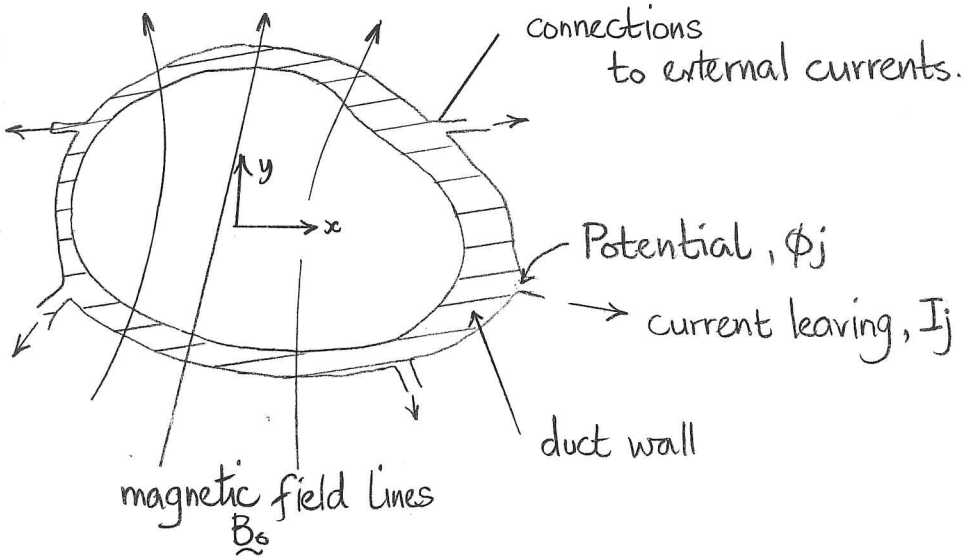

Fig 2.1. Cross-section of an arbitrarily shaped duct with external electrical connections.

2.3. The equations, boundary conditions and uniqueness theorem for MHD duct flows.

2.3.1. Formulation of the problem.

We now consider steady flows through ducts under the action of a transverse magnetic field. In this and the next two sections we will confine ourselves to examining flows in ducts of constant cross-sectional area which are fully developed, that is to say the velocity, the magnetic field, the electric field and the electric current do not vary along the length of the duct. Thus all the variables except pressure are independent of z, (see fig.2.1). (We show subsequently that it follows dp/dz is also independent of z).

The duct may be connected to external electric circuits. Then, if the current leaving the duct per unit length and the electric potential at each of these connections are I_j and Φ_j respectively, we assume that the external circuits uniquely define Φ_j in terms of I_j or vice versa; a condition satisfied in all practical circuits. Now, given the flux density of the imposed magnetic field, we want to find the distribution of velocity, pressure, electric potential and electric current in the duct given the following data:

(1) either the mean pressure drop per unit length in the z-direction Δ_p, (we subsequently show that the pressure drop must be independent of x and y) or the volume flowrate, Q, and

(2) either I_j or Φ_j at each connection of the duct with its external circuits.

The problem may now be expressed mathematically as follows:-

Find $\underset{\sim}{q} = \{\underset{\sim}{v}, p, \phi, \underset{\sim}{j}, \underset{\sim}{B}\}$ which satisfies the equations (2.2.1. - 2.2.8) when $d/dt = 0$ given Δ_p or Q and I_j or Φ_j, provided the following boundary conditions are satisfied:

(i) at the fluid-wall interface of the duct:

$$\underset{\sim}{v} = 0, \qquad 2.3.1.$$

$$(\underset{\sim}{j}\cdot\underset{\sim}{n})_f = (\underset{\sim}{j}\cdot\underset{\sim}{n})_\omega, \qquad 2.3.2.$$

$$(\nabla\phi\times\underset{\sim}{n})_f = (\nabla\phi\times\underset{\sim}{n})_\omega, \qquad 2.3.3.$$

where $\underset{\sim}{n}$ is in the direction into the fluid and the subscripts f, w indicates the value of the quantity inside the bracket at the fluid side and wall side of the interface respectively.

(ii) The boundary conditions at the exterior of the wall of the duct is:

$$\underset{\sim}{j} \cdot \underset{\sim}{n} = 0 , \qquad 2.3.4.$$

except at the connections to the external electric circuits. (The equations for the wall are the same as 2.2.3 - 2.2.8 with $\underset{\sim}{v} = 0$).

(iii) As $|x|, |y| \to \infty$, $\underset{\sim}{B} \to \underset{\sim}{B}_0 (x,y)$, 2.3.5.

where $\underset{\sim}{B}_0$ is the imposed magnetic field. Since $\underset{\sim}{B}_0$ is produced by currents outside the duct, it satisfies the equations:

$$\nabla \times \underset{\sim}{B}_0 = 0 ,$$

$$\nabla . \underset{\sim}{B}_0 = 0 .$$

We assume $\underset{\sim}{B}_0$ to be given in our problem.

2.3.2. Uniqueness theorem.

By considering the energy dissipated in the duct we now prove that thereis a unique solution for $\underset{\sim}{q}$. (This analysis is similar to that of Moffatt (1964), though more general in that we consider inertial terms and make no restriction on R_m, the magnetic Reynolds number).

From (2.2.1) and (2.2.3) we can eliminate $\underset{\sim}{B}$ to obtain:

$$\sigma^{-1} |\underset{\sim}{j}|^2 - \tilde{\eta}\, \underset{\sim}{v} . \nabla^2 \underset{\sim}{v} = - \underset{\sim}{v} . \nabla p - \underset{\sim}{j} . \nabla \phi - \rho \underset{\sim}{v} . \left((\underset{\sim}{v} . \nabla) \underset{\sim}{v} \right)$$

Now integrate this equation unit distance along the duct and across the duct but not including the duct walls. Call this volume V_f and its surface S_f. Then, using Gauss' theorem and equations (2.2.2) and (2.2.8), we obtain:

$$\int_{V_f} \sigma^{-1} j^2 \, dV - \tilde{\eta} \int_{V_f} (\underset{\sim}{v} . \nabla^2 \underset{\sim}{v}) \, dV = - \int_{S_f} \left\{ (\underset{\sim}{v} . \underset{\sim}{n}) p + \phi (\underset{\sim}{j} . \underset{\sim}{n}) \right\} ds$$

$$- \rho \int_{V_f} \left\{ \underset{\sim}{v} . \nabla \left(v^2 / 2 \right) - \underset{\sim}{v} . (\underset{\sim}{v} \times \underset{\sim}{w}) \right\} dV \qquad 2.3.6.$$

where $\underset{\sim}{w} = \nabla \times \underset{\sim}{v}$. Now

$$\int_{V_f} \underset{\sim}{v} \nabla^2 \underset{\sim}{v}\, dV = -\int_{V_f} (\nabla \times \underset{\sim}{v})^2 dV + \int_{S_f} \left\{ (\underset{\sim}{v} \times \underset{\sim}{w}) \cdot \underset{\sim}{n} \right\} dS,$$

$$= -\int_{V_f} \underset{\sim}{w}^2 dV,$$

since $\underset{\sim}{v} = 0$ on the walls and $\partial \underset{\sim}{v}/\partial z = 0$.

Since $(\underset{\sim}{v} \cdot (\underset{\sim}{v} \times \underset{\sim}{w}) = 0$ and $\underset{\sim}{v} = 0$ on the walls,

$$\rho \int_{V_f} \left(\underset{\sim}{v} \nabla (v^2/2) - \underset{\sim}{v} \cdot (\underset{\sim}{v} \times \underset{\sim}{w}) \right) dV = \rho \int_{V_f} \nabla \cdot \left(\frac{v^2}{2} \underset{\sim}{v} \right) dV = 0$$

Since $\partial \underset{\sim}{v}/\partial z = \partial \underset{\sim}{j}/\partial z = \partial \underset{\sim}{B}/\partial z = 0$,

$$\frac{\partial}{\partial z} \left\{ \rho (\underset{\sim}{v} \nabla) \underset{\sim}{v} - \underset{\sim}{j} \times \underset{\sim}{B} - \tilde{\eta} \nabla^2 \underset{\sim}{v} \right\} = -\partial (\nabla p)/\partial z = 0$$

Therefore $p = -z \Delta p + f(x, y)$ where Δp is now a constant.

Therefore

$$\int_{S_f} (\underset{\sim}{v} \cdot \underset{\sim}{n})\, p\, dS = \int_A \Delta p\, v_z\, dA = Q \Delta p$$

where A is the cross-sectional area of the duct and Q the volume flow rate, and thence (2.3.6) becomes:

$$\int_{V_f} \left\{ \sigma^{-1} |\underset{\sim}{j}|^2 + \tilde{\eta} |\underset{\sim}{w}|^2 \right\} dV = Q \Delta p - \int_{S_f} (\phi \underset{\sim}{j} \cdot \underset{\sim}{n})\, dS \qquad 2.3.7.$$

Now consider the walls of the duct. If the walls are non-conducting, $\underset{\sim}{j} \cdot \underset{\sim}{n} = 0$ on the walls and (2.3.7) becomes:

$$\int_{V_f} \left(\sigma^{-1} |\underset{\sim}{j}|^2 + \tilde{\eta} |\underset{\sim}{w}|^2 \right) dV = Q \Delta p$$

If the walls are conducting, the potential ϕ is continuous across the wall-fluid interface and $\underset{\sim}{j} \cdot \underset{\sim}{n}$ is also continuous. By integrating in a volume V_w of the wall also of unit length along the duct, with an external surface area of S_w, its internal surface area being S_f, we obtain:

$$\int_{V_w} \sigma_w^{-1} |\underset{\sim}{j}|^2 dV = \int_{S_f} \left(\phi (\underset{\sim}{j} \cdot \underset{\sim}{n}) \right) dS - \int_{S_w} \left\{ \phi (\underset{\sim}{j} \cdot \underset{\sim}{n}) \right\} dS,$$

$$= \int_{S_f} \phi (\underset{\sim}{j} \cdot \underset{\sim}{n})\, dS - \sum_j \Phi_j I_j,$$

since $\underset{\sim}{j} \cdot \underset{\sim}{n} = 0$ on the external surface of the duct except at the connections with the external circuits.

Thence (2.3.7) becomes:

$$\int_{V_f}\left(\sigma^{-1}|\underset{\sim}{j}|^2+\tilde{\eta}|\underset{\sim}{w}|^2\right)dV+\int_{V_w}\left(\sigma_w^{-1}|\underset{\sim}{j}|^2\right)dV$$

$$=\mathcal{Q}\Delta p-\sum_j \Phi_j I_j \,.$$

2.3.8.

Now suppose that $q_{\sim}' = \{\underset{\sim}{v}', p', \phi', \underset{\sim}{j}', \underset{\sim}{B}'\}$ is a second solution of the equation (2.2.1 - 2.2.8) satisfying the same boundary conditions as $q_{\sim}$ with $\Delta p' = \Delta p$ or $\mathcal{Q}' = \mathcal{Q}$ and $I_j' = I_j$ or $\Phi_j' = \Phi_j$ at each connection, depending on which condition was specified for the solution $q_{\sim}$. Let

$$\hat{q}_{\sim} = q_{\sim} - q_{\sim}'$$

be the difference between the two solutions. Then $\hat{q}_{\sim}$ satisfies the equations (2.2.1 - 2.2.8) and the boundary conditions (2.3.1. - 2.3.5.), but

$$\Delta\hat{p} = 0 \quad \text{or} \quad \hat{\mathcal{Q}} = 0 \quad \text{and} \quad \hat{I}_j = 0 \quad \text{or} \quad \hat{\Phi}_j = 0.$$

Then (2.3.8) becomes:

$$\int_{V_f}\left(\sigma_f^{-1}|\underset{\sim}{\hat{j}}|^2+\tilde{\eta}|\underset{\sim}{\hat{w}}|^2\right)dV+\int_{V_w}\left(\sigma_w^{-1}|\underset{\sim}{\hat{j}}|^2\right)dV = 0$$

Hence $\underset{\sim}{\hat{j}} = 0$ and $\underset{\sim}{\hat{w}} = 0$. Then since $\partial/\partial z = 0$, we can write $\hat{v}_x = \partial\psi/\partial y$ and $\hat{v}_y = -\partial\psi/\partial x$ and since $\underset{\sim}{\hat{w}} = 0$,

$$\nabla^2\psi = 0.$$

Therefore $\hat{\psi} = \hat{v}_x = \hat{v}_y = \hat{p} = 0$ and since $\hat{w}_x = \hat{w}_y = 0$, $\hat{v}_z = 0$ and thence, since $\underset{\sim}{\hat{j}} = 0$, $\hat{p} = 0$ and $\underset{\sim}{\hat{B}} = 0$.
Thus $\hat{q}_{\sim} = 0$ and $q_{\sim}' = q_{\sim}$, which shows that there is only one solution to the problem.

There are some interesting aspects of this uniqueness theorem. Firstly it is valid for all values of the magnetic Reynolds number, R_m. Therefore even if the induced magnetic field is of the same order as the imposed magnetic field, the result is not affected. Secondly the result is independent of the orientation and distribution of the imposed magnetic field. Thirdly the result is not affected by having the walls of the duct conducting. Lastly we note that, in general, specifying Q and dp/dz

or Φ_j and I_j does not uniquely determine the solution e.g. a current flowing between the walls perpendicular to the magnetic field in the duct examined by Hunt (1965) does not affect the flow and therefore, of course, specifying I_j and Φ_j would give no information about the flow. On the other hand in the flow examined by Hunt & Stewartson (1965) specifying the current and potential between the electrically conducting walls does uniquely determine Q and Δp, given $\underset{\sim}{B}_0$. This case is the exception.

2.3.3. The MHD duct flow equations

Since we have shown that there is only one solution to the problem of fully developed duct flow given suitable boundary conditions, if we assume a given flow and show that such a flow satisfies the equations and the boundary conditions, then we have found the solution to the problem.

We assume that there is no secondary flow and that the imposed magnetic field is constant i.e.

$$\underset{\sim}{B}_0 = (0, B_0, 0)$$

Then, making the same assumptions as in §2.3.1, that the cross-sectional area, $\underset{\sim}{v}$, ϕ , $\underset{\sim}{j}$ and $\underset{\sim}{B}$ do not vary in the z-direction, and using the result of §2.3.2. that dp/dz is a constant, and $\partial p/\partial x$ and $\partial p/\partial y$ are functions of x and y only, the equations (2.2.1 - 2.2.8) reduce to:

$$0 = -\partial p/\partial x + j_y \mu_0 H_z , \qquad 2.3.9.$$

$$0 = -\partial p/\partial y - j_x \mu_0 H_z \qquad 2.3.10.$$

$$0 = -\partial p/\partial z + j_x B_0 + \tilde{\eta}\left(\frac{\partial^2}{\partial x^2} + \frac{\partial^2}{\partial y^2}\right) v_z , \qquad 2.3.11.$$

$$j_x = \sigma(-\partial p/\partial x - v_z B_0) , \quad j_y = \sigma(-\partial \phi/\partial y) , \qquad 2.3.12.$$

$$j_x = \partial H_z/\partial y , \quad j_y = -\partial H_z/\partial x , \qquad 2.3.13.$$

$$\partial j_x/\partial x + \partial j_y/\partial y = 0 . \qquad 2.3.14.$$

These equations may be rewritten in terms of p, H_z and v_z:

$$0 = \partial/\partial x\left(p + \frac{\mu_0 H_z^2}{2}\right) , \qquad 2.3.15.$$

$$0 = -\partial/\partial y\left(p + \frac{\mu_0 H_z^2}{2}\right), \qquad 2.3.16.$$

$$0 = -\frac{\partial p}{\partial z} + B_0 \frac{\partial H_z}{\partial y} + \eta^2\left(\frac{\partial^2}{\partial x^2} + \frac{\partial^2}{\partial y^2}\right) v_z, \qquad 2.3.17.$$

and
$$0 = B_0 \frac{\partial v_z}{\partial x} + \frac{1}{\sigma}\left(\frac{\partial^2}{\partial x^2} + \frac{\partial^2}{\partial y^2}\right) H_z, \qquad 2.3.18.$$

Thus p has the form deduced in §2.3.2. Also note that, given the boundary conditions dp/dz or Q and I_j or Φ_j we can find v_z and H_z by only considering (2.3.17) and (2.3.18), which were first deduced by Shercliff (1953). When the walls of the duct are conducting, to find the value of H_z at the fluid-wall interface, in addition to examining (2.3.17) and (2.3.18) we have to analyze the current distribution in the walls of the duct and use the boundary conditions (2.3.1 - 2.3.5) to match the solution in the walls to that in the duct and to the external electrical circuit. We now write down the equation for H_z in the wall and these matching conditions in terms of H_z and v_z. Let s be the co-ordinate parallel to the wall. Then, in the wall, H_z satisfies:

$$0 = \left(\frac{\partial^2}{\partial x^2} + \frac{\partial^2}{\partial y^2}\right) H_z, \qquad 2.3.19.$$

provided the conductivity of the wall is constant, and the matching conditions at the fluid-wall interface are:

$$v_z = 0,$$

$$\left(\frac{\partial H_z}{\partial s}\right)_f = \left(\frac{\partial H_z}{\partial s}\right)_w \qquad 2.3.20.$$

and
$$\frac{1}{\sigma}\left(\frac{\partial H_z}{\partial x}\right)_f = \frac{1}{\sigma_w}\left(\frac{\partial H_z}{\partial n}\right)_w \qquad 2.3.21.$$

where σ_w is the conductivity of the wall.
At the outer boundary of the duct wall,

$$\partial H_z/\partial s = 0 \qquad 2.3.22.$$

except where the duct wall connects with an external circuit.

If the duct walls are non-conducting, the boundary conditions on H_z becomes simply,

$$\left(\partial H_z / \partial s\right) = 0 \qquad \text{2.3.23.}$$

and the condition on $\partial H_z / \partial n$ is then ignored because in the wall the electric field

$$\left(-\partial \phi / \partial s\right) \neq -\frac{1}{\sigma_w}\left(\partial H / \partial n\right).$$

Shercliff (1956) pointed out that these boundary conditions and the equation for H_z in the wall may be simplified when the thickness of the wall, t, is small compared to the duct size.

Then $\frac{\partial H_z}{\partial x} \gg \frac{\partial H_z}{\partial s}$ and (2.3.19) becomes

$$\partial^2 H_z / \partial n^2 = 0,$$

$$\left(\partial H / \partial n\right)_w = \left(\left(H_z\right)_w - \left(H_z\right)_o\right)/t.$$

Consequently except where the duct wall connects with an external circuit, $(H_z)_w$ and $(H_z)_o$ being the value of H_z at the outside and the inside of the duct wall respectively. From (2.3.20),

$$\left(H_z\right)_w = \left(H_z\right)_f .$$

Therefore the condition (2.3.21) becomes:

$$\frac{\partial H_z}{\partial n} = \frac{\sigma}{\sigma_N}\,\frac{H_z - H_{z_o}}{t} . \qquad \text{2.3.24.}$$

2.4. Magnetohydrodynamic flow in rectangular ducts. I.

2.4.1. Introduction to Hunt (1965)

In §§2.4 and 2.5 we merely introduce the work we have already published on steady fully developed flow in rectangular ducts of fluids with uniform properties under the action of a transverse magnetic field. In this section we refer to the author's paper, Hunt (1965), in which we generalize the mathematical solution of Chang & Lundgren (1961) and Shercliff (1953) to examine the flow in two kinds of rectangular ducts:

(i) those whose walls parallel to the magnetic field (AA) are of arbitrary conductivity and whose walls perpendicular to the magnetic field (BB) are perfectly conducting;

(ii) those whose walls (AA) are non-conducting and walls (BB) are of arbitrary conductivity.

In the paper we concentrated on the interesting physical effects which occur when $M \gg 1$, (as have already been described in §2.1.3) and were led to make some speculation on the stability of the resulting flows in the conclusion of the paper. Since then we have examined the stability of these flows in greater detail and our conclusions are presented in §2.4.2. Finally in §2.4.3 we compare our theoretical results with the experimental results of Alty (1966).

Since the publication of Hunt (1965), we have found two papers by Chang, Atabek and Lundgren (1961) and Uflyand (1962) in which were analysed the flow in a duct whose walls (BB) are perfectly conducting and walls (AA) are non-conducting. However, owing to the form of solution used in these papers, the interesting properties of the flow as $M \to \infty$ could not easily be seen and no physical discussion of the problem was attempted. A recent book by Hughes and Young (1966) also analyses the same problem using the same cumbersome techniques as Chang, Atabek and Lundgren (1961), but the book is of interest since velocity profiles and current stream lines have been computed in great detail for various values of M.

2.4.2. The stability of the flows when $M \gg 1$.

In this section we discuss the stability of the high Hartmann number flows analysed in our paper, Hunt (1965), using the results of our

general analysis of the stability of MHD duct flows in §5.3.

In §5.3 it is shown that the analysis of the stability of a flow in a rectangular duct is simpler when $M \gg 1$ than when $M = 0$. The reason is that, when $M \gg 1$ a core flow develops in the centre of the duct and boundary layers form on the side walls and therefore the stability of the flow is determined by that of the boundary layers, which are simpler to analyse than the flow found at $M = 0$ which varies equally in two directions. Furthermore, it is found that the most unstable disturbances, which determine the stability of the boundary layers, are unaffected by the magnetic field. Therefore in examining the stability of these flows we can use our knowledge of the stability of boundary layers where there is no magnetic field.

Let us examine the stability of the boundary layers on the walls AA in a duct with perfectly conducting walls perpendicular to the field and insulating walls parallel to the field ($d_A = 0$, $d_B = \infty$). In this case as $M \to \infty$ the velocity profile in the boundary layer becomes:

$$V = \sum_{j=0}^{\infty} \frac{2(-1)^j \cos(\alpha_j/2)}{M \alpha_j^2} \exp\left(-\tilde{\zeta}\sqrt{\frac{\alpha_j}{2}}\right) \sin\left(-\tilde{\zeta}\sqrt{\frac{\alpha_j}{2}}\right),$$

where $\tilde{\zeta} = M^{\frac{1}{2}} \zeta$ and thus (MV) becomes a function of $\tilde{\zeta}$ only. The stability of this boundary layer is then determined solely by the value of the Reynolds number for the layer $R_{b.l.}$, since the velocity profile, suitably expressed, is independent of M. We now have to determine the value of $R_{b.l.}$ in terms of M and R, the overall Reynolds number ($= a \bar{v}_z / \nu$), where $\bar{v}_z$ is the mean velocity, for various shapes of duct.

If $a/b \ll M^{-\frac{1}{2}}$, i.e. a very thin duct with walls AA much shorter than walls BB, the mean velocity in the duct, $\bar{v}_z$, closely approaches the core velocity and most of the flow is in the core. (For $a/b \gg M^{-\frac{1}{2}}$ most of the flow is in the boundary layers on AA, Section 3 of Hunt (1965)). Then the mean velocity in the boundary layers on the walls AA is $O(M)\bar{v}_z$ and since the thickness of these boundary layers is $O(aM^{-\frac{1}{2}})$, the Reynolds number of the boundary layer $R_{b.l.} = O(aM^{\frac{1}{2}} \bar{v}_z / \nu)$, where ν is the kinematic viscosity. Hence,

$$R_{b.l.} = O(M^{\frac{1}{2}})R,$$

where R is the overall Reynolds number, ($R = a\bar{v}_z/\nu$). Thus for given R, $R_{b.l.}$ increases with M: hence the critical overall Reynolds number at which the boundary layers become unstable is reduced by increasing M. Note, however, that away from the remote walls AA the flow would be very stable.

Now consider an approximately square duct with a/b = O(1). We see from equation (24) of Hunt (1965) that in this case most of the flow is in the boundary layers on AA. The mean velocity in the boundary layers on AA is $O(M)v_c$, where v_c is the core velocity and, since the thickness of these boundary layers is given by $\delta = O(aM^{-\frac{1}{2}})$,

$$\bar{v}_z = O\left[(M v_c a^2 M^{-1/2} + v_c ab)/ab\right] = O\left[M^{1/2} v_c a/b\right]$$

Hence, if a/b = O(1), $R = O(M^{\frac{1}{2}} a v_c/\nu)$,
and since $R_{b.l.} = O(M^{\frac{1}{2}} a v_c/\nu)$, $R \simeq R_{b.l.}$
It is important to realise that the forms of the velocity profiles are a function of M and not R. Thus velocity over-shoot and reversed flow can occur in the boundary layers on AA at arbitrarily small Reynolds number. Using the usual sufficiency condition for boundary layer flows we can show that below a certain value of R the flow is stable. Since the velocity profile is in the form of a jet with an infinite number of points of inflection and since the critical Reynolds numbers of free jets vary between about 4 and a few hundred it would seem that in this type of duct, when $M \gg 1$, $R_{crit} < 1000$ whereas when M = 0, $R_{crit} \simeq 3000$. If it could be shown that when $M \gg 1$, $R_{crit} < 1000$ then, by definition, our hypothesis that the magnetic field has a destabilizing effect would be verified.

When the walls of the ducts are all perfectly conducting ($d_A = d_B = \infty$), the velocity profile of the boundary layer also contains points of inflection (fig.4 of Hunt (1965)), and hence raising M reduces the Reynolds number at which the boundary layers become unstable. But in this case, for $M \gg 1$, the velocity in the boundary layers on AA is of the same order as the core velocity and since the boundary layer thickness is $O(aM^{-\frac{1}{2}})$, $R_{b.l.} = O(M^{-\frac{1}{2}})R$. In this case, provided $a/b < M^{\frac{1}{2}}$, the shape of the duct is irrelevant. Raising M at a constant value of R may first tend to destabilize the boundary flow and then stabilize it.

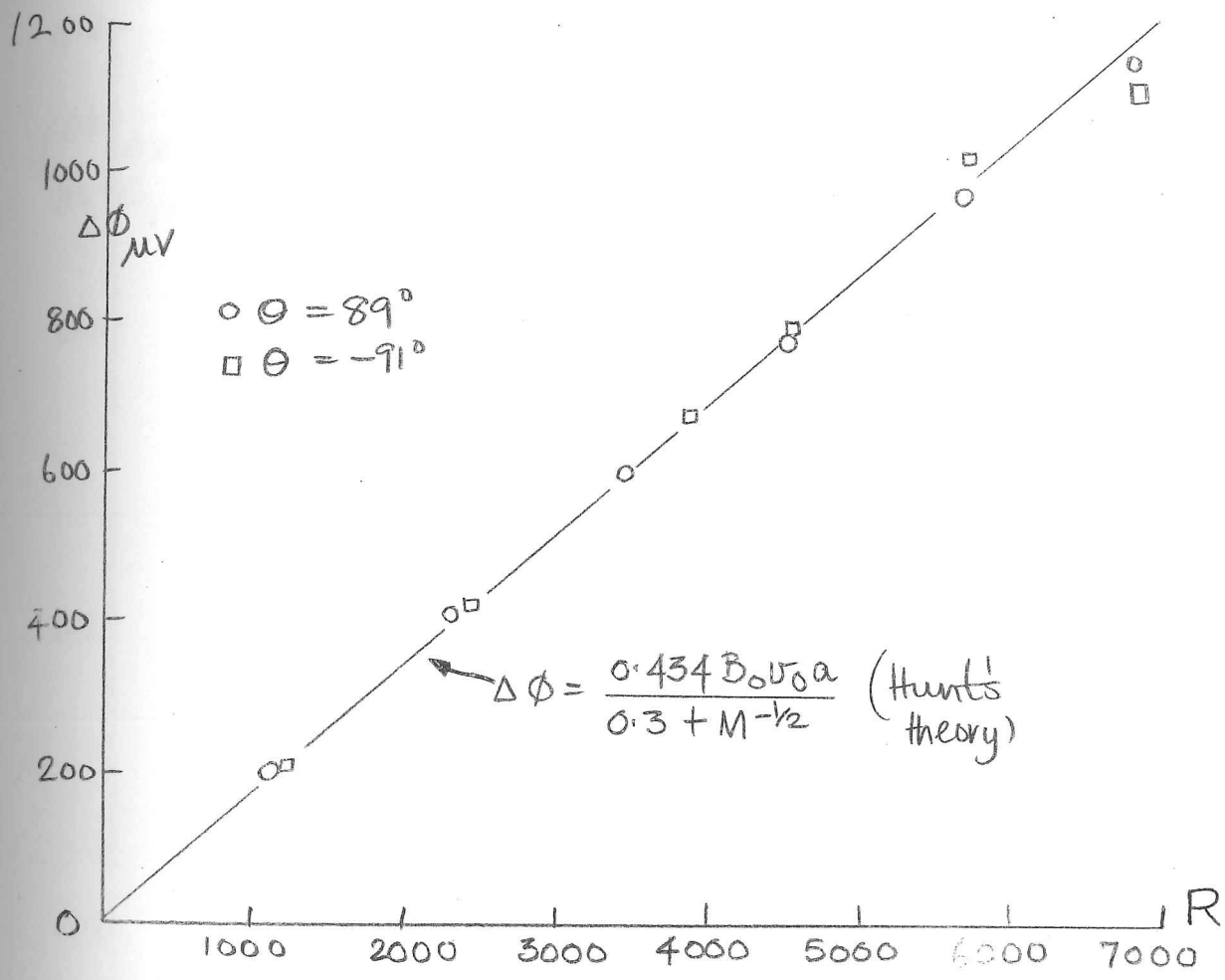

Fig 2.2. The potential at the mid-point of one insulating wall against Reynolds number
½" duct: $\Theta \simeq \pm 90°$, $M = 227$
(Alty, 1966)

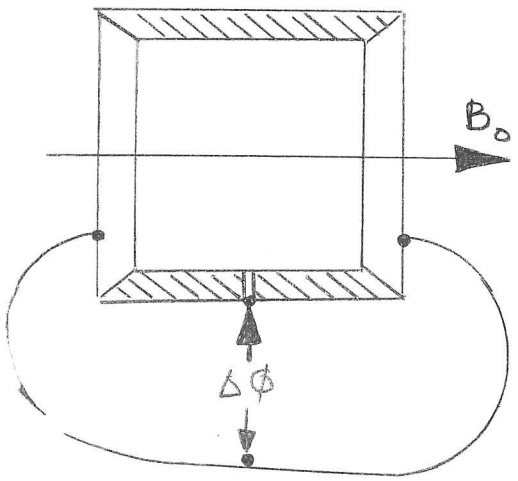

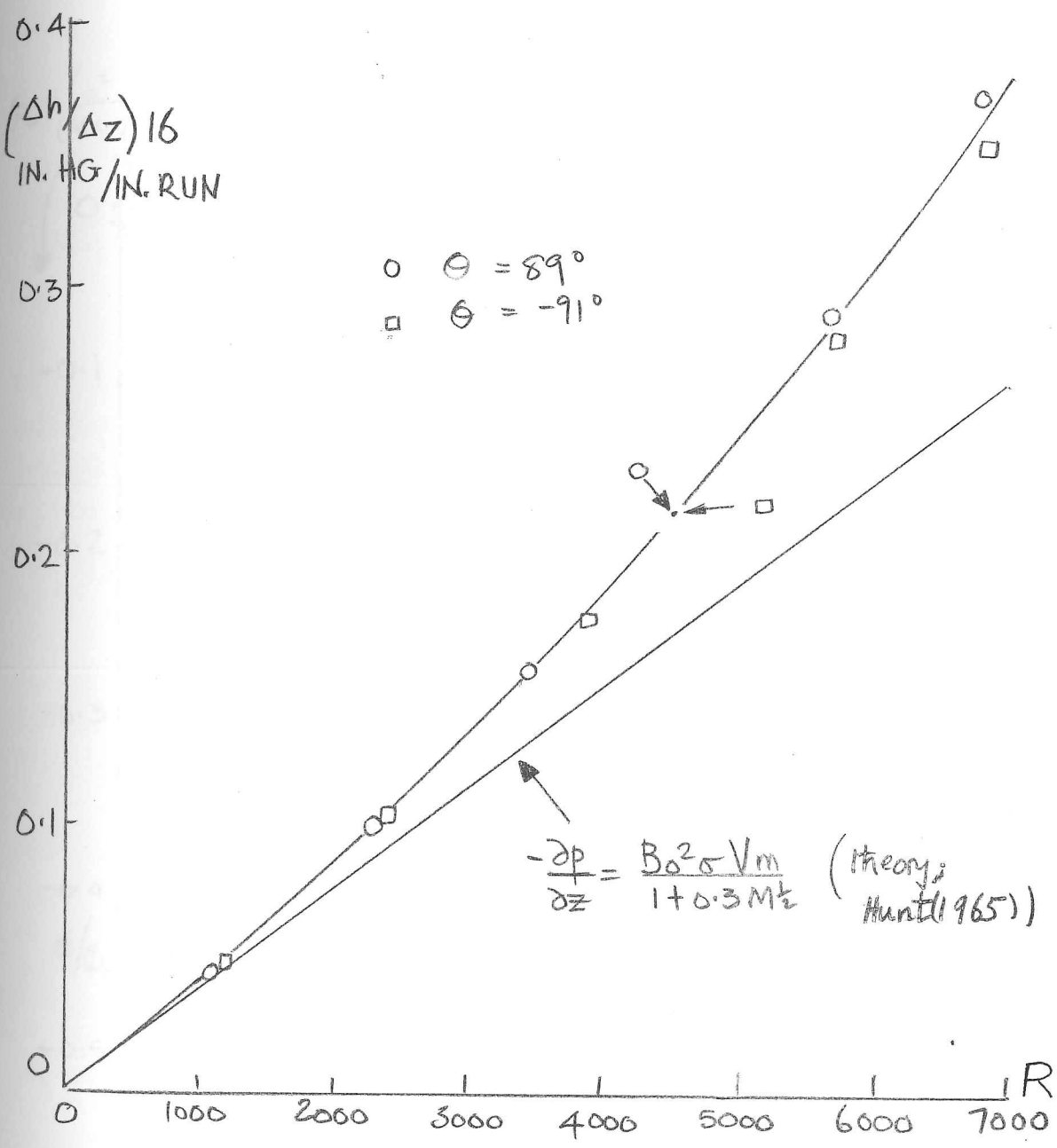

Fig 2.3. Pressure gradient against Reynolds number. ½" duct: $\theta \simeq \pm 90°$, M = 227. (Alty, 1966)

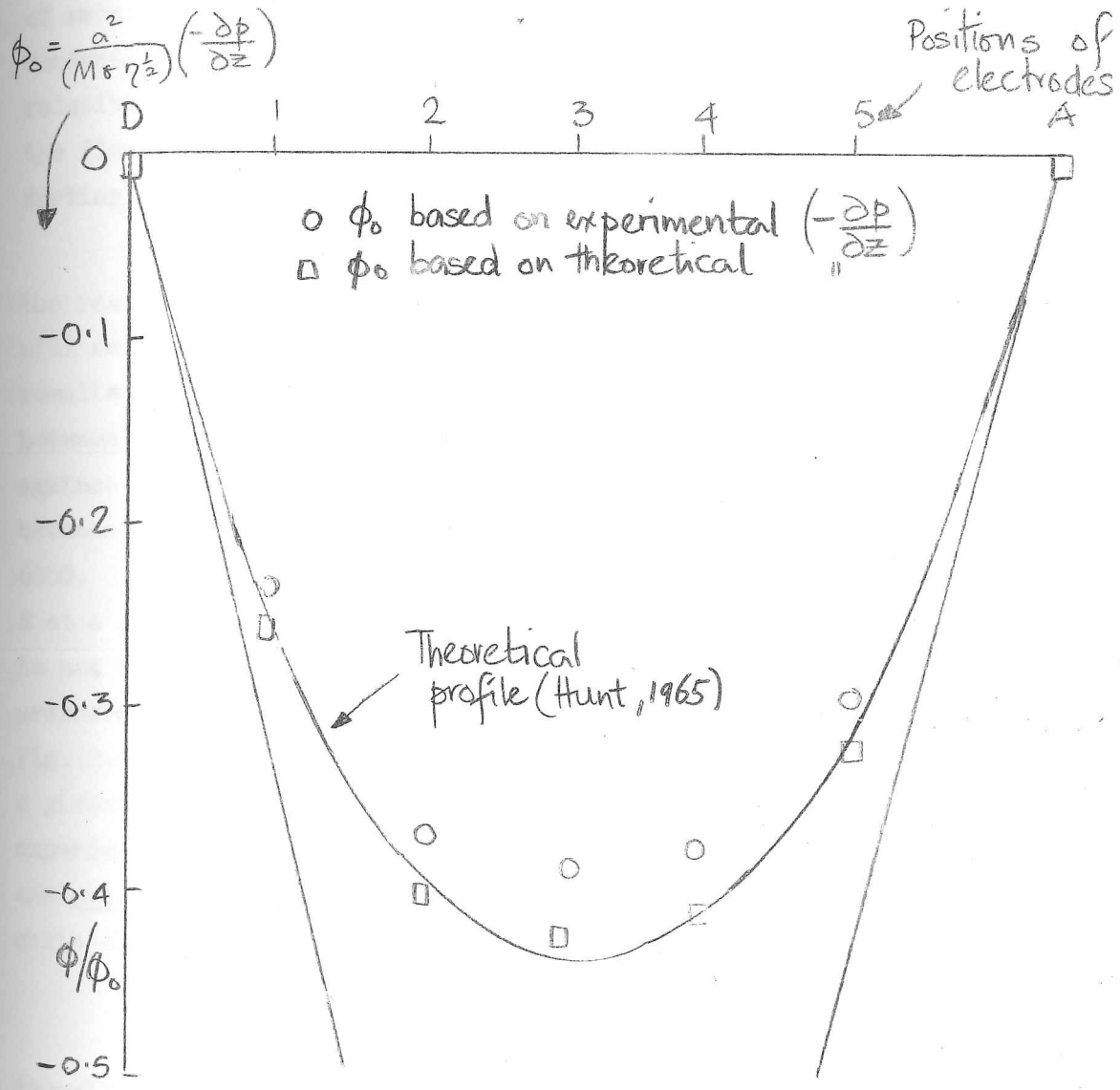

Fig 2.4 Potential profile along the insulating wall.

$\frac{3}{8}$" duct : $\theta = 90°$, $M = 159$, $R \approx 800$.

from Alty (1966)

2.4.3. Experimental results of Alty.

Since the publication of Hunt (1965), Alty has performed a series of experiments on the effect of a transverse magnetic field on the flow of mercury through a square duct with two walls conducting and two non-conducting. He was able to vary the direction of the magnetic field relative to the duct and in one series of experiments he investigated the flow when the magnetic field was perpendicular to the highly conducting walls.

In his Ph.D. thesis Alty has made a detailed comparison between the results predicted by our theory and his experimental results. We will merely present the three relevant figures which show most of the results. Fig.(2.2.) is a graph of the electric potential difference between the mid-point of a nonconducting wall and a conducting wall, $\Delta\phi$, against the overall Reynolds number, R. Note the close agreement between the theoretical and exerimental values up to a value of R of 6000. Fig.(2.3) is a graph of the variation of pressure gradient with R at a given value of M, ($M \gg 1$), and shows that for $R > 1000$ the flow is not laminar, i.e. it is unstable, and also that for R low enough the pressure gradient becomes very close to that predicted theoretically. Fig.(2.4) shows the distribution of ϕ along the non-conducting wall at a given value of R and M. The theoretical values only agree with experimental values if the potential is calculated from the mean velocity and <u>not</u> the pressure gradient, though the explanation for this is not quite clear.

These experimental results have proved the following:

(i) The magnetic field, if sufficiently large, can lower the Reynolds number at which the flow in a duct becomes unstable.

(ii) In the particular duct flow studied, for a given value of $M(\gg 1)$, the flow can be stabilised if R is reduced low enough, as was shown in §2.4.2.

(iii) The theory of MHD flow in a duct with conducting walls can accurately predict the values of ϕ, (dp/dz) etc., found experimentally.

The experiments have also shown that various interesting effects occur when the boundary layer becomes unstable which we do not understand.

2.5. Magnetohydrodynamic flows in rectangular ducts II.

2.5.1. Introduction.

In this section we continue our examination of flow in rectangular ducts whose walls are electrically conducting. We begin by referring to the paper written jointly with Professor K.Stewartson, Hunt & Stewartson (1965), hereinafter referred to as H & S. In this paper we considered the case where the walls parallel to the magnetic field (AA) are perfectly conducting and those perpendicular to the field (BB) are non-conducting, this being the kind of duct used in MHD pumps and generators, which are usually connected to an external electric circuit. In our analysis, which is only valid when $M \gg 1$, we considered the effects of such circuits, though it is found that for this particular duct they do not make the problem more difficult. (The demarcation of the work in the paper was precise in that Stewartson performed the asymptotic analysis of §2, while I wrote the other sections).

In the following sub-section we extend the order of magnitude argument of the paper to the duct flow examined in §2.4 and then compare the flow in rectangular ducts with all combinations of conducting and non-conducting walls. Finally we compare our results with the exact numerical solution of Tani (1962). Since the publication of our paper, the translation of a paper by Berezin (1963) has become available, in which he considers the same problem for all values of M. However, he merely reduces the problem to a single infinite series of algebraic equations, which, he claimed, can be solved by the method of successive approximation. This does not seem to us a great step forward.

2.5.2. Comparison of all types of duct flow.

In this section we use the method of §§4.1 and 4.2 of H & S to deduce the main result of Hunt (1965), namely that most of the flow occurs in the boundary layers on the walls (AA) if the walls (AA) are non-conducting and the walls (BB) are perfectly conducting. We call this type of duct flow case (iii).

Case (iii)

We use the same notation as for case (i) and note that for case (iii),

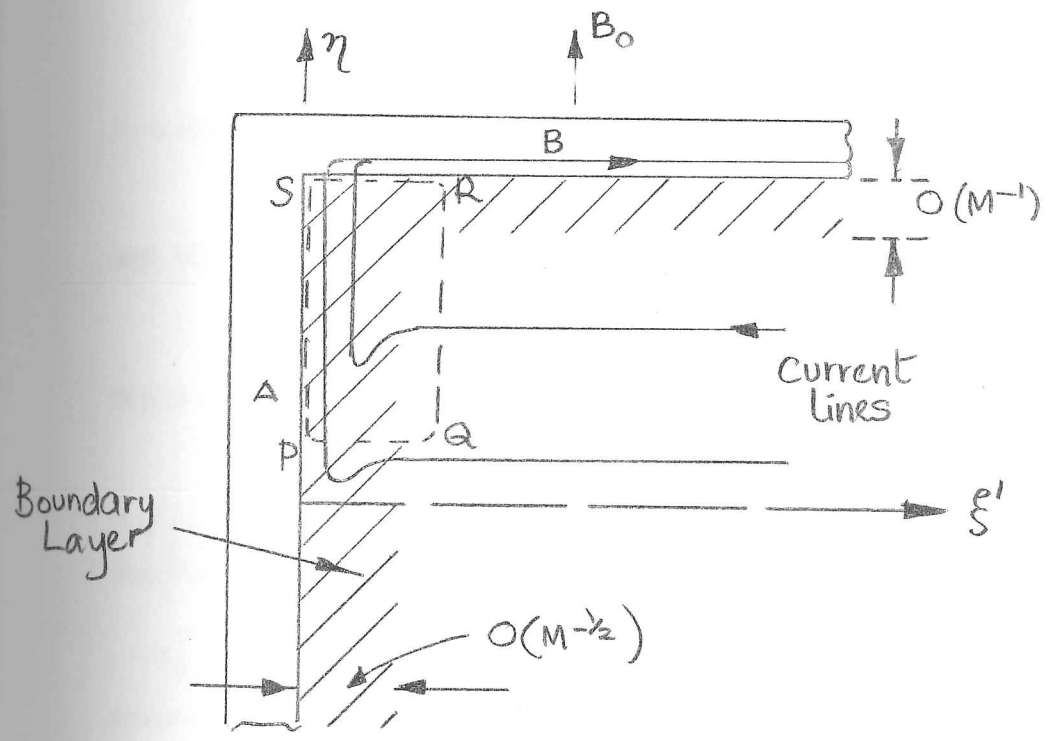

Fig 2.5 Cross-section of the duct when $d_A = 0$ and $d_B = \infty$ $(M \gg 1)$.

as may be seen from Hunt (1965), the core values of current and velocity, j_c and v_c, are also the same,

i.e. $$j_c = -B_0 v_c/\sigma = (\partial p/\partial z)/B_0 . \qquad 2.5.1.$$

We consider the integral $\oint \underset{\sim}{E} . d\underset{\sim}{\ell}$ taken round the path PQRS in fig. (2.5) Then, since Ey = 0 in the core and $E_x = 0$ on the walls BB, and since

$$\oint \underset{\sim}{E} . d\underset{\sim}{\ell} = 0 ,$$

$$\int_P^Q E_x dx + \int_S^P E_y dy = 0 . \qquad 2.5.2.$$

By considering current continuity in the secondary boundary layer:

$$j_y = -O[j_c y/\delta] ,$$

and therefore,

$$\int_S^P E_y dy = \int_S^P \frac{j_y dy}{\sigma} = -O[j_c a^2/\sigma\delta] . \qquad 2.5.3.$$

Since $E_x = 0$ in the core, $j_c/\sigma + B_0 v_c = 0$, and therefore

$$\int_P^Q E_x dx = \int_0^\delta \frac{j_s dx}{\sigma} + B_0 \int_0^\delta v_s dx .$$

Now since $j_x = 0$ on the wall it follows that $j_s = -O[j_c]$.

Therefore, using (2.5.2) and (2.5.3)

$$-O[j_c a^2/\sigma\delta] = O[-j_c \delta/\sigma] + B_0 \int_P^Q v_s dx ,$$

whence $B_0 v_s S = -O[j_c a^2/\sigma\delta]$, since $\delta \ll a$. 2.5.4.

From the equation of motion, since $j_s = -O[j_c]$,

and $\left|\frac{\partial v_s}{\partial x^2}\right| = O\left[\frac{v_s}{\delta^2}\right]$, it follows that $\frac{\bar{\mu} v_s}{\delta^2} = O[j_c B_0]$, 2.5.5.

where $\bar{\mu}$ is the viscosity in this case.

Then dividing (2.5.4) by (2.5.5)

$$\delta^4/a^4 = O[\bar{\mu}/\sigma B_0^2 a^2] .$$

or $$\delta = O[a M^{-1/2}] .$$

Thence (2.5.4) leads to:

$$v_s = -O[j_c M/\sigma B_0]$$

Therefore, from (2.5.1)

$$v_s = O(M)\, v_c,$$

$$\text{and} \int_0^\delta v_s \, dx = O\left[\frac{-(\partial p/\partial z)\, a^2}{\bar{\mu}\, M^{3/2}}\right], \qquad 2.5.6.$$

which result is the same as that of Hunt (1965).

As was mentioned in H & S, the form of the boundary layer on the walls AA is best explained in terms of the secondary currents induced in these layers. We now draw up a table showing the orders of magnitude of the secondary currents, relative to both the core current and the core velocity, including in this list the case (iv) where all the walls are non-conducting analyzed by Shercliff (1953). d_A and d_B are as defined by Hunt (1965), being proportional to the conductivities of the walls AA and BB respectively.

Case Number	d_A	d_B	
(i)	∞	∞	$j_s = -O(j_c M^{-1}) = -O(M^{-1}\sigma B_0 v_c)$
(ii) (open circuit)	∞	0	$j_s = -O(j_c) = -O(M^{-1}\sigma B_0 v_c)$
(ii) (short circuit)	∞	0	$j_s = -O(M^{-1} j_c) = -O(M^{-1}\sigma B_0 v_c)$
(iii)	0	∞	$j_s = -O(j_c) = -O(\sigma B_0 v_c)$
(iv)	0	0	$j_s = -O(j_c) = -O(M^{-1}\sigma B_0 v_c)$

From case (ii) we see that the value of the secondary currents relative to the core currents may vary, yet expressed as a fraction of v_c, j_s is of the same order in both cases. This must be so for the viscous and electromagnetic forces to balance in the boundary layer. The most significant result from this table is that $j_s = -O(M^{-1}\sigma B_0 v_c)$ in every case except (iii) and, as we saw in §§4.1 and 4.2 of H & S, this means that in each of these cases $v_s = -O(v_c)$. It is only in case (iii) where j_s, relative to v_c, is O(M) times the value of j_s in the other cases and where, in consequence, the viscous stresses must be O(M) times as great, that $v_s = O(M)\, v_c$. Other important differences are shown up by the order of magnitude arguments. This crude table only indicates the gross difference between the secondary boundary layer in case (iii) and the other cases.

2.5.3. Comparison with others' results.

Although the analysis in H & S is only valid when $M \gg 1$, Tani (1962) has provided a suitable variational method for calculating the velocity profiles and the volume flow rate, Q, at values of M below about 25. It is interesting to compare his values for Q in a square duct when M = 25 and M = 15, with those calculated from our result (1.5.48).

M	$\bar{\mu}Q/((-\partial p/\partial z)4a^4)$	
	Tani	From (3.5) of H & S
15	.047	.0458
25	.0368	.0371

We see that the difference at M = 25 is about 1%. Thus for square ducts, at least, the entire range of M is now covered.

It should be noted that in the analysis of H & S we found that the velocity profile was unchanged by an external circuit. This is only true if the conductivity of the walls AA is high enough. By analogy with the result of Hunt (1965) that, for given d_A, as $M \to \infty$, such that $d_A M^{\frac{1}{2}} \to \infty$, the solution becomes identical to that of the case where $d_A = \infty$, it is likely that a similar result will hold when d_A is finite and $d_B = 0$. The physical reason is the same namely the relative resistance of the wall to the boundary layer on the wall AA decreases as $M \to \infty$, because of the decreasing thickness and consequently conductance of the boundary layers. (This point has been analysed more rigorously by Chiang (1965)).

In the same series of experiments mentioned in §2.4.3. C.J.N.Alty examined the flow in his duct when the conducting walls were parallel to the field and the non-conducting walls were perpendicular. The conducting walls, AA, were connected together, the resistance between them being very small so that they were virtually short circuited. Therefore in measuring Q as a function of (dp/dz), the flux deficit due to the boundary layers on the walls AA is $O(M^{-3/2})$ that of the core, as shown in (3.9) of H & S. With $M > 100$, this term was too small to measure so these experiments gave no test to the theory of the secondary boundary layers. However, in some experiments on electrically driven flows in a curved duct with dp/dz = 0, J.A.Baylis (1966) has provided a critical test of the theory. We describe the theory for the flow and Baylis' results in the next section.

2.6. Flow in Curved Channels.

2.6.1. Equations for cylindrical flow.

We now consider the extension of the theory of H & S to flow in curved rectangular ducts. (See fig.2.6). We will only examine the flow when the secondary or radial velocities due to the curvature of the duct are very small compared to those in the θ direction. Also, we assume that flow does not vary in the θ or streamwise direction and therefore the pressure gradient in the streamwise direction must be zero, the energy of the flow coming from electrical energy fed in at the walls. The equations (2.2.1 - 2.2.8) for steady flow written in cylindrical, (r, θ, z) co-ordinates when $\partial/\partial\theta = 0$ are (Chandrasekhar, 1961):

$$\rho\left(v_r \frac{\partial v_r}{\partial r} + v_z \frac{\partial v_r}{\partial z} - \frac{v_\theta^2}{r}\right) = -\partial p/\partial r + j_\theta B_0 + \eta\left\{\frac{\partial^2}{\partial r^2} + \frac{1}{r}\frac{\partial}{\partial r} - \frac{1}{r^2} + \frac{\partial^2}{\partial z^2}\right\} v_r, \quad 2.6.1.$$

$$\rho\left(v_r \frac{\partial v_\theta}{\partial r} + v_z \frac{\partial v_\theta}{\partial z} + \frac{v_r v_\theta}{r}\right) = -j_r B_0 + \eta\left(\frac{\partial^2}{\partial r^2} + \frac{1}{r}\frac{\partial}{\partial r} - \frac{1}{r^2} + \frac{\partial^2}{\partial z^2}\right) v_\theta \quad 2.6.2.$$

$$\rho\left(v_r \frac{\partial v_z}{\partial r} + v_z \frac{\partial v_z}{\partial z}\right) = -\frac{\partial p}{\partial z} + \eta\left(\frac{\partial^2}{\partial r^2} + \frac{1}{r}\frac{\partial}{\partial r} + \frac{\partial^2}{\partial z^2}\right) v_z, \quad 2.6.3.$$

$$\frac{\partial v_r}{\partial r} + \frac{\partial v_z}{\partial z} + \frac{v_r}{r} = 0, \quad 2.6.4.$$

$$j_r = \sigma\left(-\partial\phi/\partial r + v_\theta B_0\right), \quad 2.6.5a.$$

$$j_\theta = \sigma v_r B_0, \quad 2.6.5b.$$

$$j_z = \sigma\left(-\partial\phi/\partial z\right), \quad 2.6.5c.$$

$$j_r = -\partial H_\phi/\partial z, \quad j_z = \frac{1}{r}\frac{\partial}{\partial r}\left(r H_\theta\right). \quad 2.6.6.$$

We now determine the conditions under which $v_r, v_z \ll v_\theta$, when $M \gg 1$. Differentiate (2.6.1) w.r.t. z, and (2.6.3) w.r.t. r, and subtract the equations. Assuming $v_\theta \gg v_r, v_z$, we have in the primary or Hartmann boundary layers at $z = \pm a$,

$$-\rho \frac{\partial\left(v_\theta^2/r\right)}{\partial z} \simeq \sigma B_0^2 \frac{\partial v_r}{\partial z} + \eta \frac{\partial^3 v_r}{\partial z^3}.$$

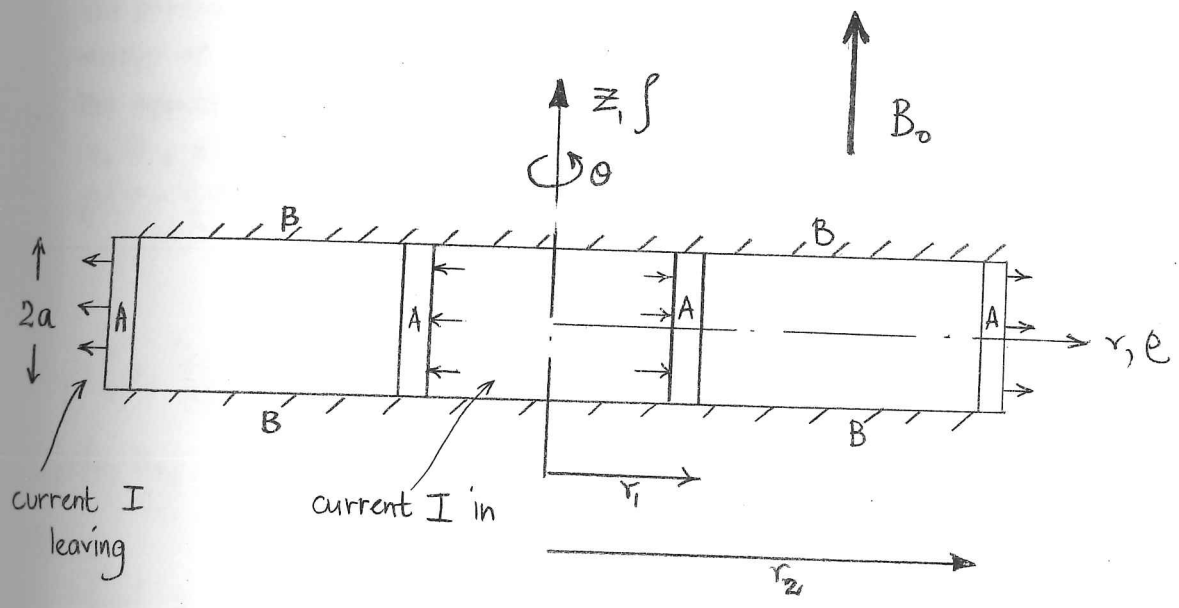

Fig 2.6 Cross-section of annular rectangular channel (Walls AA are perfectly conducting walls BB are non conducting.)

2.6. Flow in Curved Channels.

2.6.1. Equations for cylindrical flow.

We now consider the extension of the theory of H & S to flow in curved rectangular ducts. (See fig.2.6). We will only examine the flow when the secondary or radial velocities due to the curvature of the duct are very small compared to those in the θ direction. Also, we assume that flow does not vary in the θ or streamwise direction and therefore the pressure gradient in the streamwise direction must be zero, the energy of the flow coming from electrical energy fed in at the walls. The equations (2.2.1 - 2.2.8) for steady flow written in cylindrical, (r, θ, z) co-ordinates when $\partial/\partial\theta = 0$ are (Chandrasekhar, 1961):

$$\rho\left(v_r \frac{\partial v_r}{\partial r} + v_z \frac{\partial v_r}{\partial z} - \frac{v_\theta^2}{r}\right) = -\partial p/\partial r + j_\theta B_0 + \eta\left\{\frac{\partial^2}{\partial r^2} + \frac{1}{r}\frac{\partial}{\partial r} - \frac{1}{r^2} + \frac{\partial^2}{\partial z^2}\right\} v_r, \quad 2.6.1.$$

$$\rho\left(v_r \frac{\partial v_\theta}{\partial r} + v_z \frac{\partial v_\theta}{\partial z} + \frac{v_r v_\theta}{r}\right) = -j_r B_0 + \eta\left(\frac{\partial^2}{\partial r^2} + \frac{1}{r}\frac{\partial}{\partial r} - \frac{1}{r^2} + \frac{\partial^2}{\partial z^2}\right) v_\theta \quad 2.6.2.$$

$$\rho\left(v_r \frac{\partial v_z}{\partial r} + v_z \frac{\partial v_z}{\partial z}\right) = -\frac{\partial p}{\partial z} + \eta\left(\frac{\partial^2}{\partial r^2} + \frac{1}{r}\frac{\partial}{\partial r} - \frac{1}{r^2} + \frac{\partial^2}{\partial z^2}\right) v_z, \quad 2.6.3.$$

$$\frac{\partial v_r}{\partial r} + \frac{\partial v_z}{\partial z} + \frac{v_r}{r} = 0, \quad 2.6.4.$$

$$j_r = \sigma\left(-\partial\phi/\partial r + v_\theta B_0\right), \quad 2.6.5a.$$

$$j_\theta = \sigma v_r B_0, \quad 2.6.5b.$$

$$j_z = \sigma\left(-\partial\phi/\partial z\right), \quad 2.6.5c.$$

$$j_r = -\partial H_\phi/\partial z, \quad j_z = \frac{1}{r}\frac{\partial}{\partial r}\left(r H_\theta\right). \quad 2.6.6.$$

We now determine the conditions under which $v_r, v_z \ll v_\theta$, when $M \gg 1$. Differentiate (2.6.1) w.r.t. z, and (2.6.3) w.r.t. r, and subtract the equations. Assuming $v_\theta \gg v_r, v_z$, we have in the primary or Hartmann boundary layers at $z = \pm a$,

$$-\rho \frac{\partial\left(v_\theta^2/r\right)}{\partial z} \simeq \sigma B_0^2 \frac{\partial v_r}{\partial z} + \eta \frac{\partial^3 v_r}{\partial z^3}.$$

Since in these boundary layers $\partial/\partial z = O(M)$ and $v_\theta = O(v_c)$, where v_c is the core velocity, we have:

$$\frac{v_r}{v_c} = O\left[\frac{a}{r} \cdot \frac{\rho v_c}{\sigma B_o^2 a}\right] = K \qquad 2.6.7.$$

Therefore provided K is small enough we can ignore v_r and v_z compared to v_θ, but it is important to realise that however small v_θ is, v_r is always present.

2.6.2. Flow in a rectangular annulus.

Consider the flow in a rectangular annulus of sides 2a and $(r_2 - r_1)$ with walls parallel and perpendicular to the field being perfectly conducting and non-conducting respectively, as shown in fig.(2.6). The flow is driven by a total current I and therefore from (2.6.6) the boundary conditions on H_θ are:

$$\text{at } z = \pm a, \quad \frac{\partial}{\partial r}(r H_\theta) = 0,$$

$$\text{at } r = r_1, r_2, \quad \frac{\partial}{\partial r}(r H_\theta) = 0.$$

Then let $H_\theta = I_1/2\pi r$ at $z = +a$,

and $H_\theta = I_2/2\pi r$ at $z = -a$,

where I_1, I_2 are constants so that,

$$2\pi r \int_{-a}^{+a} j_r \, dz = I_2 - I_1 = I.$$

We now normalize v_θ, H_θ by writing:

$$v_\theta = v\, I/(4\pi a \sqrt{\sigma\eta}), \quad h_\theta = \frac{I_1 + I_2}{4\pi r} + \frac{hI}{4\pi a},$$

$$M = a B_o (\sigma/\eta)^{1/2}, \quad \rho = r/a, \quad \xi = z/a. \qquad 2.6.8.$$

Then v and h satisfy:

$$\left.\begin{aligned} \left(\frac{\partial^2 v}{\partial \xi^2} + \frac{\partial^2 v}{\partial \rho^2} + \frac{1}{\rho}\frac{\partial v}{\partial \rho} - \frac{v}{\rho^2}\right) + M\frac{\partial h}{\partial \xi} = 0 \\ \left(\frac{\partial^2 h}{\partial \xi^2} + \frac{\partial^2 h}{\partial \rho^2} + \frac{1}{\rho}\frac{\partial h}{\partial \rho} - \frac{h}{\rho^2}\right) + M\frac{\partial v}{\partial \xi} = 0 \end{aligned}\right\} \qquad 2.6.9.$$

subject to:

$$\left.\begin{aligned} v = 0, \quad h = \pm 1/\rho \quad &\text{when } \xi = \pm 1, \\ v = 0, \quad \frac{\partial h}{\partial \rho} + \frac{h}{\rho} = 0 \quad &\text{when } \rho = \rho_1, \rho_2. \end{aligned}\right\} \qquad 2.6.10.$$

Dividing up the duct into similar zones as in H & S, we can perform a similar asymptotic analysis when $M \gg 1$.

(i) Core: Since $\frac{\partial}{\partial \xi} \sim \frac{\partial}{\partial \rho} = O(1)$,

$$v_c = g(\rho) \quad \text{and} \quad h_c = f(\rho),$$

where g and f are functions of ρ to be determined by the primary boundary layers.

(ii) Primary boundary layers; Since $\frac{\partial}{\partial \rho} \gg \frac{\partial}{\partial \xi}$, (2.6.6) becomes:

$$\frac{\partial^2 v_p}{\partial \xi^2} + M \frac{\partial h_p}{\partial \xi} = 0, \quad \frac{\partial^2 h_p}{\partial \xi^2} + M \frac{\partial v_p}{\partial \xi} = 0 \qquad 2.6.11.$$

where $v = v_p + v_c$, $h = h_c + h_p$ and h_p, v_p are subject to:

$$v_p = -v_c, \quad h_p = -\frac{1}{\rho} - h_c \qquad \text{at } \xi = 1,$$

$$v_p = -v_c, \quad h_p = \frac{1}{\rho} - h_c \qquad \text{at } \xi = -1,$$

$$v_p \to 0, \quad h_p \to 0 \qquad \text{away from walls.}$$

Then in the boundary layer at $\xi = 1$

$$v_p = \frac{1}{\rho} e^{-M(1-\xi)}, \quad h_p = -\frac{1}{\rho} e^{-M(1-\xi)} \qquad 2.6.12a.$$

and at $\xi = -1$,

$$v_p = \frac{1}{\rho} e^{-M(1+\xi)}, \quad h_p = \frac{1}{\rho} e^{-M(1+\xi)} \qquad 2.6.12b.$$

It follows that $f(\rho) = 0$ and $g(\rho) = \frac{1}{\rho}$ so that,

$$v_c = -1/\rho, \quad h_c = 0 \qquad 2.6.13.$$

(iii) Region d

The analysis for this region follows that in §2.5.2 with the result that on the wall $\xi = 1$,

$$v_s(\rho, 1) + h_s(\rho, 1) = 0,$$

where $v = v_c + v_p + v_s$, $h = h_c + h_p + h_s$. Thus we have a boundary condition on $(v_s + h_s)$ at $\eta = 1$, which we need for the analysis of the secondary boundary layer - region (c).

(iv) Secondary boundary layer

In this region we assume, as in H & S (§2), that:

$$\partial/\partial\rho \gg \partial/\partial\zeta$$

However in this case we make the additional assumption that,

$$\partial/\partial\rho \gg 1/\rho \,. \qquad 2.6.14.$$

or in other words $\delta = O(aM^{-\frac{1}{2}}) \ll r_1$, the radius of the inner wall. Clearly if the condition is satisfied when $\rho = \rho_1$, it is also satisfied when $\rho = \rho_2$. Then, in the layer on the wall at $\rho = \rho_1$, if $v_s = -(M/\rho_1)v_s'$ and $h_s = (M/\rho_1)h_s'$, v_s' and h_s' satisfy (2.25) of H & S, namely:

$$\frac{\partial^2 v_s'}{\partial\rho^2} + M\frac{\partial h_s'}{\partial\zeta} = 0, \quad \frac{\partial^2 h_s'}{\partial\rho^2} + M\frac{\partial v_s'}{\partial\zeta} = 0$$

and the boundary conditions:

$$v_s' = -\frac{1}{M}, \quad \frac{\partial h_s'}{\partial\rho} = 0 \qquad \text{when } \rho = \rho_1,$$

since $\partial h_s/\partial\rho \gg \frac{h_s}{\rho_1}$, in virtue of (2.6.14). Now we can use the solutions for v_s and h_s in §2 of H & S. The result for the velocity deficiency on the wall $\rho = \rho_1$, is:

$$\int_0^\infty \int_{-1}^{+1} v_s \, \partial\bar{\rho}\,\partial\zeta = \frac{M}{\rho}\frac{(-\frac{1}{4})!\,2^{\frac{1}{2}}}{(-\frac{1}{4})!\,M^{3/2}}, \quad \text{where } \bar{\rho} = (\rho-\rho_1)M^{\frac{1}{2}},$$

and on the wall $\rho = \rho_2$:

$$= M(-\tfrac{1}{4})!\,2^{\frac{1}{2}}/((\tfrac{1}{4})!\,M^{3/2}\rho_2).$$

Thus $\int_{\rho_1}^{\rho_2}\int_{-1}^{+1} v\,\partial\rho\,\partial\zeta = -2\ln(\rho_2/\rho_1) + \frac{(-\frac{1}{4})!\,2^{\frac{1}{2}}}{(-\frac{1}{4})!\,2^{\frac{1}{2}}}\left(\frac{1}{\rho_1}+\frac{1}{\rho_2}\right) + \frac{2\ln(\rho_2/\rho_1)}{M} + \ldots$

This may be rewritten:

$$Q = \int_{r_1}^{r_2}\int_{-a}^{+a} v_\theta \, dr\, dz,$$

$$= -\frac{I\ln(r_2/r_1)}{2\pi\sqrt{\sigma\eta}}\left[1 - \frac{.956(r_2+r_1)a}{M^{\frac{1}{2}}r_1r_2\ln(r_2/r_1)} - \frac{1}{M}\right] \qquad 2.6.15.$$

Now if we integrate (2.6.5a) across the duct, then:

$$\int_{r_1}^{r_2}\int_{-a}^{+a}\left(\frac{-\partial\phi}{\partial r}\right)dr\,dz = 2a\Delta\phi \text{ where } \Delta\phi \text{ is the fall in potential from}$$

the wall at $r = r_1$, to that $r = r_2$. Thence

$$2a\,\Delta\phi = -B_0 \int_{r_1}^{r_2}\int_{-a}^{+a} v_\theta \, dr\, dz + \int_{r_1}^{r_2}\int_{-a}^{+a} \frac{jr}{\sigma}\, dr\, dz$$

$$= -B_0 \mathcal{Q} + \int_{r_1}^{r_2} I/(\sigma 2\pi r)\, dr$$

Therefore $\Delta\phi = B_0\mathcal{Q}/2a - I\ln(r_2/r_1)/(4\pi a\sigma)$. 2.6.16.

From (2.6.16) and (2.6.15) we obtain an expression for the resistance of the channel i.e. the ratio of $\Delta\phi$ to I:

$$\frac{\Delta\phi}{I} = \frac{M\ln(r_2/r_1)}{4\pi a\sigma}\left[1 - \frac{.956(r_2+r_1)a}{M^{1/2} r_1 r_2 \ln(r_2/r_1)} + O(M^{-3/2})\right] \quad 2.6.17.$$

2.6.3. Experimental results.

J.A.Baylis performed some experiments in the Cambridge University Engineering Laboratory on electrically driven flows in square annular channels at high Hartmann number (Baylis, 1966). Although secondary flow was present in all his experiments, when the field was high enough and the current low enough it was negligible. (When secondary flow occurs, $\Delta\phi$ does not increase linearly with I, as is to be expected from (2.6.17), and is detected in this way). In order to analyze the experimental results in the non-linear regime, Baylis plotted the variable $P_1 = IB_0a^3/(\pi R M \tilde{\eta}\mathcal{Q})$ as a function of M, where Q is calculated from (2.6.16). The theoretical value of P from (2.6.16) and (2.6.17) is:

$$P = \left[\frac{R}{2a}\left(\ln\left(\frac{R+a}{R-a}\right)\right)\left(1 - \frac{.956(2Ra)}{M^{1/2}(R^2-a^2)\ln(R+a/R-a)} - M^{-1} + O(M^{-3/2}) \ldots\right)\right]^{-1} \quad 2.6.18.$$

where $R = (r_2 + r_1)/2$. The experimental results are compared with the theoretical in the table below.

M	R/a	$P_{theor.}$	$P_{exp.}$
16.31	35	1.41	$1.4 \pm .1$
16.37	17	1.41	$1.5 \pm .1$
16.74	8	1.41	$1.4 \pm .1$
32.37	17	1.25	$1.19 \pm .04$

M	R/a	$P_{theor.}$	$P_{exp.}$
32.86	8	1.24	$1.23 \pm .04$
64.93	8	1.15	$1.12 \pm .03$
65.8	3.5	1.12	$1.12 \pm .03$
129.8	3.5	1.062	$1.045 \pm .02$

Thus, although most of the experimental results differ from the theoretical by less than the experimental error, they are systematically below the theoretical value, for which there is no ready explanation.

We note that the value of M is low enough for the term in $(M^{-\frac{1}{2}})$ to be appreciable, so that the theory for the secondary boundary layers may be considered to be fairly well tested. Also the values of R/a are low enough for the effects of the curvature of the duct to be appreciable, so that the modification of the H & S theory for curved ducts may be considered satisfactory.

2.7. Magnetohydrodynamic flow in channels of variable cross section with strong transverse magnetic fields.*

2.7.1. Introduction.

In section 2.7 we consider the effects of a strong uniform magnetic field,

$$\underline{B_0} = (0, B_0, 0),$$

on steady two-dimensional flows, whose velocities are given by,

$$\underline{v} = (v_x(x,y), v_y(x,y), 0)$$

through ducts with walls at

$$y = f_t(x), f_b(x) \text{ and } z = \pm b,$$

where we assume $b \gg (f_t - f_b)$ (The effects on the flow of boundary layers on the walls at $z = \pm b$ are considered negligible). The analysis also enables us to examine the flow over a body placed in such a duct. Unlike a wind tunnel, a duct for investigating MHD flow over bodies has to be placed in a magnet whose gap is usually small. Consequently the duct size is severely limited and, for flow over a practical size of body, wall effects cannot be ignored even outside the boundary layers. We examine the inviscid regions taking into account the effects of the wall and we also examine the boundary layers on the walls.

Ludford (1961) and Ludford & Singh (1963) have developed much of the existing theory for external flows in transverse magnetic fields over two and three dimensional bodies. They assume that the magnetic field is strong, and that the conductivity is weak enough to ignore the induced magnetic field. This is equivalent to assuming that the interaction parameter $N (= \sigma B_0^2 a/\rho U_0) \gg 1$, and that the magnetic Reynolds number $R_m (= \mu\sigma U_0 a) \ll 1$, where B_0, σ, ρ, μ are the flux density of the imposed transverse magnetic field and the fluid's density, conductivity and magnetic permeability, respectively. U_0 and a are the characteristic velocity and length.

Making this approximation for two-dimensional flow, Ludford (1961)

---

* The analysis presented here is the same as that submitted jointly with Dr.S.Leibovich in a paper to the Journal of Fluid Mechanics. In the paper the problem of flow over 2 dimensional bodies was considered in greater detail, this part of the paper being written by Leibovich. The work presented in this thesis is my own in all essentials.

found that in the 'inner' region near the body the inertial terms in the momentum equation are negligible compared to the electromagnetic and pressure forces, except in singular zones at the front and rear of the bodies. In the 'outer' region sufficiently far in the field, or y direction from the body he found that inertia forces again became important. He discussed their effect by compressing the y co-ordinate to retain the influence of inertia and found expressions for lift and drag. The singularities in the inner region were left and the question of how these may affect the flow was not resolved.

We apply Ludford's approximations to flows in ducts in which we also consider viscous effects in boundary layers at the walls. Then the region outside the boundary layers where viscous forces are negligible corresponds to Ludford's 'inner' region and we treat this region in a similar manner to Ludford, though, unlike Ludford, we succeed in analysing the singular zones which occur whenever the duct wall curvature is O(N). We then examine the boundary layers by assuming that the Hartmann number $M \gg 1$. We are able to extend the usual analysis of these layers (Stewartson 1960) by calculating the higher order approximations, which is possible because of the simplicity of the core flow solution (away from the singular zones), for which an expansion in inverse powers of N may easily be found.

The approximation used by Ludford has also been used very successfully by Bornhorst (1965) to calculate the effect of a magnetic field on the free surface of a mercury flow when $N \gg 1$. The fact that the theory accurately predicted the free surface profiles found experimentally demonstrates the usefulness of the approximation. It is worth observing that, in general, it is not difficult to devise laboratory experiments which satisfy our criteria that $N \gg 1$, $R_m \ll 1$ and $M \gg 1$, while having the Reynolds number large enough for accurate readings of pressure, velocity, etc to be taken. With regard to the practical usefulness of our approximation, our criteria are not satisfied by the flows in most MHD devices at the moment, (e.g. in the biggest MHD generators N is only O(1)). However, as their size and their field strength increase, so that N increases, our approximate methods may become increasingly useful in examining the flows in MHD pumps, generators, etc.

2.7.2. Statement of the problem.

The Magnetohydrodynamic (MHD) equations for steady, incompressible flow when the fluid properties are constant are:

$$\rho(\underset{\sim}{v}\cdot\nabla)\underset{\sim}{v} = -\nabla p + \underset{\sim}{j}\times\underset{\sim}{B} + \eta\nabla^2\underset{\sim}{v}, \qquad 2.7.1.$$

$$\nabla\cdot\underset{\sim}{v} = 0, \qquad 2.7.2.$$

$$\underset{\sim}{j} = \sigma(\underset{\sim}{E} + \underset{\sim}{v}\times\underset{\sim}{B}), \qquad 2.7.3.$$

$$\nabla\times\underset{\sim}{E} = 0, \qquad 2.7.4.$$

$$\underset{\sim}{j} = \frac{1}{\mu}\nabla\times\underset{\sim}{B}, \qquad 2.7.5;$$

$$\nabla\cdot\underset{\sim}{B} = 0, \qquad 2.7.6.$$

where $\underset{\sim}{v}$, p, $\underset{\sim}{j}$, $\underset{\sim}{B}$, $\underset{\sim}{E}$ are velocity, pressure, current density, magnetic flux density and electric field respectively. When $R_m \ll 1$, we can ignore the induced magnetic field due to $\underset{\sim}{j}$ and assume that, in equations (2.7.1) and (2.7.3)

$$\underset{\sim}{B} = \underset{\sim}{B_0},$$

where $\underset{\sim}{B_0}$ is the imposed magnetic field.

If now we consider a two-dimensional flow in the x-y plane, such that

$$v_z = \partial/\partial z = 0$$

then,

$$\partial E_x/\partial z = \partial E_y/\partial z = 0$$

and hence from (2.7.4)

$$\partial E_x/\partial x = \partial E_z/\partial y = 0$$

Whether the walls at $y = f_t(x), f_b(x)$ are conducting or not, provided there are no current sources or sinks along these walls, it may be shown that $E_x = E_y = 0$. (If the electrical boundary conditions on the walls at $z = \pm b$ vary rapidly in the x-direction then it follows that $\partial/\partial z \neq 0$ and $E_x \neq 0$; thus the applicability of the basic assumptions to real flows must always be carefully checked. We discuss this point further in the conclusion). If the magnetic field $\underset{\sim}{B_0}$ lies in the y-direction and if we reduce the parameters to a non-dimensional form in terms of Q, the total flow rate through the duct per unit depth, $\underset{\sim}{B_0}$, and a, a representative channel width, the equations become:

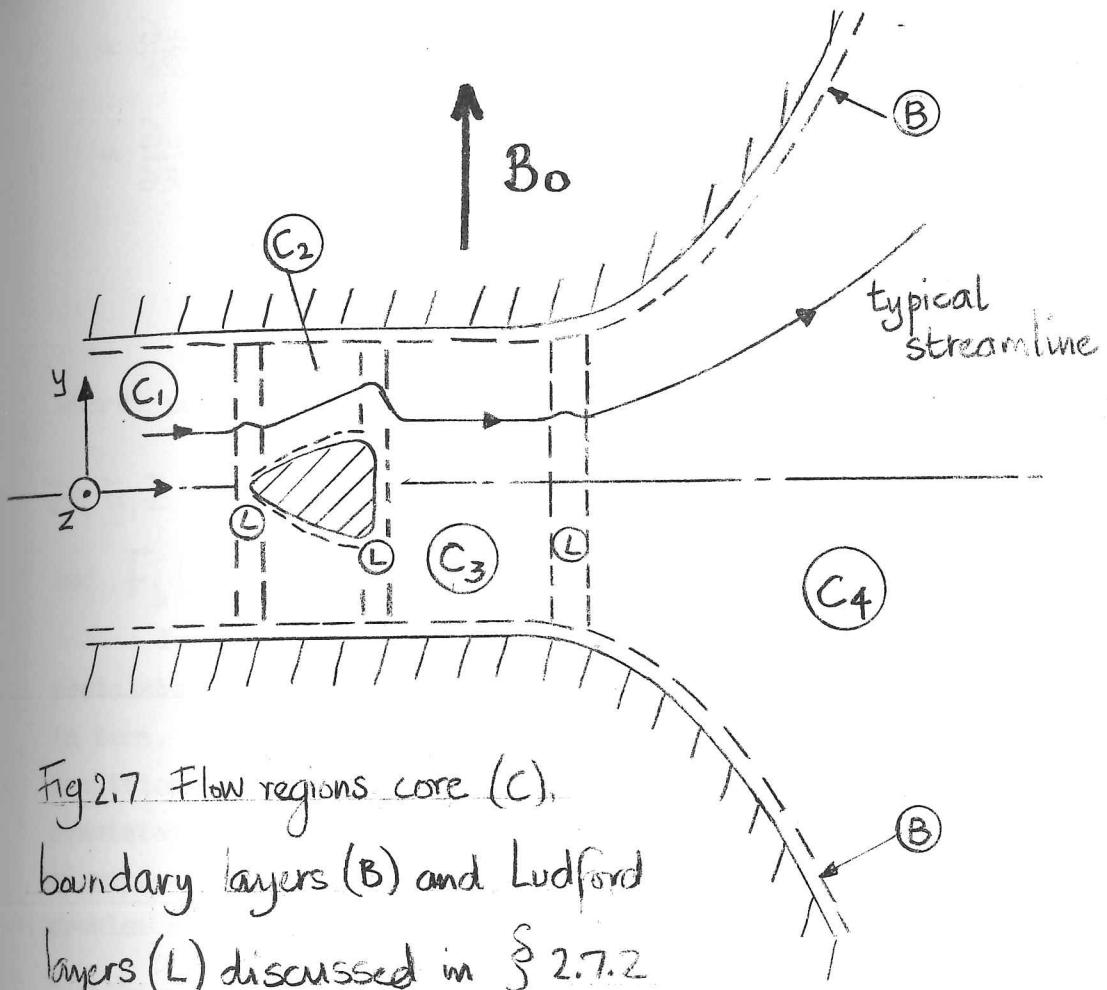

Fig 2.7 Flow regions core (C), boundary layers (B) and Ludford layers (L) discussed in § 2.7.2

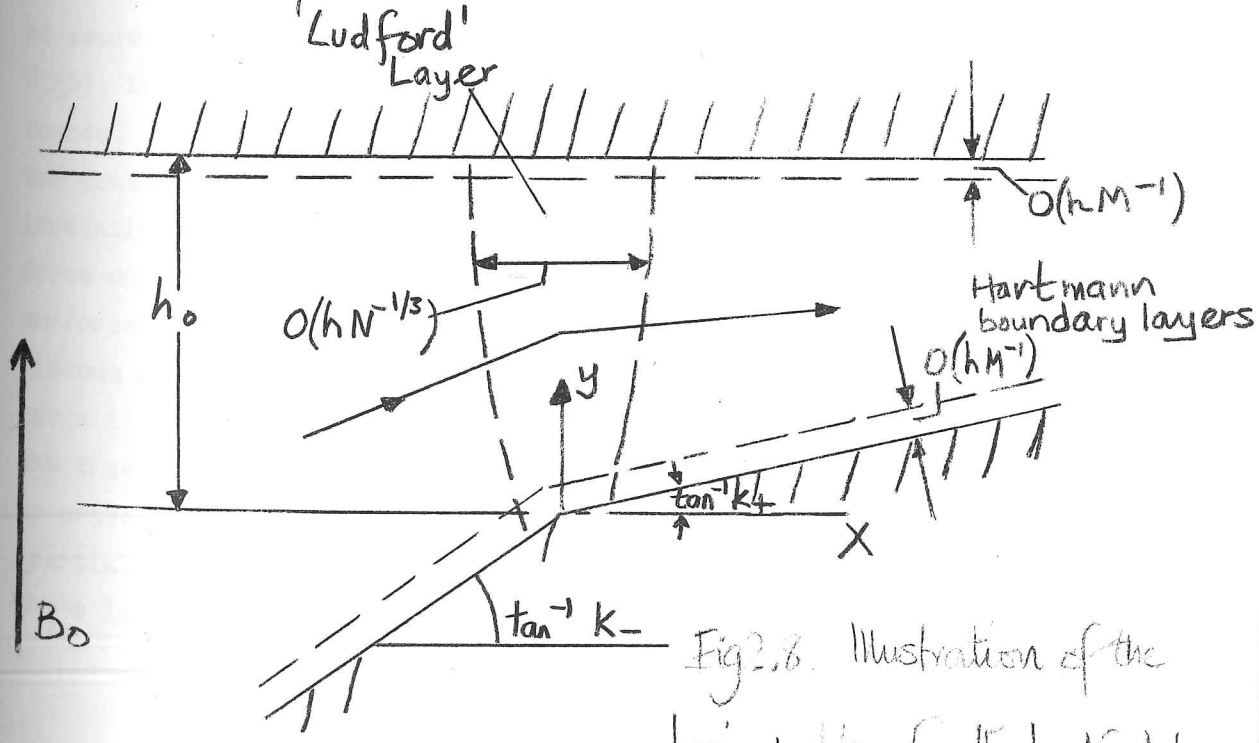

Fig 2.8 Illustration of the basic problem for the Ludford layer

$$u\frac{\partial u}{\partial \tilde{x}} + v\frac{\partial u}{\partial \tilde{y}} = -\frac{\partial \tilde{p}}{\partial \tilde{x}} - N(u + E_0) + R^{-1}\nabla^2 u,$$

$$u\frac{\partial v}{\partial \tilde{x}} + v\frac{\partial v}{\partial \tilde{y}} = -\frac{\partial \tilde{p}}{\partial \tilde{y}} + R^{-1}\nabla^2 v,$$

$$0 = -\frac{\partial p}{\partial \tilde{z}}, \qquad \text{2.7.7.}$$

$$\frac{\partial u}{\partial \tilde{x}} + \frac{\partial v}{\partial \tilde{y}} = 0,$$

where $u = v_x/(Q/a)$, $v = \sigma_y/(Q/a)$, $\tilde{p} = p/(\rho Q^2/a^2)$, $E_0 = E/(Q B_0/a)$

$\tilde{x}, \tilde{y}, \tilde{z} = x, y, z/a$, $N = \sigma B_0^2 a^2/\rho Q$ and $R = \rho Q a/\eta$. Also let $F_t(\tilde{x}) = f_t(x)/a$ and $F_b(\tilde{x}) = f_b(x)/a$.

To solve these equations and satisfy the boundary conditions we postulate the existence of various regions in the flow, which we examine in turn. The solutions which are found to satisfy the boundary conditions, match each other at the boundaries of the regions and are consistent with the original assumptions. We will now discuss the approximations to be used (see figure 2.7) by looking at the general problem of flow over a body placed in a duct with diverging walls.

Regions C (core flow).

In these regions, away from the boundaries, velocity gradients may be assumed to be O(1) so that viscous forces are negligible and, since $N \gg 1$, the electromagnetic forces are very much greater than the inertial forces. Thus in these regions the electromagnetic force is balanced by the pressure gradient, and consequently the body force, $\underset{\sim}{j} \times \underset{\sim}{B}$, is irrotational. Since, as pointed out by Shercliff (1965), the $\underset{\sim}{j} \times \underset{\sim}{B}$ force only affects the motion of an incompressible fluid with no free surfaces when it is rotational, it appears paradoxical that, when no viscous effects are present, as the $\underset{\sim}{j} \times \underset{\sim}{B}$ force becomes sufficiently large it becomes irrotational. The explanation is that, although in the final flow pattern the $\underset{\sim}{j} \times \underset{\sim}{B}$ force is irrotational, in the setting-up process the $\underset{\sim}{j} \times \underset{\sim}{B}$ force has to be rotational. Note that, when the inertial forces are negligible, the velocity is very simply determined by Ohm's Law and the continuity equation, as shown in §3. But, as Ludford

has shown, this approximation breaks down in the region near a discontinuity in the slope of the boundary walls, as illustrated by the kink in the streamlines between C_1, C_2 and C_2 C_3 in figure 2.7.

Regions L. (Ludford Layers).

These regions emanate in the field direction from places where the slope of the boundary walls changes rapidly. Consequently U' changes rapidly in the x direction and therefore in these regions the inertial and viscous forces are appreciable. These are the singular regions near the front and rear of a body which Ludford did not analyse. The structure of these regions, which we shall call 'Ludford' layers, is analysed in §4 and is shown to depend on the relative size of M and R. For the parameter range of interest it is shown that the thickness of these layers is $O(N^{-1/3})$. Our analysis assumes the slopes of the boundaries is always finite, though their rate of change may be infinite. This means we do not analyse the layers emanating from the rear of the body in figure 2.7, but only from the front. However, since duct walls usually have finite slopes, the analysis is valid for most practical situations.

Regions B.

In these regions boundary layers are formed. We shall assume that their thickness is small compared with the size of the duct and that in these layers the dominant forces are viscous and electromagnetic. These assumptions are shown in §5 to be equivalent to assuming $N \gg 1$ and $M \gg 1$, the thickness of the boundary layer being $O(M^{-1})$. In this analysis we implicitly assume that, as a result of several experimental and theoretical investigations, if N and M are sufficiently large there is no separation of the boundary layers. In experimental investigations of the flow over cylinders, spheres and flat plates, (Tsinober, 1963, and Tsinober, Shtern & Shcherbinin, 1963), and flow through a diverging channel, (Heiser, 1964), it was shown that when the magnetic field is sufficiently great, it can completely suppress the separation of a boundary layer, while some theoretical evidence for this phenomenon has been provided by Moreau (1964) who demonstrated that a transverse magnetic field can suppress the separation of boundary layers on a flat plate and on a cylinder.

2.7.3. Core flow.

As Ludford (1961) has shown, in the limit $N \to \infty$, equations (2.7.7) reduce to

$$\text{(a)}\quad \partial\tilde{p}/\partial\tilde{x} + N(u + E_0) = 0,$$
$$\text{(b)}\quad \partial(\tilde{p}/N)/\partial\tilde{y} = 0,$$
$$\text{(c)}\quad \partial u/\partial\tilde{x} + \partial v/\partial\tilde{y} = 0, \qquad 2.7.8.$$

on allowing p to grow large with N and assuming that velocity gradients are o(N). Equations (2.7.8) have the solution

$$u = -f'(\tilde{x}),\quad \tilde{p} = N[f(\tilde{x}) - \tilde{x}E_0],\quad v = \tilde{y}f''(\tilde{x}) + g(\tilde{x}). \qquad 2.7.9.$$

Clearly, this solution cannot satisfy the no-slip condition $u = 0$, $v = 0$ at the walls. In fact, Hartmann layers must form there, of thickness $O(M^{-1})$ to reduce the tangential velocity of the core flow (2.7.9) to zero. (See § 2.7.5). We therefore relax the no-slip condition, and require only that the normal velocity at the walls vanish.*

For flow in a duct the top and bottom walls of which are described by the equations $\tilde{y} = F_t(\tilde{x})$, $\tilde{y} = F_b(\tilde{x})$ respectively the boundary conditions are satisfied if

$$F_t f''(\tilde{x}) + g(\tilde{x}) = F_t' u,\quad F_b f'' + g = F_b' u,$$

$$\text{or}\quad g(\tilde{x}) = \frac{F_b F_t' - F_t F_b'}{F_b - F_t}\left[-f(\tilde{x})\right] \qquad 2.7.10.$$

Furthermore, to satisfy the continuity requirement,

$$Q\int_{F_b}^{F_t} u\, d\tilde{y} = Q = (-f')(F_t - F_b)Q, \qquad 2.7.11.$$

Thus,

$$u = \frac{1}{F_t - F_b},\quad v = \frac{1}{(F_t - F_b)^2}\left[F_t'(\tilde{y} - F_b) + F_b'(F_t - \tilde{y})\right], \qquad 2.7.12.$$

* Ludford (1961) also deals with the solution (3.2). Since he is concerned with an infinite domain, however, he must take f' = constant, and cannot satisfy boundary conditions at infinity. These are satisfied by considering inertial effects for large y.

and $\tilde{p}$ may be found in terms of E and Q by integration.

If now a body is placed in the duct the top and bottom walls of which are at $\tilde{y} = c_t(\tilde{x})$, $\tilde{y} = c_b(\tilde{x})$, $(l_1 < \tilde{x} < l_2)$, then the solution when $l_1 < \tilde{x} < l_2$ for the flow between the body and the top wall is:

$$u = \frac{1}{f_t - c_t}, \quad v = \frac{1}{(f_t - c_t)^2}\left[f_t'(\tilde{y} - c_t) + c_t'(f_t - \tilde{y})\right], \qquad 2.7.13a.$$

and for the flow between the body and the bottom wall is:

$$u = \frac{1}{c_b - f_b}, \quad v = \frac{1}{(c_b - f_b)^2}\left[c_b'(\tilde{y} - f_b) + f_b'(c_b - \tilde{y})\right] \qquad 2.7.13b.$$

The solution for $\tilde{x} < l_1$, and $\tilde{x} > l_2$ is unaltered by the presence of the body. Thus the flow over a body in a duct is identical to the flow in two separate ducts, their walls being the top and bottom walls of the duct, the dividing streamlines and the top and bottom walls of the body. Therefore in the following analysis, where we only mention flows in ducts, we are implicitly treating flows over bodies as well.

Our duct flow solution (2.7.12) (or pseudo duct flow (2.7.13)) holds whenever the wall slopes and curvatures are finite, since

$$\frac{1}{N}\frac{\partial v}{\partial x} = \frac{1}{N(f_t - f_b)^2}\left[f_t''(\tilde{y} - f_b) + f_b''(f_t - \tilde{y}) - 2\frac{f_t' - f_b'}{f_t - f_b}\left[f_t'(\tilde{y} - f_b) + f_b'(f_t - \tilde{y})\right]\right].$$

However, if $f_{t,b}''$ or $f_{t,b}^{12} = O(N)$, (2.7.8) fails to hold. As discussed in §2, we only deal with the case where $f_{t,b}' = O(1)$, so that we only consider situations where (2.7.12) fails to hold owing to the curvature being $O(N)$. (The solution (2.7.13) always fails at the front and rear of a body except in the unlikely event of the body being cusp shaped at these points).

The solution (2.7.12) may be regarded as the leading terms in an asymptotic expansion:

$$\left.\begin{aligned} u &= u_0 + N^{-1}u_1 + N^{-2}u_2 + \dots \\ v &= v_0 + N^{-1}v_1 + N^{-2}v_2 + \dots \\ \tilde{p} &= N(p_0 + N^{-1}p_1 + \dots) \end{aligned}\right\} \qquad 2.7.14.$$

To consider the higher approximations and still ignore viscous effects M has to be sufficiently large. But since we are only interested in the first or second order approximations, if $M \gg N$ we can ignore viscous effects in the core . To find u_1 , v_1 , p_1 we substitute (2.7.14) into (2.7.7) and equate terms of $O(1)$.

The solutions for u_1 and v_1 that satisfy the boundary condition that the normal velocity vanishes at the walls are

$$u_1 = \left[\frac{1}{2}\tilde{y}^2 - \frac{F_t^3 - F_b^3}{6(F_t - F_b)}\right]\frac{dG_1}{d\tilde{x}} - \left[\tilde{y} - \frac{F_t + F_b}{2}\right]\frac{dG_2}{d\tilde{x}},$$

$$v_1 = -\frac{\partial}{\partial \tilde{x}}\left[\left\{\frac{\tilde{y}^3 - F_b^3}{6} - \frac{(F_t^3 - F_b^3)(\tilde{y} - F_b)}{6(F_t - F_b)}\right\}\frac{dG_1}{d\tilde{x}}\right. \qquad 2.7.15.$$

$$\left. - \left\{\frac{\tilde{y}^2 - F_b^2}{2} - \frac{(F_t + F_b)(\tilde{y} - F_b)}{2}\right\}\frac{dG_2}{d\tilde{x}}\right],$$

where $$G_1 = \frac{1}{(F_t - F_b)^2}\frac{d}{d\tilde{x}}\left(\frac{F_t' - F_b'}{F_t - F_b}\right),$$

$$G_2 = \frac{1}{(F_t - F_b)^2}\frac{d}{d\tilde{x}}\left(\frac{F_t F_b' - F_b F_t'}{F_t - F_b}\right). \qquad 2.7.16.$$

We note that if the wall slope becomes $O(N^{1/3})$, N^{-1} becomes of the same order as U_0, so that F_t', $F_b' \ll O(N^{1/3})$ for the first approximation to be valid.

2.7.4. The Ludford layer equations.

In regions where the wall curvature is $O(N)$ the inertial forces cannot be neglected and the solution for the core flow, (2.7.12), is no longer valid. Suppose such a region exists at $x = 0$, then we see from (2.7.12) that v_0 has an $O(1)$ jump while U_0 is continuous at this point. (Note that v_1 , u_1 and higher order terms are, in general, all discontinuous. See the example of §2.7.6). Now let us assume that the width of this region in the streamwise direction, δ , is very much less than the width of the channel, i.e. $\delta \ll 1$, and that the region appears to be a discontinuity in the limit $N \to \infty$. Then the problem is to show that such a layer can exist by finding a solution for u , v in the layer which matches u_0, v_0 in the core (See figure 2.8).

We first stretch the x-co-ordinate according to the rule:

$$\tilde{x} = \delta X.$$

2.7.17.

Then, since v_0 has an O(1) jump in the layer, if the change in the layer is Δu, $\Delta u = O(\delta)$. Accordingly, in the layer put

$$u = 1/h(o) + \delta(u(x, \tilde{y})), \quad \tilde{p} = P/\delta,$$

2.7.18.

where $h(\tilde{x}) = F_t(\tilde{x}) - F_b(\tilde{x})$ is the channel width at station . Also let $h(o) = h_o$. (In the following analysis we assume that

$$\delta \gg O(N^{-1})$$

2.7.19.

in order that we can ignore higher order approximations to the core flow).

In terms of U, v, P, X, $\tilde{y}$, equations (2.7.7) are

$$\left.\begin{aligned}
&(a)\ \frac{1}{h_o}\frac{\partial u}{\partial X} + \delta u\frac{\partial u}{\partial X} + \delta v\frac{\partial u}{\partial \tilde{y}} = -\frac{1}{\delta^2}\frac{\partial P}{\partial X} - \delta N u - N\left(E_o + \frac{1}{h_o}\right) + \frac{1}{R\delta}\frac{\partial^2 u}{\partial X^2},\\
&(b)\ \frac{1}{h_o}\frac{\partial v}{\partial X} + \delta u\frac{\partial v}{\partial X} + \delta v\frac{\partial v}{\partial \tilde{y}} = -\frac{\partial P}{\partial \tilde{y}} + \frac{1}{R\delta}\frac{\partial^2 v}{\partial X^2},\\
&(c)\ \partial u/\partial X + \partial v/\partial \tilde{y} = 0,
\end{aligned}\right\}$$

2.7.20.

where terms of $O(R^{-1})$ have been neglected compared to those of $O(\delta^2 R^{-1})$. All unknown quantities appearing in (2.7.20) and their derivatives, are assumed to be O(1). Equation (2.7.20a) is then

$$\frac{\partial P}{\partial X} = -\delta^3 N u - \delta^2 N\left(E_o + \frac{1}{h_o}\right) + O(\delta^2) + O(\delta R^{-1})$$

2.7.21.

while (2.7.20b) is

$$\frac{1}{h_o}\frac{\partial v}{\partial X} = -\frac{\partial P}{\partial y} + \frac{1}{R\delta}\frac{\partial^2 v}{\partial X^2} + O(\delta)$$

2.7.22.

On eliminating the pressure and the core value of the $\underset{\sim}{j} \times \underset{\sim}{B}$ force, and ignoring the error terms, one obtains the equation

$$\frac{\partial^2 v}{\partial X^3} + h_o\delta^3 N\frac{\partial^2 v}{\partial \tilde{y}^2} - \frac{h_o}{R\delta}\frac{\partial^4 v}{\partial X^4} = 0,$$

2.7.23.

which is also satisfied by U.

Depending on the values of N and R four possible situations may arise, leading to different values of δ :

(a) Electromagnetic-viscous balance: $\delta^4 NR = \delta^4 M^2 = 1$, and $\delta R \ll 1$. Thus $\delta = M^{-\frac{1}{2}}$, and $M \gg R^2$ is the requirement for the existence of such a layer. (This condition satisfies the criterion (4.3) for ignoring higher order terms).

(b) Inertial-viscous balance: $\delta = R^{-1}$ and $\delta^3 N \gg 1$, which holds if $1 \ll R^{\frac{1}{2}} \ll M \ll R^2$. (To satisfy (2.7.19) this condition must be altered to $1 \ll R \ll M \ll R^2$).

(c) Inertial-viscous-electromagnetic balance: $\delta^3 N = k^2 = O(1)$, $\delta = R^{-1}$ which holds if $M = KR^2$. (This also satisfies 2.7.19),

(d) Inertial-electromagnetic balance: $\delta = (h_0/N)^{1/3} \ll 1$, $R\delta \gg 1$, which holds if $1 \ll R^{\frac{1}{2}} \ll M \ll R^2$ (Since $\delta = O(N^{-1/3})$, $\delta \gg O(N^{-1})$ and (2.7.19) is satisfied).

We now concentrate on the type of layer which occurs when M, R and N have typical experimental values, e.g. M = 500, R = 5000, N = 50. Thus we can ignore situations (a) and (c), but we have to consider both the situations (b) and (d) since they may both occur in the same range of M and R. However, there is no solution to (2.7.23) which satisfies the required boundary condition as $X \to \pm\infty$, if the electromagnetic term is neglected and a balance of the inertial and viscous forces is supposed to exist. Therefore we must consider the very much thicker layer which occurs in situation (d) where $\delta = O(N^{-1/3})$. We call this layer the Ludford layer in recognition of the similarities between this work and that of his 1961 paper and assume its structure to be governed by the equation

$$\frac{\partial^3 v}{\partial X^3} + h_0^2 \frac{\partial^2 v}{\partial \tilde{y}} = 0 \qquad 2.7.24.$$

We find that it is possible to construct a solution to this equation satisfying the boundary conditions and therefore we conlude that the errors, due to neglecting the higher order terms in (2.7.23) of $O(N^{-1/3})$, and due to neglecting the viscous terms of $O(M/R^2)^{2/3}$, do not affect the solution to this order of approximation.

It is important to note that, with this length scale, the boundary curvature still tends to infinity with N; in fact it is $O(N^{-1/3})$ in (X, y) space, Thus, the wall still has an abrupt change of slope at X = 0.

Since the problem is linear, we may break it into two parts. The core flow, from (2.7.12), may be written as $v_0 = v_1 + v_2$ where

$v_1 = F_t'(\tilde{y} - F_b)/h^2$, $v_2 = F_b'(F_t - \tilde{y})/h^2$, and separate solutions for the Ludford layer may be found which match with v_1 and v_2 as $X \to \pm\infty$. Thus, without loss of generality, we may assume that it is the bottom wall which curves abruptly and consider only the problem of matching with v_2. Let $k_- = \lim_{x \to 0-} (F_0'(x)/h)$, $k_+ = \lim_{x \to 0+} (F_0'(x)/h)$, and put $F_t(0) - \tilde{y} = h(0)(1-Y) = h_0(1-Y)$.

The lower wall is then given by Y = 0 in the layer. The boundary conditions on v(X,Y) in the layer are then

$$v(X,1) = 0, \qquad 2.7.25.$$

$$\left.\begin{aligned} v(X,0) &= k_-, \quad X < 0 \\ &= k_+, \quad X > 0 \end{aligned}\right\} \qquad 2.7.26.$$

$$v \to k_-(1-Y) \text{ as } X \to -\infty, \qquad 2.7.27.$$

$$v \to k_+(1-Y) \text{ as } X \to +\infty, \qquad 2.7.28.$$

in order to match with v_2.

Structure of the layer.

The problem for v may be further divided by writing

$$v = k_-(1-Y) + (k_+ - k_-)v^*, \qquad 2.7.29.$$

where

$$\left.\begin{aligned} v^*(X,1) &= 0 \\ v^*(X,0) &= 0, \quad X < 0 \\ &= 1, \quad X > 0 \\ v^* &\to 1-Y \text{ as } X \to +\infty \\ &\to 0 \text{ as } X \to -\infty \end{aligned}\right\} \qquad 2.7.30.$$

and

$$\frac{\partial^3 v^*}{\partial X^3} + \frac{\partial^2 v^*}{\partial Y^2} = 0 \qquad 2.7.31.$$

The solution to (2.7.31) may be found by separating the variables and using a Fourier series solution first making the further simplication:

$$v^* = 1 - Y + v_1^* \quad \text{for } X \geq 0,$$

$$= v_2^* \quad \text{for } X < 0.$$

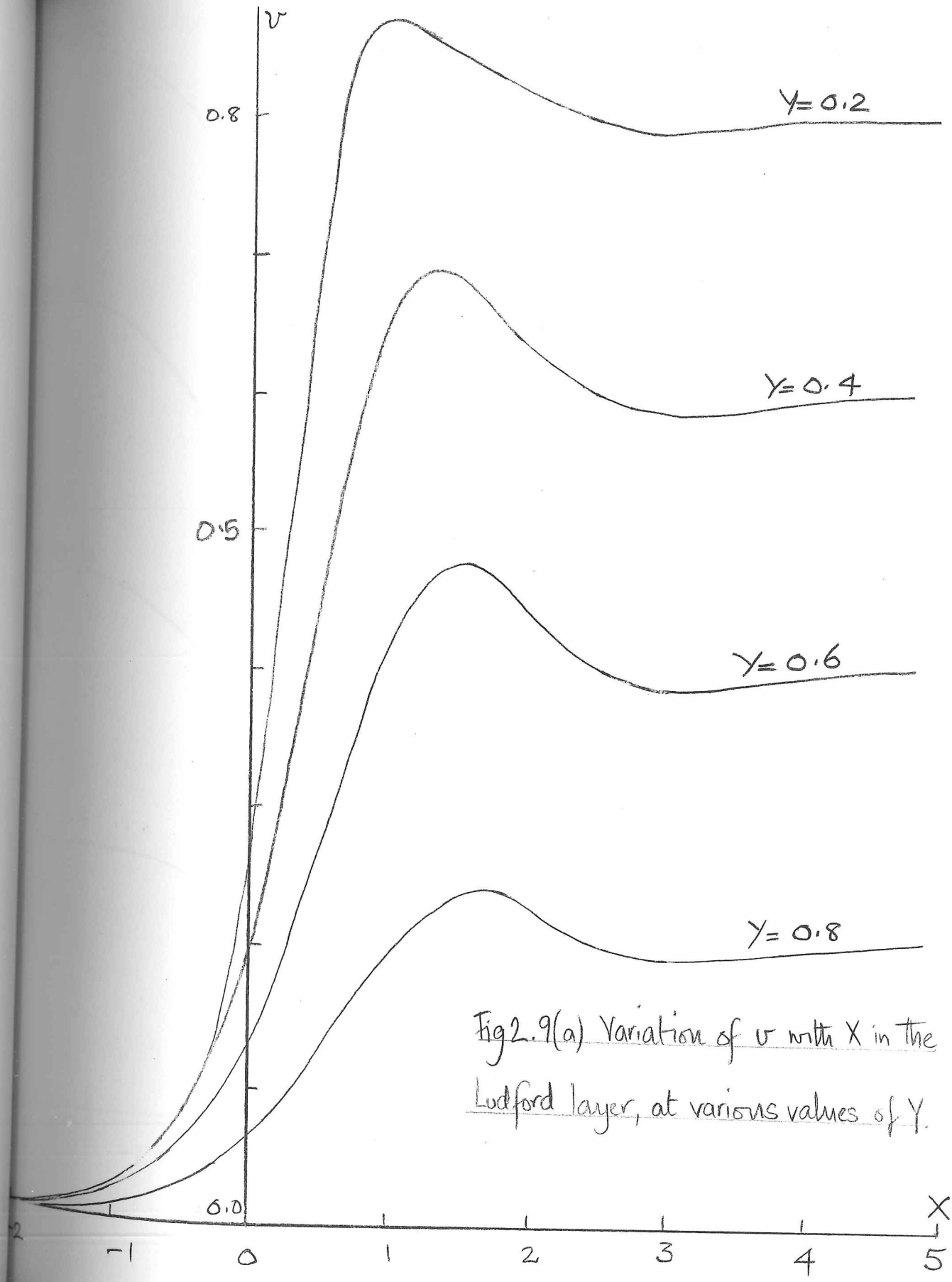

Fig 2.9(a) Variation of v with X in the Ludford layer, at various values of Y.

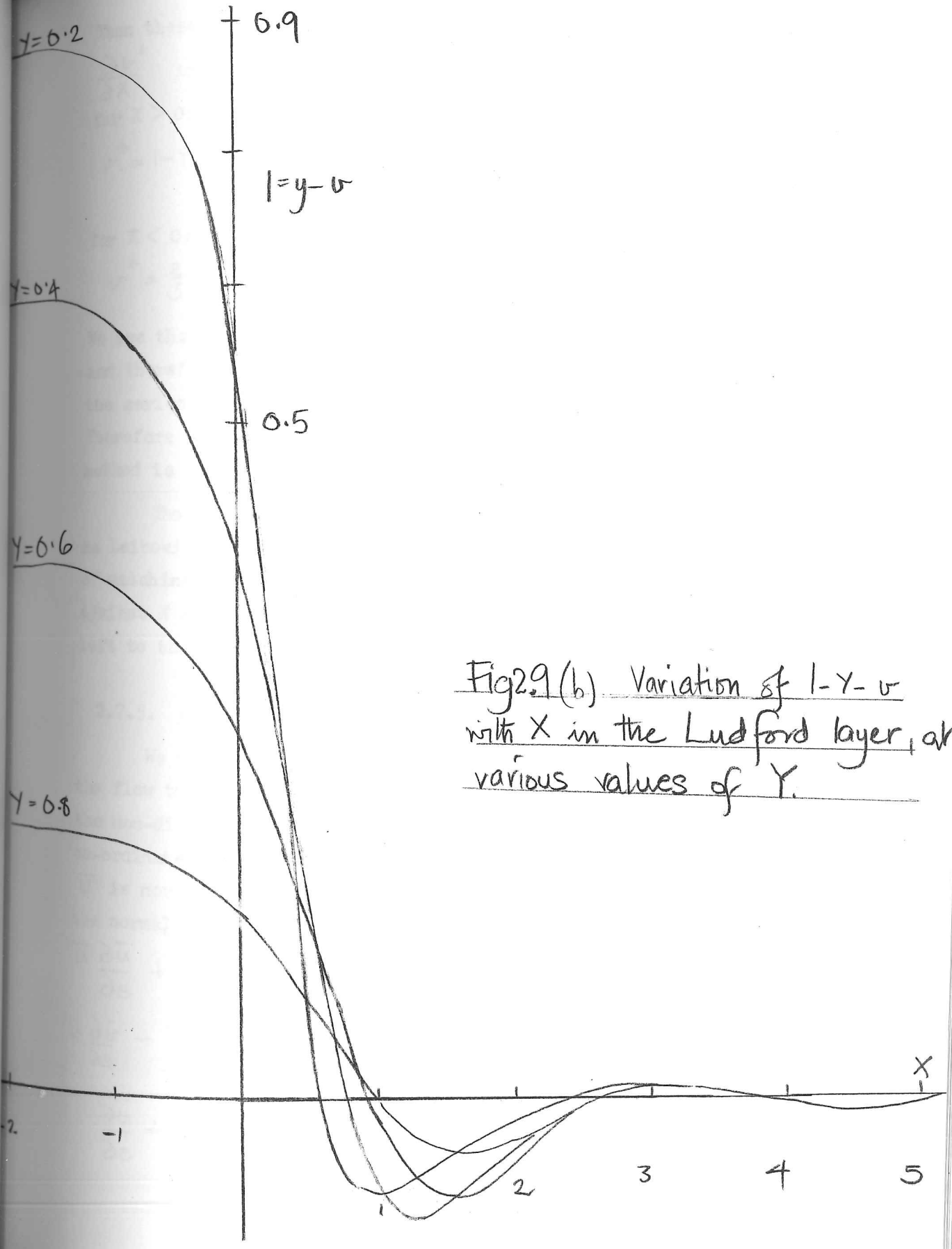

Fig 2.9 (b) Variation of 1-Y-v with X in the Ludford layer, at various values of Y.

Then these two solutions for v_1^* and v_2^* are found by matching v^*, $\frac{\partial v^*}{\partial X}$ and $\frac{\partial^2 v^*}{\partial X^2}$ at $X = 0$. The solution is:

for $X > 0$:

$$v^* = 1 - Y - \frac{4}{3}\sum_{n=1}^{\infty} \frac{(-1)^{n+1}}{n\pi} \cos\left(\frac{(n\pi)^{1/3}\sqrt{3}}{2} X\right) e^{-\frac{(n\pi)^{2/3}}{2}X} \sin\left(n\pi(1-Y)\right) \qquad 2.7.32a.$$

for $X < 0$:

$$v^* = \frac{2}{3}\sum_{n=1}^{\infty} \frac{(-1)^{n+1}}{n\pi} e^{(n\pi)^{2/3}X} \sin\left(n\pi(1-Y)\right) \qquad 2.7.32b.$$

We see that these series for $\frac{\partial v^*}{\partial X}$ and $\partial^2 v^*/\partial X^2$ are <u>divergent</u> at $X = 0$, and therefore our method involves matching divergent series. However, the series are <u>convergent</u> for $|X| = \epsilon$ for ϵ as small as we like. Therefore if we equate $\partial^2 v^*/\partial X^2$ at $X = -\epsilon$ to $\partial^2 v^*/\partial X^2$ at $X = +\epsilon$, our method is legitimate.

These series for v^* may also be derived using a Fourier Integral, as Leibovich has shown, (Hunt & Leibovich (1967)) and then the difficulty of matching diverging series is avoided. Graphs of v^* and $1 - Y - v^*$ against X are plotted in figure 2.9; the discussion of the graphs is left to the conclusion of §2.7.

2.7.5. <u>Hartmann boundary layers</u>.

We turn now to the boundary layers, B, and show how to calculate the flow there to the same order of accuracy as in the core. Consider the non-dimensional equations (2.7.7) written in terms of the s, n, z co-ordinate shown in figure 2.10 so that $\bar{u}$ is parallel to the wall and $\bar{v}$ is normal to the wall, and the magnetic field is at an angle α to the normal of the wall. We have;

$$\bar{u}\frac{\partial \bar{u}}{\partial s} + \bar{v}\frac{\partial \bar{u}}{\partial n} = -\frac{\partial \tilde{p}}{\partial s} - N\cos\alpha\left(E_0 + \bar{u}\cos\alpha - \bar{v}\sin\alpha\right) + \frac{1}{R}\nabla^2\bar{u}, \qquad 2.7.33.$$

$$\bar{u}\frac{\partial \bar{v}}{\partial s} + \bar{v}\frac{d\bar{v}}{\partial n} = -\frac{\partial \hat{p}}{\partial s} - N\sin\alpha\left(E_0 + \cos\alpha - \bar{v}\sin\alpha\right) + \frac{1}{R}\nabla^2\bar{v}, \qquad 2.7.34.$$

$$\frac{\partial \bar{u}}{\partial s} + \frac{\partial \bar{v}}{\partial n} = 0 \qquad 2.7.35.$$

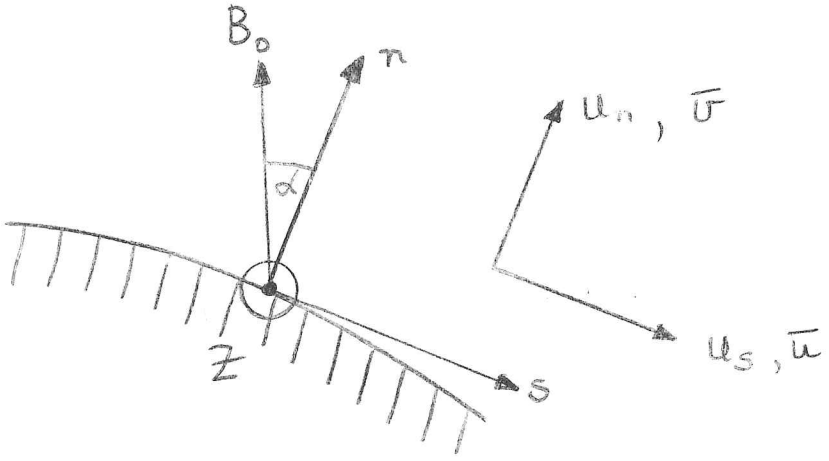

Fig 2.10 Notation for the boundary layer analysis in §2.7.5

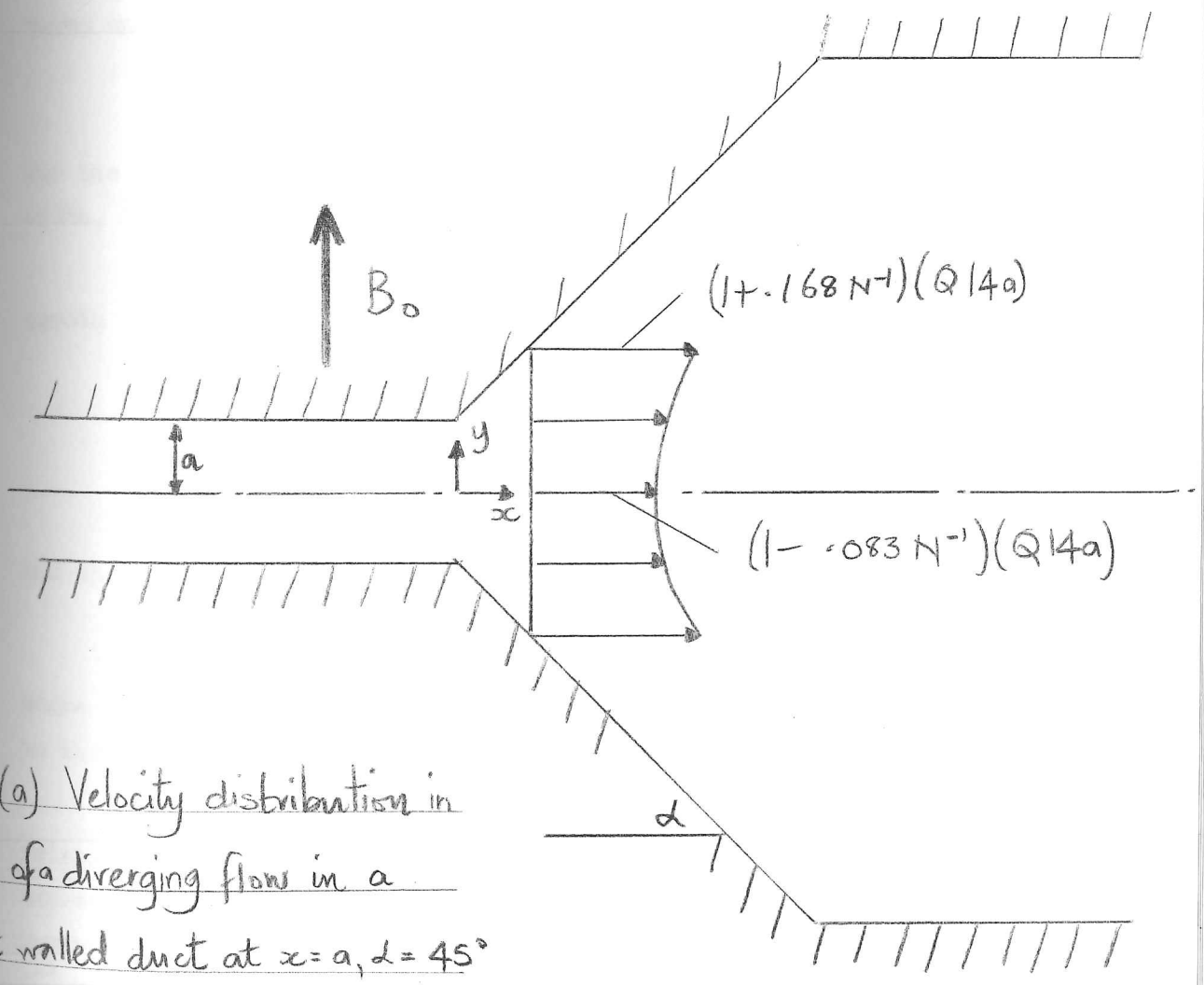

2.11(a) Velocity distribution in core of a diverging flow in a straight walled duct at $x=a$, $\alpha=45°$

These equations may be simplified by ignoring terms of order, δ_1, where $\delta_1 (\ll 1)$, is the non-dimensional boundary layer thickness. Then if we write $\zeta = n/\delta$, and $\bar{V} = \bar{v}/\delta_1$, the above equations become:

$$\bar{u}\frac{\partial \bar{u}}{\partial \zeta} + \bar{V}\frac{\partial \bar{u}}{\partial \zeta} = -\frac{\partial \tilde{p}}{\partial s} - N\cos\alpha\left(E_0 + \bar{u}\cos\alpha\right) + \frac{1}{\delta_1^2 R}\frac{\partial^2 \bar{u}}{\partial \zeta^2} + o(\delta_1, N),$$

$$0 = -\frac{\partial \tilde{p}}{\partial \zeta} + o(\delta_1, N) + o(R^{-1}), \qquad 2.7.36.$$

$$\frac{\partial \bar{u}}{\partial s} + \frac{\partial \bar{V}}{\partial \zeta} = 0$$

As with the 'Ludford' layer, the structure of this boundary layer also depends on the relative sizes of M and R. In this case if $N(=M^2/R) \gg 1$ there is only one possible type of boundary layer i.e. one in which the electromagnetic and viscous terms are very much greater than the inertial terms and balance each other. Hence it follows from (2.7.36) that

$$N = o(\delta_1^2 R)^{-1}$$

$$\text{or } \delta_1 = o(NR)^{-\frac{1}{3}} = o(M^{-1}) \qquad 2.7.37.$$

For the boundary layer thickness to be small compared with the duct width, δ_1 must be small, or $M \gg 1$.

With this approximation and, using (2.7.37) we can obtain the zeroth order solution for $\bar{u}$, $\bar{u}_0$, which satisfies

$$0 = -\frac{1}{N}\frac{\partial \tilde{p}}{\partial s} - \cos\alpha\left(E_0 + \bar{u}_0\cos\alpha\right) + \frac{\partial^2 \bar{u}_0}{\partial \zeta^2} \qquad 2.7.38.$$

$$= -\frac{1}{N}\frac{\partial \tilde{p}}{\partial \zeta}$$

and the no slip condition at the wall. The solution is

$$\bar{u}_0 = \bar{u}_{0\infty}\left(1 - e^{-\zeta\cos\alpha}\right), \qquad 2.7.39.$$

where $\bar{u}_{0\infty}$ is the component of the zeroth order core velocity parallel to the wall (Stewartson 1960).

The higher order approximations to $\bar{u}$, $\bar{v}$ and $\tilde{p}$ depend on the relative magnitude of M and N, $(=M^2/R)$, since $\bar{u}$, $\bar{v}$ and $\tilde{p}$ may be expressed as asymptotic expansions in M^{-1}, N^{-1}, or in a combination of powers of M^{-1} and N^{-1}. Let us consider the two limiting cases when $N^{-1} \gg M^{-1}$ and $M^{-1} \gg N^{-1}$ and the expansion may be written:

$$\bar{u} = \bar{u}_0 + \left(N^{-1}\bar{u}_{1n} + N^{-2}\bar{u}_{2n} + \dots\right) + \left[M^{-1}\bar{u}_{1m} + M^{-2}\bar{u}_{2m} + \dots\right],$$

$$\bar{v} = \bar{v}_0 + \left(N^{-1}\bar{v}_{1n} + N^{-2}\bar{v}_{2n} + \dots\right) + \left[M^{-1}\bar{v}_{1m} + M^{-2}\bar{v}_{2m} + \dots\right],$$

$$\bar{p} = N\left\{p_0 + \left(N^{-1}p_{1n} + N^{-2}p_{2n} + \dots\right) + \left[M^{-1}p_{1n} + \dots\right]\right\},$$

where the expansion in either the square or round brackets vanish in the two cases. Then, in the first case, i.e. $N^{-1} \gg M^{-1}$, the expansion can only proceeed until $N^{-r} \sim M^{-1}$ for some r, at which point it must either be terminated or a new mixed expansion of the form $N^{-r} M^{-s}$ must be considered. We may note that in this case M and R have the same relative magnitudes as in our analysis of the Ludford layer, i.e.

$$R^{\frac{1}{2}} \ll M \ll R^2,$$

which is a condition satisfied in many experiments. Also in the first case it is important to realise that the higher order approximations may be matched to those in the core.

In the second case, i.e. $M^{-1} \gg N^{-1}$, $M \gg R$, the expansion is carried out in terms of M^{-1}, or equivalently δ_1 which means that at the wall the core velocity is not regarded as parallel to it. Therefore the core velocity also has to be expressed as a series in δ_1 and has to be matched to the boundary layer solution in such a way that the core velocity ceases to be independent of the boundary layer flow. We ignore this expansion since it is of no practical use and concentrate on the first case.

We first find $\bar{u}_{1n}$, using the zeroth order solution (2.7.39); $\bar{u}_{1n}$ satisfies

$$\bar{u}_0 \frac{\partial \bar{u}_0}{\partial s} + \frac{\partial \bar{u}_0}{\partial \zeta}\left(-\int_0^{\zeta} \frac{\partial \bar{u}_0}{\partial s}\, d\zeta\right) = -\frac{\partial p_{1n}}{\partial s} - \bar{u}_{1n}\cos^2\alpha + \frac{\partial^2 \bar{u}_{1n}}{\partial \zeta^2}, \qquad 2.7.40.$$

$$0 = -\partial p_{1n}/\partial \zeta .$$

Hence

$$\frac{\partial^2 \bar{u}_{1n}}{\partial \zeta^2} - \bar{u}_{1n}\cos^2\alpha = \bar{u}_{0\infty}\frac{d(\bar{u}_{0\infty})}{ds}\left[(1-e^{-\zeta\cos\alpha})^2 - \cos\alpha\, e^{-\zeta\cos\alpha}\left(\zeta - \frac{1-e^{-\zeta\cos\alpha}}{\cos\alpha}\right)\right] + \frac{\partial p_{1n}}{\partial s}, \qquad 2.7.41.$$

Outside the layer $\bar{u}_{in} = \bar{u}_{1\infty}$ and

$$\frac{\partial p_{in}}{\partial s} = -\bar{u}_{1\infty}\cos^2\alpha - \bar{u}_{\infty}\frac{d\bar{u}_{0\infty}}{ds}$$

Hence we can rewrite (2.7.41) as

$$\frac{\partial^2 \bar{u}_{in}}{\partial \rho^2} - \bar{u}_{in}\cos^2\alpha = \frac{d(\bar{u}_{0\infty}^2/2)}{ds}\left[-(1+\rho\cos\alpha)e^{-\rho\cos\alpha}\right] - \bar{u}_{1\infty}\cos\alpha$$

The solution for $\bar{u}_{in}$, is

$$\bar{u}_{in} = \bar{u}_{1\infty}\left(1-e^{-\rho\cos\alpha}\right) + \left(d(\bar{u}_{0\infty}^2)/ds\right)\left[\frac{(3\rho+\rho^2\cos^3\alpha)\,e^{-\rho\cos\alpha}}{8\cos\alpha}\right] \quad 2.7.42.$$

To find $\bar{u}_{1\infty}$ and $\bar{u}_{0\infty}$ we use the results of §2.7.3. noting that

$$\bar{u}_{0\infty} = u_0\cos\alpha + v_0\sin\alpha,$$

and $$\bar{u}_{1\infty} = u_1\cos\alpha + v_1\sin\alpha,$$

where $\tan\alpha = F_b'$ and u_0, v_0, u_1, v_1, are as defined in §2.7.3.

In principle, higher order terms in the expression for $\bar{u}$ may be found, since only linear equations need be solved. The algebra is complicated, however.

2.7.6. Example: flow through a straight-walled converging and diverging ducts.

We now consider the flow through a simple duct as an example.

Let it have walls at:

$$\tilde{y} = \pm 1 \quad \text{for } \tilde{x} \lesseqgtr 0 \text{ and } \tilde{y} = \pm(1+\tilde{x}\tan\alpha) \text{ for } \tilde{x} \gtreqless 0,$$

where the upper inequality is appropriate for the diverging duct and the lower for the converging.

Then the zeroth order solution outside the Ludford layers is

$\tilde{x} \leq 0$ core; $u_0 = 1$, $v_0 = 0$,

$$\partial p_0/\partial\tilde{x} = -N(1+E_0), \quad 2.7.43.$$

boundary layer; $u_0 = 1-e^{-\rho}$. 2.7.44.

$\tilde{x} \geq 0$ core: $u_0 = \dfrac{1}{2(1+\tilde{x}\tan\alpha)}$, $v_0 = \dfrac{\tilde{y}\tan\alpha}{2(1+\tilde{x}\tan\alpha)^2}$,

$$\partial p_0/\partial\tilde{x} = -N\left[\frac{1}{2(1+\tilde{x}\tan\alpha)} + E_0\right], \quad 2.7.45.$$

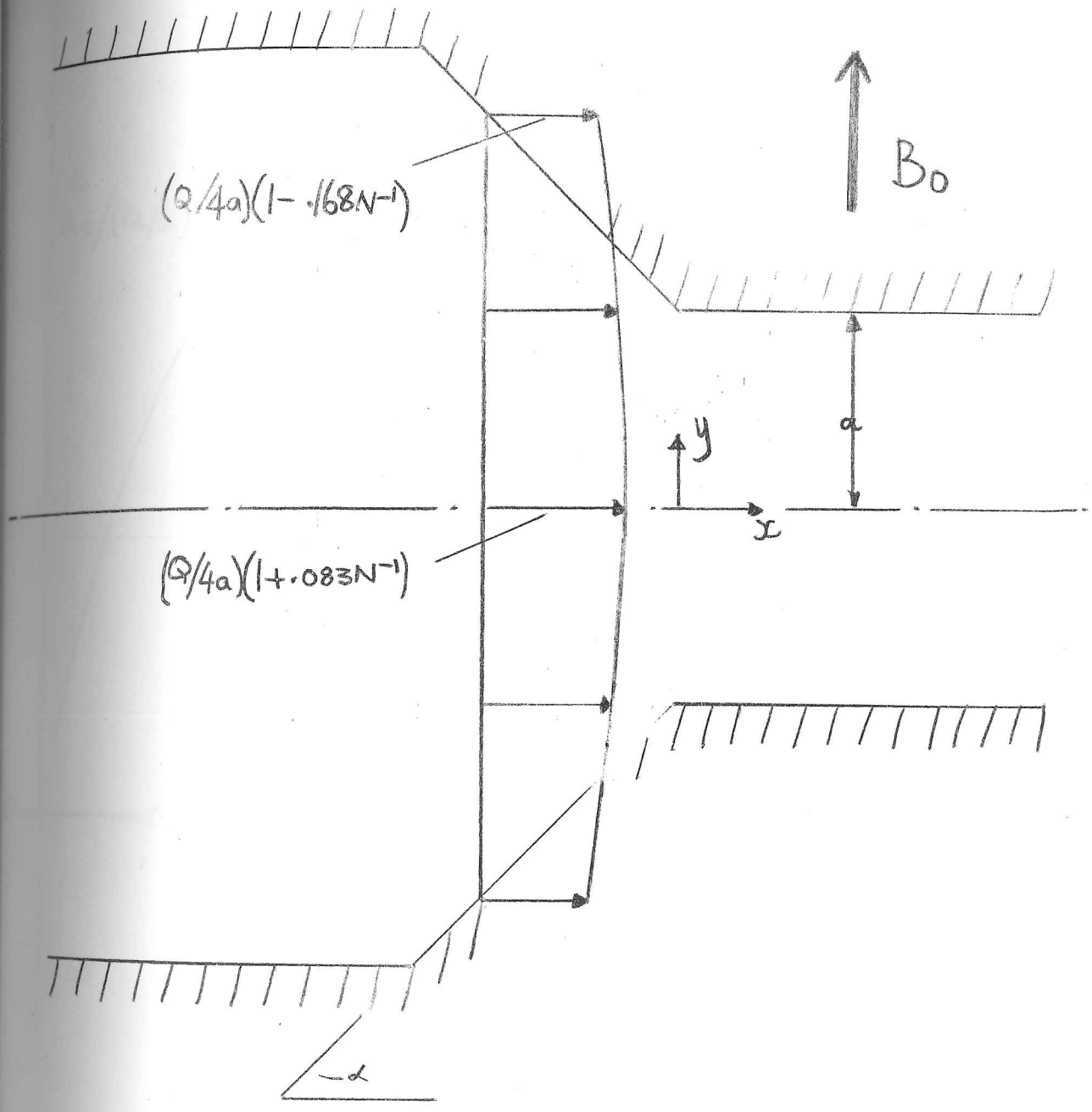

Fig 2.11.(b) Velocity distribution in the core of a converging flow in a straight walled duct at $x = -a$, $\alpha = -45°$

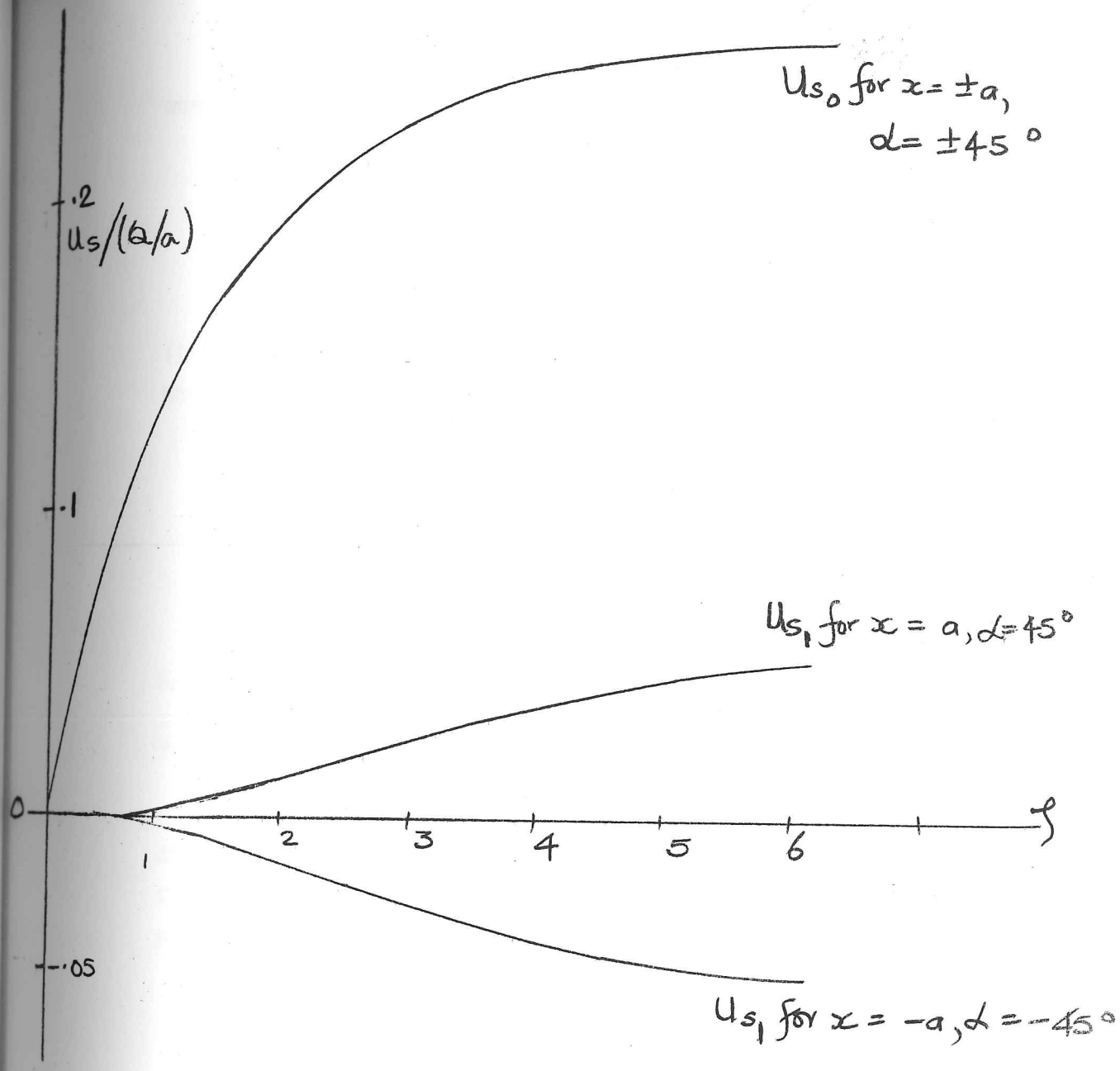

Fig. 2. Velocity profiles of U_{s_0} and U_{s_1} in the boundary layer where $x = \pm a$, $\alpha = \pm 45°$. (Note that $U_s = U_{s_0} + N^{-1} U_{s_1}$ and $\zeta = M^{-1} n$, where n is the co-ordinate normal to the wall.)

boundary layer: $\bar{u}_0 = (1-e^{-\zeta})/(2\cos\alpha(1+\tilde{x}\tan\alpha))$ 2.7.46.

where $\zeta = M(1-\tilde{y})$ for $\tilde{y} > 0$, $\tilde{x} \gtrless 0$

$= M(1-\tilde{y})$ for $\tilde{y} < 0$, $\tilde{x} \gtrless 0$

$= (1+\tilde{x}\tan\alpha-\tilde{y})M\cos\alpha$ for $\tilde{y} > 0$, $\tilde{x} \gtrless 0$

$= (1+\tilde{x}\tan\alpha+\tilde{y})M\cos\alpha$ for $\tilde{y} < 0$, $\tilde{x} \gtrless 0$

When $\tilde{x} \gtrless 0$ the first order solution is:

$$u_1 = v_1 = \partial p_1/\partial x^2 = 0$$

(All higher orders are also zero).

When $x \gtrless 0$ the first order solution is:

core: $$u_1 = \frac{\tan^3\alpha}{2(1+\tilde{x}\tan\alpha)^3}\left(\tilde{y}^2-\frac{(1+\tilde{x}\tan\alpha)^2}{3}\right), \quad v_1 = \frac{\tilde{y}\tan^4\alpha\, x}{2(1+\tilde{x}\tan\alpha)} \times \left(\frac{5\tilde{y}^2}{3}-(1+x^2\tan\alpha)^2\right)$$

$$\partial p_1/\partial x^2 = -\left\{u_0\frac{du_0}{d\tilde{x}} + u_1\right\}, \quad = \frac{\tan\alpha}{(1+\tilde{x}\tan\alpha)^3}\left[\frac{1}{4}+\frac{\tan^2\alpha}{6}-\frac{\tilde{y}^2\tan^2\alpha}{2(1+\tilde{x}\tan\alpha)^2}\right], \qquad 2.7.47.$$

boundary layer:

$$\bar{u}_1 = \frac{\tan^3\alpha}{3\cos\alpha(1+\tilde{x}\tan\alpha)^3}\left\{1-\left(1+\frac{9\cos\alpha}{16\sin^2\alpha}\zeta+\frac{5\cos^3\alpha}{16\sin^2\alpha}\zeta^2\right)e^{-\zeta}\right\} \qquad 2.7.48.$$

In figure 2.11 we show velocity profiles in the core for flow in diverging and converging ducts, i.e. positive and negative α, and in figure 2.12 we show velocity profiles for the components of velocity parallel to the wall, $\bar{u}$, in the boundary layers.

2.7.7. Discussion.

a) Core and boundary layers.

The example presented in §2.7.6 reveals some of the effects of considering higher order terms in the core and boundary layer flows. Although the zeroth order approximations for the core flow are identical in converging and diverging ducts (except for direction, of course), the first order approximations differ, and in a surprising way, in that, for a given value of x, the core velocity in a straight walled diverging duct, such as that considered in §2.7.6 is greater near the walls and least in the centre, whereas for flow in a converging duct the reverse is true.

There seems to be no obvious physical explanation for this effect, which only occurs in certain types of duct since, if the duct width is proportional to $1/(1-\tilde{x})$ for $1 \geq \tilde{x} \geq 0$, the velocity is greatest in the centre for a diverging duct and least in a converging duct. Thus we conclude that the first and, presumably, higher approximations to the velocity profiles are very sensitive to the rate of change of the duct width with distance along it.

It is of interest to compare the values of u_0 and u_1 in our example of §2.7.6 in order to calculate the value of N which enables the required condition, $N^{-1} u_1 \ll u_0$ to be satisfied. For example, when $\alpha = 45^\circ$, $\tilde{x} = 1$ and $\tilde{y} = 0$, $\frac{u_1}{u_0} = 1/12$, so that, even if N is as low as 5, the conditions for the analysis of the core would be well satisfied. On the other hand, for the analysis of the Ludford layers we must satisfy the condition that $N^{1/3} \gg 1$ so that in an experiment where $N \simeq 10$, say, the experimental core flow would be adequately described by our theory but not the experimental Ludford layers.

Figure 2.12 indicates how inertial effects become apparent in the Hartmann boundary layers when the first order approximation is considered, so that, when the core flow is decelerating as in a diverging duct, there is a slight tendency for back flow to develop near the wall, whereas when the core flow is accelerating, the flow near the wall is faster. It is interesting that the tendency for back flow to develop in a diverging duct is very much greater when $\bar{u}_{1\infty} < 0$, as in a duct whose width is proportional to $1/(1-\tilde{x})$, than when $\bar{u}_{1\infty} > 0$, as in the example of §2.7.6 which indicates that the first order approximation of the core flow has an important effect on the boundary layer flow.

b) Ludford layers and the relation between Ludford's solution and the duct flow problems.

We have considered the structure of the Ludford layer when the core flow is continuous in U_0 and when the predominant forces are pressure, inertial and electro-magnetic, the criteria to be satisfied by M and R for our analysis being

$$R^2 \gg M \gg R^{\frac{1}{2}} \qquad 2.7.49.$$

In this case the thickness of the layer, δ, being $O(N^{-1/3})$. The key to a physical understanding of the layer lies in the role of the pressure gradients; the pressure gradient in the y-direction, $\partial\tilde{p}/\partial\tilde{y}$, is $O(N^{-1})$ in the core while in the Ludford layer it is $O(N^{1/3})$, because it is the pressure gradient which accelerates the fluid in the y-direction, not, of course, the electromagnetic force. Since the pressure varies in the y-direction, there must be a component of dp/dx of $O(N^{2/3})$ which also varies in the y-direction, i.e. different from the core value of dp/dx = O(N), and this secondary component of dp/dx is balanced by the $\tilde{j}\times\tilde{B}$ force produced by a perturbation velocity U of $O(N^{-1/3})$. The practical significance of the pressure gradient is that, since pressures are measured more easily than velocities, probably the best way to confirm the existence of Ludford layers is to check whether the pressure difference across an asymmetric channel at a point where the wall slope changes suddenly is $O(N^{1/3})$.

Note that the graphs of v^* and $(1-Y-v^*)$ shown in figure 2.6. can be interpreted directly since v^*, $(=v/k_+)$ is proportional to v when $k_-=0$, that is, for a straight duct joining a diverging duct; and $(1-Y-v^*)$ $(=v/k_-)$ is proportional to v when $k_+=0$, that is, for a converging duct joining a straight duct. From v^* and $(1-Y-v^*)$ we can calculate v for the general case in which k_+ and k_- are both non-zero. Also note that the damped wave, for which there is no obvious explanation, always occurs downstream of any change in the duct wall.

c) Limitations of the analysis.

Our analysis has been for two-dimensional flows, but since experiments have to be performed in finite sized ducts the effects of the side walls parallel to the fields must be considered. Also it is only by considering the side walls that we can determine E_z. These walls may be non-conducting, or, if conducting, they may be split up into segments. They may also diverge in the z-direction. In these cases E_z may vary in the x direction and E_x is likely to be non-zero, in which case secondary flows may result, and our analysis will not hold except perhaps in the centre of the duct away from the side walls. However, our analysis is expected to be most applicable in a duct with

continuous conducting walls parallel to B_o since then E_z will be uniform in the core and $E_x = 0$. E_z will then be determined by considering the external electrical circuit and the total current leaving the duct. Even in this case the analysis will fail where the conducting-electrode walls end at the edge of the power extraction or injection region.

A preliminary analysis of the effect on <u>compressible</u> duct flows of very strong magnetic fields was given at the conference on MHD Power Generation at Salzburg. (Hunt, 1966b).

3. Some electrically driven flows in magnetohydrodynamics.

3.1. Introduction and summary

A common feature of many magnetohydrodynamic flows where the magnetic field strength is very high is the existence of narrow regions extending in the direction of the magnetic field across which discontinuities in velocity, electric potential or current density occur. The universality of such regions was first hinted at by Braginskii (1960) in examining the MHD equations, since when many specific flows have been analysed in which such regions have been found to occur e.g. the various 'wakes' which occur in the flow over bodies placed in transverse and parallel magnetic fields, (Hasimoto, 1960, Ludford, 1961, and Childress, 1963). Although Braginskii himself outlined the possibility of such regions being caused by sudden changes in the electrical boundary conditions, he did not analyse any particular physical situation so as to conclusively demonstrate the existence of such a layer. However, various analyses have recently been made of such situations and since they are not widely known it is pertinent to briefly describe them.

Yakubenko (1963) examined the pressure-driven, laminar, incompressible flow of a uniformly conducting fluid in a rectangular duct whose walls perpendicular to the magnetic field, BB, are very much longer than the walls parallel to the magnetic field AA, and whose walls BB are perfectly conducting for $x<0$ and non-conducting for $x>0$. Then, when the Hartmann number $M \gg 1$, the velocity expressed in terms of the pressure gradient is $O(M^{-2})$ when $x<0$ and $O(M^{-1})$ when $x>0$, so that some shear layer must exist near $x=0$. Although Yakubenko obtained an exact solution to this problem by means of the Wiener-Hopf technique he did not interpret the result physically nor did he produce any numerical data.

Waechte (1966) has recently analysed the flow in the same long duct in which there is no pressure gradient, the walls AA are non-conducting, the wall B at $y=a$, for $x<0$ is perfectly conducting and held at a potential ϕ_0, the wall B at $y=-a$ for $x<0$ is also perfectly conducting but held at a potential $-\phi_0$, and both the walls BB are non-conducting for $x>0$. In this case there is no flow in the core when $x<0$ and therefore no discontinuity in the velocity. However, there is a

discontinuity at $x = 0$ in $\partial\phi/\partial y$, which necessitates the existence of a layer at $x = 0$ in which the velocity is non-zero. Such a layer was first discussed by Moffatt (1964) who examined the case where the wall at $y = a$ is perfectly conducting and held at a potential ϕ_0 for $x > 0$ and for $x < 0$ is also perfectly conducting but held at zero potential. There has to be an infinitely small insulating segment of wall at $x = 0$. The wall at $y = -a$ is perfectly conducting, and held at zero potential; Again in this case there is a layer at $x = 0$, through which $\partial\phi/\partial y$ is discontinuous and in which the velocity is non-zero. Moffatt discussed in detail the physics of such a layer, though which there is a discontinuity in the electric field parallel to it, so that we now have a clear physical picture of what to expect when such a discontinuity occurs.

However, there were some anomalies in his mathematical solution which Waechte (1966) has now clarified.

Alty (1966) examined an altogether more difficult problem; he undertook a theoretical and experimental investigation of the pressure driven flow in a square duct, two of whose walls are highly conducting and two non-conducting, when a uniform magnetic field is imposed at an arbitrary angle to the walls. By only considering the flow when $M \gg 1$, by dividing the flow up into various regions, which he investigated in turn, and by using some of the results of Moffatt's (1964) analysis he was able to provide an approximate asymptotic analysis in which he discovered the existence of thin layers emanating from the corners of the duct in the direction of the magnetic field. In these layers the velocity and electric field changed discontinuously, in a similar way to the layers of Yakubenko and Moffatt. The existence of these layers was confirmed by the experiments, though indirectly from pressure and electric potential measurements at the walls, no probes being inserted into the flow.

The main interest in these studies has been on the curious layers which emanate in the direction of the magnetic field from the places where the conductivity changes. In each case different layers are found; yet, despite their similarities, a complete analysis and description of these layers in pressure or electrically driven flows is still awaited.

The mathematical difficulty is similar to that of analysing MHD duct flows in that two coupled linear partial differential equations of second order must be solved (equations (2.4) and (2.5) of H & S). These equations may be decoupled by increasing their order as shown by Braginskii (1960), though in that case the boundary conditions for the various parameters, e.g. velocity and potential, then become coupled, this being the method of Moffatt and Waechte. This method is only suitable for the simplest boundary conditions and types of boundary.

The other approach to solving the coupled equations is to add and subtract them, as originally performed by Shercliff (1953), and as we did in H & S. Then, provided the current distribution along the boundary is specified, we can obtain a solution, the problem becoming the transformation of the current boundary condition to that required, e.g. the specification of the potential, or matching to a finitely conducting electrode, which in general requires the solution of an integral equation, one such being that solved in §2 of H & S. The great advantage of this method, particularly when $M \gg 1$, is that one is dealing with an elliptic second order equation whose asymptotic properties are fairly well understood. In this chapter we adopt the latter approach (suggested to me by Professor Shercliff) to examine the flow produced by various electrode configurations.

In §3.2 we examine the simplest situation in which two line electrodes are placed opposite and parallel to each other in parallel non-conducting planes; an electric current travels between the electrodes and a magnetic field is applied perpendicular to the planes. Assuming that the flow is laminar, uniform and incompressible we find an exact solution for arbitrary values of M and an asymptotic solution when $M \gg 1$. We show these are identical when $M \gg 1$, and how the results may be interpreted in physical terms. We then analyse the flow when the electrodes are displaced relative to each other, the magnetic field remaining in the same direction; this flow is similar to that discussed by Alty (1966).

In §3.3 we analyse the flows due to circular electrodes. We first analyse the flow due to point electrodes placed in non-conducting planes opposite each other, before analysing the flow due to finite circular

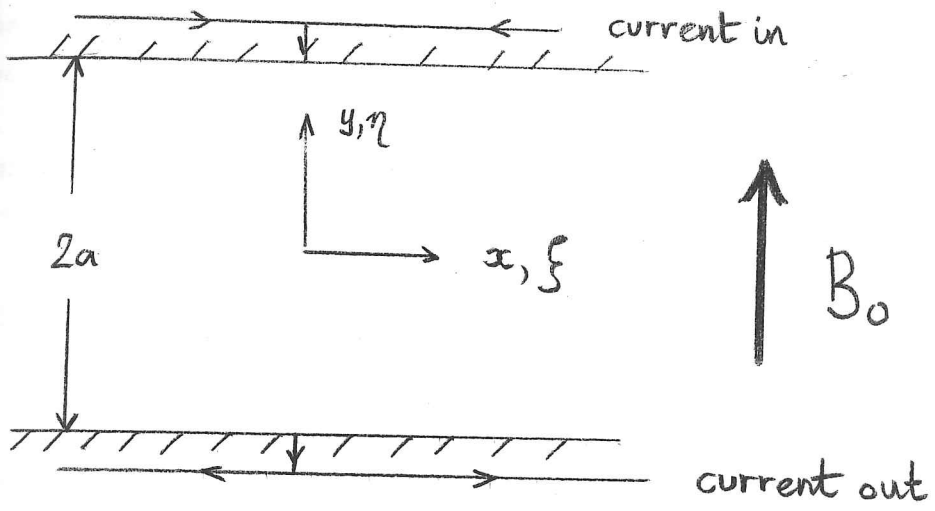

Fig 3.1 Alined line electrodes

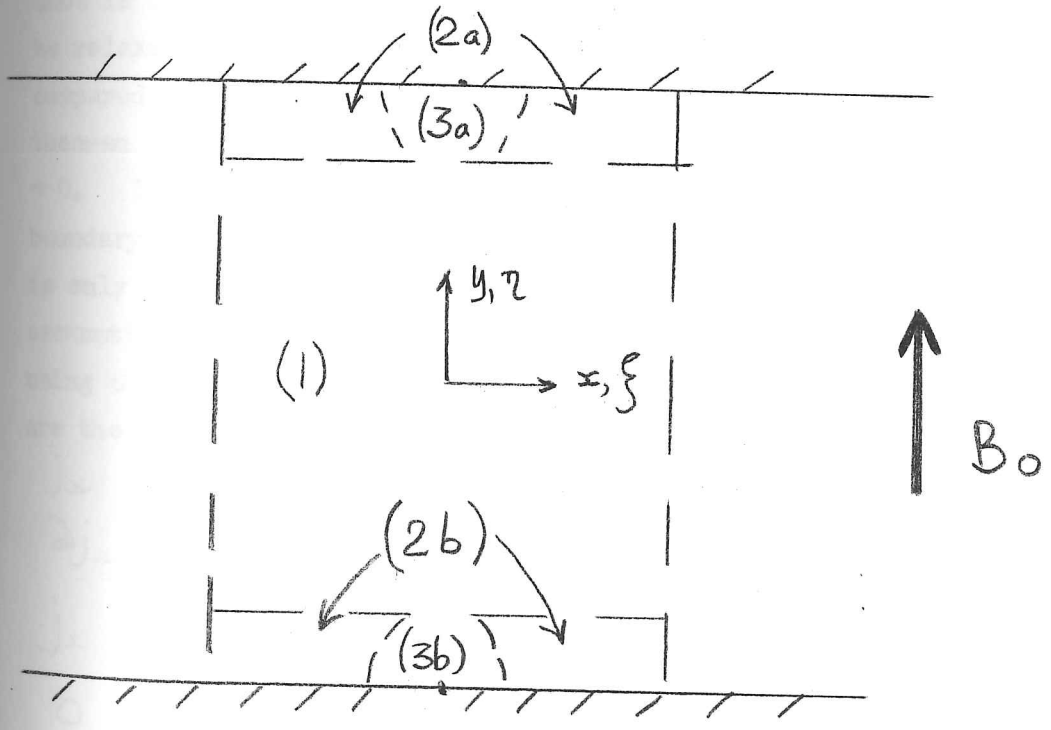

Fig 3.2. Asymptotic regions between the electrodes when $M \gg 1$

electrodes. We consider two cases where the current distribution at the electrodes is constant and where the potential of the electrodes is constant, our analysis in the latter case not being complete. Many of the salient physical phenomena found from this analysis were shown to exist in the experiments described in chapter 7.

3.2. Two-dimensional electrode configurations.

3.2.1. The Equations.

We consider the steady flow of an incompressible fluid with uniform properties driven by the interaction of imposed electric currents and a uniform, transverse magnetic field. In this section we consider two-dimensional situations, in which all the physical variables, including pressure, and the boundary conditions are functions of x and y only. Therefore any external circuit connected to the conducting walls of the duct is continuous and unvarying in the z direction. (This condition may be relaxed if the magnetic field due to the applied currents is small compared to the imposed magnetic field.) We can apply the uniqueness theorem of §2.3 to this situation, the only difference being that $dp/dz = 0$. Therefore, if we can construct a solution consistent with the boundary conditions, it is the correct one. We will assume that there is only one component of velocity (in the z-direction) and since this assumption provides a solution we are justified in making it. Then, using the axes defined in figure 3.1, the equations describing such flows are the same as those of MHD duct flow but with $dp/dz = 0$.

$$j_x = \sigma(-\partial\phi/\partial x - v_z B_0), \quad j_y = \sigma(-\partial\phi/\partial y), \tag{3.2.1.}$$

$$\partial j_x/\partial x + \partial j_y/\partial y = 0, \tag{3.2.2.}$$

$$j_x = \partial H_z/\partial y, \quad j_y = -\partial H_z/\partial x, \tag{3.2.3.}$$

$$0 = -\frac{\partial}{\partial x}\left(p + \mu H_z^2/2\right), \tag{3.2.4.}$$

$$0 = -\frac{\partial}{\partial y}\left(p + \mu H_z^2/2\right), \tag{3.2.5.}$$

$$0 = j_x B_0 + \tilde{\eta}\left(\frac{\partial^2 v_z}{\partial x^2} + \frac{\partial^2 v_z}{\partial y^2}\right) \tag{3.2.6.}$$

We can ignore equations (3.2.4) and (3.2.5) since we do not consider free surfaces and we can rewrite the rest of the equations to give two coupled second order partial differential equations in U_z and H_z. By normalising in terms of some reference value of H_z, H_1 say, such that,

$$v = v_z / (H_1/\sqrt{\sigma\eta}),$$

$$h = H_z / H_1,$$

and $\xi = x/a$, $\eta = y/a$, where a is some characteristic length, then the governing equations become:

$$\frac{\partial^2 v}{\partial \xi^2} + \frac{\partial^2 v}{\partial \eta^2} + M\frac{\partial h}{\partial \eta} = 0, \qquad 3.2.7.$$

$$\frac{\partial^2 h}{\partial \xi^2} + \frac{\partial^2 h}{\partial \eta^2} + M\frac{\partial v}{\partial \eta} = 0, \qquad 3.2.8.$$

where $M = B_0 a(\sigma/\tilde{\eta})^{\frac{1}{2}}$, is the Hartmann number, We can rewrite these equations in terms of $X, = v + h$, and $Y, = v - h$, by adding and subtracting them as follows:

$$\left(\frac{\partial^2}{\partial \xi^2} + \frac{\partial^2}{\partial \eta^2}\right)X + M\frac{\partial X}{\partial \eta} = 0, \qquad 3.2.9.$$

and

$$\left(\frac{\partial^2}{\partial \xi^2} + \frac{\partial^2}{\partial \eta^2}\right)Y + M\frac{\partial Y}{\partial \eta} = 0. \qquad 3.2.10.$$

3.2.2. Alined line electrodes.

We now analyze the flow between two walls at $y = \pm a$ induced by a current I per unit length in the z- direction entering the fluid at a line electrode (i.e. one of vanishingly small width in the x- direction) at $x = 0$, $y = +a$, and leaving the fluid at $x = 0$, $y = -a$. A magnetic field is imposed in the y-direction. Let $H_1 = I/2$: then the boundary conditions are:

$$\left.\begin{cases} v_z = 0, & H_z = H_1, & x > 0, & y = \pm a, \\ v = 0, & h = 1 & \xi > 0, & \eta = \pm 1 \end{cases}\right\}$$

$$\left.\begin{cases} v_z = 0, & H_z = -H_1, & x < 0, & y = \pm a, \\ v = 0, & h = -1, & \xi < 0, & \eta = \pm 1 \end{cases}\right\} \qquad 3.2.11.$$

We can rewrite these boundary conditions in terms of X as

$$X = 1, \quad \xi > 0, \quad \eta = \pm 1,$$
$$X = -1, \quad \xi > 0, \quad \eta = \pm 1, \qquad 3.2.12.$$

and therefore we need only consider this combined variable. v and h may be found independently from the relations,

$$v(\xi,\eta) = \tfrac{1}{2}\left[X(\xi,\eta) - X(\xi,-\eta)\right],$$
$$h(\xi,\eta) = \tfrac{1}{2}\left[X(\xi,\eta) + X(\xi,-\eta)\right].$$

We can obtain a solution for X as a Fourier series in η, by finding solutions for $\xi > 0$ and $\xi < 0$ and equating them at $\xi = 0$. We obtain for $\xi > 0$:

$$X = 1 - 2\sum_{j=0}^{\infty} (-1)^j e^{-(M/2)\eta}\left[\frac{d_j \cosh(M/2)\, e^{-\lambda_j \xi} \cos\alpha_j \eta}{\lambda_j^2} - \frac{\beta_j \sinh(M/2)\, e^{-\mu_j \xi} \sin\beta_j \eta}{\mu_j^2}\right],$$

and for $\xi < 0$:

$$X = -1 + 2\sum_{j=0}^{\infty} (-1)^j e^{-(M/2)\eta}\left[\frac{\alpha_j \cosh(M/2)\, e^{\lambda_j \xi} \cos(\alpha_j \eta)}{\lambda_j^2} - \frac{\beta_j \sinh(M/2)\, e^{\mu_j \xi} \sin(\beta_j \eta)}{\mu_j^2}\right]$$

where

$$\alpha_j = (j+\tfrac{1}{2})\pi, \quad \beta_j = j\pi, \quad \lambda_j^2 = M^2/4 + \alpha_j^2, \quad \mu_j^2 = M^2/4 + \beta_j^2$$

This solution for X is convergent when $\xi = 0$ and therefore we match convergent series at $\xi = 0$. Also the solution is valid for all values of M.

Asymptotic solution for large M.

As $M \to \infty$, the flow may be examined separately in certain regions (see fig.3.2). We examine these regions in turn making approximations in each. Showing that a solution exists consistent with the approximations and the boundary conditions justifies the approximations. In this case we can also show that the asymptotic solution is equal to the exact solution for large values of M by comparing values of X computed for various points.

$$X = 1, \quad \xi > 0, \quad \eta = \pm 1,$$
$$X = -1, \quad \xi > 0, \quad \eta = \pm 1, \qquad 3.2.12.$$

and therefore we need only consider this combined variable. v and h may be found independently from the relations,

$$v(\xi,\eta) = \tfrac{1}{2}\left[X(\xi,\eta) - X(\xi,-\eta)\right],$$
$$h(\xi,\eta) = \tfrac{1}{2}\left[X(\xi,\eta) + X(\xi,-\eta)\right].$$

We can obtain a solution for X as a Fourier series in η, by finding solutions for $\xi > 0$ and $\xi < 0$ and equating them at $\xi = 0$. We obtain for $\xi > 0$:

$$X = 1 - 2\sum_{j=0}^{\infty} (-1)^j e^{-(M/2)\eta}\left[\frac{d_j \cosh(M/2)\, e^{-\lambda_j \xi} \cos \alpha_j \eta}{\lambda_j^2} - \frac{\beta_j \sinh(M/2)\, e^{-\mu_j \xi} \sin \beta_j \eta}{\mu_j^2}\right],$$

and for $\xi < 0$:

$$X = -1 + 2\sum_{j=0}^{\infty} (-1)^j e^{-(M/2)\eta}\left[\frac{\alpha_j \cosh(M/2)\, e^{\lambda_j \xi} \cos(\alpha_j \eta)}{\lambda_j^2} - \frac{\beta_j \sinh(M/2)\, e^{\mu_j \xi} \sin(\beta_j \eta)}{\mu_j^2}\right]$$

where

$$\alpha_j = \left(j + \tfrac{1}{2}\right)\pi, \quad \beta_j = j\pi, \quad \lambda_j^2 = M^2/4 + \alpha_j^2, \quad \mu_j^2 = M^2/4 + \beta_j^2$$

This solution for X is convergent when $\xi = 0$ and therefore we match convergent series at $\xi = 0$. Also the solution is valid for all values of M.

Asymptotic solution for large M.

As $M \to \infty$, the flow may be examined separately in certain regions (see fig.3.2). We examine these regions in turn making approximations in each. Showing that a solution exists consistent with the approxi= mations and the boundary conditions justifies the approximations. In this case we can also show that the asymptotic solution is equal to the exact solution for large values of M by comparing values of X computed for various points.

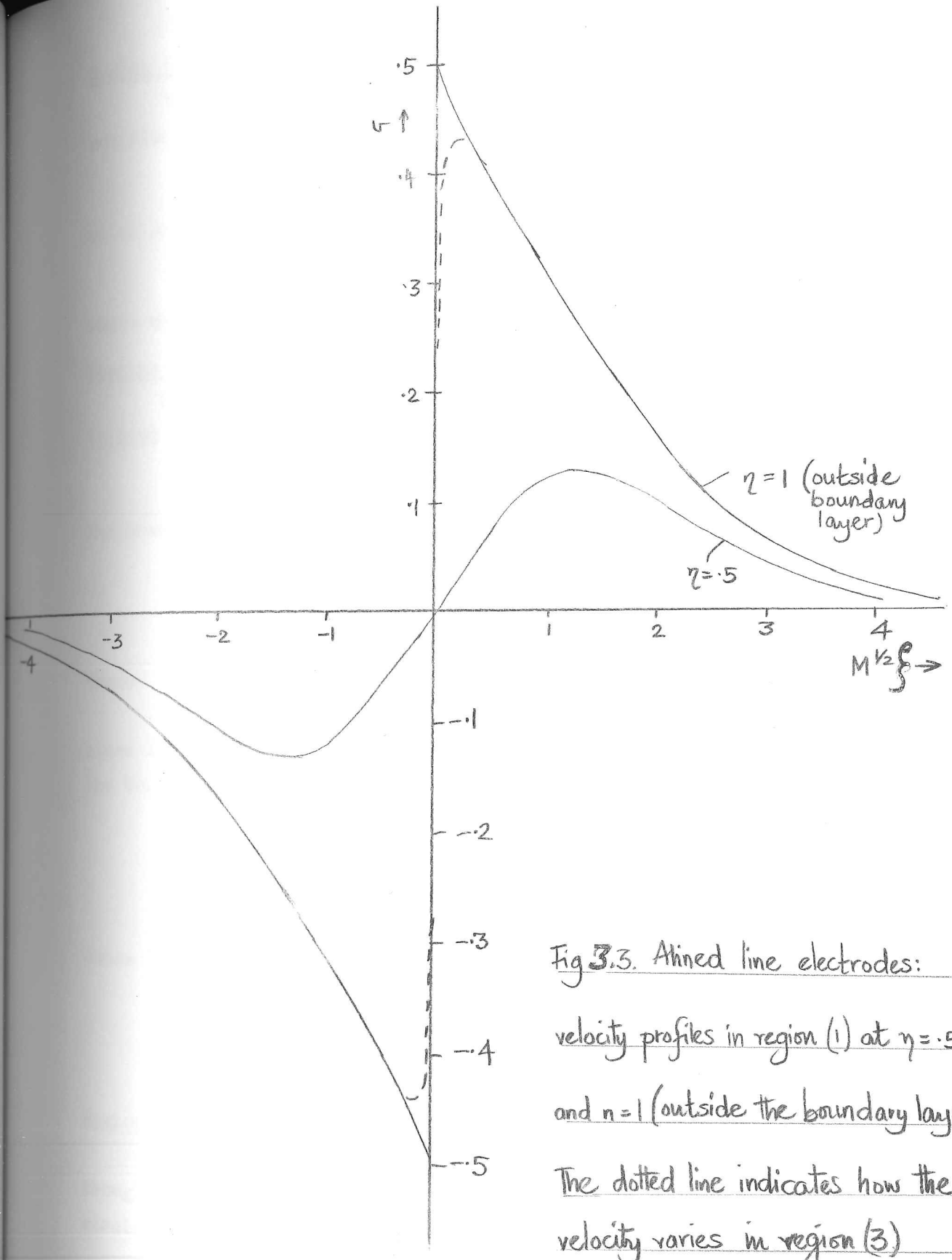

Fig 3.3. Aligned line electrodes: velocity profiles in region (1) at $\eta = \cdot 5$ and $\eta = 1$ (outside the boundary layer) The dotted line indicates how the velocity varies in region (3)

Region (1).

Here $\partial/\partial\eta = O(1)$ and $\partial/\partial\xi = O(M^{\frac{1}{2}})$. Hence $\partial/\partial\xi \gg \partial/\partial\eta$ and equation (3.2.9) becomes:

$$\frac{\partial^2 X}{\partial \xi^2} + M\frac{\partial X}{\partial \eta} = 0 \qquad 3.2.13.$$

which has the solution:

$$X_1 = \operatorname{erf}\left(\xi\sqrt{M}/2\sqrt{1-\eta}\right), \qquad 3.2.14.$$

where the suffix refers to the value of X in region (1).

Regions (2a) and (2b).

Here $\partial/\partial\eta = O(M)$ and $\partial/\partial\xi = O(M^{\frac{1}{2}})$. Hence $\partial/\partial\eta \gg \partial/\partial\xi$ and equations (3.2.9) become:

$$\frac{\partial^2 X}{\partial \eta} + M\frac{\partial X}{\partial \eta} = 0 . \qquad 3.2.15.$$

The boundary conditions for (2a) are:

$X = 1$ for $X > 0$, $= 1$

$X = -1$ for $X < 0$, $= 1$

$X \to X_1(\eta = 1)$ as $(1-\eta)M \to \infty$

Hence

$$X_{2a} = 1 \text{ for } X > 0$$
$$= -1 \text{ for } X < 0 \qquad 3.2.16.$$

since X_1 satisfies the boundary conditions of X_{2a} at $\eta = 1$.

The boundary conditions for (2b) are:

$X = 1$ for $X > 0, \eta = -1$

$X = -1$ for $X < 0, \eta = -1$

$X \to X_1(\eta = -1)$ as $[(1+\eta)M] \to \infty$.

Hence $X_{2b} = e^{-M(1+\eta)} + \left[\operatorname{erf}\left(\frac{\xi\sqrt{M}}{\sqrt{8}}\right)\right]\left[1 - e^{-M(1+\eta)}\right]$ for $X > 0$,

$$= -e^{-M(1+\eta)} + \left[\operatorname{erf}\left(\frac{\xi\sqrt{M}}{\sqrt{8}}\right)\right]\left[1 - e^{-M(1+\eta)}\right] \quad \text{for } X < 0, \qquad 3.2.17.$$

Regions (3a) and (3b)

We can see that both X_{2a} and X_{2b} are discontinuous when $\xi = 0$, though X_1 is not. Hence there must be a region we call (3) near the electrodes in which $\frac{\partial}{\partial\xi} \sim \frac{\partial}{\partial\eta}$ and hence the full equation (3.2.9) must be

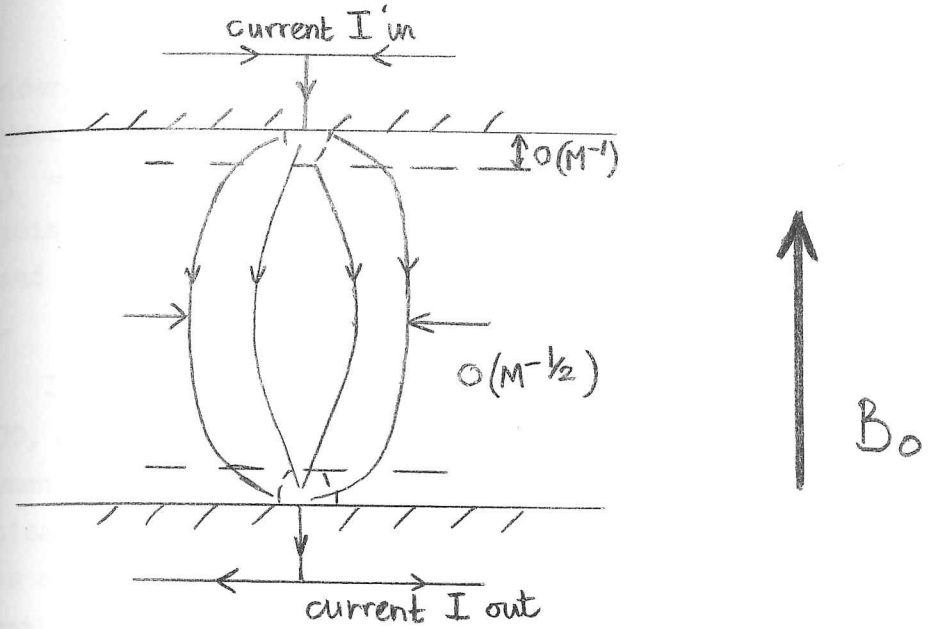

Fig 3.4 Current streamlines between line electrodes when $M \gg 1$

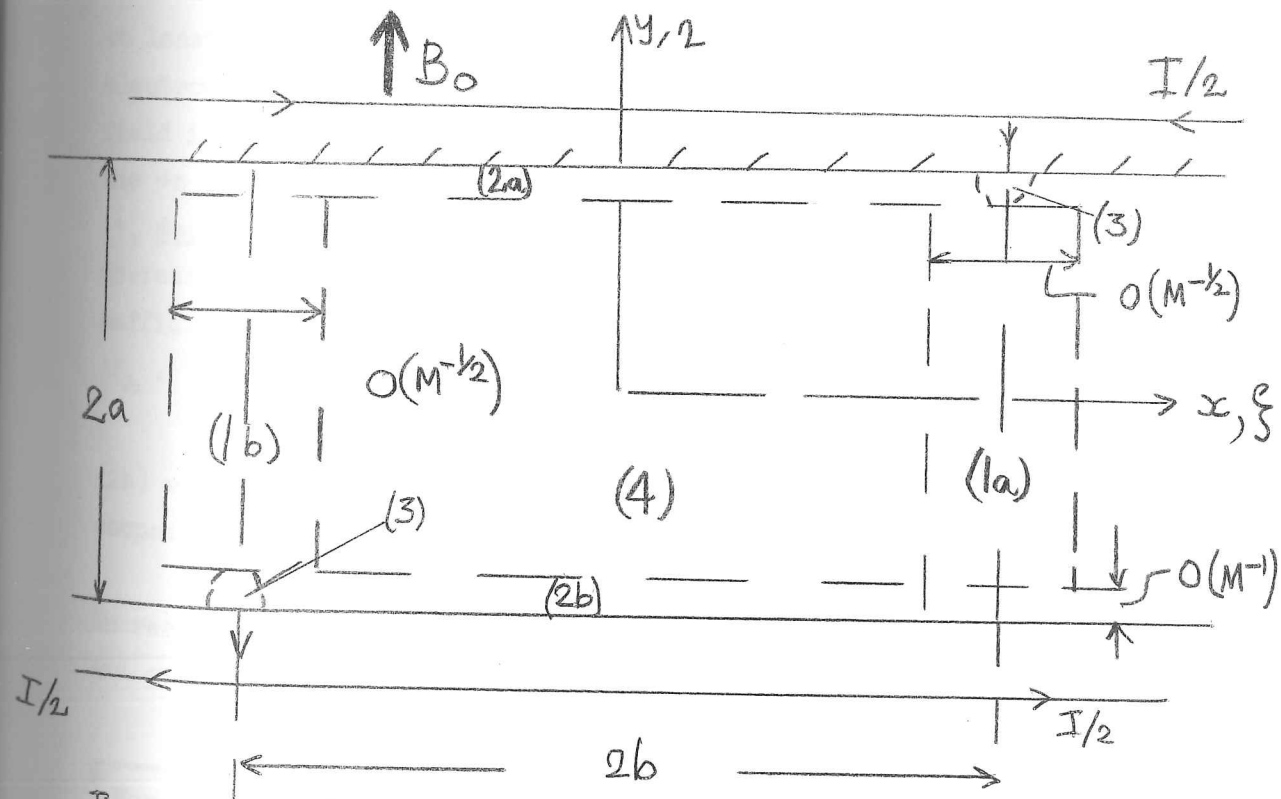

Fig 3.5 Displaced line electrodes showing asymptotic regions

considered rather than (3.2.15). Since regions (3a) and (3b) are imbedded in (2), but do not extend into (1), $\partial/\partial\eta = O(M)$. Hence $\partial/\partial\xi = O(M)$ and thus these regions extend a distance $O(M^{-1})$ round the points $\xi = 0$, $\eta = \pm 1$. Since these regions are small compared to (1) and (2) and do not exert any controlling influence, we can ignore them.

If we compare the values of X computed from the exact solution at M = 20, 40 and those taken from the asymptotic solution we find that the agreement is clearly good enough to show that these two solutions are identical when $M \to \infty$*. In fig.(3.3) the velocity profiles for two values of η are shown and in fig.(3.4) the current lines are shown schematically.

The best way of understanding the physical reasons for the distribution of velocity and current is by considering what happens to the current and the velocity when the magnetic field is turned on. When there is no magnetic field there is no velocity and a current passes between the electrodes the current spreads out from the top electrode at least a distance of order 2a before curving back to the bottom electrode. Let us consider the quadrant $\xi > 0, \eta > 0$ when the magnetic field is applied; the large component of $\underset{\sim}{j} \times \underset{\sim}{B}_o$ accelerates the fluid in the +z direction. However, as v_z <u>increases</u> v_z B_o increases and thus j_x <u>decreases</u>. Then, since $j_x B_o$ <u>decreases</u>, the acceleration of v_z decreases. This process continues until j_x is reduced to a value sufficient for the $j_x B_o$ force to balance the viscous stresses produced by v_z.

Thus as we see from figs(3.3) and (3.4) in the regions (2a) and (2b) where the viscous stresses are greatest, i.e. $O(M^2)$, there is a large component of current perpndicular to the magnetic field such that

$$\underset{\sim}{j} \times \underset{\sim}{B}_o = O(M^2)$$

In region (1), however, the viscous stresses are much less, i.e. O(M), and consequently the current has a smaller component perpendicular to $\underset{\sim}{B}_o$.

It is perhaps worth noting that we can construct a solution for

* More recently Prof. Williams has shown analytically that the asymptotic and exact solutions are identical as $M \to \infty$. (Hunt & Williams, 1967).

electrodes which have a finite thickness, δ, where $\delta \ll a$, provided we specify the current distribution on the electrodes. Then it is easily shown that as $\delta \to 0$, the solution becomes that of the line electrodes. Therefore our solution is a limiting solution of the electrode thickness tending to zero.

3.2.3. Displaced line electrodes.

We now analyze the flow between two walls when the electrodes are displaced sideways by a distance, 2b. See figure (3.5). If $b/a = \ell$ and $H_1 = I/2$, the boundary conditions are:

$$v = 0 \ , \ h = X = 1 \ , \quad \xi > \ell, \quad y = a,$$
$$\xi > -\ell, \quad y = -a,$$
$$v = 0, \quad h = X = 1 \ , \quad \xi < \ell, \quad y = a,$$
$$\xi < -\ell, \quad y = -a.$$

v and h may be found independently from the relations:

$$v = \tfrac{1}{2}\left\{ X(\xi, \eta) + X(-\xi, -\eta) \right\},$$
$$h = \tfrac{1}{2}\left\{ X(\xi, \eta) - X(-\xi, -\eta) \right\}. \qquad 3.2.18.$$

Although it is possibe to obtain a Fourier Series solution there is little interest in doing so. We move straight on to the asymptotic solution.

Asymptotic solution.

We now consider the solution when $M \to \infty$. We will assume that M is large enough to satisfy the condition that $aM^{-\frac{1}{2}} \ll b$. Then in this situation there is one new type of region not found in the alined electrode problem. This is the region, (4) (see fig.3.5), where

$$\ell - \alpha(M^{-\frac{1}{2}}) > \xi > -\ell + O(M^{\frac{1}{2}}),$$
$$1 - O(M^{-1}) > \eta > -1 + O(M^{-1}),$$

in other words this region lies between the Hartmann layers on the walls and the layers of thickness $O(M^{-\frac{1}{2}})$ emanating from the electrodes. The solution in this region is simply,

$$X = -1 \qquad 3.2.19.$$

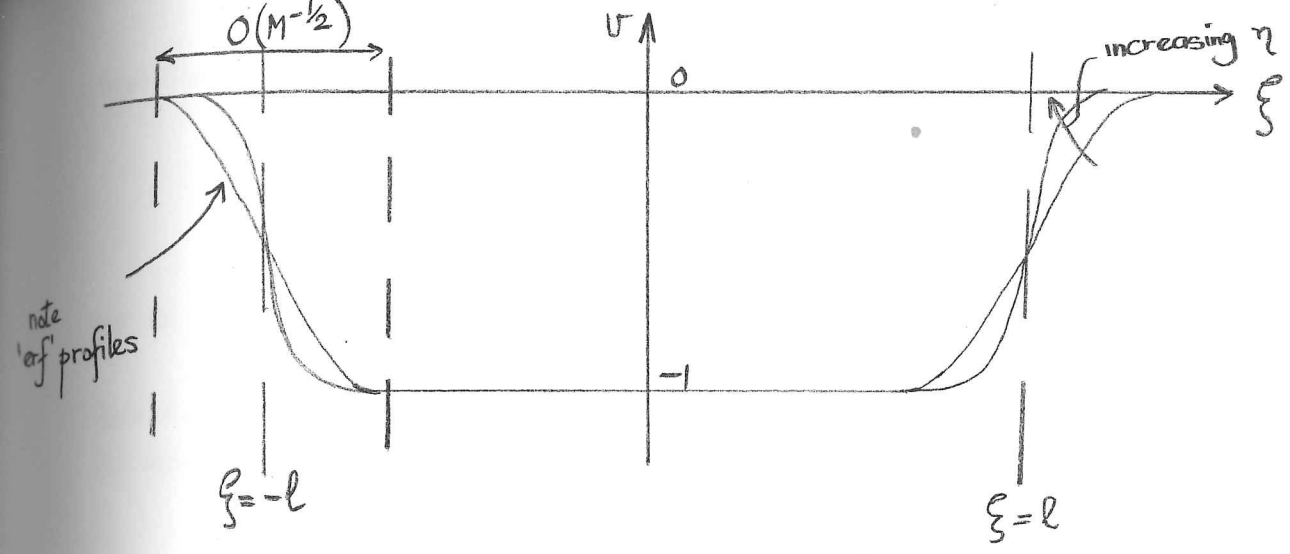

Fig 3.6a. Velocity profiles for flow between displaced line electrodes in regions (1) and (4) – profiles are schematic (M≫1)

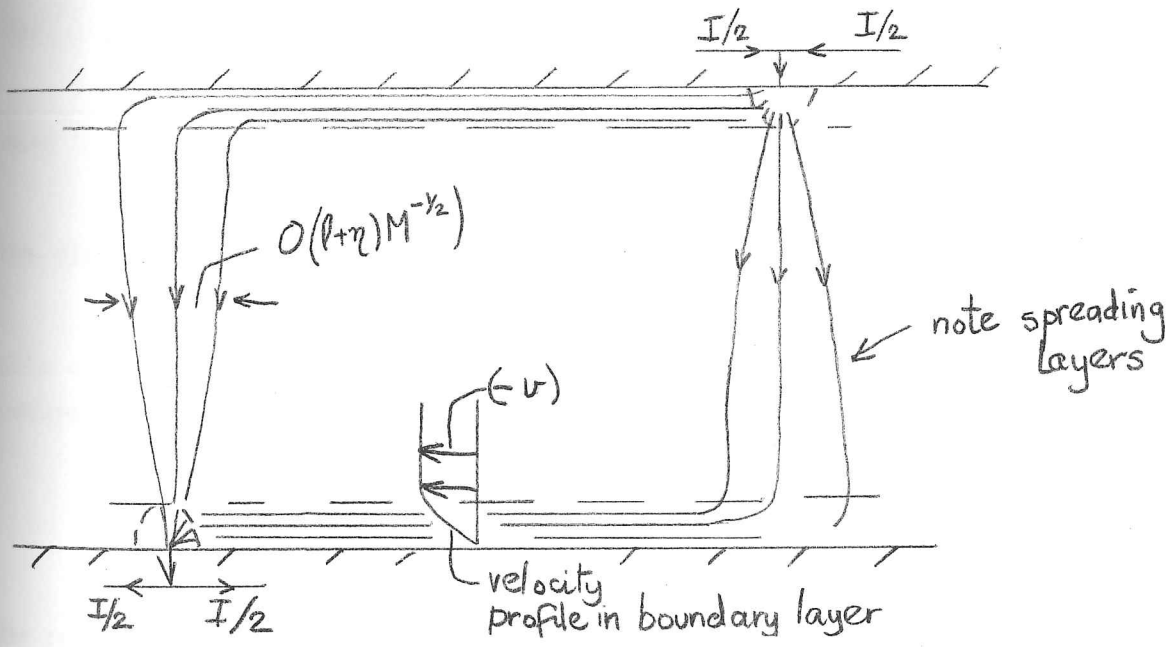

Fig 3.6b. Current streamlines for flow between displaced line electrodes when M≫1. (Velocity profile in region (2) is also shown)

Therefore $v = -1, \quad h = 0$.

3.2.20.

The solution for region (1a) is

$$X = \operatorname{erf}\left[\frac{(\xi - \ell)\sqrt{M}}{2\sqrt{1-\eta}}\right], \qquad 3.2.21.$$

and in (1b):

$$X = -1 .$$

Thus X does not change in (1b) which is to be expected since $X = -1$ in (4) and $X \to -1$ as $\xi \to -\infty$.

The solution for (2a) is much the same as for the alined line electrodes, i.e.

$$X = 1, \quad \xi > \ell .$$
$$X = -1 \quad \xi < \ell .$$

and the solution for (2b) is:

$$\xi > -\ell : X = -e^{-M(1+\eta)} + \operatorname{erf}\left(\frac{(\xi - \ell)\sqrt{M}}{\sqrt{8}}\right)\left[1 - e^{-M(1+\eta)}\right]$$

for $(\ell - \xi)\sqrt{M} \gg 1$ this becomes:

$$X = -1 + 2e^{-M(1+\eta)}$$

when $\xi < -\ell$, $X = -1$.

Thus we again must have two regions (3) with thickness $O(M^{-1})$ near the electrodes in which $\partial/\partial\xi$ is of the same order as $\partial/\partial\eta$.

We see from (3.2.19) and (3.2.20) and fig (2.6a) that the major difference between this case and the alined electrode situation is that a net flow is induced. This is simply calculated to be:

$$\int_{-\infty}^{+\infty}\int_{-1}^{+1} v\, d\xi\, d\eta = -4\ell\left(1 - \frac{1}{M}\right),$$

or

$$a\int_{-\infty}^{+\infty}\int_{-a}^{+a} v_z\, dx\, dy = -\frac{2Iab}{\sqrt{\sigma\eta}}\left(1 - \frac{1}{M}\right). \qquad 3.2.22.$$

The reason for this net flow is that, since the current must pass between the electrodes, and since there can be no current in the inviscid core (region (4)) because the flow is steady and there is no pressure gradient, all the current has to pass along Hartmann boundary layers on the two walls, a current I/2 along each. See fig 2.6(b). Now Shercliff (1965) has shown that the relation between the total current flowing along a Hartmann boundary layer (I/2 in our case) and the velocity outside it

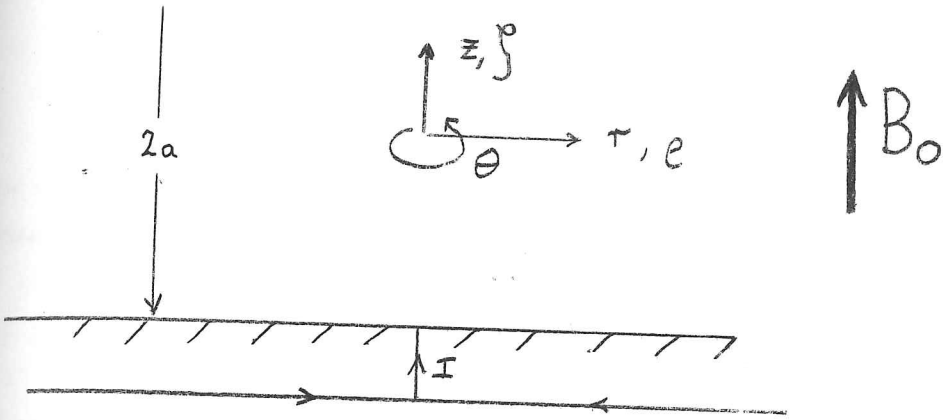

Fig 3.7 Notation for alined point electrodes

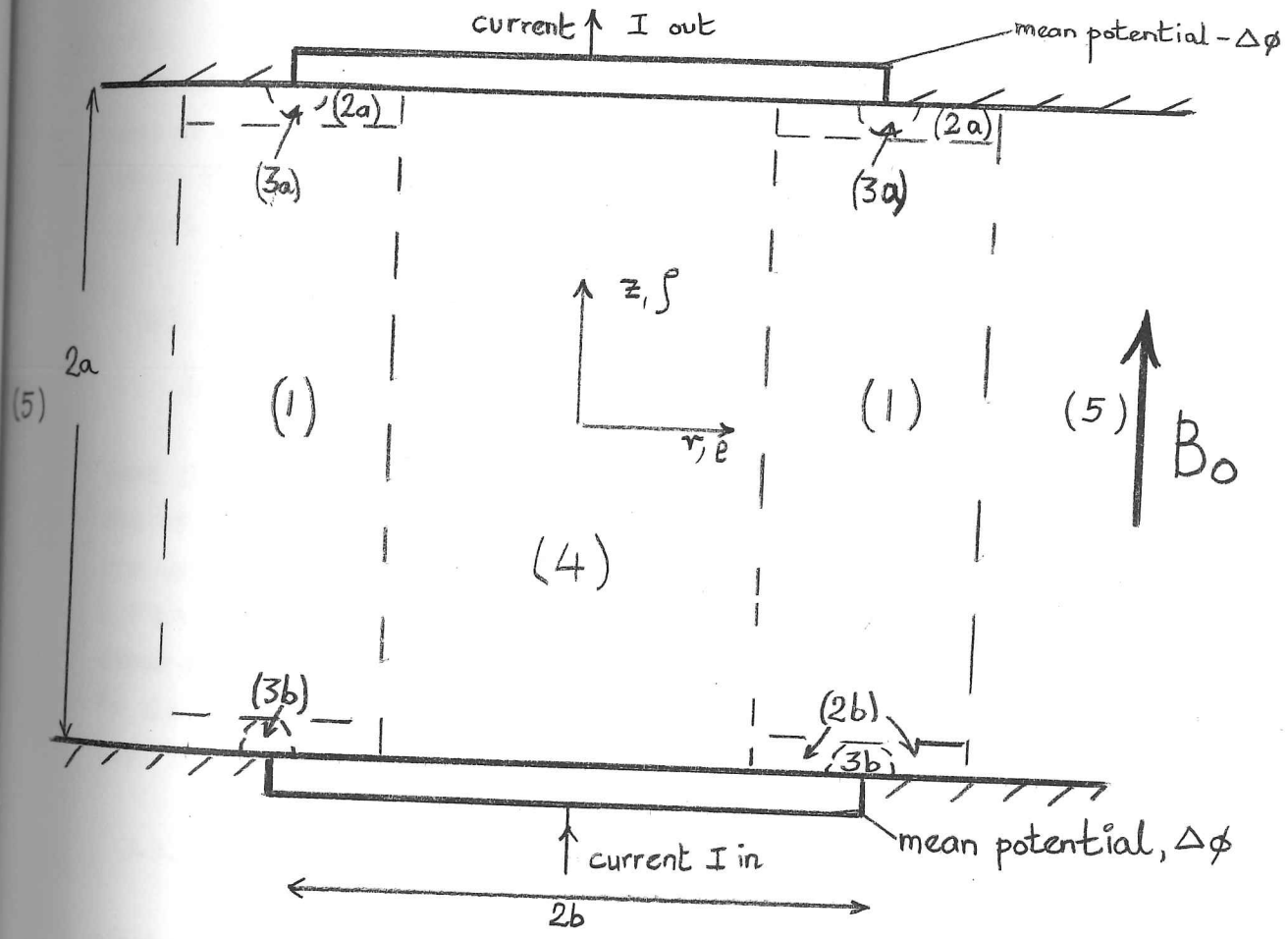

Fig 3.8 Aligned circular electrodes with asymptotic regions

V is:

$$V = I/(2\sqrt{\sigma\eta}),$$

whence we can obtain the first term in our expression for Q. It is important to note that the first term (3.2.22) is independent of the value of B_o, though if the electrodes were finite such that there was a finite potential difference between them, $\Delta\phi$, it would be found that the relation between Q and $\Delta\phi$ depends on B_o. This result was to be expected from § 3 of H & S where we examined the flow in a rectangular duct with perfectly conducting walls parallel to the field and showed that for such a flow when there is no pressure gradient the first term in the Q - I relation is independent of B_o, whereas the $Q - \Delta\phi$ relation is not. It is also worth noting that the first term in (3.2.21) is the same as that of the Q - I relation for a rectangular duct with sides 2a and 2b which is to be expected since Shercliff's Hartmann layer relation shows that the distribution of current along the lines $X = \pm b$ does not affect the first term in (3.2.22).

3.3. Circular Electrodes.

3.3.1. Introduction

The disadvantage of studying flows due to line electrodes is that such flows are difficult to produce experimentally. Inevitably at the end of the container enclosing the fluid some recirculation occurs which may upset the flow elsewhere. However if circular flows are used there are no such end effects, although the flows, being more unstable, entail other problems. In this section we examine the theory of flows produced by circular electrodes and thence predict some of the effects found experimentally, as shown in chapter 7.

3.3.2. Alined point electrodes.

We consider the axisymmetric flow induced between two point electrodes set in insulating planes opposite to each other (see fig.3.1). We discoverd in §2.6 how such flows induced radial pressure gradients which in turn induce radial flow and why, if the magnetic field is strong enough, these effects may be ignored. We make the same assumption again,

only considering the azimuthal or swirl component of velocity, and the radial and axial components of current. Then, in terms of v_θ and H_θ, the azimuthal components of velocity and induced magnetic field, the governing equations are:

$$0 = B_0 \frac{\partial H_\theta}{\partial z} + \eta^2 \left(\frac{\partial^2}{\partial r^2} + \frac{1}{r}\frac{\partial}{\partial r} - \frac{1}{r^2} + \frac{\partial^2}{\partial z^2} \right) v_\theta , \qquad 3.3.1.$$

$$0 = B_0 \frac{\partial v_\theta}{\partial z} + \frac{1}{\sigma} \left(\frac{\partial^2}{\partial r^2} + \frac{1}{r}\frac{\partial}{\partial r} - \frac{1}{r^2} + \frac{\partial^2}{\partial z^2} \right) H_\theta . \qquad 3.3.2.$$

Let the current entering the electrode on the wall at $z = -a$ and leaving the electrode on the wall at $z = +a$, be I, then the boundary conditions are:

at $z = \pm a$: $\quad r H_\theta = I/2\pi$, $\quad v_\theta = 0$

at $z = 0$, $\quad v_\theta$ and H_θ are continuous.

We now non-dimensionalize in terms of I:

$$v = \frac{v_\theta}{(I/2\pi a\sqrt{\sigma\eta})} \; ; \; h = \frac{H_\theta}{I/(2\pi a)} \; ; \; \Phi = \frac{\phi}{I/(2\pi a \sigma)} \; ; \; \rho = r/a \; ; \; \xi = z/a$$

and $M = B_0 a \sqrt{\sigma/\eta}$

Then (3.3.1) and (3.3.2) become:

$$\frac{M}{\partial \xi} \frac{\partial h}{\partial \xi} + \frac{\partial}{\partial \rho} \left(\frac{1}{\rho} \frac{\partial (\rho v)}{\partial \rho} \right) + \frac{\partial^2 v}{\partial \xi^2} = 0 \qquad 3.3.3.$$

and $$\frac{M}{\partial \xi} \frac{\partial v}{\partial \xi} + \frac{\partial}{\partial \rho} \left(\frac{1}{\rho} \frac{\partial (\rho h)}{\partial \rho} \right) + \frac{\partial^2 h}{\partial \xi^2} = 0 \qquad 3.3.4.$$

We can rewrite these equations as one in $\rho(v+h)$:

$$\frac{M}{\rho} \frac{\partial}{\partial \xi} \left(\rho (v+h) \right) + \left(\frac{1}{\rho} \frac{\partial^2}{\partial \xi^2} + \frac{\partial}{\partial \rho} \left(\frac{1}{\rho} \frac{\partial}{\partial \rho} \right) \right) \left[\rho (v+h) \right] \qquad 3.3.5.$$

and the boundary conditions become:

$$\rho (v+h) = 1 \quad \text{at} \quad \xi = \pm 1. \qquad 3.3.6.$$

The solution of (3.3.5) subject to the boundary condition (3.3.6)

$$v + h = \frac{1}{\rho} - 2 \sum_{j=0}^{\infty} \left\{ \frac{(-1)^j \alpha_j \cosh[M/2] \, K_1(\lambda_j \rho) e^{-M/2 \xi} \cos \alpha_j \xi}{\lambda_j} \right.$$

$$\left. - \frac{(-1)^j \beta_j \sinh(M/2) \, K_1(\mu_j \rho) e^{-M/2 \xi} \sin \beta_j \xi}{\mu_j} \right\} \qquad 3.3.7.$$

where

$$\alpha_j = (j + \tfrac{1}{2})\pi, \quad \beta_j = j\pi, \quad \lambda_j^2 = \alpha_j^2 + M^2/4, \quad \mu_j^2 = \beta_j^2 + M^2/4.$$

As we have found before, the asymptotic solution is simpler and physically clearer. Dividing the flow into 3 regions, as in (fig.3.2), with region (1) lying between the electrodes, regions (2a) and (2b) lying on the two walls, and regions (3) extending a distance $O(M^{-1})$ round the electrodes. Then in regions (2a) and (2b), (3.3.5) becomes:

$$\left(\frac{\partial^2}{\partial \xi^2} + M\frac{\partial}{\partial \xi}\right)\left(\rho(v+h)\right) = 0 \qquad 3.3.8.$$

and the solution in (2a) is:

$$\rho(v+h) = 1$$

In region (1), $\partial/\partial\xi = O(1)$, $\frac{\partial}{\partial\rho} \simeq O(M^{\frac{1}{2}})$ and $\rho = O(M^{-\frac{1}{2}})$ and therefore (3.3.5) becomes:

$$\left(M\frac{\partial}{\partial \xi} + \frac{\partial}{\partial \rho}\left(\frac{1}{\rho}\frac{\partial}{\partial \rho}\right)\right)\left(\rho(v+h)\right) = 0 \qquad 3.3.9.$$

The boundary conditions are:

$$\rho(v+h) = 1 \quad \text{as} \quad \rho \to \infty \qquad \text{and when} \quad \xi = 1$$

Thence

$$\rho(v+h)_1 = 1 - \exp\left[-M\rho^2/4(1-\xi)\right] \qquad 3.3.10.$$

In region (2b), the solution to equation (2.3.7) is:

$$\rho(v+h)_{2b} = 1 - e^{-M\rho^2/(4(1-\xi))}\left[1 - e^{-M^*(1+\xi)}\right] \qquad 3.3.11.$$

By considering the symmetry of the flow we see that in (1),

$$v = \frac{1}{2\rho}\left\{e^{-M\rho^2/4(1+\xi)} - e^{-M\rho^2/(4(1-\xi))}\right\} \qquad 3.3.12.$$

and

$$h = \frac{1}{2\rho}\left\{2 - e^{-M\rho^2/(4(1-\xi))} - e^{-M\rho^2/4(1-\xi)}\right\} \qquad 3.3.13.$$

Though the form of the velocity profile is similar to that for the line electrode, the important difference is that in this case

$$v \quad = O(M^{\frac{1}{2}}),$$

---

* Prof.Williams has again shown analytically that, as $M \to \infty$, this asymptotic solution is equivalent to the exact solution (3.3.7). Hunt & Williams, 1967).

whereas for a line electrode,

$$v = O(1).$$

We can also deduce this result by an order of magnitude argument:

In the region (1),

$$B_0 v_\theta \simeq \partial\phi/\partial r$$
$$= O[\phi r = o/\delta], \text{ where } \delta = O(aM^{-\frac{1}{2}}) \text{ is the}$$

thickness of region (1) and, since at $r = 0$, $\phi = O(Ia/\sigma\pi\delta)$

$$= O(IM/a\sigma),$$

$$v_\theta = O\left[\frac{IM}{\sigma a} \times \frac{M^{\frac{1}{2}}}{a} \times \frac{1}{B_0}\right],$$

$$= O\left[\frac{IM^{\frac{1}{2}}}{a\sqrt{\sigma\eta}}\right]$$

For a line electrode, at $x = 0$,

$$\phi = O[Ia/\sigma\delta],$$

and thence $v_\theta = O\left[I/\sqrt{\sigma\eta}\right]$

where I in this case is the current passing between the electrodes per unit length. Thus the different values of v_θ in terms of M result from the much higher potential which occurs in the point electrode case than the line electrode case.

3.3.3. Asymptotic analysis of alined circular electrodes.

In this section we examine the flow induced by current passing between the two electrodes shown in fig.(3.8) when $M \gg 1$. The analysis presented is not complete, but even in this incomplete form it is useful in interpreting the experimental results presented in chapter 7. We will only examine the flows when the Hartmann number is large, since the interesting physical effects are then seen most easily both analytically and experimentally.

We first analyse the flow when the electrodes are perfectly conducting using the same non-dimensionalized parameters as in §3.3.2. Thus we consider the current I to be given and the electric potential, $\Delta\phi$, on the electrodes to be a dependent variable. We have one further parameter, if the radius of the electrodes is b and $\ell = b/a$ then

the boundary conditions in non-dimensionalized form are:

$$\zeta = \pm 1, \quad \rho < \ell, \quad \frac{\partial h}{\partial \zeta} = 0, \quad v = 0,$$
$$\rho > 0, \quad h = 1/\rho, \quad v = 0,$$
$$\rho' \to \infty, \quad h = 1/\rho \quad v \to 0$$

Now in order to solve this problem, following the method used to examine the boundary layers on walls AA in H & S, we specify the value of h on the electrodes and then find an equation which this distribution of h must satisfy in order that $\partial h/\partial \zeta = 0$ on the electrode. Let $h = f(\rho)$ on $\zeta = \pm 1, \rho < \ell$, where $f = 0$ when $\rho = 0$ and $f = 1/\ell$ when $\rho = \ell$. The latter condition follows from the necessity of h being continuous on the wall.

As before we divide the flow into various regions as shown in fig. 3.8. For this analysis we assume that M is large enough to satisfy the two criteria: $M \gg 1$ and $\ell \gg O(M^{-\frac{1}{2}})$.

Region (4).

$$\partial/\partial\zeta = O(1), \quad \partial/\partial\rho = O(\ell^{-1}) \ll O(M^{1/2}).$$

Therefore (3.3.5) becomes:

$$\frac{\partial(\rho(v+h))}{\partial\zeta} = 0,$$

and therefore

$$v = 0$$
$$\text{and } h = f(\rho).$$

Therefore,

$$-\frac{\partial \Phi}{\partial \zeta} = \frac{1}{\rho}\frac{\partial}{\partial \rho}(\rho f),$$

and since Φ is constant at $\zeta = \pm 1$, it follows that:

$$\frac{1}{\rho}\frac{\partial}{\partial \rho}(\rho f) = 2\lambda\ell,$$

where λ is some constant to be determined. Therefore:

$$f = \lambda\rho/\ell^2 \qquad 3.3.14.$$

Region (5).

In this region $(\rho - \ell) \gg O(M^{-\frac{1}{2}})$ and $v = 0$ and $h = 1/\rho$. We see that though v and h may be continuous at $\rho = \ell$, as calculated in

regions (4) and (5), $\partial h/\partial \rho$ and $\partial \Phi/\partial \zeta$ are discontinuous. Therefore regions must exist in which $\partial \Phi/\partial \zeta$ changes from its value in (4) to zero in (5), these being (1) and (2).

Regions (2a) and (2b).

We treat these regions as in §3.3.2. $\partial/\partial \zeta = O(M)$, $\partial/\partial \rho = O(M^{\frac{1}{2}})$ and therefore $\partial/\partial \zeta \gg \partial/\partial \rho$ so that (3.3.5) becomes:

$$\left(\frac{\partial^2}{\partial \zeta} + M\frac{\partial}{\partial \zeta}\right)(v+h) = 0. \qquad 3.3.15.$$

Thence, in (2a),

$$v + h = f_1(\rho) \quad \text{for } \rho < \ell,$$
$$= 1/\rho \qquad \rho > \ell. \qquad 3.3.16.$$

Region (1).

Let us postulate that:

$$\partial/\partial \rho = O(M^{\frac{1}{2}}), \text{ and } \partial/\partial \zeta = O(1).$$

Then since $\ell \gg O(M^{-\frac{1}{2}})$

$$\partial/\partial \rho \gg 1/\rho.$$

and (3.3.5) becomes:

$$\left(\frac{\partial^2}{\partial \rho^2} + M\frac{\partial}{\partial \zeta}\right)(v+h) = 0 \qquad 3.3.17.$$

The boundary conditions in this region are:

$$\zeta = 1, \quad \left.\begin{matrix}\rho' < 0 \\ \rho' \to -\infty\end{matrix}\right\} \; v + h = f(\rho)$$

$$\zeta = 1, \quad \left.\begin{matrix}\rho' > 0 \\ \rho' \to \infty\end{matrix}\right\} \; v + h = 1/\rho \simeq 1/\ell - \rho/\ell^2$$

where $\rho' = \rho - \ell$. $\rho' = O(M^{-\frac{1}{2}})$ in region (1).

Thence, using the standard solution to the heat conduction equation, (3.3.17),

$$(v+h)_1 = \frac{M^{1/2}}{2\sqrt{\pi(1-\zeta)}} \int_{-\infty}^{0} f(t) \exp\left[-(t-\rho')^2 M/4(1-\zeta)\right] dt$$

$$+ \frac{M^{\frac{1}{2}}}{2\sqrt{\pi(1-\zeta)}} \int_{0}^{\infty} \frac{\ell - t}{\ell^2} \exp\left[-(t-\rho')^2 M/4(1-\zeta)\right] dt. \qquad 3.3.18.$$

Region (2b).

Using the solution for (1) we can now write down the solution for (2b) viz:

$$\text{for } \rho' < 0, (v+h)_{2b} = f(\rho')\, e^{-M(1+\zeta)} + (v+h)_{1(\zeta=-1)}\left[1-e^{-M(1+\zeta)}\right],$$

$$\rho' > 0, (v+h)_{2b} = \frac{l-\rho'}{l^2}\, e^{-M(1+\zeta)} + (v+h)_{1(\zeta=-1)}\left[1-e^{-M(1+\zeta)}\right] \qquad 3.3.19.$$

where $(v+h)_{1\,(\zeta=-1)}$ is the value of $(v+h)_1$ when $\zeta = -1$. Note that, except when $\rho' = 0$, $\partial(v+h)_{1(\zeta=-1)}/\partial\rho = O(M^{\frac{1}{2}})$ compared with $\partial(v+h)/\partial\zeta = O(M)$, and therefore our solution for this region is consistent with our assumption.

To find $f(\rho)$.

We now find an equation for which $f(\rho)$ must be a solution in order that $\partial h/\partial\zeta = 0$ at $\zeta = \pm 1$ when $\rho < l$.

Now
$$\frac{\partial h(\rho,\zeta)}{\partial\zeta} = \frac{\partial[(v+h)(\rho,\zeta)]}{\partial\zeta} - \frac{\partial[(v+h)(\rho,-\zeta)]}{\partial\zeta},$$

and therefore, since in (2a),

$$\partial(v+h)/\partial\zeta = 0$$

and since $\partial h/\partial\zeta = 0$, when $\zeta = \pm 1, \rho < l$,

$$\left|\partial[(v+h)(\rho,\zeta)]/\partial\zeta\right|_{\zeta=-1} = 0 \qquad 3.3.20.$$

In order to satisfy (3.3.20), we use our solution for region (2b).

Thence, when $\rho < l$ or $\rho' < 0$,

$$\left|\frac{\partial[(v+h)(\rho,+\zeta)]}{\partial\zeta}\right|_{\zeta=-1} = -M\left\{f(\rho') - \frac{M^{\frac{1}{2}}}{2\sqrt{2\pi}}\int_{-\infty}^{0} f(t)\exp\left[-(t-\rho')^2 M/8\right]dt\right.$$

$$\left. - \frac{M^{\frac{1}{2}}}{2\sqrt{2\pi}}\int_{0}^{\infty}\frac{l-t}{l^2}\exp\left[-(t-\rho')M/8\right]dt + O(M^{-\frac{1}{2}})\right\} \qquad 3.3.21.$$

Thus, to find $f(\rho)$, we have to solve this integral equation (3.3.21), to do which we first need to know the boundary conditions.

However, before determining the boundary conditions on f in the

regions (2a) and (2b), we must consider the regions (3). Since when $\rho' < 0$ $\partial h/\partial \zeta = 0$ and when $\rho' > 0$, $\frac{\partial h}{\partial \zeta} \neq 0$, a discontinuity exists at $\rho' = 0$, which implies that some regions (3a) and (3b) must exist in which $\frac{\partial}{\partial \zeta} = 0\left(\partial/\partial\rho\right) = O(M)$.

Now in the regions (3a) and (3b) for line electrodes, (§3.2.2), h changes from +1 to -1, so that we have to determine whether the change in (3) is comparable with that in (2). We now show that this must be the case for the integral equation (3.3.21) to be satisfied.

The equation (3.3.21) specifies $f(\rho)$ such that, when $\rho' < 0$ in region (1), v + h has the same value at $\zeta = -1$ as at $\zeta = +1$. If the change of f in region (3) is negligible, when in region (2) $f = (v+h)_{(\zeta=1)} = 1/\ell$ when $\rho' = 0$.

Therefore the maximum value of (v + h) in region (2) when $\rho' < 0$ and $\zeta = 1$ is the maximum value anywhere in the plane $\zeta = 1$. Since in region (1), (v + h) satisfies the heat conduction equation (3.3.17), the maximum value of v + h at the boundary between regions (1) and (2b) is less than that at $\zeta = 1$. Therefore it is impossible to satisfy the equation (3.3.21) and the boundary condition $f = 1/\ell$ when $\rho' = 0$. However, if the change of f in region (3) is comparable with that in (2), so that the boundary condition for f in region (2) at $\rho = 0$ is:

$f = \mu/\ell$, where $\mu < 1$ it follows that it may be possible to find values of μ and λ as well as a solution for f in region (2) by means (3.3.21). This result implies that $\partial\phi/\partial y$ is $O(M^{\frac{1}{2}})$ in (3) and thus, near $\zeta = 1$ when $\rho' = O(M^{-1})$, $\partial\phi/\partial x$ is $O(M^{\frac{1}{2}})$, whereas for $\rho' = -O(M^{-\frac{1}{2}})$, $\partial\phi/\partial x = 0$ near $\zeta = 1$. We believe that we can find μ and λ by invoking the minimum dissipation theorem mentioned by Moffatt (1964).

Since the materials used for electrodes in experiments are not perfectly conducting it would be of interest to examine the effects of finitely conducting walls. But, since no analysis has been developed for this situation, as a first approximation to a finitely conducting electrode we make the assumption that the current distribution is uniform over the electrode. Then

$$f(\rho) = \rho/\ell^2,$$

and, dividing up the flow into regions as before, we find that in region (4)

Fig 3.9 Graph of $(-\Phi)\ell^{2/2}$ $(\equiv (-\phi)\pi b^2\sigma/Ia)$ against $\rho' M^{\frac{1}{2}}$ at $\delta = 1.0$ (The current density across the electrode is assumed constant)

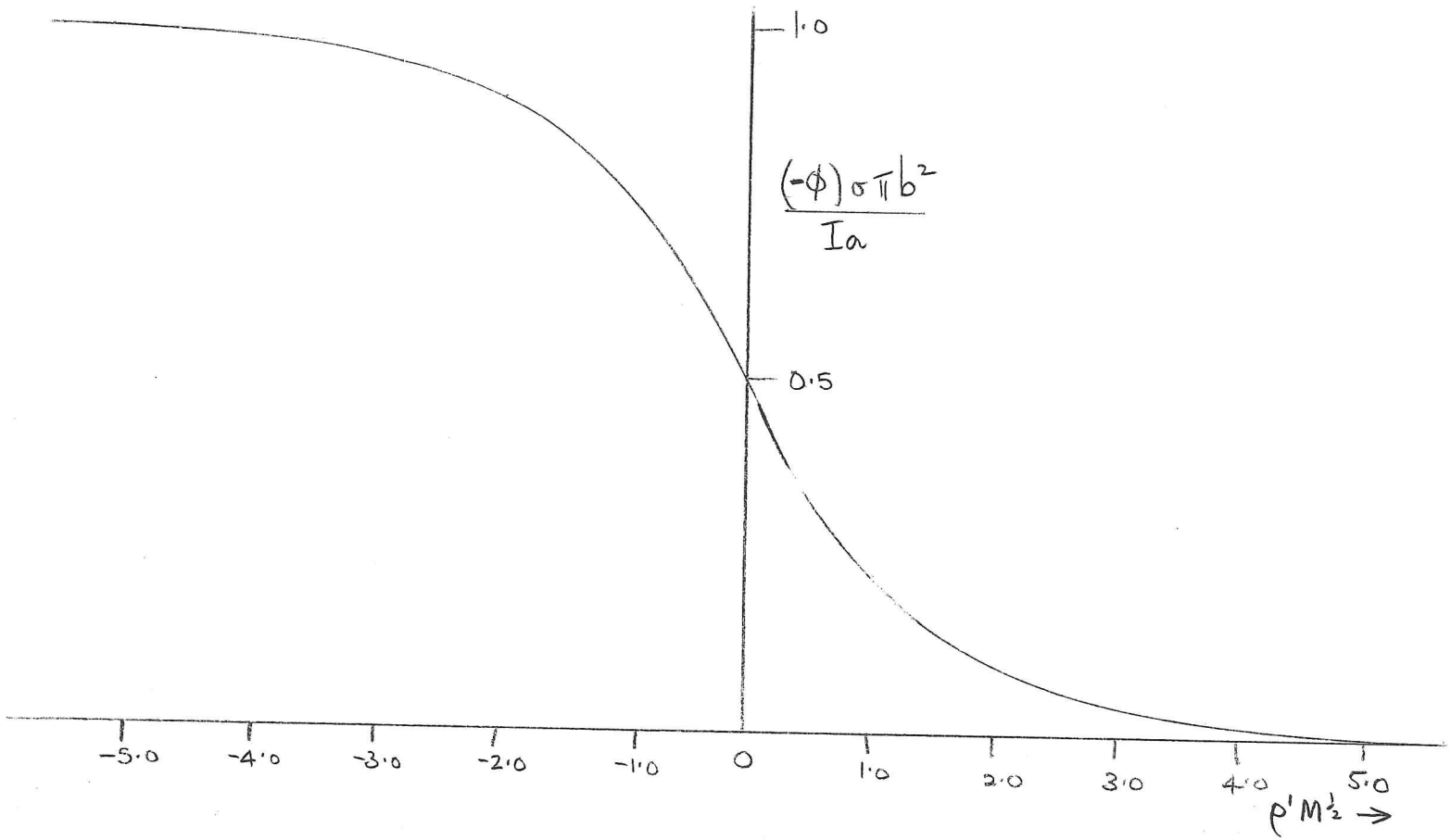

$v = 0$, $h = \rho/\ell^2$, in region (5)

$v = 0$, $h = 1/\rho$, in region (1)

$$v+h = \frac{\rho'}{\ell^2}\left[\frac{\ell}{\rho'} - \operatorname{erf}\alpha - \frac{1}{\alpha\sqrt{\pi}}\exp(-\alpha^2)\right], \qquad 3.3.22.$$

where

$$\alpha = \rho'\sqrt{M}/(2\sqrt{1-\zeta}).$$

$(v + h)$ for region (2b) can be calculated as before.

It is interesting to see how the electric potential varies along the electrode when we make the assumption that the current distribution is constant. Using the solution for region (2b) i.e.

$$v+h = \frac{\ell+\rho'}{\ell^2}e^{-M(1+\zeta)} + \frac{\rho'}{\ell^2}\left[\frac{\ell}{\rho'} - \operatorname{erf}\bar{\rho} - \frac{1}{\bar{\rho}\sqrt{\pi}}\exp(-\bar{\rho}^2)\right]\left[1-e^{-M(1+\zeta)}\right]$$

where

$$\bar{\rho} = \rho'\sqrt{M}/\sqrt{8},$$

we find $\partial h/\partial\zeta$ at $\zeta = \pm 1$ and hence,

$$\left.\frac{-\partial\Phi}{\partial\rho}\right|_{\zeta=1} = \left.\frac{\partial h}{\partial\zeta}\right|_{\zeta=1}$$

$$= M\left\{\frac{\rho'+\ell}{\ell^2} - \frac{\rho'}{\ell^2}\left(\frac{\ell}{\rho'} - \operatorname{erf}\bar{\rho} - \frac{1}{\bar{\rho}}\exp(-\bar{\rho}^2)\right)\right\}$$

Therefore,

$$\Phi_{\zeta=1} = \frac{2\phi\pi a}{I} = \frac{2}{\ell^2}\left[-1 + (\rho^{-2}+\tfrac{1}{2})(1+\operatorname{erf}\bar{\rho}) + \frac{1}{\sqrt{\pi}}\bar{\rho}\,e^{-\bar{\rho}^2}\right] \qquad 3.3.23.$$

A graph of $(\phi\pi b^2\sigma/Ia)$ against $\rho' M^{\frac{1}{2}}$ is plotted in fig.(3.9) and we see that the potential rises from its constant value in region (4) to half that value when $\rho = \ell$ or $\rho' = 0$. Note that, on $\zeta = 1$, Φ is negative and that this change in potential occurs in a distance $O(M^{-\frac{1}{2}})$, so that, as M increases, the potential across the disc near the edge of the disc becomes more nearly uniform. Thus for the potential across the electrode to be constant it follows that the current density near $\rho = \ell$ must increase, which we found when examining perfectly conducting electrodes. It also shows why in a finite conductor the distribution of the current density on the electrode or

is likely to depend on the value of M. As regards the flow, the chief significance of this potential rise is that it implies the existence of a current of density $O(M^{\frac{1}{2}})$ parallel to the electrode and consequently a velocity of $O(M^{-\frac{1}{2}})$ outside the Hartmann boundary on the electrode. When the potential of the electrode is constant, although a velocity of $O(M^{-\frac{1}{2}})$ exists outside the boundary layer on the insulator where $\rho' > 0$, there is no current parallel to the disc when $\rho' < 0$ and consequently there the velocity is zero, to first order.

We now show that if $f(\rho)$ is a function of $\rho'\sqrt{M}$ in region (2), then in region (1) the distribution of Φ for a given value of ζ is similar for all values of $M \gg 1$. If we let

$$f(\rho) = \frac{1}{\ell} + \frac{1}{\ell^2 M^{\frac{1}{2}}} g(\rho'\sqrt{M}),$$

then in region (1)

$$v + h = \frac{M^{\frac{1}{2}}}{2\sqrt{\pi(1-\zeta)}} \left\{ \int_{-\infty}^{0} \left(\frac{1}{\ell} + \frac{1}{\ell^2 M^{\frac{1}{2}}} g(t\sqrt{M}) \right) \exp\left(\frac{-(t-\rho')^2 M}{4(1-\zeta)} \right) dt \right.$$

$$\left. + \int_{0}^{\infty} \frac{\ell - t}{\ell^2} \exp\left[\frac{-(t-\rho')^2 M}{4(1-\zeta)} \right] dt \right\},$$

whence,

$$v = \frac{1}{4\ell^2\sqrt{\pi M}} \left\{ \int_{-\infty}^{0} g(2\sqrt{1-\zeta}\, t) \exp(-(t-\rho_-)^2)\, dt \right.$$

$$- \int_{-\infty}^{0} g(2\sqrt{1+\zeta}\, t) \exp(-(t-\rho_+)^2)\, dt - \int_{0}^{\infty} (2\sqrt{1-\zeta}\, t) \exp(-(t-\rho_-)^2) dt$$

$$\left. + \int_{0}^{\infty} (2t\sqrt{1+\zeta}) \exp(-(t-\rho_+)^2)\, dt \right\},$$

where

$$\rho_- = \rho'\sqrt{M}/(2\sqrt{1-\zeta}), \quad \rho_+ = \rho'\sqrt{M}/(2\sqrt{1+\zeta}).$$

Thus for given ζ, $v\sqrt{M}$ is a function of $\rho'\sqrt{M}$ only. (Note that the case of uniform current distribution is covered by this analysis). Now in region (1), since $\partial h/\partial\zeta = O(M^{-\frac{1}{2}})$ and $Mv = O(M^{\frac{1}{2}})$, it follows that $\partial\Phi/\partial\rho = Mv$ (3.3.24), as was first noted by Moffatt (1964). Thence

$$\Phi = \int_{0}^{\rho'} (M^{\frac{1}{2}} v)\, d(\rho'\sqrt{M}),$$

and therefore Φ is a function of $(\rho'\sqrt{M})$ only, for a given value of ζ.

We use the converse of this result in chapter 7 to deduce from our experimental results that $f(\rho)$ is a function of $\rho' \sqrt{M}$.

We now show how the resistance between the two discs may be calculated for an arbitrary distribution of current and why the resistance must always tend to the same limiting value as $M \to \infty$. We define the resistance, R, between the two discs as follows.

$$R = 2\Delta\bar{\phi}/I \qquad 3.3.25.$$

where

$$2\bar{\Delta}\phi = -\frac{1}{\pi b^2}\int_0^b \left[\phi(r)\right]_{-a}^{+a} 2\pi r\,dr,$$

is the mean value of the potential difference between the two discs. Since,

$$-\partial\phi/\partial z = \frac{1}{\sigma r}\frac{\partial}{\partial r}(rH_\theta),$$

$$2\bar{\Delta}\phi = \frac{2}{\sigma b}\int_{-a}^{+a} |H_\theta|_{r=b}\,dz,$$

which may be rewritten in a non-dimensionalized form as:

$$R = \frac{2}{\pi\sigma b}\int_{-1}^{+1} |h|_{\rho=\ell}\,d\zeta \qquad 3.3.26.$$

If $h = f(\rho)$ at $\zeta = \pm 1$, then in region (1) near $\rho = 1$, we can use the same formula to find $(v + h)$ in terms of $f(\rho)$, which we found in our investigation of perfectly conducting electrodes, namely,

$$v + h = \frac{M^{\frac{1}{2}}}{2\sqrt{\pi(1-\zeta)}}\left\{\int_{-\infty}^{0} f(r)\exp\left[-(r-\rho')^2 M/4(1-\zeta)\right]dr + \int_{\rho}^{\infty}\frac{1-r}{\ell^2}\exp\left[-r^2 M/4(1-\zeta)\right]dr\right\}.$$

Since $f = 1/\ell$ when $\rho = \ell$, (we are only considering region (1) and not considering any distinction between regions (2) and (3), as in our discussion of a perfectly conducting electrode), it follows that when $M \to \infty$

$$v + h = 1/\ell \quad \text{when } \rho = \ell.$$

Then, since v is antisymmetric in ζ,

$$\int_{-1}^{+1} |h|_{\rho=\ell} \, d\zeta = \int_{-1}^{+1} |v+h|_{\rho=\ell} \, d\zeta = 2/\ell ,$$

and from (3.3.26) it therefore follows that

$$R = R_\infty = \frac{2a}{\pi + b^2} . \qquad 3.3.27.$$

Note that this result only depends on the condition that $f = 1/\ell$ when $\rho = \ell$. It does not depend on the form of f and therefore the value of R will be the same whether the electrodes emit current at a constant potential or with a constant current density.

To calculate R when the current desnity is constant we use (3.3.26) whence

$$R = \frac{2}{\pi ab} \int_{-1}^{+1} \frac{1}{\ell} \left(1 - \frac{2\sqrt{1-\zeta}}{\sqrt{\pi}\, \ell M^{\frac{1}{2}}} \right) d\zeta ,$$

or

$$R = R_\infty \left(1 - \frac{1.064}{\ell M^{\frac{1}{2}}} \ldots \right) . \qquad 3.3.28.$$

Thus the form of the current distribution on the electrodes will only be indicated by how the resistance varies with M and not by its ultimate value. We expect the form of the variation of R with M to be similar for all types of electrode because the thickness of the region (1) is always $O(M^{-\frac{1}{2}})$ and therefore the current density in the z direction, for given I, is reduced by $O(\ell M^{\frac{1}{2}})^{-1}$. This implies that $(\partial\phi/\partial z)$ and consequently the resistance are also reduced by $O(\ell M^{\frac{1}{2}})^{-1}$.

4. On the use of pitot tubes and electric potential probes in MHD flows.

4.1. Introduction and summary.

In fluid mechanics and MHD when a flow can be theoretically analysed, e.g. Poiseuille flow in a tube, then measurements of pressure, electric potential, electric current etc, taken at the boundaries of the flow, e.g. on the walls of a duct or on the surface of an aerofoil, can be compared with those theoretically predicted and, if they are in agreement, the analysis is considered to be verified. However, if no such analysis has been made, then external measurements often give little indication as to the nature of the flow, and in that case direct, internal, measurements of velocity, electric potential etc, become necessary. To take such measurements we need to use pitot tubes, static pressure probes, electric potential probes, and hot wire anemometers to name a few.

In fluid mechanics we measure total and static pressure and velocity whereas in MHD we can measure several more variables, e.g. the electric potential and induced magnetic field (Ahlstrom 1964), so that in principle we have a further check on our measurements. However, this advantage is more apparent than real in that the difficulties of measuring all these variables are very much greater in MHD flows, in particular a magnetic field changes the relation between the velocity and the total pressure measured by a pitot tube, the velocity and reading of a hot-wire anemometer, and the electric potential and that measured by an electric potential (e.p.) probe. In this chapter we analyse the way in which these relations are affected for Pitot and e.p. probes. (D.G.Malcolm of the University ofWarwick is investigating the behaviour of hot-wire anemometers).

Most of the internal measurements of MHD flows have been in gases where the magnetic field has not been strong enough to induce errors in the probes, but where the errors, particularly with e.p. probes, have resulted from electronic and ionic phenomena. The only investigations of the continuum errors have been made by those interested in liquid metal flows, (as we are). Lecocq (1964) developed some of the basic theory of pitot and e.p. probes which we develop further, however his experiments were such that he could not test his theory since the magnetic

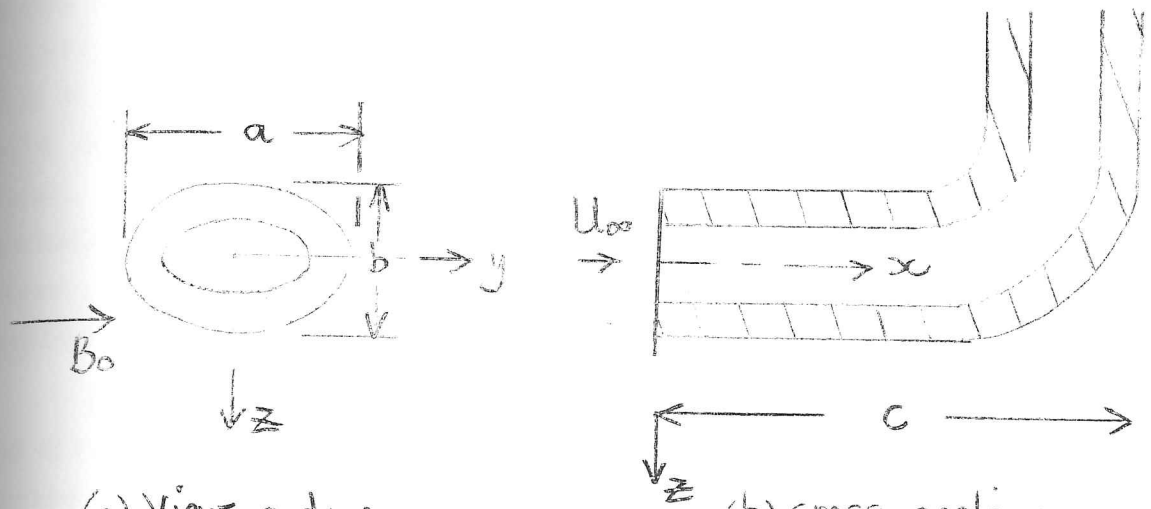

(a) View end on (b) cross-section

Fig 4.1. Notation for Pitot tubes and electric potential probes.

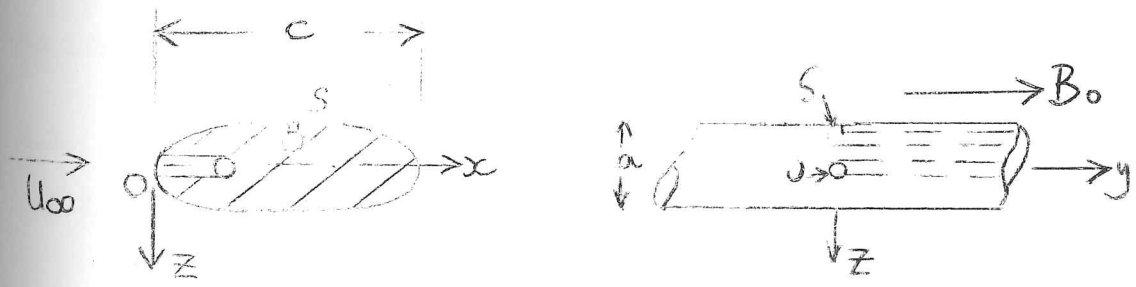

(a) section (b) view end on

Fig 4.2. Error free Pitot-static tube.

field effects were so small. He measured velocity profiles by means of Pitot and e.p. probes, but did not correlate his results between the probes and, since the flows were turbulent so that no theory for the velocity profiles exists, the experimental results could not be correlated with theoretical results. East (1964) performed some experiments on pitot tubes to determine the MHD errors involved in measuring uniform flows; he did not use the pitot to examine shear flows or flows with electric currents present. Moreau (1966) has used a pitot tube to examine turbulent velocity profiles where the MHD probe errors are negligible.

In §4.2 we consider Pitot tubes in uniform flows where the magnetic and electric fields are perpendicular to the flow and analyse in detail various special probes, finding that the MHD error is highly dependent on the probe shape. We then give a physical explanation for the prominent effects and discuss some of the practical consequences of our analysis.

In §4.3. we consider e.p. probes, though in this case we do consider the errors of using such probes in shear flows. We first find that with uniform flows there is no probe error, owing to the symmetry of the flow, but when the flows are non-uniform certain interesting effects occur. We examine these analytically and then discuss the physical reasons for the errors.

In chapters 7 and 8 we make use of the results of this chapter in the interpretation of our experimental results.

4.2. Pitot tubes

4.2.1. Non-dimensional equations, boundary conditions.

In this section we consider the relation between the pressure at the tip of a blunt body, i.e. a Pitot tube, and the velocity of the uniform flow impinging on it, and examine how this relation is affected by the application of a magnetic field to the flow. The three major assumptions we make are: (1) $R_m \ll 1$; (2) the velocity to be measured is uniform; (3) the shape of the probe near its tip is symmetric about the planes $y = o$ and $z = o$, with the point O, $x = y = z = o$, being the centre of the total pressure measuring aperture (See fig.4.1). If for

example the probe is supported by a stem well downstream of the tip, we assume its effect on the flow at the tip is negligible.

In order to non-dimensionalize the equations we use a characteristic length, d, which may for example be equal to a, b or c. Then the following forms are the most suitable for the non-dimensional variables:

$$\underset{\sim}{\tilde{v}} = \underset{\sim}{v}/\bar{u} = (u, v, w)/\bar{u},$$

$$\underset{\sim}{\tilde{b}} = \underset{\sim}{b}/R_m B_0, \quad \underset{\sim}{\tilde{j}} = \underset{\sim}{j}/\sigma \bar{u} B_0, \quad \tilde{p} = p/\rho \bar{u}^2$$

$$\tilde{\phi} = \phi/d\bar{u}B_0, \quad \tilde{x}, \tilde{y}, \tilde{z} = x, y, z/d, \quad \underset{\sim}{\tilde{y}} = \underset{\sim}{B_0}/|\underset{\sim}{B_0}| \qquad 4.2.1.$$

and $N = \sigma B_0^2 d/\rho\bar{u}$, $R = \bar{u}d\rho/\eta$, $R_m = \sigma\mu\bar{u}d$,

where $\bar{u}$ is a characteristic velocity (e.g. the value of u_∞ at y = z = o). Then the equations (2.2.1) to (2.2.6) become:

$$\left.\begin{aligned} (\underset{\sim}{\tilde{v}}.\nabla)\underset{\sim}{\tilde{v}} &= -\nabla\tilde{p} + N(\underset{\sim}{\tilde{y}} \times \underset{\sim}{\tilde{j}}) + \frac{1}{R}\nabla^2 \underset{\sim}{u}, \quad (a), \\ \nabla.\underset{\sim}{\tilde{u}} &= 0, \quad (b), \quad \underset{\sim}{\tilde{j}} = -\nabla\tilde{\phi} + \underset{\sim}{\tilde{y}} \times \underset{\sim}{\tilde{v}}, \quad (c), \\ \underset{\sim}{\tilde{j}} &= \frac{1}{R_m}\nabla \times \underset{\sim}{\tilde{b}}, \quad (d), \text{ and } \nabla.\underset{\sim}{\tilde{b}} = 0, \quad (e), \end{aligned}\right\} \qquad 4.2.2.$$

where $\nabla \equiv (\partial/\partial\tilde{x}, \partial/\partial\tilde{y}, \partial/\partial\tilde{z})$ (We assume the flow is steady). Since $R_m \ll 1$ we deduce from (4.2.2c) to (4.2.2e) that

$$0 = \frac{\partial \underset{\sim}{\tilde{v}}}{\partial y} + \frac{1}{R_m}\nabla^2 \underset{\sim}{\tilde{b}}, \qquad 4.2.3.$$

with an error of order R_m.

In specifying the boundary conditions in the free stream we consider some typical flows in which pitot tubes are likely to be used, which include the flows we examined experimentally, described in chapters 7 and 8. As regards boundary conditions on the probe we will consider two kinds of probe: (a) those which are non-conducting or, which amounts to the same thing, probes whose surface contact resistance is very large, (b) those whose conductivity is large compared to that of the fluid.

In the free stream (or $|\tilde{x}|, |\tilde{y}|, |\tilde{z}| \to \infty$),

$$\left.\begin{aligned} \underset{\sim}{\tilde{v}} &= \underset{\sim}{\tilde{v}}_\infty = (u_\infty, 0, 0), \quad (a) \\ \nabla\tilde{\phi} &= \nabla\tilde{\phi}_\infty = (0, 0, \frac{\partial\tilde{\phi}_\infty}{\partial\tilde{z}}), \quad (b) \end{aligned}\right\} \qquad 4.2.4.$$

whence $$\frac{\partial \tilde{p}_\infty}{\partial \tilde{x}} = -N(u_\infty - \partial\tilde{\phi}_\infty/\partial z), \frac{\partial \tilde{p}_\infty}{\partial \tilde{y}} = \frac{\partial \tilde{p}_\infty}{\partial \tilde{z}} = 0, \quad 4.2.5.$$

$$\left.\begin{aligned} \tilde{j}_{x_\infty} &= \frac{1}{R_m}\left\{\frac{\partial \tilde{b}_{z_\infty}}{\partial \tilde{y}} - \frac{\partial \tilde{b}_{y_\infty}}{\partial \tilde{z}}\right\} = 0, \quad \tilde{j}_{y_\infty} = \frac{1}{R_m}\left\{\frac{\partial \tilde{b}_{x_\infty}}{\partial \tilde{z}} - \frac{\partial \tilde{b}_{z_\infty}}{\partial \tilde{x}}\right\} = 0 \\ \tilde{j}_{z_\infty} &= \frac{1}{R_m}\left\{\frac{\partial \tilde{b}_{y_\infty}}{\partial \tilde{x}} - \frac{\partial \tilde{b}_{x_\infty}}{\partial \tilde{y}}\right\} = u_\infty - \partial\tilde{\phi}_\infty/\partial\tilde{z}\,. \end{aligned}\right\} \quad 4.2.6.$$

The conditions on the probe are:

a) Non-conducting probe

$$\left.\begin{aligned} \tilde{\underset{\sim}{v}} = 0\,, \quad \nabla\tilde{\phi}.\tilde{\underset{\sim}{n}} = (\nabla\times\tilde{\underset{\sim}{b}}).\tilde{\underset{\sim}{n}} = 0. \qquad (a) \\ \text{E.n} \end{aligned}\right\} \quad 4.2.7.$$

b) Highly conducting probe

$$\left.\begin{aligned} \tilde{\underset{\sim}{v}} = 0\,, \quad \nabla\phi.\underset{\sim}{s} = 0\,, \qquad (b) \\ \text{E.s} \end{aligned}\right\}$$

where $\tilde{\underset{\sim}{n}}$ and $\underset{\sim}{s}$ are vectors normal and tangential to the probe surface. We will assume that the highly conducting probe's walls are electrically insulated from the fluid inside the probe, to avoid a further source of error. (East (1964))

4.2.2. The general problem and some special cases.

In order to use the probe as a Pitot tube we have to calculate the pressure at the point 0, ($\tilde{p}_0$), either relative to the pressure far from the pitot or, if a pressure gradient exists in the free stream, relative to the pressure at 0 in the absence of the probe ($\tilde{p}'_0$). However, we first deduce an important symmetry condition relating to the general flow over a symmetric body, subject to the boundary conditions (4.2.4) and (4.2.7).

If we consider the governing equations written in terms of $\tilde{\underset{\sim}{v}}$ and $\tilde{\underset{\sim}{b}}$ so that:

$$\left.\begin{aligned} (\tilde{\underset{\sim}{v}}.\nabla)\tilde{\underset{\sim}{v}} &= -\nabla\tilde{p} + NR_m(\tilde{\underset{\sim}{y}}\times\nabla\times\tilde{\underset{\sim}{b}}) + \nabla^2\tilde{\underset{\sim}{v}}/R, && (a) \\ \nabla.\tilde{\underset{\sim}{v}} &= 0\,, && (b) \\ 0 &= \partial\tilde{\underset{\sim}{v}}/\partial\tilde{y} + \frac{1}{R_m}\nabla^2\tilde{\underset{\sim}{b}}\,, && (c) \\ \nabla.\tilde{\underset{\sim}{b}} &= 0 && (d) \end{aligned}\right\} \quad 4.2.8.$$

Then we see that if $\tilde{y} = -\tilde{y}$ the equations and boundary conditions are

consistent with the following result:

$$[u', v', w', \tilde{b}_x', \tilde{b}_y', \tilde{b}_z'] = [u, -v, w, -\tilde{b}_x, \tilde{b}_y, -\tilde{b}_z],$$

where the prime refers to the value of the variable at the same value of $\tilde{x}$ and $\tilde{z}$, but at $\tilde{y} = -\tilde{y}$. If $\tilde{z} = -\tilde{z}$ we have:

$$[u', v', w', \tilde{b}_x', \tilde{b}_y', \tilde{b}_z'] = [u, v, -w, \tilde{b}_x, \tilde{b}_y, -\tilde{b}_z],$$

where the prime now refers to the value of the variable at the same value of $\tilde{x}$ and $\tilde{y}$, but at $\tilde{z} = -\tilde{z}$. Thence we conclude that for the symmetric probes we consider, on the line $y = z = 0$,

$$v = w = \partial \tilde{b}_y / \partial \tilde{x} = \tilde{b}_z = 0, \qquad 4.2.9.$$

whatever the value of the magnetic field.

We now integrate (4.2.2a) from $\tilde{x} = -L$ to $\tilde{x} = 0$ along the line $y = z = 0$, where $L (\gg a/b)$ is such that $\lim_{L \to \infty} \tilde{q}(x = -L) = \tilde{q}_\infty$, where $\tilde{q} = (\tilde{v}, \nabla\phi, \nabla \times \tilde{b})$. Then, using (4.2.2.c) and $L \to \infty$ the result of our symmetry condition (4.2.9) we have:

$$\tilde{p}_0 - \tilde{p}_{\tilde{x}=-L} = \frac{\tilde{u}_\infty^2}{2} + N \int_{\tilde{x}=-L}^{x=0} (\partial\tilde{\phi}/\partial\tilde{z}^2 - u) d\tilde{x}$$

$$+ \frac{1}{R} \int_{x=-L}^{x=0} \left(\frac{\partial^2 u}{\partial \tilde{y}^2} + \frac{\partial^2 u}{\partial \tilde{z}^2} \right) d\tilde{x}. \qquad 4.2.10.$$

In this equation we have ignored the error due to the velocity not being zero at the aperture in the probe at $x = 0$, which is generally considered negligible. Now, when $R > 100$, even though the probe is used in a shear flow it has been shown experimentally that the error due to the viscous term is negligibe ($< 1\%$), (Rosenhead, 1964). (This assumes, of course, that the probe is not used in shear flows whose characteristic length is much less than d, though it may be of the same order). If $\partial\tilde{\phi}_\infty/\partial\tilde{z} \neq \tilde{u}_\infty B_0$, so that $\partial\tilde{p}_\infty/\partial\tilde{x} \neq 0$, we are interested in calculating $\Delta\tilde{p}$, where

$$\Delta\tilde{p} = \tilde{p}_0 - \tilde{p}_0'. \qquad 4.2.11.$$

Using (4.2.5) and assuming $R > 100$, we have

$$\Delta\tilde{p} = \frac{\tilde{u}_\infty^2}{2} + N \int_{x=\infty}^{x=0} \left(\frac{\partial}{\partial z}(\tilde{\phi} - \tilde{\phi}_\infty) + (\tilde{u}_\infty - u) \right) d\tilde{x}. \qquad 4.2.12.$$

In order to calculate the extra electromagnetic term, (the error), in general we need to solve the set of equations (4.2.2), using the boundary conditions (4.2.4) and (4.2.7). (We could concentrate solely on $\tilde{p}$, $\underset{\sim}{\tilde{v}}$ and $\underset{\sim}{\tilde{b}}$, but with less physical insight). However such a task is in general beyond us at the present time, so we concentrate on certain simplified situations.

(i) $N \ll 1$.

In many instances the value of N is low enough for us to make the approximation that $N \ll 1$ and that $\underset{\sim}{\tilde{v}}$, $\tilde{p}$, $\tilde{\phi}$ etc., may be expanded as a series in ascending powers of N, e.g.

$$\underset{\sim}{\tilde{v}} = (u, v, w) = (u_0, v_0, w_0) + N(u_1, v_1, w_1) + N^2(u_2, v_2, w_2) + \ldots \quad 4.2.13.$$

This approximation has often been used to examine the flow over bodies with various types of magnetic field and has been shown by Ludford to have certain singularities associated with it (Ludford, 1963). However, if we confine ourselves to examining the first order approximation only we avoid such difficulties. We will ignore boundary layer effects since $R \gg 1$ and $N \ll 1$, which means that we must reconsider the boundary conditions (4.2.7).

Using the expansion (4.2.11) and matching powers of N:

$$\Delta p_0 = \frac{u_\infty^2}{2}$$

and

$$\Delta p_1 = \int_{x=-\infty}^{\tilde{x}=0} \left[(u_\infty - u_0) - \left(\partial\tilde{\phi}_\infty/\partial z - \partial\tilde{\phi}_0/\partial z\right)\right] d\tilde{x}, \quad 4.2.14.$$

where u_0 is found from the potential flow solution over the pitot, and $\partial\phi_0/\partial z$ is calculated from

$$\nabla^2\phi_0 = \underset{\sim}{\tilde{y}} \cdot \operatorname{curl} \underset{\sim}{\tilde{v}}_0 = 0, \quad 4.2.15.$$

since $\underset{\sim}{\tilde{v}}_0$ is irrotational. The boundary conditions on ϕ_0 are:

$$\left.\begin{aligned} &\text{In the free stream: } \nabla\phi_0 = \left(0, \quad 0 \quad \partial\tilde{\phi}_\infty/\partial\tilde{z}\right) \\ &\text{outside the probe boundary layer:} \\ &(a)\ \left(-\nabla\phi_0 + \underset{\sim}{\tilde{y}} \times \underset{\sim}{\tilde{v}}_0\right) \cdot \underset{\sim}{\tilde{n}} = 0, \quad (b)\ \nabla\phi_0 \cdot \underset{\sim}{\tilde{s}} = 0 \end{aligned}\right\} \quad 4.2.16.$$

Since there is no general solution to (4.2.15) subject to the boundary conditions (4.2.16), we cannot write down a more easily calculable

expression than (4.2.14). However, there are two special cases where we can:

a) $N \ll 1$, $\nabla\phi_\infty = 0$, highly conducting.

In this case, if $\nabla\phi_\infty = 0$, the only solution to (4.2.15) subject to the boundary condition in the highly conducting probe i.e. (4.2.16b) is:

$$\nabla\phi_0 = 0,$$

whence it follows that (4.2.12) becomes simply:

$$\Delta\tilde{p}_1 = \int_{\tilde{x}=-L}^{\tilde{x}=0} (u_\infty - u_0)\, d\tilde{x} \quad . \quad * \qquad 4.2.17.$$

Knowing the potential solution, u_0, enables us to calculate $\Delta\tilde{p}$, directly. Note that in this case there is a static pressure gradient in the free stream and that to find $\Delta\tilde{p}$ one would normally make two measurements of $\tilde{p}_0 - \tilde{p}_{x=-L}$ and $\tilde{p}_{x=-L} - \tilde{p}_0'$, the first with the probe and the other in its absence. (In this situation $\partial\tilde{p}_\infty/\partial\tilde{y} = \partial\tilde{p}_\infty/\partial\tilde{z} = 0$ and we are assuming that static pressure can be measured error free at the boundary of the flow, e.g. pressure tappings on the wall of a duct).

b) $N \ll 1$, $a \ll b$.

When the pitot tubes shape is such that $a \ll b$, then near the centre of the probe the flow will be such that $\partial/\partial\tilde{y} \gg \partial/\partial\tilde{z}$ Then it follows from the fact that $\operatorname{curl} \underline{E} = 0$ that

$$\frac{\partial E_z}{\partial y} \simeq \frac{\partial E_z}{\partial x} \simeq 0,$$

so that we can regard E_z as approximately constant in the flow round the pitot. Then (4.2.14) becomes:

$$\Delta p_1 = \int_{x=-L}^{\tilde{x}=0} (u_\infty - u_0)\, d\tilde{x}, \qquad 4.2.18.$$

so that, in this case, knowing u_0 enables us to calculate Δp_1. Ostensibly this result is the same whatever the conductivity of the probe, but clearly if $\underline{E} = 0$ in the probe, unless the probe short circuits the external flow, our result is not valid and therefore the conductivity of the probe determines the ratio of a to b for the approximation to be valid. The application of the result (4.2.18) to a particular probe

* Lecocq (1964) appeared to be groping for this result, but his analysis contains so many obscurities as to be unintelligible.

should be made with care.

As an example we now evaluate Δp, for uniform flow over a two-dimensional probe with a square end. Using the potential flow solution of Milne Thompson (1962, pp 273-275), we find that

$$\Delta p_1 = \frac{u_\infty a/2}{d\pi},$$

so that $p_0 - p_0' = \frac{1}{2}\rho U_\infty^2\left(1 + \frac{\sigma B_0^2 a}{\pi \rho u_\infty}\right)$. * 4.2.19.

It is important to realise also that the degree to which the flow is two dimensional depends on the value of N.

(ii) $\underline{a \gg b}$

When the pitot tubes shape is such that $a \gg b$, then we can assume that $\partial/\partial y \ll \partial/\partial z$ in the centre of the probe, so that

$$\frac{\partial \tilde{j}}{\partial y} \simeq \frac{\partial \tilde{v}}{\partial y} \simeq 0, \qquad 4.2.20.$$

and therefore the flow over the pitot tube is unaffected by the magnetic field (Shercliff, 1965). Then we can express the non-dimensional $\underset{\sim}{j} \times \underset{\sim}{B}$ force $(-N\tilde{j}_z, 0, N\tilde{j}_x)$ as $(-\partial \tilde{b}_y/\partial \tilde{x}, 0, -\partial \tilde{b}_y/\partial \tilde{z})$ so that

$$\tilde{p}_{x=0} - \tilde{p}_{x=-L} = \frac{u_\infty^2}{2} - N\tilde{b}_{y\tilde{x}=0} + N\tilde{b}_{y_{x=-L}} \qquad 4.2.21.$$

Now in the free stream $\partial \tilde{b}_y/\partial \tilde{x} = \partial \tilde{b}_{y\infty}/\partial \tilde{x} = -\partial \phi_\infty/\partial \tilde{z} + u_\infty$, and by definition $\tilde{b}_{y(x=-L)} = (b_{y\infty})_{(x=-L)}$, so that

$$\Delta \tilde{p} = \frac{u_\infty^2}{2} + N\left(b_{y\tilde{x}=0} - b_{y\tilde{x}=0}\right). \qquad 4.2.22.$$

Now it also follows from (4.2.20) that (4.2.8) becomes:

$$0 = \nabla^2 \tilde{b}, \qquad 4.2.23.$$

whence we can calculate b_y, given the boundary conditions. We will again consider two special cases for which simple solutions exist.

a) $\underline{a \gg b,\ \tilde{j}_\infty = 0}$

If $\tilde{j}_\infty = 0$, $\nabla \times \underset{\sim}{\tilde{b}}_\infty = 0$ whence, using (4.2.23) and the boundary conditions on the probe (4.2.7), i.e. actually on the probe not at the edge of the boundary layer, it follows that $\nabla \times \underset{\sim}{\tilde{b}} = 0$ everywhere. Therefore (4.2.22) becomes:

---

* This result may be compared with example 4.13 in Shercliff's book where he finds the error for flow round a circular cylinder to be π times as great as this.

$$\Delta\tilde{p} = \frac{u_\infty^2}{2}$$

4.2.24.

This important result is valid for all values of N; again its limitation is that we do not know, except by more detailed calculation, what the ratio a/b needs to be for this result to be accurate. (The conductivity of the probe does not affect this result).

b) $\underline{a \gg b,\ a \gg c}$, probe used as Pitot-Static tube.

If now we consider the probe to be supported at $y = \pm\infty$, its length C being comparable with b, and if we also use the probe as a pitot-static tube, then we can show that such a probe is error free whatever the value of $\hat{j}_\infty$ and N, provided it is non-conducting. (This result has already been given by Lecocq, (1964)).

Let the probe be constructed as shown in figure 4.2, with a static pressure tapping (S) on the flat face at $\tilde{x} = t$, so that $\tilde{p}_s - \hat{p}(x=t, z=-\infty) = 0$. Now if the probe is non-conducting the boundary condition (4.2.7) leads to $\partial b_y/\partial s = 0$ along the surface of the probe whence the value of b_y at O is the same as that at S. From the conditions at infinity it follows that

$$\tilde{p}(x=t, z=-\infty) - \hat{p}(x=-L, z=0) = \tilde{E}_{y\infty}\big|_{x=-L} - b_{y\infty}\big|_{x=t}$$

and thence from (4.2.21) that

$$\Delta\tilde{p} = u_\infty^2/2$$

This result may be extended to compressible flows in that the electromagnetic error term is still zero. The use of a conventional pitot-static tube may incur large errors in such flows due to the Hall effect and therefore this result may be of some practical use in those circumstances, (Hunt, 1966c).

c) $\underline{a \gg b,\ a \gg c}$.

We examine a simple but unrealistic kind of pitot tube in order to calculate the error if $\hat{j}_\infty \neq 0$. We consider a non-conducting probe which is a circular cylinder of diameter non-dimensional $\tilde{a}$, whose centre is at $\tilde{x} = \tilde{a}/2$, $\tilde{y} = 0$, $\tilde{z} = 0$. Then to find the error, we have to solve (4.2.23) with boundary conditions:

Free stream: $b_{y\infty} = R_m(\tilde{x} - \tfrac{1}{2})\hat{j}_{z\infty}$; on the probe $\partial b_y/\partial\tilde{s} = 0$.

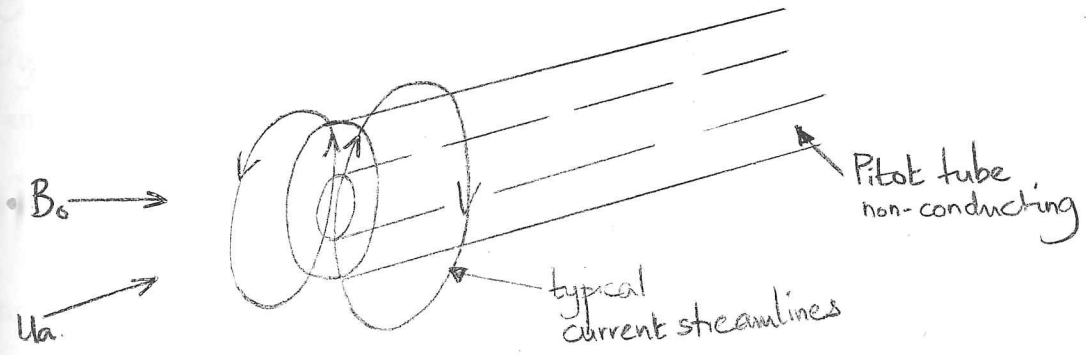

(a) $\underset{\sim}{j}_\infty = 0$ (3-D view of non-conducting probe.)

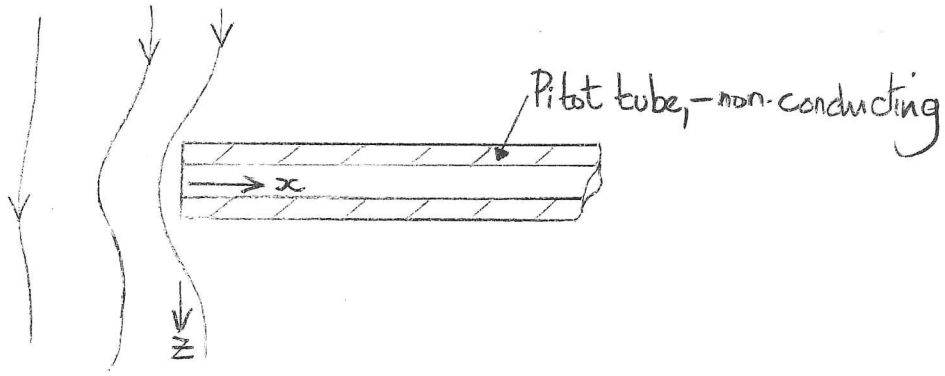

(b) $\underset{\sim}{j}_\infty = (0, 0, j_{z\infty})$. (Section thro' non-conducting probe)

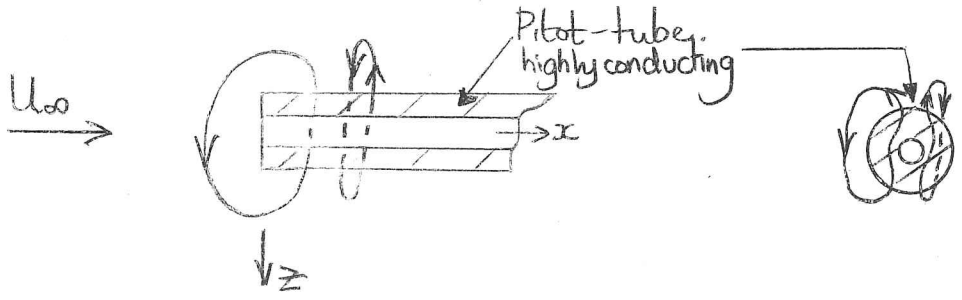

(c) $\underset{\sim}{j}_\infty = 0$, (Sections through highly conducting probe)

Fig 4.3 Current streamlines round Pitot tubes.

Then the solution for $\tilde{b}_y$ along the line $\tilde{y} = \tilde{z} = 0$ is:

$$\tilde{b}_y = \tilde{j}_{z\infty} \left(\frac{\tilde{x}^2 - \tilde{a}\tilde{x}}{-\tilde{x} + \tilde{a}/2} \right) Rm ,$$

and thence from (4.2.22) it follows that

$$\Delta\tilde{p} = \frac{u_\infty^2}{2} - N j_{z\infty} \tilde{a}/2 , \qquad 4.2.25.$$

which shows how in some circumstances the error can be negative.

4.2.3. A physical discussion of pitot tube errors.

In this section we consider the physical reasons for the MHD error in pitot tubes, where possible comparing our conclusions with the analysis of §4.2.2.

We examine two limiting situations for simplicity.

(i) $u_\infty = \partial\phi_\infty / \partial z$

In this case $j_{z\infty} = 0$, but, owing to the fact that u has to reduce to zero at the probe tip and that $\partial\phi/\partial z$ does not decrease proportionally, currents are induced in the vicinity of the probe. If the probe is non-conducting then the currents flow in the -z direction infront of the probe and return in the regions where the fluid moves faster (fig. 4.3a). If the probe is conducting then the electric field induces currents in the (-z) direction through the probe. Some of these currents return near the probe tip (as in fig.4.3b). Thus in the former case we expect that near the tip $j_z B_0 > 0$, and in the latter case $j_z B_0 < 0$. In (4.2.18) we showed that $\Delta p_i > 0$ when $a \ll b$ which agrees with our conclusion for a non-conducting probe. We noted in §4.2.2 that (4.2.18) is not a good approximation for a finite probe which was highly conducting in agreement with our physical reasoning which is also supported by the results of East (1964) who found experimentally that the error term was negative when the circular probe he used was highly conducting.

(ii) $\nabla\phi_\infty = 0$

In this case $j_{z\infty} = \sigma u_\infty B_0$ and $\partial p/\partial x = -\sigma u_\infty B_0^2$ so that near the probe tip where u decreases, j_z decreases and $\partial p/\partial x$ becomes less than its free stream value. Then, due to this effect, although the pressure at the probe tip may be less than the pressure far from the probe upstream, the pressure is greater than at the point $x = y = z = 0$ if no probe were

present, as demonstrated by (4.2.17).

When $j_{z_\infty} \neq 0$ there is another effect, namely that caused by the obstruction of the free stream current by the pitot tube. We showed in §4.2.2 how this can lead to an increase in j_z infront of the pitot so that $j_z B_o > j_{z_\infty} B_o$ and therefore the error may be negative. Fig 4.3(c).

Finally, we have to mention that, though the velocity distribution is altered as the magnetic field is increased, the only affect of this is to alter the term $N \int_{\tilde{x}=-\frac{t}{2}}^{\tilde{x}=0} (\hat{j}_{z_\infty} - \hat{j}_z)\, d\tilde{x}$ and not the dynamic pressure term, $\frac{u_\infty^2}{2}$, on account of the general result (4.2.9) of §4.2.2.

4.2.4. Conclusion.

The most significant result of our analysis of §4.2.2 is that, if we design a probe for which $a \gg b$, then if $\tilde{j}_\infty = 0$ we can use it as an error free pitot tube and if $\tilde{j}_\infty \neq 0$ we can use it as an error free pitot static tube. Therefore we expect that the shape of a pitot tube will have a significant effect on its behaviour when a magnetic field is present. It is important to note that one cannot imply from our results that the greater the ratio a/b the less the error because the velocity near the end of a conventional circular pitot tube increases as $(1-r^{-3})$ compared to a more two-dimensionally shaped pitot where it increases as $(1-r^{-2})$. Therefore, in the former case $\int_{\tilde{x}=-\frac{t}{2}}^{\tilde{x}=0} (u_\infty - u_o)\, d\tilde{x}$ maybe less than in the latter. Clearly the fact that no currents are induced as $a/b \to \infty$ finally reduces the probe error to zero when $\tilde{j}_\infty = 0$, but for finite values of a/b it is an open question as to which effect dominates. While increasing the ratio a/b lead to a reduction in probe error, clearly such a flattened tube is unpractical for examining Hartmann boundary layers but is very suitable for those on walls parallel to . Thus increasing a/b is not always possible.

It would seem that using conducting pitot tubes can lead to negative errors while non-conducting tubes have positive errors. However, any attempt to find that value of conductivity, σ_p, which leads to zero MHD error would be useless, since the error would only be zero in one or two situations. It is unlikely that a value of σ_p exists which gives no error in all circumstances.

We note that if the probe error is thought to be appreciable in a given MHD flow, then $\Delta\tilde{p}$ should be plotted against u_∞^2 and if the resulting curve is not linear, then some MHD error is present. We use this principle in the experiments described in chapters 7 and 8 to detect and measure the MHD error term.

We have not investigated the effects of a magnetic field on the behaviour of a pitot tube in a shear flow, but since for two-dimensional shear flow round a cylinder there is no effect on u along the line $y=z=0$ it would appear that the MHD error term is not greatly affected. However, this problem needs further investigation.

4.3. Electric potential probes.

4.3.1. On the use of such probes.

Electric potential probes were first used by Lecocq (1964) to measure the turbulent flow through a square duct. He was interested in comparing the results from those probes with those from pitot tubes and therefore had to convert his potential readings to velocities. From Ohm's Law, (2.2.3), and (2.2.8):

$$\nabla^2\phi = B_o(\nabla \times \underset{\sim}{v}), \qquad 4.3.1.$$

which may be integrated to find v_z in a fully developed duct flow:

$$v_z(x,y) = \frac{1}{B_o}\int_{-b}^{x}\left(\frac{\partial^2\phi}{\partial x^2} + \frac{\partial^2\phi}{\partial y^2}\right)dx, \qquad 4.3.2.$$

where the duct's walls are at $x = \pm b$, $y = \pm a$, and the magnetic field is in the y-direction. Using this equation one should be able, in such a high velocity flow as Lecocq's, to deduce the value of v_z in the boundary layers on the walls parallel to the magnetic field, and in the central region, but not in the boundary layers on the walls perpendicular to the field which entails measuring ϕ very accurately in the corners which cannot easily be done. Therefore we begin this section by noting that electric potential probes are most suitable for measuring electric potential, Φ, but if they are to be used to calculate the velocity then it is important to realise this involves even greater errors than those in measuring ϕ.

4.3.2. The general problem and some special cases.

We shall consider a probe whose external shape is similar to that of the pitot tube (figure 4.2). The difference is that we measure electric potential at O, $x = y = z = 0$, instead of pressure. Since the probe has to transmit its information of the potential at O to an instrument outside the fluid there has to be an electrically isolated region inside the probe, along its length, which may be an electric wire or simply the conducting fluid. (For a practical example of the type of probe used see figure 7.2). Since this 'information transmitting region' of the probe needs to be supported, (an electric wire being too weak), the probe has walls which may be electrically conducting or non-conducting. Thus the probe-fluid boundary conditions are the same as those for a pitot probe, i.e. (4.2.7). As regards the free stream boundary conditions they are the same as (4.2.4) only we now consider that $\partial\tilde{\phi}_\infty/\partial\tilde{y}$ and $\partial\tilde{\phi}_\infty/\partial\tilde{z}$ may be functions of y and z.

Using the same notation as in §4.2.2, the x-component of Ohm's law may be written:

$$\tilde{J}_x = -\partial\tilde{\phi}/\partial\tilde{x} - \tilde{w} \quad . \qquad 4.3.3.$$

Now if $\tilde{\phi}$ is to be measured in a flow determined by the free stream conditions (4.3.4) then we need to calculate $\Delta\tilde{\phi}$, where

$$\Delta\tilde{\phi} = \tilde{\phi}_o - \tilde{\phi}_{\tilde{x}=-L} \qquad 4.3.3.$$

$$\Delta\tilde{\phi} = -\int_{-L}^{o} \tilde{J}_x \, d\tilde{x} - \int_{-L}^{o} \tilde{w} \, d\tilde{x} \, . \qquad 4.3.4.$$

As in §4.2.2. we examine various special cases which can analyse in greater detail.

(i) Uniform free-stream flow and electric field.

If the probe is symmetric about y = o and z = o and if $\partial\tilde{\phi}_\infty/\partial\tilde{y} = 0$ and $\partial\tilde{\phi}_\infty/\partial\tilde{z}$ is uniform then we can use the result (4.2.9), which showed that on the line $\tilde{y} = \tilde{z} = 0$, $v = w = b_y = b_z = 0$, to deduce from (4.3.4) that

$$\Delta\tilde{\phi} = 0 \qquad 4.3.5.$$

This result was first proved by Lecocq, but for a restricted situation. Our result only assumes uniformity of the free stream conditions and of the probe shape, the value of N being arbitrary. (If $\partial\tilde{\phi}_\infty/\partial\tilde{y} \neq 0$ and $\partial\tilde{\phi}_\infty/\partial\tilde{z} = 0$, (4.3.5) still holds But if $\partial\tilde{\phi}_\infty/\partial\tilde{y} \neq 0$ and $\partial\tilde{\phi}_\infty/\partial\tilde{z} \neq 0$ and $B_0 \neq 0$, (4.3.5) does not).

(ii) a $\gg$ b. Non-uniform free stream flow.

In this and the next special case we consider the situation found in boundary layers parallel to the magnetic field in MHD duct flows and in the curious 'free' shear layers analysed in chapter 3, where, when $M \gg 1$,

$$\partial \tilde{\phi}_\infty / \partial \tilde{z} = u_\infty(z). \qquad 4.3.6.$$

$\partial \tilde{\phi}_\infty / \partial x$, $\partial \tilde{\phi}_\infty / \partial \tilde{y}$, and $\tilde{j}_\infty$ are $O(M^{-\frac{1}{2}})$ and may be ignored, when $M \gg 1$. We now attempt to estimate the probe error when the probe size is comparable with the distance, δ, in which u_∞ varies, since such situations arose in our experiments.

We make the assumption that $a \gg b$, so that $\frac{\partial}{\partial y} \ll \frac{\partial}{\partial z}$ and (4.2.8) becomes $\nabla^2 \tilde{b} = 0$. Then, since we assume that $j_\infty = 0$, whether the probe is conducting or non-conducting, it follows that $\tilde{j} = 0$. Thence (4.3.4) becomes $\Delta\phi = -\int_L \tilde{w}\, d\tilde{x}$. If we consider as an example a probe which is a circular cylinder with its axis $\tilde{x} = -b/2$, $\tilde{z} = 0$ and radius $b/2$, and if we assume that $\partial u_\infty / \partial \tilde{z}$ is a constant, then, using the standard result for an unconstrained shear flow over a cylinder, we find that

$$\Delta\tilde{\phi} = (\partial u_\infty / \partial \tilde{z})(\tilde{a}^2/4). \qquad 4.3.7.$$

Thus for a general shape of probe we expect that

$$\Delta\tilde{\phi} = O\left[(\partial \tilde{u}_\infty / \partial \tilde{z})\tilde{a}^2\right],$$

or, in normal variables, $\Delta\phi = O\left[a^2 B_0 (\partial u_\infty / \partial z)\right]$. 4.3.8.

In general of course w is less in a three-dimensional flow than a two-dimensional flow so that the estimate (4.3.8) will tend to be high.

(iii) a $\gg$ b. Boundary layer flow-probe on the wall.

When the probe is on the wall, $\tilde{z} = -\tilde{a}/2$, in a boundary layer flow, $u_\infty = \tilde{z}(\partial u_\infty / \partial z)$ where $\partial u_\infty / \partial z$ is a constant, then, of course, w is positive in contrast to the unrestrained shear flow where it is negative. For a two-dimensional probe square ended probe of width by considering the continuity of flow we easily deduce that

$$\Delta\tilde{\phi} = -\tilde{a}^2 (\partial u_\infty / \partial z)/8,$$

so that for a general flow we expect that

$$\Delta\phi = -O\left[B_0 (\partial u_\infty / \partial z) a\right], \qquad 4.3.9.$$

4.3.3. Physical discussion and conclusion.

We mention here briefly the physical reasons for the errors which may be made in using electric potential probes. The first point to be made about such a probe is that it is like a static pressure probe in that, unlike a pitot tube, it does not necessarily have to disturb the flow to perform its function. It does have to disturb the flow, however, in transmitting the information of the potential at a point to a measuring instrument outside the flow and the errors are incurred by the disturbance to the flow of the 'information transmitting region' of the probe.

If an electric potential probe is used in a fluid in which there is no flow but only electric currents, an error may be caused by the obstruction of these currents. We have shown in §4.3.2 that this effect only affects $\phi_{x=0}$ if the currents are non-uniform or are parallel to the x-axis of the probe, (in our notation of fig.4.1). In general the error in $\phi_{x=0}$ is easily seen to be $O\left[|j_\infty| d/\sigma\right]$

The second cause of error is due to the disturbance of the flow velocity. In fact, as we showed in §4.3.2, this only affects $\phi_{x=0}$ if the flow is non-uniform.

We may conclude our examination of these probes by saying that for most situations the powerful symmetry condition (4.3.5) ensures no probe error. But, if some non-uniformity of the flow or current exists, we can estimate the direction and the magnitude of the error. Finally we note that we have only considered a symmetric probe, whereas in fact most probes are supported downstream of their tip by a stem which only exists in one direction (fig.7.3). This may be a cause of error, e.g. it could short circuit the flow, but if it is far enough downstream should have negligible effect on the probe reading.

5. On the stability of incompressible flows in magnetohydrodynamics.

5.1. Introduction.

5.1.1. Summary.

The third part of this dissertation has three main aspects.

The first is an examination of the effect of a uniform magnetic field, $\underset{\sim}{B}_0 = (B_0 \cos\phi, 0, B_0 \sin\phi)$ on the stability of parallel shear flows described by:

$$\underset{\sim}{v} = (U_0(y), 0, 0)$$

The main result of our examination is that a magnetic field can never completely stabilize a parallel flow, i.e. stabilize it for all values of the Reynolds number.

The second is a new physical interpretation for the stability of MHD flows, thereby explaining some of the effects found in this dissertation as well as those found previously by others.

The third aspect is a demonstration how the results of investigating the stability of parallel flows can be used to examine the stability of the boundary layers found in the MHD flow in rectangular ducts, and the shear layers found in our study of electrically driven flows in part two.

5.1.2. Purposes.

Since still very little is known about the stability of viscous incompressible flows when there is no magnetic field present, it might be thought bold to attempt to understand the stability of MHD flows. However, in a few simple cases of rotating flows, the theory has been found adequate to predict the effect of a magnetic field on the onset of secondary flow, (Chandrasekhar, 1961), though there have been no experiments to confirm the theoretical predicitions for the onset of instability in parallel shear flows.

Despite the lack of experimental confirmation of the existing theory in parallel shear flows, we intend to develop it further; first, though, correcting some erroneous conclusions of previous workers. The reason for our interest in these flows is that we want to know, firstly,

how, if at all, the magnetic field stabilizes the various flows which it induces in rectangular ducts, as shown in part one, or in electrically driven flows, as in part two. Our second reason is that it is of some practical importance to understand the stability of the flows which are found in experiments used for examining very hot gases, e.g. in thermonuclear fusion research, where jets of highly conducting gas are injected along the magnetic field lines in the area where the magnetic field contains the plasma, as in the 'cusp' geometry, or where the gas is ejected along the field lines, as in the 'theta pinch' (Taylor and Weston, 1965).

5.1.3. Contents.

The major part of this chapter consists of the paper 'On the stability of parallel flows with parallel magnetic fields', Hunt (1965a) which is an examination into the effects of a uniform parallel magnetic field on the stability of plane parallel flows of fluids with finite viscosity and conductivity, uniform properties, and no free surfaces. We prove that, when a uniform magnetic field is parallel to the flow and sufficiently large, the wave number vector of the most unstable disturbance is not, in general, parallel to the flow, i.e. it is a three-dimensional disturbance. Our result invalidates the conclusion of Michael (1953) and Stuart (1954) who asserted that the wave number vector of the most unstable disturbance was parallel to the flow, i.e. a two-dimensional disturbance. Using this erroneous assumption, Stuart (1954), Velikhov (1959), and Tarasov (1960), examined the stability of plane Poiseuille flow with a parallel magnetic field. Drazin (1960) has examined some general aspects of the stabilizing influence of a parallel magnetic field on a plane parallel flow, also considering only two-dimensional disturbances. Wooler (1961) has examined the stability of a plane parallel flow when $R_m \ll 1$ and when the magnetic field lies in the plane of the flow but is not parallel to it. He found that three-dimensional disturbances can be the most unstable; however, he did not point out that, even when the magnetic field is parallel to the flow, three-dimensional disturbances can still be the most unstable. For all values of R_m we show how results obtained for two-dimensional disturbances can be modified to take into account three-dimensional disturbances

and thence draw some general conclusions about the stabilizing influence of a parallel magnetic field on a plane parallel flow. In particular we prove that a parallel magnetic field can never completely stabilize a flow, i.e. stabilize it for all values of the Reynolds number. (Our conclusions have recently been used by Abbas (1966) to investigate the stability of duct flows.)

In our paper we also discuss the stability of MHD flows from a new physical point of view so as to demonstrate that the effect of a magnetic field on small disturbances in an MHD flow is different from that in a static situation; usual discussions make no differentiation between these two situations. We first examine the currents induced by a disturbance, pointing out the important difference between electromagnetic and mechanical disturbances, and then examine the electromagnetic $\underline{j} \times \underline{B}$ force. By considering the rotationality of the $\underline{j} \times \underline{B}$ force we find under what conditions the magnetic field affects the forces acting on the disturbance. We particularly concentrate on the importance of the relative directions of the mean flow, the magnetic field, and the line along which the disturbance travels.

In §5.2 we examine the same situation as Wooler (1961), reaching the same conclusion when $R_m \ll 1$. We extend his analysis to include the case of R_m being arbitrary and then show that the stabilizing effect of a magnetic field which is not parallel to the flow is less than one which is parallel.

In §5.3. we discuss the stability of the boundary layers found in our examination of MHD flows in rectangular ducts in chapter 2, and the layers found in our examination of electrically driven flows in chapter 3. We conclude that the magnetic field has no effect on the disturbances which determine the onset of instability of these layers and therefore that the oscillatory velocity profiles found in Hunt (1965) and §3.2. are extremely unstable.

Finally we present an Appendix in which we expand on the derivation of the equations in §3.2 of Hunt (1965a).

5.2. Parallel flows with coplaner but non-parallel magnetic fields.

We now consider the stability of plane parallel flows $\left(\underline{U} = (U(y), 0, 0)\right)$ with magnetic fields which lie in the plane of the

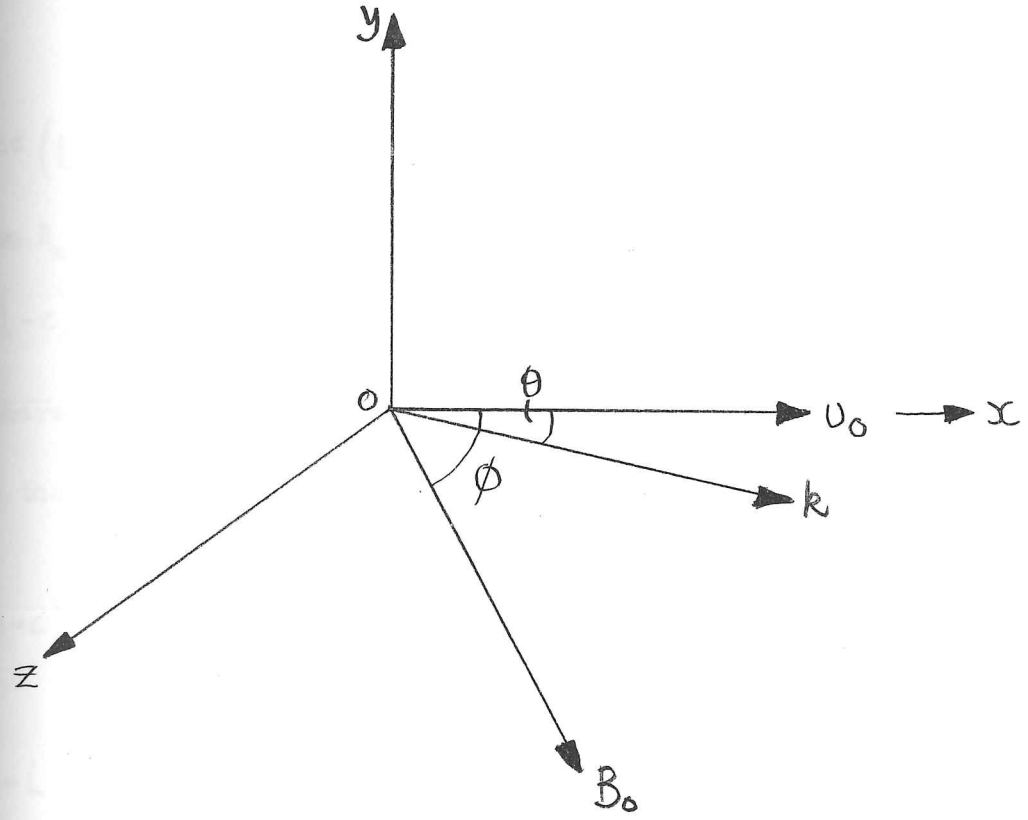

Fig 5.1. Notation of analysis of §5.2.

flow but are not parallel to it, $B_0 = (B_0 \cos\phi, 0, B_0 \sin\phi)$, (see figure 5.1). Wooler (1961) has deduced the equations of a disturbance travelling at an angle Θ to the main flow. Using the same notation as in §3 of Hunt (1965a) the equations are

$$(U-c)(v''-\lambda^2 v) - vU'' - \frac{B_0 \cos(\Theta-\phi)}{\rho \bar{u} \cos\Theta}(\psi''-\lambda'\psi) = \frac{-i}{\lambda \bar{R}}(v^{IV} - 2\lambda^2 v'' + \lambda^4 v) \qquad 5.2.1.$$

and $$(U-c)\psi - \frac{B_0 \cos(\Theta-\phi)}{\bar{u}\cos\Theta} = \frac{-i}{\lambda \bar{R}_m}(\psi''-\lambda^2\psi). \qquad 5.2.2.$$

When $R_m \ll 1$ these equations may be written as

$$(U-c)(v''-\lambda^2 v) - vU'' + i\lambda \bar{q} v = \frac{-i}{\lambda \bar{R}}(v^{IV} - 2\lambda^2 v'' + \lambda^4 v) \qquad 5.2.3.$$

where $$\bar{q} = \frac{\sigma B_0^2 l \cos^2(\Theta-\phi)}{\rho \bar{u} \cos\Theta} = \frac{q_0 \cos^2(\Theta-\phi)}{\cos\Theta} \qquad 5.2.4.$$

for the same reasons as given in §3.2 of our stability paper.

When R_m is arbitrary the equations may be rewritten in terms of :

$$\left[(U-c)^2 - \bar{A}^2 - \frac{iU''}{\lambda \bar{R}_m}\right](D^2-\lambda^2)\psi + 2U'(U-c)\psi'$$

$$= -i\left[\frac{(D^2-\lambda^2)[(U-c)\psi]}{\lambda \bar{R}} + \frac{(U+c)(D^2-\lambda^2)^2\psi}{\lambda \bar{R}_m} + \frac{(D^2-\lambda^2)^3\psi}{\lambda^2 \bar{R}\bar{R}_m}\right], \qquad 5.2.5.$$

where

$$A = \frac{B_0^2 \cos^2(\Theta-\phi)}{\mu \rho \bar{u}^2 \cos^2\Theta}.$$

We first consider the case where $R_m \ll 1$, then it follows from (5.2.4) that, given $\pi/2 > \phi > 0$, $\bar{q}$ is least when $\Theta \leq 0$ (in particular $\bar{q} = 0$ when $\phi - \Theta = \pi/2$) and for given $\Theta (<0)$ and q_0, $\bar{q}$ is less than its value when $\phi = 0$, since

$$q_0 \frac{\cos^2(\Theta-\phi)}{\cos\Theta} < q_0 \cos\Theta \text{ if } \pi/2 > \Theta > 0 \text{ and } \Theta < 0.$$

Then, if we assume that $\bar{R}_{crit.}$ increases as $\bar{q}$ increases, the lowest value of $R_{crit.}$ for given q_0 when $\pi/2 > \phi > 0$ will occur when $\theta \leq 0$ and from the previous result it follows that this value of $R_{crit.}$ is less than the lowest value of $R_{crit.}$ for the same value of q_0 when $\phi = 0$.

Thus, as Wooler pointed out, for a sufficiently large value of the magnetic field the most unstable disturbances travel at an angle $|\theta| > 0$ when the magnetic field is not aligned with the flow, i.e. $|\phi| > 0$. Wooler did not realise, however, that the most unstable disturbances also tend to travel at an angle $|\theta| > 0$ when $\phi = 0$. Also we see that when $|\phi| > 0$, the $q_0 - R_{crit.,min.}$ curve will lie below the curve deduced for $\phi = 0$. In other words a non-aligned magnetic field is less stabilizing than an aligned one, though we cannot find a simple construction in this case for determining the lowest value of $R_{crit.}$

When R_m is arbitrary and we have to consider the higher order differential equation (5.2.5) the problem is more complicated. When $\phi = 0$ the Alfvén number for the equivalent two-dimensional disturbance, $A = B_0/(\bar{U}\sqrt{\mu\rho})$ is the same for all values of θ whereas when $|\phi| > 0$ the Alfvén number of the distrubance, $A = B_0/(\bar{U}\sqrt{\mu\rho})$ varies with θ. Given $\pi/2 > \phi > 0$ and $\theta < 0$, then $\bar{A} < A$. Also, given θ, $\bar{R}$ and $\bar{R}_m$ are independent of ϕ. Then, if $R_{crit.}$ increases as A increases, for given $\bar{R}_m$, given $\theta (< 0)$ and $\bar{R}_m$, it follows that $\bar{R}_{crit.}$ and hence $R_{crit.}$ are lower when $\phi > 0$, since then $\bar{A} < A$. In other words, if the effect of increasing the conductivity (or R_m) and the applied magnetic field (or A) is to <u>stabilize</u> the flow, then a magnetic field which is not aligned with the flow will have reduced stabilizing influence. Clearly, if the effect of increasing the conductivity or the magnetic field is to <u>destabilize</u> the flow then we cannot predict whether an aligned or non-aligned field will have a more destabilizing influence.

We can now generalise the results of §3.3. and 4 of Hunt (1966a) and state that, when a magnetic field is coplanar with a parallel flow, in the sense we have defined, there is always some finite value of the Reynolds number for which the flow is unstable.

The other conclusion to be drawn from these equations is that when $\phi = \pi/2$ and $\theta = 0$ the equation for U (5.2.1), has no electromagnetic

term. Therefore, in this case the velocity perturbation is unaffected by the magnetic field and since this particular disturbance is the most unstable when there is no magnetic field, it follows that the stability of the flow is unaffected by the magnetic field when it is perpendicular to it.

5.3. On the stability of MHD flow in rectangular ducts.

Using the results of §3 of Hunt (1965) and §3.2 we now examine some general aspects of the stability of MHD flows in rectangular ducts. The conclusions we reach have already been used in the detailed discussion of the duct flows in chapter 2 (§2.4.2).

When there is no applied magnetic field, the velocity in a rectangular duct varies across the duct in the x and y directions. (We use the notation of fig.2.1). Very little theory has yet been developed for examining the stability of flows which vary in more than one dimension and none for the stability of laminar flow in a rectangular duct.

When B_o is such that $M \gg 1$, the problem is simpler since a uniform core flow develops in the centre and boundary layers form on the walls. Let us consider these boundary layers and the effect of the magnetic field on their stability, concentrating on the practical situations where $R_m \ll 1$.

Boundary layers of the walls ⊥⊥. These boundary layers always have the same velocity profile whatever the various wall conductivities, the thickness of these layers being $O(M^{-1})$. In examining the stability of these layers we must consider the induced magnetic field, B_z, as well as the applied field, B_o. Although the induced field, B_z, has no effect on the mean flow it may influence the stability of the flow. It is easily seen that the maximum value of $B_z = O(R_m) B_o$, when $R_m \ll 1$. Therefore before ignoring this term it is advisable to calculate the value of $q_o = \sigma B_o^2 \delta / \rho V_c$, where δ is the boundary layer thickness and V_c is the core velocity. Thus for the effects of B_z on the stability of boundary layers on ⊥⊥ to be negligible, it is necessary that

$$M R_m^2 / R \ll 1.$$

The stability of these layers was first examined by Lock (1955) who assumed $R_h \ll 1$ and that B_z was negligible. He found that the magnetic field has a negligible effect compared to that of viscosity on the velocity perturbations, even though the interaction parameter, q_o, for the boundary layer, $= O(M/R)$, is of the same order in M and R as the reciprocal of the local Reynolds number, also $O(M/R)$. (In the case of the flows we examined where $\underline{B}_o$ was parallel to $\underline{U}$, q_o and R^{-1} were not related since $\underline{B}_o$ and $\underline{U}$ could be varied separately.) Thus the magnetic field tends to make such boundary layers stable by affecting the mean velocity profile rather than the actual disturbances. Lock's conclusion was that the flow is unstable when $R > 50,000M$.

Boundary layers on the walls AA. The velocity profile in the boundary layers on the walls AA depends on the conductivity of the various walls, but there is one property in common of all such boundary layers which is that their thickness is $O(M^{-\frac{1}{2}})$. Therefore, though the velocity varies in the y-direction, in these layers $\frac{\partial}{\partial x} \gg \frac{\partial}{\partial y}$ and at any value of y we can consider the velocity profile to be a function of x only, i.e.

$$\underline{U} = (0, \quad 0, \quad U(x)).$$

If the induced field is to be negligible,

$$M^{3/2} \, R_{mc}/R \ll 1,$$

where R_{mc} is based on the core velocity and R is based on a and the maximum velocity in the boundary layer, and then we need only consider the effect of

$$\underline{B}_o = (0, \quad B_o, \quad 0).$$

This combination of mean flow and magnetic field is the same as that mentioned in §5.2 for $\phi = \pi/2$ when we showed that in this case the magnetic field has no effect on the most unstable disturbances, i.e. those travelling parallel to $\underline{U}$. The physical reason for this was made clear in §2 of Hunt (1965) where we showed that if the vorticity of a disturbance is parallel to $\underline{B}_o$ it is unaffected. Therefore we can examine disturbances of the form:

$$u = \left(u(x) \exp\left[i(\alpha z - \beta t)\right], 0, w(x) \exp\left[i(\alpha z - \beta t)\right]\right)$$

by the usual Orr-Somerfeld equation, and conclude that the onset of instability is unaffected by the magnetic field. However, since it has been shown experimentally and theoretically that at large growth rates

the disturbances growing most rapidly are often three-dimensional, it seems that the magnetic field must affect the ultimate transition to turbulence of the boundary layer flow.

Two-dimensional shear layers.

It is interesting to note that in the two-dimensional electrically driven flows examined in §3.2, the vorticity of the shear layers away from the walls is parallel to the magnetic field, B_o and consequently the most unstable disturbances, whose vorticity is parallel to that of the mean flow, are unaffected by B_o. This shows that the flows predicted are likely to be highly unstable.

Appendix to chapter 5.

In this appendix we discuss the approximations made in deducing equation (3.5) from (3.4) in §3 of Hunt (1965a). This approximation which is the same as that made by Stuart (1954), has been criticised for its reasoning by both Hains (1965) and Tatsumi (1962), though they both agreed with Stuart's results. Put simply, their objection was that, if

$$\frac{|b|}{B_o} = O\left[\frac{|u|}{|U|}\right]$$

then the correct approximation for ψ in (3.4) when $R_m \ll 1$ is:

$$\psi'' - \lambda^2\psi = \frac{c\alpha R_m}{i}\psi$$

What this implies physically is that the oscillations in b induced by an oscillating field outside the fluid are much larger than those induced by the velocity perturbations. However the oscillations thereby produced in u are of such a high frequency that they cannot be amplified by the mean flow and are damped by viscosity. If β is low enough for

$$\psi'' - \lambda^2\psi = 0$$

then there is no electromagnetic force term in (3.3) and therefore, when oscillations in b occur of this magnitude they have no effects on the stability of the flow.

However, if $|b|/B_o = O[R_m] = |u|/|U|$,

and if only the oscillations of wavelength $O[l]$ and frequency $O[U/l]$,

are considered, (3.4) becomes:

$$-\frac{B_0 v}{U} = \frac{-i}{\alpha R_m}\left(\psi'' - \lambda^2 \psi\right). \qquad 3.2.5.$$

This approximation must be justified, a posteriori, in any particular case using the values of α and c found in the analysis, but in all known cases this approximation has been found to be valid for disturbances of interest.

6. Experimental apparatus.

6.1. Introduction.

6.1.1. Purpose of experiments.

The main object of the experiments described in chapters 7 and 8, was to investigate certain flows by means of direct measurements of velocity and electric potential (e.p), using Pitot and e.p. probes. There were four main reasons for these investigations. The first was to confirm, at least qualitatively, the existence of some of the remarkable phenomena predicted by the theory of chapters 2 and 3, which occur when $M \gg 1$. The second was to see whether the results of the two probes could be correlated against each other. The third was to use the probes to measure the velocity and potential in some simple, well understood, MHD duct flows and compare the results with those calculated from external pressure measurements in order to calculate the probe errors induced by a magnetic field; we hoped, thereby, to confirm some of the ideas of chapter 4. The fourth reason was to show that the use of such probes can indicate how unstable and turbulent flows develop, in a way that external measurements cannot.

Although there are still some experiments which need doing, the study of MHD duct flows, turbulent and laminar, by means of external measurements of static pressure and electric potential has now provided virtually as much information as it can about the internal mechanics of the flow. Owing to the paucity of the theory of unstable and turbulent MHD duct flows, we can only extend our understanding by internal flow measurements. (For the latest review of the duct flow literature see Branover, et al (1966)). This was the reason for Branover & Lielausis (1962), Lecocq (1964), and Moreau (1966) using probes in mercury flows, and clearly many more workers will have to in the future. Therefore we hoped that an investigation into the use of such probes in known or approximately understood flows would enable future experimentalists to have greater confidence in the use of these probes.

6.1.2. Requirements of the apparatus.

The apparatus which was needed for our experiments had to have

five main elements. We outline here the main requirements for each of these:

(i) The electro-magnet had to satisy three criteria; the first was that the magnetic flux density, B_o, and the gap between the pole pieces, 2a, were great enough to satisfy the condition that $M \gg 1$, where $M = B_o a(\sigma/\tilde{\eta})^{\frac{1}{2}}$, because we were interested in the curious flows which then occur; the second was that the gap be great enough for the boundary layers and shear layers which occur when $M \gg 1$ to be investigated by probes, the smallest of which were about .025" in diameter; the third was that the length of the magnet, l, be great enough for laminar, and, if possible, turbulent, flows to become fully developed when $M \gg 1$. The criterion for the development of laminar flows in a non-conducting pipe is that $l \simeq aR/M$, where R is the Reynolds number, so that, for given M, l was determined by the minimum value of R for accurate enough readings to be taken with the pitot and e.p.probe. We do not have a criterion for the development of MHD turbulent flows; this needs finding out. Shercliff (1956)

(ii) A rectangular duct was needed in which we could investigate the flows analysed in §2.4 and, if possible, many other kinds of flow as well. The requirements of the duct we designed were these; firstly that its walls perpendicular to the magnetic field (BB) should be such as to have no contact resistance with mercury and to have a very much lower resistance than that of the volume of mercury in the duct, i.e. $\Delta_B \left(= \sigma_w w/\sigma a\right) \gg 1$, where σ_w is the wall's conductivity and w its thickness; secondly that $w \ll a$ so that the distance in the fluid parallel to the magnetic field should be maximised; thirdly the walls of the duct parallel to the magnetic field (AA) had to be non-conducting. We also hoped to design the duct so that the conductivity of its walls could be changed and that its walls could be removed to insert smaller ducts inside, to place bodies in the flow or to place grids in the flow for turbulence experiments, in other words design the duct as a flexible 'mercury-tunnel'.

(iii) A probe mechanism was needed to move the probes in the plane perpendicular to the axis of the duct, i.e. x-y plane.

(iv) A flow circuit was required to pump mercury through the duct

Fig 6.1. I – B_0 curve of electromagnet calibration.

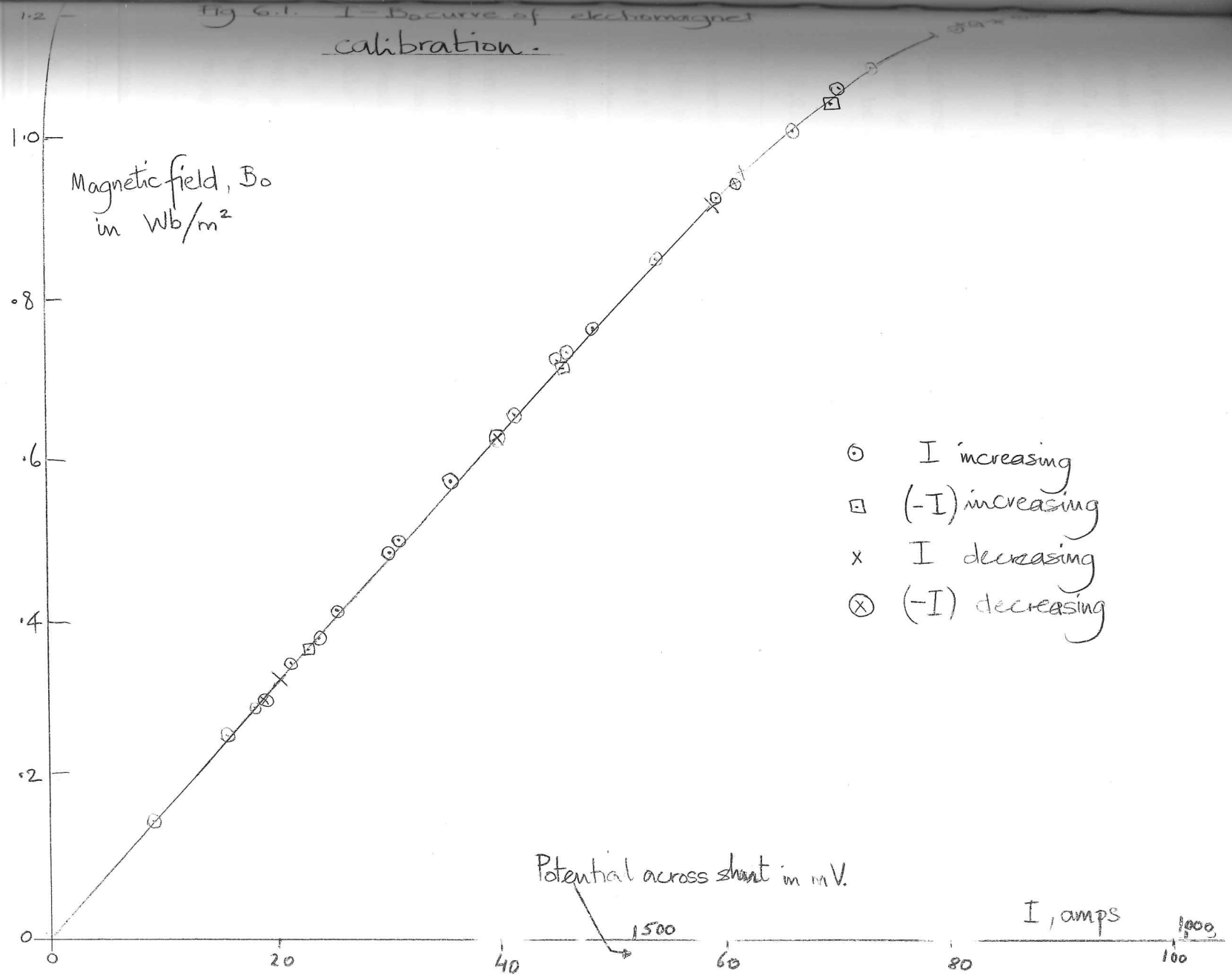

at rates varying from approximately .004 litres/sec to .05 litres/sec, these flow rates corresponding to Reynolds numbers of about 250 to about 3000, i.e. the range in which Alty found the duct flow, described in §2.4, unstable. Also a flow meter was required to measure these flow rates.

(v) Instruments: we needed a manometer to measure as low pressure differences as possible ($\simeq$ .020" meths), consistent with a reasonable time to take a reading and with the fast flows to be measured would not all be completely steady. We also needed a sensitive potentiometer.

6.2. The electromagnet.

Having considered the requirements for the magnet and its cost, we ordered an electromagnet from Lintott Engineering. The magnet has an iron core and is energized by water-cooled copper coils which are wound so as to be flush with the pole faces of the magnet; the coils can take up to 60 volts at 1000 amps, D.C. The pole face area is 60" x 9" and the gap between the poles is 3".

We calibrated the magnet by measuring the flux density, B_o, in the centre of the gap with a search coil and Cambridge fluxmeter, as a function of the potential across a shunt placed in series with the magnet. We measured the hysteresis affect on B_o, but no discernible effect was found (fig.6.1). We then measured the flux density near the edge of the pole faces to examine the uniformity of the field, finding that when $B_o = .78 \text{ wb/m}^2$ the field was uniform to within $\frac{1}{2}\%$ over a volume 60" x 3" x 3" but when $B_o = 1.24 \text{ wb/m}^2$ the field was uniform to within $\frac{1}{2}\%$ 8" in from the edges of the pole faces, 1%, 2" in, and 6% over the 60" x 3" x 3" volume.

The cooling water rate required for the magnet is about $3\frac{1}{2}$ g.p.m. a pressure switch setting off an alarm if the flow dropped below this rate. The magnet pole faces tend to move together as the current is increased so spaces are needed to prevent this distortion; lengths of 1" brass rod were found to be sufficiently strong.

6.3. The rectangular duct.

To satisfy the requirements that $d_A \gg 1, \omega \ll a$, and that no contact

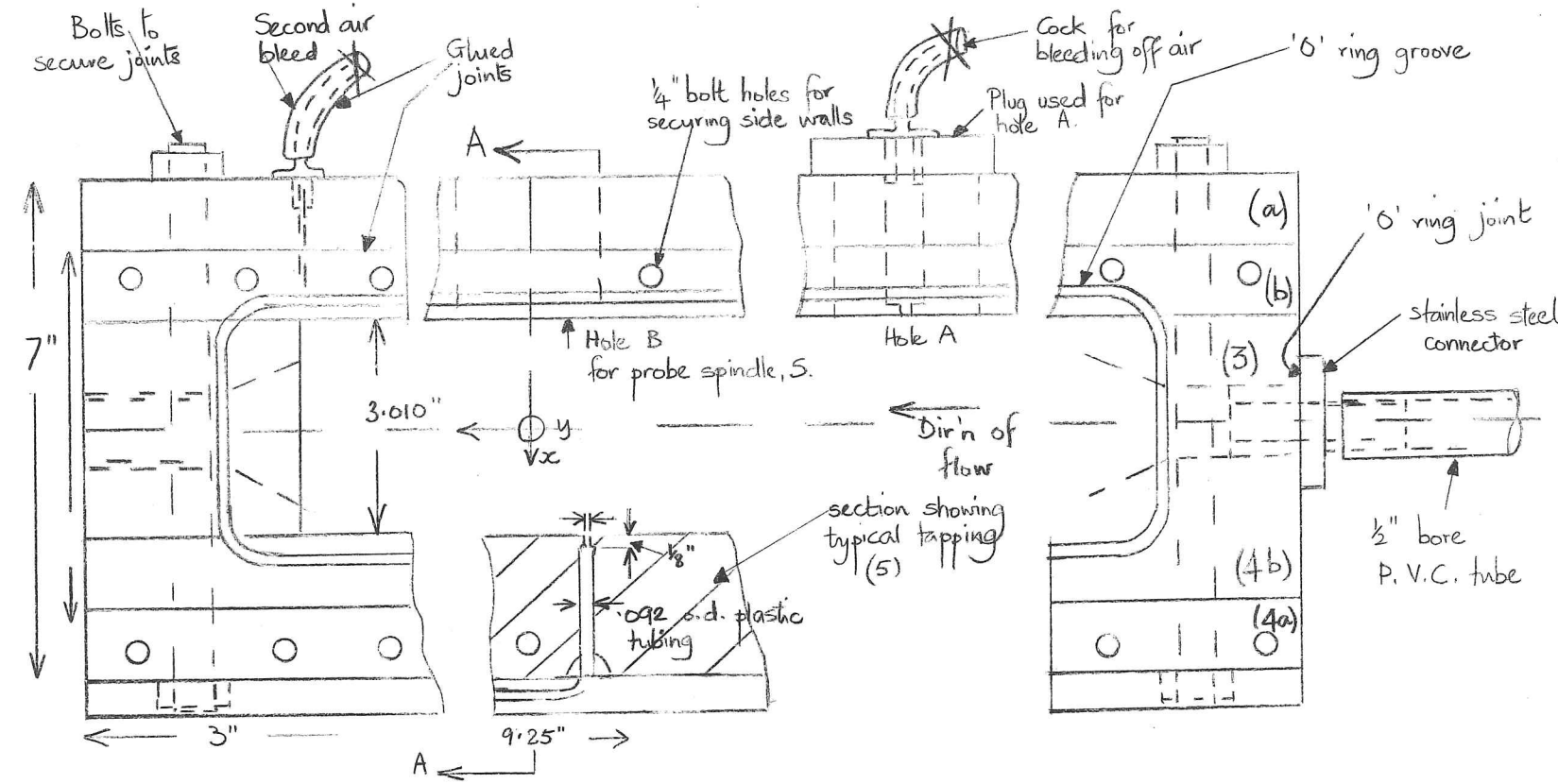

(a) Side view with copper side walls removed, showing section thro' bottom of duct at typical tapping (5) and stainless connectors

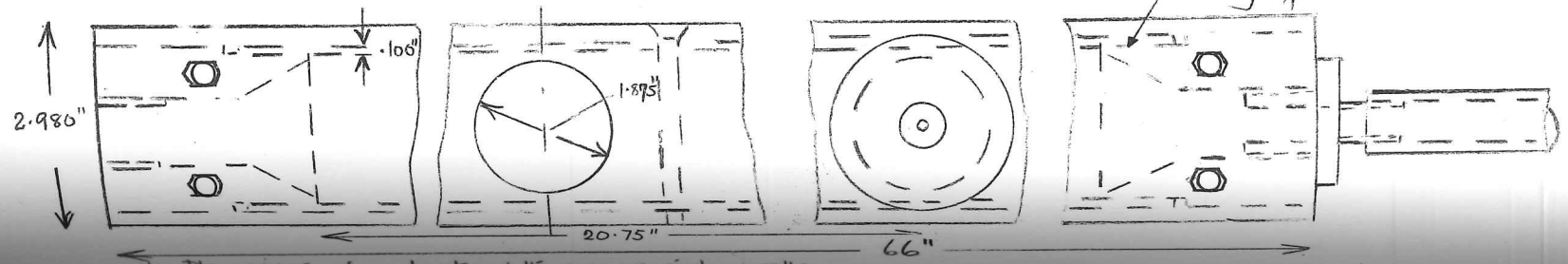

(b) Plan views of duct with copper side walls.

Fig 6.2. Main, 66" long duct. (approx to scale : 1 cm = 1 inch)

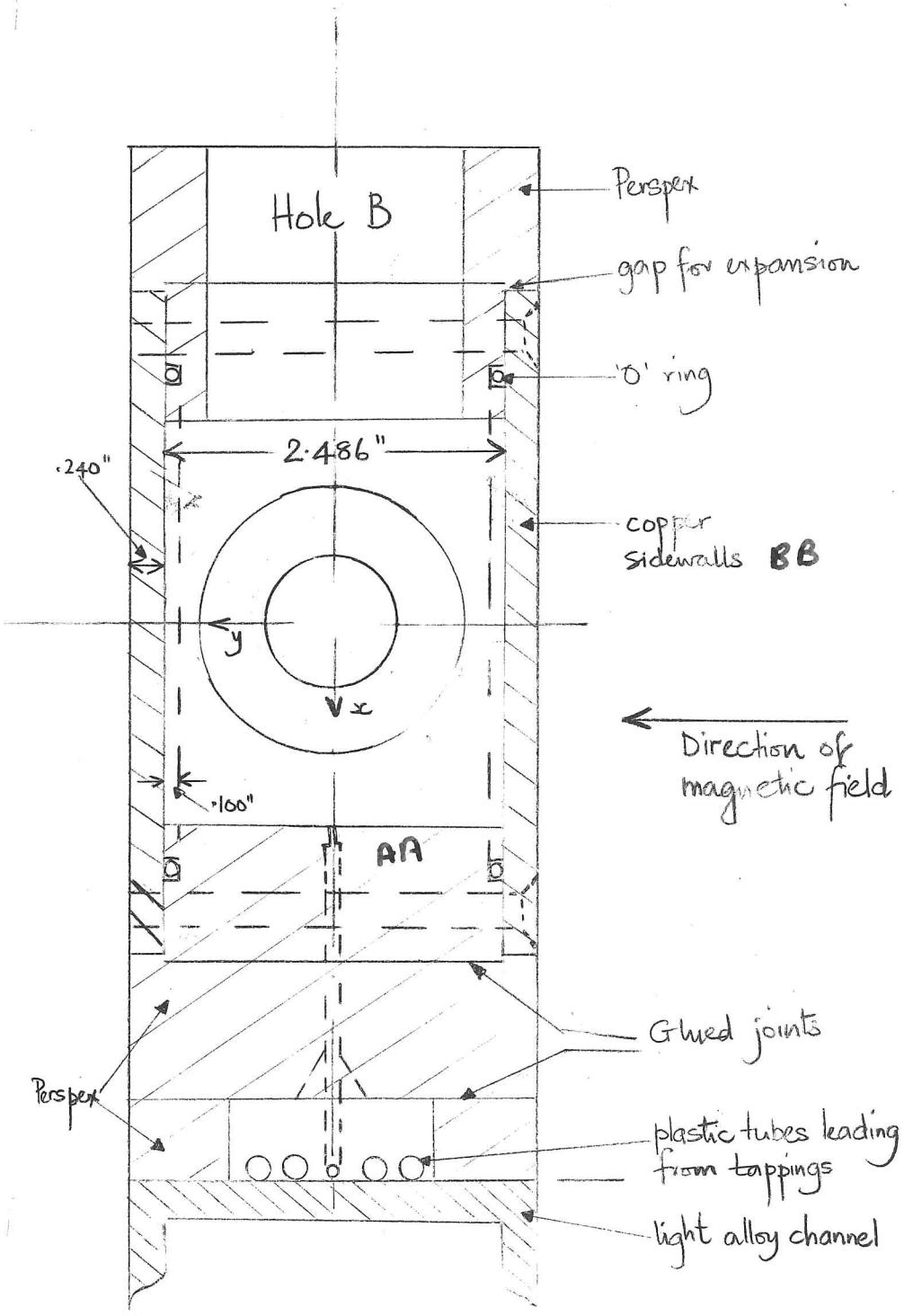

Fig 6.2 (c) Section AA showing duct supported on light alloy channel.

resistance should be present in the walls (AA), the only ~~must~~ suitable metal is copper. To satisfy the requirement that the walls (AA) be non-conducting, we could either have used metal walls and covered them with a non-conducting layer, e.g. sellotape, or used a non-conducting material such as 'Perspex'. The problem lay in sealing the duct. The first point to establish on a small scale duct was whether it was possible to construct a duct in which all 6 constituent parts, i.e. the 4 walls and the 2 end pieces for connecting the duct to the flow circuit, could be assembled without permanently joining any of them, e.g. by glueing or welding, but by bolting them together and mechanically sealing them e.g. by rubber sheets and 'O' rings. All attempts at this, the ideal solution, failed, because leaks developed. There were then two remaining solutions; we could either make the 2 walls AA and the 2 end pieces out of one piece of copper, as Alty (1966) did, or we could weld or glue the pieces together, in either case sealing the hole thus formed with the walls AA. This solution was rejected, firstly because to machine a hole 60" x 3" x $2\frac{1}{2}$" out of a piece of copper 66" x 3" x 3" is wasteful and very difficult, and secondly because all our attempts at welding copper failed. (Glueing was out of the question because of the way in which mercury amalgamates with copper, (Alty, 1966)).

The second solution was either to make the walls AA and the end pieces out of one piece of copper or Perspex, or again to permanently join them. After our previous experience with welding copper, the simplest solution was to make the walls AA and the end pieces from Perspex and to glue them together. Then the walls BB would consist of 2 standard copper $\frac{1}{4}$" strips bolted to each other through the Perspex, the seal being made by an 'O' ring seated in a continuous groove cut into the side of the walls AA and the end-pieces. A small scale duct was constructed to this design, filled with mercury, and found not to leak. (This small scale duct was later used for the electrically driven flow experiments described in chapter 7, and is shown in fig.7.1).

We then designed a large scale duct, which is shown in figure 6.2. The Perspex part of the duct was made up from 6 separate pieces labelled 1a, 1b, 2, 3, 4a and 4b, the various parts being glued together as shown in the drawing. Great care was taken in the fabrication of the duct to

see that parts were glued together only after they had been stress relieved by annealing; also the various parts were always annealed after rough machining and before the final machining was done. (Where Perspex was used in other parts of the flow circuit and not annealed before glueing, the joints sometimes tended to leak; where Perspex was machined, but not annealed, it tended to craze under stress).

The machining of such a long piece of Perspex was difficult because of the tight tolerances required, particularly on the 'O' ring groove, and also because of the considerable thermal expansion of Perspex. The 5" x $\frac{1}{4}$" copper strips which were used for the walls AA were ground and polished to remove surface blemishes and enable a smooth amalgam to be formed. They were then drilled and tapped to take the Aluminium Bronze retaining bolts.

We now mention some further details of the design. Perhaps the most striking point about the duct to a fluid dynamicist is the fact that the flow entering the duct diverges rather than converges, so that the flow would not settle down by the time it reached the end of the duct. The reason for our design is that a magnetic field forces a flow to settle down in a shorter length and tends to suppress the eddying motion characteristic of rapidly diverging flows. Clearly, if flows are to be examined when the ratio M^2/R is very small then a new design will be required. The tappings were made along the centre line of the Perspex wall using the method of Alty (1966), and some were made along a line at right angles to the wall under the rear probe position. (The reasons for their positions will be given in chapters 7 and 8). These tappings could be used for either pressure or potential measurements. The very narrow, (.062" i.d., .095" o.d.), P.V.C. tubes which were glued into the tappings were joined to wider tubing about an inch downstream of the tapping in the cavity under the duct, this tubing in turn being joined to $\frac{1}{4}$" i.d. tubing outside the duct; the method of jointing these tubes was again the same as that of Alty. Note the presence of two air bleeds at the extreme downstream end of the wide porition of the duct and in the plug used to block the hole A, which was not used in these experiments; they were used for expelling all the air from the duct when filling it and enabling the duct to be emptied.

fig 6.3. Plate mechanism

(a) Plan view (letters A, B, C etc – described in text and fig 6.3.(b))

Scale : Full scale

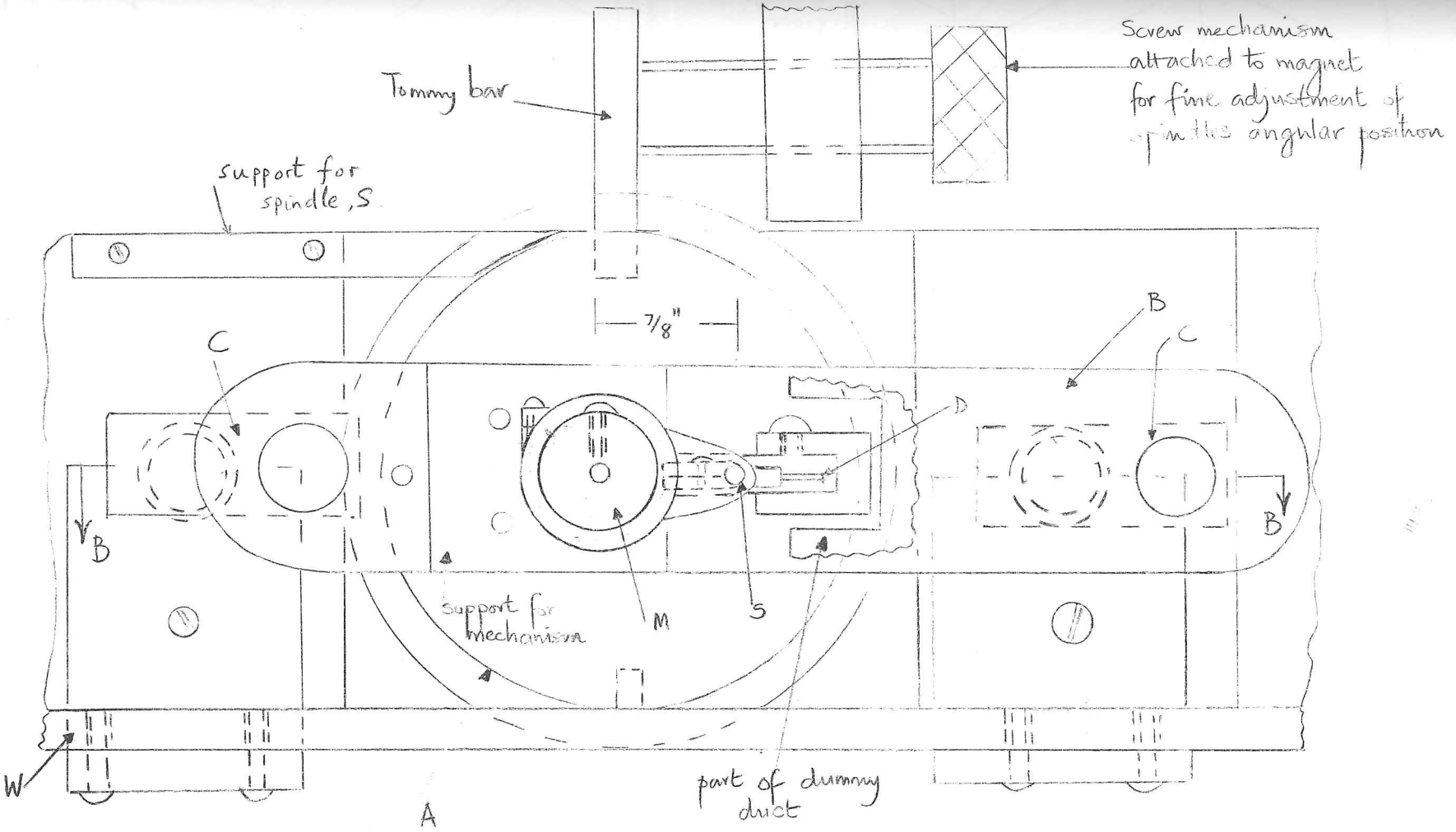

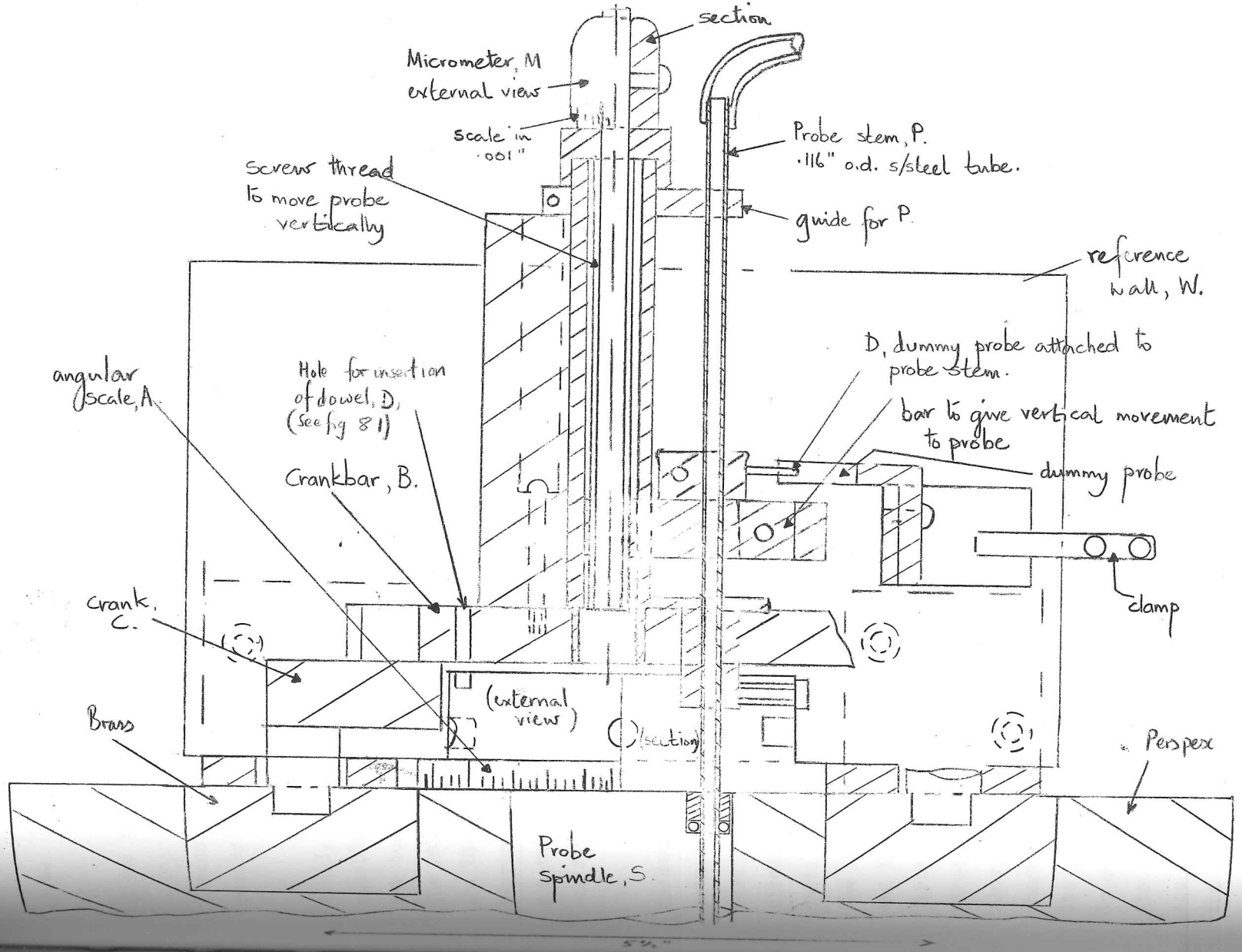

Fig 6.3(b) Section B.B. (approx. to scale : 1 cm. = ½ inch)

6.4. The mechanism for moving the probes.

The difficulties in designing a mechanism to move a probe in the plane perpendicular to the duct axis, the x-y plane, (see fig.6.2) are caused by the fact that one can only move the probes via the top walls, (AA), because the magnet's pole pieces obstruct the walls BB, and also the necessity of avoiding leaks.

Two ingenious solutions to the problem have been found by Moreau (1963, 1966). In the first he made the top of his duct a continuous movable steel ribbon through which the probe projected, a volume above the duct being full of mercury enclosed by the ribbon and side walls. The main disadvantages of this method are its extravagance with mercury and the lack of really accurate positioning required for boundary layer traverses. His second solution was more economical of mercury but again not suitable for boundary layer work, which did not worry Moreau since he was investigating jets.

We adopted the method of Lecocq (1964) who had used his probe mechanism to investigate boundary layers (see figs.6.3 and 7.1). The principle of his method was to move the probe in the y-direction by placing its stem, P , in a vertical hole drilled at a radius R in a circular cylinder, the spindle S, so that, by rotating S, whose axis is vertical, the probe stem moves in a circle, radius R, in the y-z plane. The immediate advantage of this method is the ease with which the spindle and the probe may be sealed. There are three main disadvantages. The first is that the probe is moved in the z-direction as well as the y-direction; this does not matter, of course, in a fully developed duct flow, but does matter in our electrically driven flows described in chapter 7. The second is that, if the probe is fixed to the spindle, its orientation relative to the flow changes as the spindle is rotated; to overcome this difficulty the probe must be free to rotate in S and its orientation must be fixed by some other means. The third disadvantage is that, for our type of duct design, the spindle cannot be as wide as the duct so that the probes cannot be pointing straight into the flow and touch the walls BB.

The final design we adopted is shown in figure 6.3. In order to keep the probe pointing straight into the flow when examining duct flows,

we used Lecocq's method, which entails clamping the probe to a crank bar, B. The crank bar B is constrained to be parallel to the duct's axis as each point on it traverses a circle, radius R, by means of 2 cranks C, which rest on the Perspex block which supports the whole mechanism. Placed on the crank bar is a micrometer screw to provide the vertical movement of the probe. Then the exact position of the probe should be determined by the readings of the micrometer scale, M, and of the angular scale, A, attached to the spindle. However, there are some errors in this system which have to be corrected, the first being caused by the slight 'slop' in the joints between C and B which makes the position of B to a limited extent, ($\sim 20^{\circ}$), indeterminate when the cranks are in line, i.e. 'top dead centre'. (Lecocq's apparatus did not, apparently, suffer from this defect because roller and ball bearings were used throughout rather than the simple fitting joints we used). The other fault of the system is caused by the 'O' ring seal, s, which, if tight enough to be effective, can cause twisting of the probe stem so that, even if B is parallel to the axis, the probe tip may not be. In order to avoid the first of these faults we attached a vertical plate, W, to the probe mechanism block. This plate is accurately parallel to the duct axis so that, by ensuring B to be parallel to this plate, we could ensure the probe to be correctly aligned.

The plate, W, was also used in conjunction with the 'dummy probe', D, an attachment to the probe stem which gives the position of the probe in the y-z plane; by measuring the distance between D and W we could check on the movement of the probe in the y-direction and by taking into account the value of A we could hence calculate the movement in the z-direction; we used the latter method in the experiments on electrically driven flows, as described in chapter 7. The distance moved in the z-direction could be checked further by measuring the distance between D and a set square clamped to the plate. We used the plate W in the duct flow experiments for clamping on a 'dummy duct', the purpose of which was to indicate when the probe was near the walls BB and also to enable us to measure accurately the probe's position in the y-direction by using slip gauges between the dummy duct wall and D. (see fig.6.3a). These extra measurements still did not eliminate the cause of error due

to the probe's twist. However we found when using the probe that this error was too small for measurement.

An incidental advantage of our design of the probe mechanism was that to change the probe we could lift the whole perspex block off the duct after simply undoing the retaining nuts, N (fig.7.1). In Lecocq's duct, the supporting block was an integral part of the duct so that the spindle S had to be withdrawn, and the cranks removed, which was far more complicated.

Further details on the use of the probe mechanism is left to chapters 7 and 8.

6.5. The flow circuit and its components.

Before describing the flow circuit as a whole we first describe its main components, the pump and the flow meter.

6.5.1. Pump.

The main considerations in choosing a pump was that it should not leak when used with mercury, and be fairly steady in its operation. The Orbital Lobe pump used by Alty (1966) could not deliver a sufficiently high flow rate, while the electromagnetic pump which Shercliff (1955) used was not very steady and tended to heat the mercury; the problem of using a conventional centrifugal pump seemed to be that of avoiding leaks. In the end we chose to buy a Watson-Marlow Flow Inducer, for what now appears to be very inadequate reasons. The pump operates by rotating a disc about its central axis; perpendicular to the disc face are rigidly fixed three equally spaced spindles, on which are mounted freely revolving rollers. As the disc rotates the rollers squeeze a pipe placed between them and the fixed track, which is concentric with the disc axis. (See fig.6.6). Thus the pump's motion is that of direct displacement and inconsequence is necessarily pulsating. However no leaks occur (provided the pipe does not burst), the speed of the flow can be changed, and, very important, the flow can be reversed by the flick of a switch.

It soon transpired that we would need to operate the pump at much higher pressures, up to 43 p.s.i. or 78" Hg, than its makers recommend, 20 p.s.i. Therefore we had to investigate the limitations of the pump's

Fig 6.4. Flow meter calibration rig.
(Not to scale)

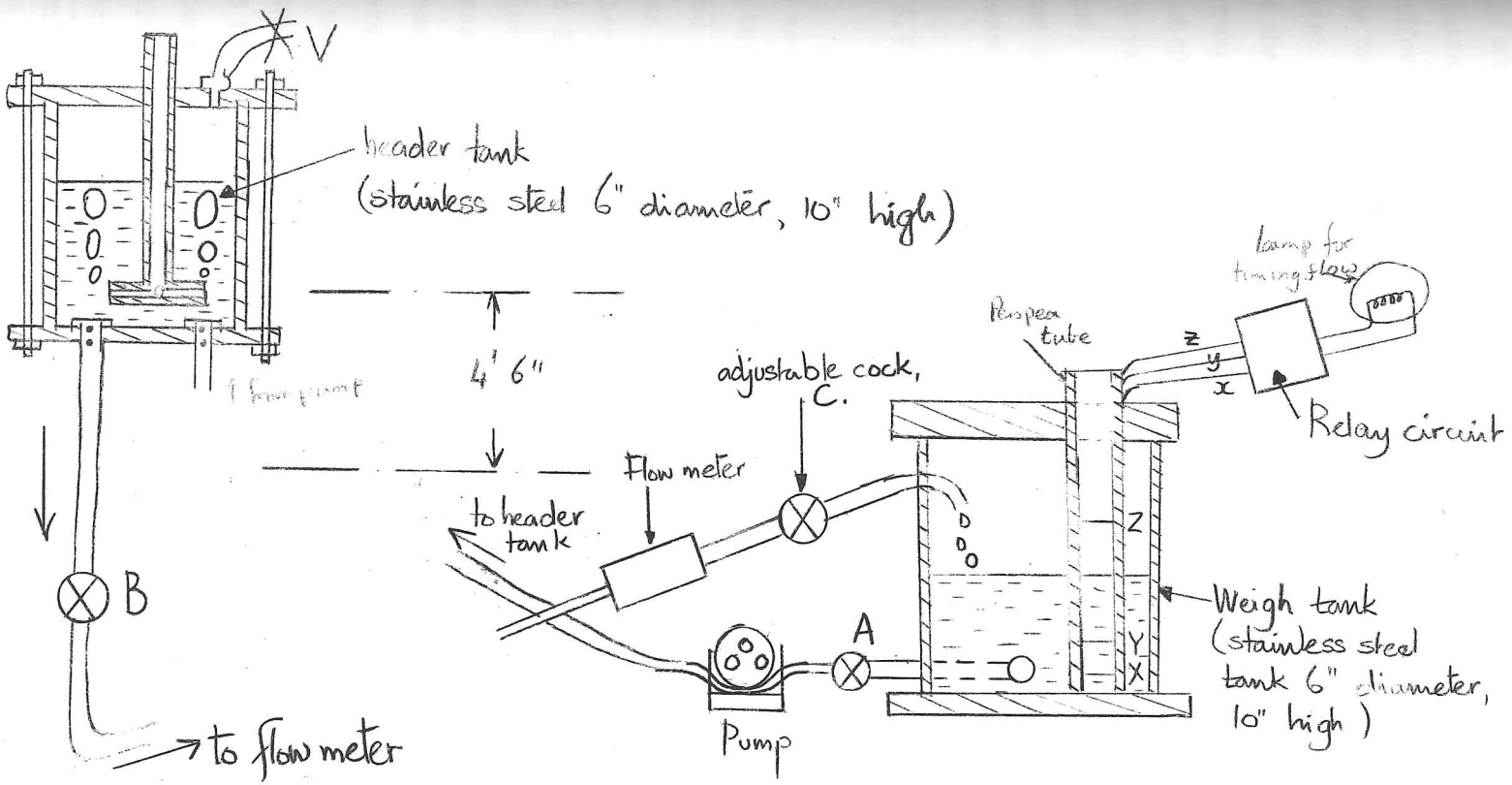

performance in these more extreme conditions. We have found that, while the stated maximum flow rate of the pump used with a $\frac{1}{2}$" diameter pipe at nominal head is .15 litres/sec, the maximum flow rate at about 60" difference in head is about .06 litres/sec. (It slightly depends on the tubing used). The other limitation, which was more serious from our point of view, was that the working life the tubing decreases very sharply at these higher pressures, so that an elastic P.V.C. pipe of $\frac{1}{2}$" diameter sprang a leak after 30 minutes of running at 43 p.s.i. as compared to the quoted lifetime of 30 hours at pressures less than 20 p.s.i. By trying out various different tubing we found that reinforced rubber tubing was best, e.g. Dunlop, Neoprene, 3 wrap reinforced tubing Type 420B, but even then had to be changed after 5 hours intermittent running, at these pressures.

6.5.2. Electromagnetic flowmeter.

To measure the rather low flowrates in our experiments we decided to use an electromagnetic flow meter and designed the first one similar to that of Shercliff (1955, fig.19), the main difference being that we used a Swift-Levick permanent magnet, which has a greater field strength (3000 gauss) than that of Shercliff's magnetron magnet, (about 1000 gauss). The flowmeter was calibrated in a slightly different way from that of Alty (1966) and Shercliff (1955), in that we recorded the time taken for a given volume to be filled at a given flowrate rather than the weight of mercury passed in a given time at a given flowrate. The apparatus used is shown schematically in fig.6.4. The header tank was similar to that of Shercliff, except that the pipe inside the tank had a 'rose' on its end to make the bubbles smaller and flow smoother. The weigh tank had two openings, at the top and the bottom; the 'Perspex' tube inside the tank had three insulated stainless steel wires, x, y, z, leading down its exterior which were bent horizontally through the tube wall and bared inside the tube at the points X, Y, Z. The process of calibration consisted, after first filling the weigh tank (w.t) with mercury, of opening the on-off cock A and pumping the mercury into the header tank (h.t), the air vent, V, being open. Then the air vent, V, and A were closed, the adjustable cock, C, was varied appropriately and the cock B was opened. Then the mercury filled the w.t. and when the mercury level

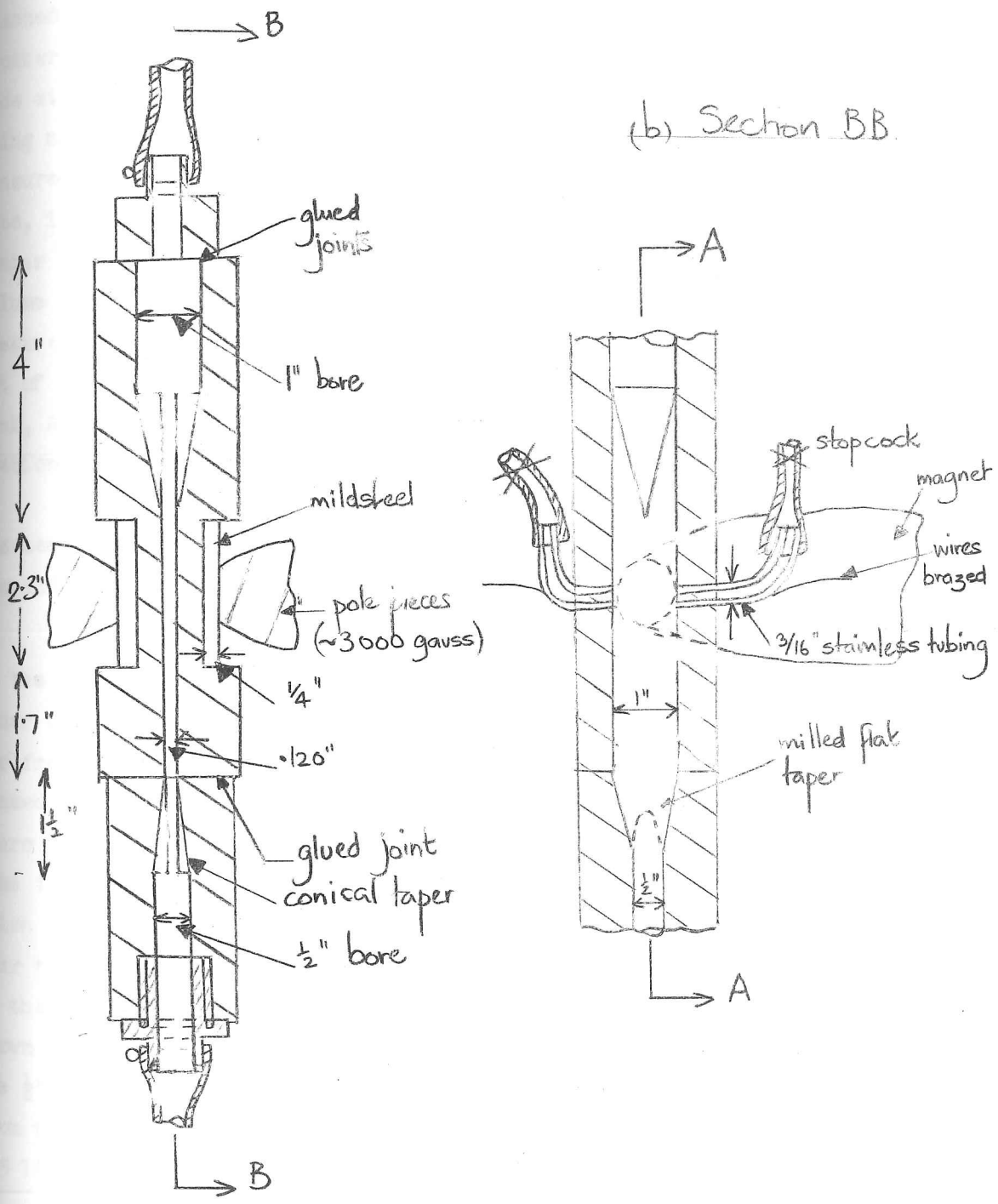

Fig 6.5. Mark II Flowmeter

reached Y, the wires x and y became connected which triggered off a relay to either start an electric counter or light an electric bulb. In general two readings of the potentiometer were taken before the level reached Z, when the wires z, y, and x were connected which stopped the counter or extinguished the bulb. We found that the flickering contact made at Y and Z led to the timing of the electric bulb by a stop watch being more accurate than using the counter. With the shortest time measured being 4 seconds we found that the variation in the measured flow rate, i.e. P x S, where P was the mean potentiometer reading and S the number of seconds the light was on, was about .5%. To measure the volume used, we put the w.t on some scales and, as we filled it by hand, measured the increase in weight while the light was on. (The tank was out of the circuit, being disconnected at the top and to the left of the cock, A). The error in weighing was about .1% so that our final calibration,

$$Q/V = (3.42 \times 10^{-3}) \text{ (litres/sec)/mV} \qquad 6.5.1.$$

was accurate to .6%: in the formula Q is the volume flowrate in litres/sec and V is the potentiometer reading in m Volts.

To avoid the complication of screening the flowmeter from the field of the main electromagnet, we decided to place the flowmeter immediately under the header tank (see §6.5.3 and fig.6.6) and therefore sufficiently far from the magnet to cause no error. However, we found that this caused bubbles of air to appear in the diverging part of the flowmeter where it changes section from a slit .035" wide to a 1" diameter tube. (The 1" section then decreases to the $\frac{1}{2}$" tubing). This phenomenon which only occurred at flow rates above .03 litres/sec led to bubbles near the flowmeter electrodes and erratic readings from the flowmeter. We then had to make a new flowmeter (Mark II) for these higher flowrates, shown in fig.6.5, in which the transition from the wider gap (.120") to the $\frac{1}{2}$" tubing was carefully made by filing. Even this flowmeter suffers from the same entrainment defect, but fortunately at flowrates above .05 litres/sec.

6.5.3. <u>The flow circuit</u>.

We now describe the flow circuit used for the experiments in the

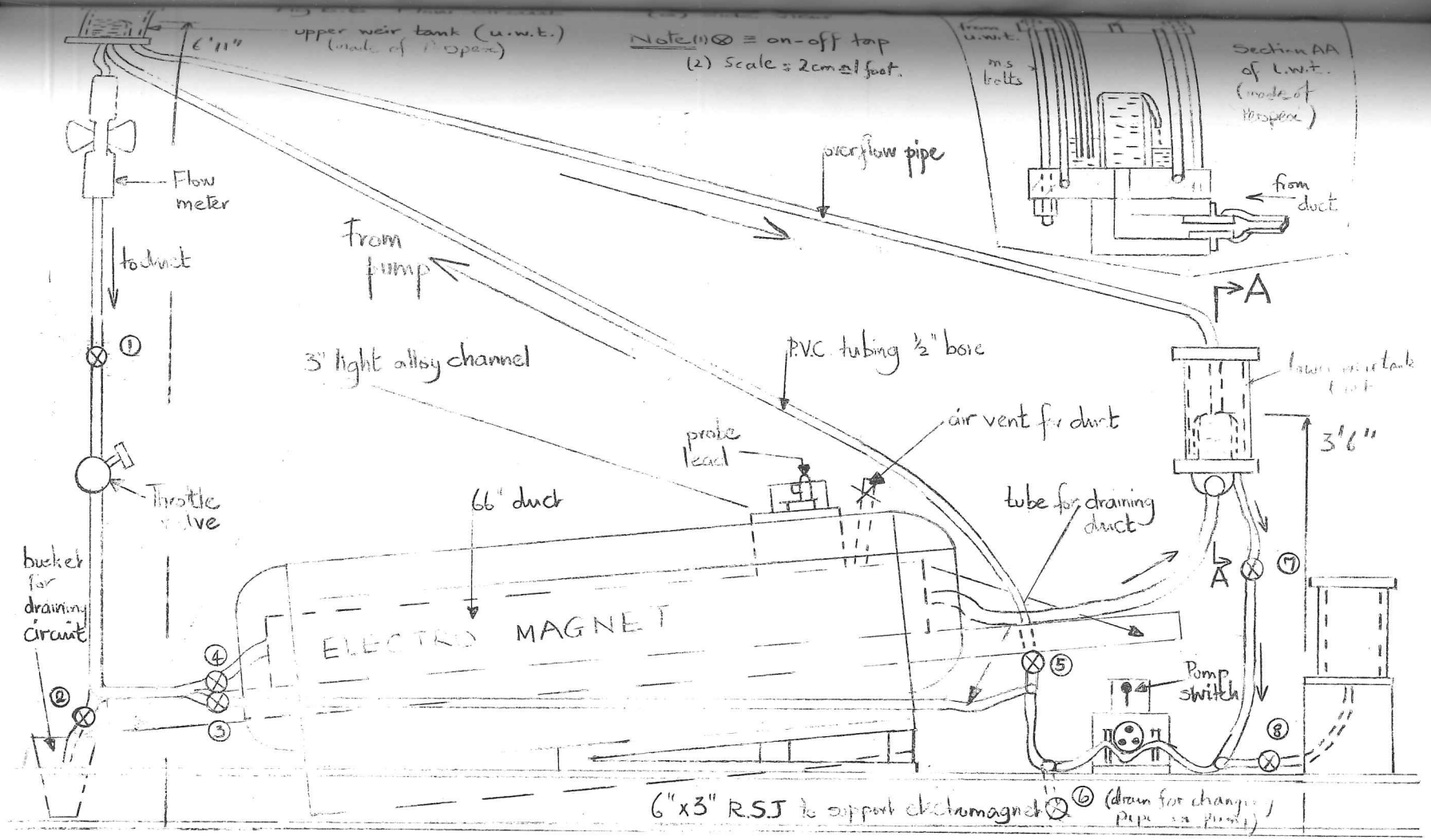
6'11"
upper weir tank (u.w.t.)
(made of Perspex)
Note (1) ⊗ ≡ on-off tap
(2) Scale = 2cm ≡ 1 foot.
from u.w.t.
m.s bolts
Section AA of u.w.t. (made of Perspex)
overflow pipe
from duct
Flow meter
to duct
from pump
A
3" light alloy channel
P.V.C. tubing ½" bore
air vent for duct
probe lead
3'6"
Throttle valve
66" duct
tube for draining duct
bucket for draining circuit
ELECTRO MAGNET
Pump switch
6"x3" R.S.J to support electromagnet
(drain for changing Pipe via pump)

Fig 6.6 (b) Plan view of flow circuit (approx. to scale : 2cm = 1 foot)

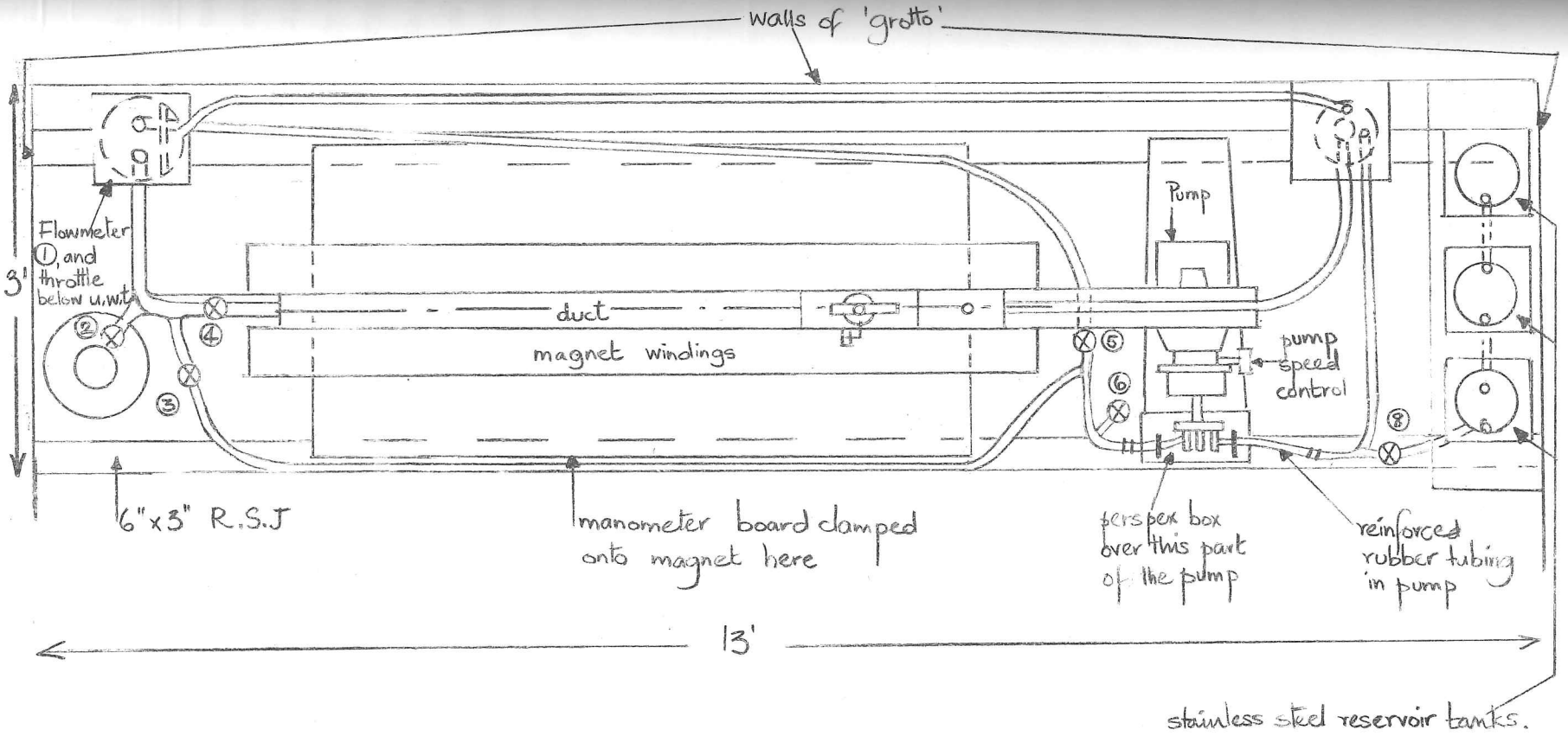

main duct and the calibration duct which are described in chapter 8. The principles of the circuit are the same as that used by Alty (1966), Lecocq (1964), and Moreau (1963), in that the pump is separated in the circuit from the experimental duct by two weirs (see figure 6.6); the mercury is pumped from the lower weir tank (l.w.t) to the upper weir tank (u.w.t), where a constant height of mercury is maintained by the mercury falling over the weir and returning to the downstream side of the l.w.t. via the overflow pipe. That which does not overflow returns to the l.w.t. via the flowmeter and the experimental duct. The main differences between our circuit and Alty's are: a) the larger scale of the circuit resulting from the higher flow rates and larger magnet used, b) the flowmeter being far from the magnet, as already mentioned, and c) the addition of an extra pipe for draining off the main duct. This extra pipe was used in the following way: first the tap (5) was closed and the taps (3) and (8) were opened, (the taps (1), and (4), and (7), being already open, (2) and (6) being closed); then the pump was started in the reverse direction to empty the contents of the l.w.t. and the duct into the reservoir tanks, the air vent on the duct being opened to speed the process. The purpose of this fast draining process was to enable us to lift off the probe block and change the probes quickly. The way in which the rest of the circuit was used in the experiments will be described in chapter 8.

It is worth commenting on some of the details of the flow circuit. $\frac{1}{2}$" bore $\frac{1}{8}$" wall, flexible, industrial, P.V.C. tubing was used throughout the circuit, except in the pump, and was found quite satisfactory for the high pressures involved, (up to 43 p.s.i). (Elastic P.V.C. tubing is liable to fracture at these pressures). In order to ease the removal of various parts of the circuit we needed easily detachable joints in the tubing. These were made of stainless steel to the same design as those of Alty (1966). In all the joints between the tubing and the various weir tanks, taps, etc, stainless steel connectors were used, which were made on the same principle as those on the main duct, jubilee clips being used to seal the connectors to the duct, tank, etc. Another example of their use is given in figure 6.7 where the on-off tap used in the circuit is shown. These taps are made by Le Bas for pressures up to 200 p.s.i.

in circuits with rigid plastic tubing; however, when modified for use with flexible tubing by means of the stainless steel connectors shown in fig. 6.7, we found that these taps did not leak and, because of their positive action, their resistance to the flow was always the same when in the on position. (The importance of this characteristic will be more apparent in chapter 8). To provide a variable resistance to the flow we first tried the method used by Alty, namely a micrometer screw adjustment of a bung in the outlet of the u.w.t, but it turned out to be unsatisfactory owing to the air being entrained in the flow round the bung which in turn led to bubbles in the flowmeter immediately below the u.w.t. We therefore used a Le Bas throttle valve below the flowmeter, as shown in figure 6.6, the valve being modified with stainless steel connectors in the same way as with the on-off taps.

6.6. Instruments.

6.6.1. Manometer.

To measure pressure differences we used a manometer similar to that built by Alty (1966), though allowing the mercury to stand with a free surface in the tubes connected to the tappings so that the existence of a pressure drop (if great enough) or the existence of bubbles in a tapping lead could be observed by the difference in height of the free surfaces. Although, theoretically the manometer could measure pressures accurately to within .001" meths, in fact it was rearely possible to do so for the many reasons described in chapters 7 and 8. One aspect of the design which has not been considered before is the electrical contact between the tappings in the manometer. In some situations if such a contact exists the fact that the two tappings or the tapping and the probe are at different potentials can lead to circulating currents which affect the measured pressure difference. Therefore we examined whether the pinchcocks used in the manometer, when closed, electrically isolated the mercury either side of the cock as well as eliminating any flow through it. We found that, if the cocks are tightened up well and placed centrally in the pinchcock, they do infact isolate the mercury either side of them. In the manometer we could either use meths over mercury, as Alty (1966) did or air over meths over mercury as Shercliff (1955); in general we used the latter method.

6.6.2. Potentiometer.

We used a Pye potentiometer to measure steady voltages, across the shunt in the electro-magnet circuit, between the electrodes in the electrically driven flows of chapter 7, between the e.p. probe and tappings in the walls of the ducts and across the flowmeter. The potentiometer used with a galvanometer can measure up to $1\mu V$, and it is sometimes possible to estimate to $\frac{1}{2}\mu V$ if the voltage is steady. When the voltage was rather unsteady we tried to use the galvanometer direct since it is calibrated, but we found that the resistance of the circuit was too great for accuracy.

7. Experiments on electrically driven flows.

7.1. Introduction.

There were two main reasons for investigating electrically driven flows as well as pressure driven flows; the first being that we had analysed these kinds of flow and found some interesting results, (described in chapter 3), which we thought would be worth while investigating experimentally; the second being that we could use these simple flows induced by current passing between two circular electrodes to test the probes and probe mechanism while the rest of the flow circuit was being constructed.

Before considering the experiments we first describe our apparatus, showing how we used the probe mechanism to examine these flows. We then apply some of the results of our analysis on the use of probes in chapter 4 to predict some of the likely errors in these experiments and in considering the best design of probe. (Many of the theoretical concepts described in chapter 4 were developed after these experiments were completed, so that our probes might well have been better designed).

In §7.3. we describe the experiments on the flow induced between finite circular electrodes. First the flows were examined to see how low the current needed to be for no secondary flows to occur, so that our results could be compared with the theory of §3.3.3. Then we measured the variation of the resistance between the electrodes with the Hartmann number, M, successfully showing that the resistance varies linearly with $M^{-\frac{1}{2}}$ when $M \gg 1$, and that, as $M \to \infty$, the resistance tends to the value predicted in §3.3.3. We used electric potential probes to investigate the curious layers joining the edges of the electrodes and were able to demonstrate that the thickness of these layers in which large potential gradients occurred is $O(M^{-\frac{1}{2}})$. To verify the existence of the velocity in these layers we traversed them with a pitot tube and examined the variation of the velocity with the current. Finally we compare the results of the two kinds of probe to draw conclusions as to the errors of the probes and the nature of the flows.

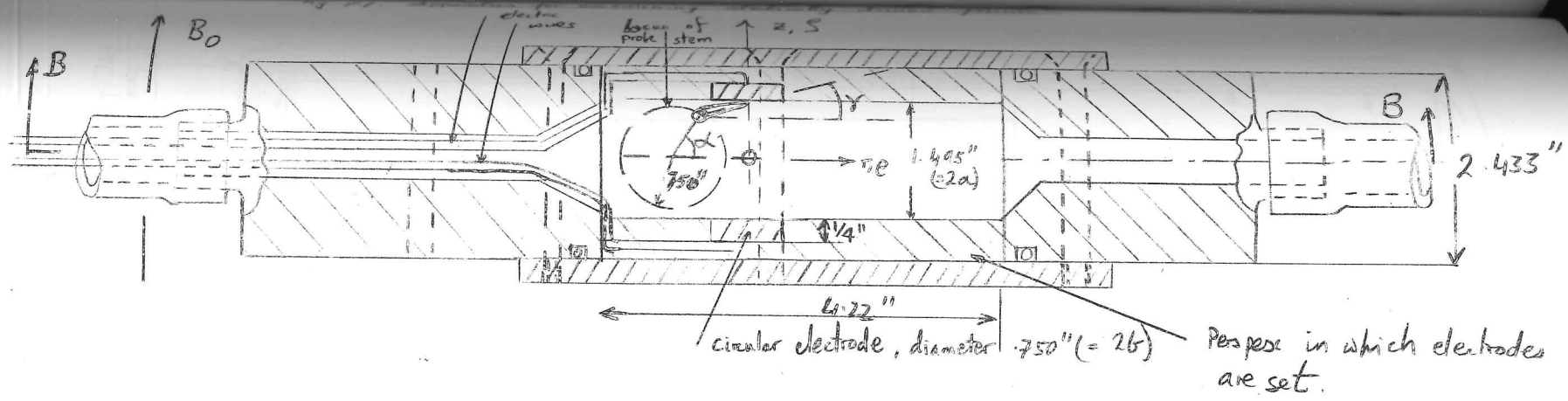

(a) Section of first apparatus

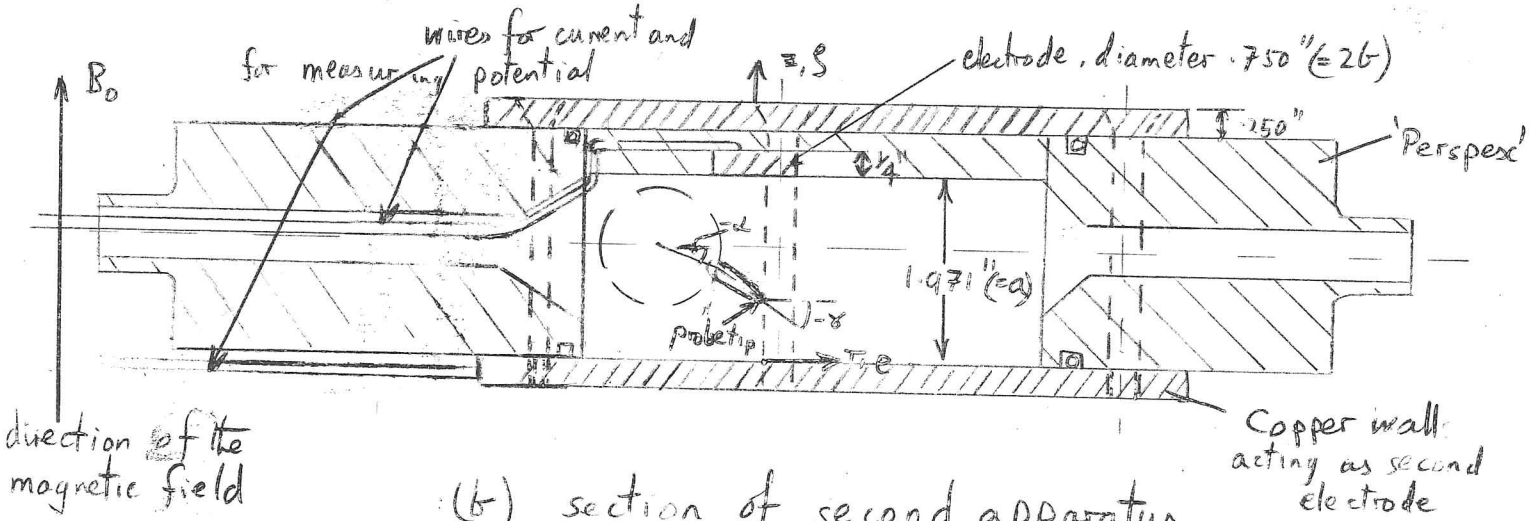

(b) section of second apparatus.

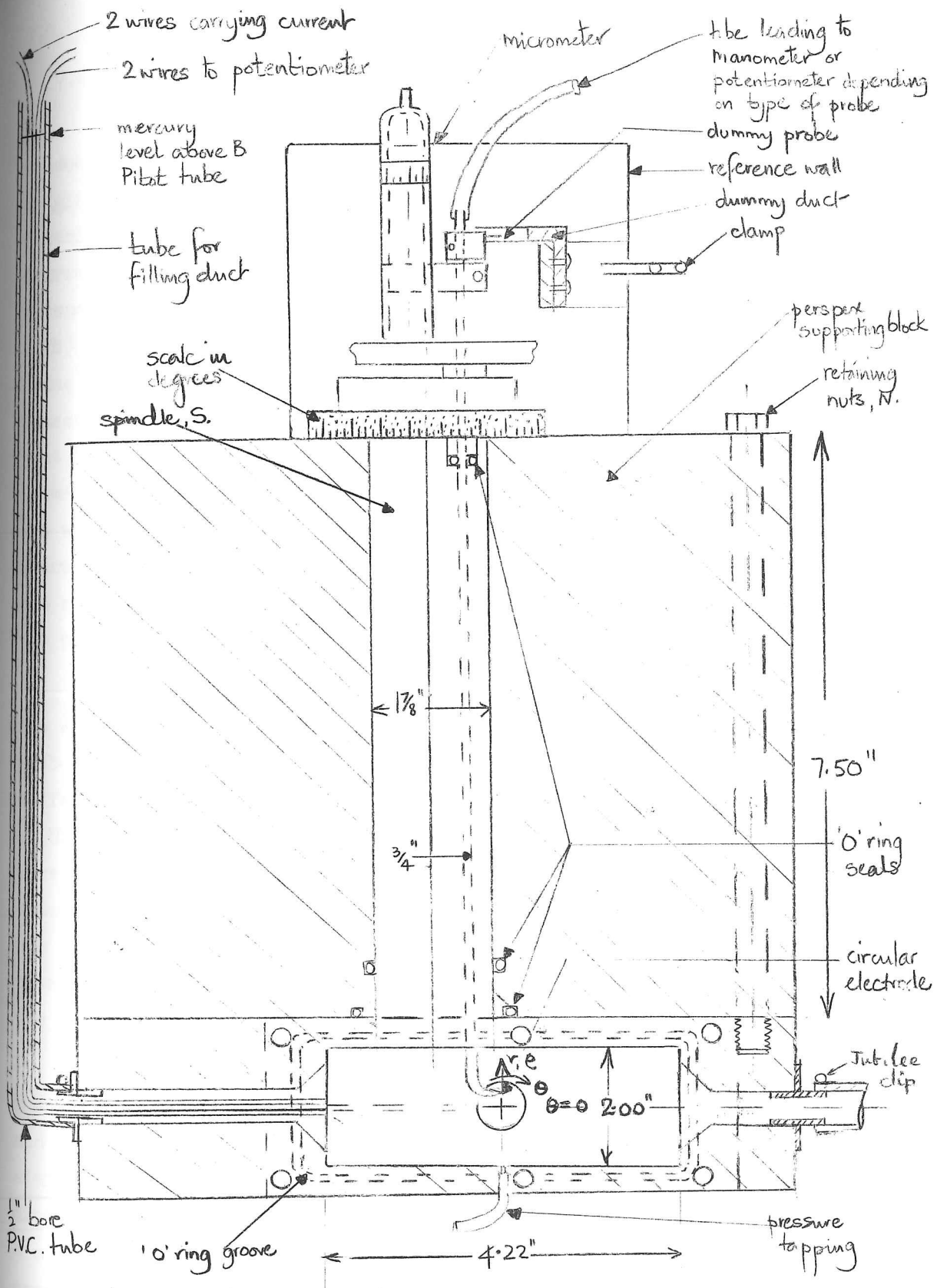

Fig 7.1 (c) Section BB

7.2. The experimental apparatus

7.2.1. The duct and the electrodes.

Our experiments on electrically driven flows using mercury as the conducting fluid were performed in the rectangular duct which had originally been constructed as a prototype for the main 66" duct, described in §6.3, and which was then modified for examining electrically driven flows (see figure 7.1). For the first set of experiments two Perspex blocks, $\frac{1}{2}$" thick, were made with copper discs $\frac{3}{4}$" in diameter (=2b) and $\frac{1}{4}$" thick, let into them, the surfaces of the copper discs being flush with those of the Perspex blocks (fig.7.1a). The blocks were placed either side of the duct with a gap of 1.47" (=2a) between them, so that $\ell = b/a = .512$. (The copper walls of the duct were isolated from its interior by rubber sheets to avoid any short circuits). Each disc had two wires connected to it, one to supply the current and the other to measure the electric potential of the disc. A fifth wire was placed in one of the tubes leading out of the duct, its purpose being to measure the potential mid-way between the discs.

We found that with this first apparatus the layers emanating from the disc edges were not sufficiently thick compared to the width of the probe and also, since we were interested in examining the flow at a different value of ℓ, we made a second set of experiments in which one of the perspex blocks and the insulation on one of the duct's copper walls were removed so that we were effectively examining only one half of the space between two discs. The distance from the disc to the copper face was 1.97" (=a) and thus $\ell = b/a = .190$ as shown in fig.7.1b. In this case we attached two wires to the plate to measure potential and transmit the current.

With the duct placed in the electro-magnet in the first apparatus the maximum value of the Hartmann number, M, based on a was about 600 and in the second about 1600. In order that the flows developed were similar to those described in the asymptotic theory of §3.3.3, two conditions had to be satisfied by the apparatus. Knowing the maximum of M attainable we can now state these conditions. The first was thay any error in the alignment of the two discs had to be very much less than the

thickness of the regions (1), i.e. the layers emanating from the disc edges, which are $O(aM^{-\frac{1}{2}}) = 0.(.030")$. We can confidently say this condition was satisfied by the two discs; with the one disc of the second apparatus this condition did not apply. The second condition was that the thickness of region (1) should be very much less than the radius of the electrodes, which required that

$$b \gg aM^{-\frac{1}{2}} \quad \text{or} \quad \ell M^{\frac{1}{2}} \gg 1.$$

The maximum values of $\ell M^{\frac{1}{2}}$ attainable in the two apparatus were 13 and 7.7. respectively, which shows that the first apparatus met the conditions of the theory better than the second. (We did not use larger electrodes for fear of the regions (1) touching the top and bottom walls of the duct).

7.2.2. Probe mechanism.

When descibring in §6.4 the design of our mechanism for moving probes in a duct where the flow was fully developed, we mentioned that we could also use the mechanism for examining electrically driven flow. To examine the flow between two circular electrodes placed in non-conducting planes opposite each other with a magnetic field parallel to the line joining their centres, we only needed to examine the flow in one plane, θ = constant, (to use the notation of fig.3.7), because, for low enough velocities, the flow is axisymmetric. Since we wanted to use the mechanism and the probes designed for examining duct flows with the minimum number of alterations, we chose to examine the flows in the plane $\theta = \pi/2$. As a result of this decision we mounted the mechanism on the duct as shown in figure 7.1.c.

The method of moving the probe in the plane, $\theta = \pi/2$, using the notation of fig.7.1, may be understood by referring to figure 7.1a, where the locus of the probe stem is shown in the r-z plane ($\theta = o$). To move the probe tip in the $\theta = \pi/2$ plane, we could not keep the angle γ between the probe and the duct axis, ($\zeta = o, \theta = o$) constant; but, by specifying the distance, z, we could calculate the angle α at which the probe spindle, S, should be set in order for the probe tip to lie in the $\theta = \pi/2$ plane. To set the probe we first turned S to the appropriate value of α and then twisted the probe on its own axis until the distance between the dummy probe and the dummy duct in the z-direction was the same as that required between the probe tip and the

electrode, the dummy duct being made so that its wall was vertically above the electrode. As a consequence of this method of moving the probes, being $\frac{3}{4}$" from their tip to the centre line of their stem, the probes were only able to face into the flow when $z \simeq +a$, $f \simeq 1$ and, in the first apparatus at $z \simeq -a$, $f \simeq -1$, and in the second at $z \simeq .25a$, $f \simeq .25$. Therefore, without making new probes of differing lengths, the pitot tubes could only be used near these values of z, such a probe being accurate to 1% if it faces into the flow to within 10°. However, the electric probes could be used at all values of z, since they do not critically depend on pointing into the flow, or being at right angles to the current path. But, if γ is the angle between the line joining the probe's tip to the axis of its stem and the duct's axis, (see fig.7.1a, b), it is clear from our analysis of chapter 4 that the probe errors are reduced if γ is kept to a minimum. When the probe tip was on the duct's centre line, γ took its maximum value, about 45°.

7.2.3. Electric potential probes.

We mention here a few of the considerations which led to the design of the e.p. probe we used in the experiments, bearing in mind the analysis of chapter 4. On the one hand such a probe needs to be as small as possible when used in flows such as these where the gradients of velocity and electric potential are large, for the reasons given in chapter 4, the probe size also needed to be minimised to reduce the size of the vortices shed by the probe which, being carried round, would tend to affect the potential at the probe tip. On the other hand the probe must be sufficently rigid for its position to be determinate, particularly since in this experiment the probe would not always be facing into the flow; also the conducting region inside the probe must have a sufficient diameter for its resistance to be reasonably low and this wire has to be insulated from the probe's exterior if made of metal.

The fact that the strongest small diameter tubing easily available is made of stainless steel determined our choice of the material for the probe's exterior. The main alternative was Pyrex tubing which Lecocq used; this suffers from the disadvantage of being brittle and therefore easily broken if the probe was inadvertently pushed against the wall and also it is less easily bent to the required shape than stainless steel.

(a) Pitot tube

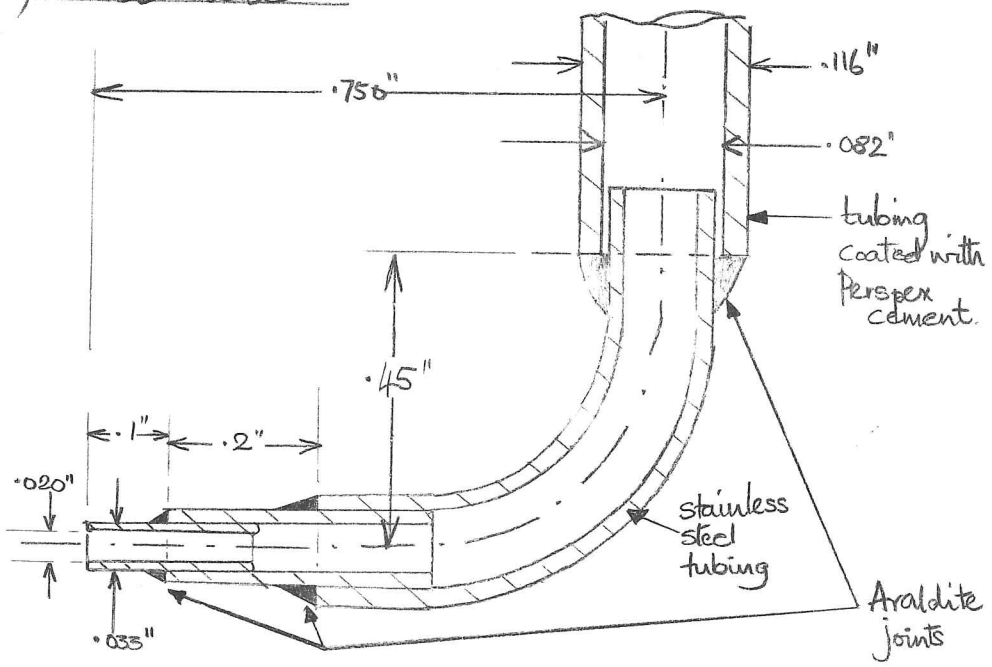

(b) Electric Potential probe

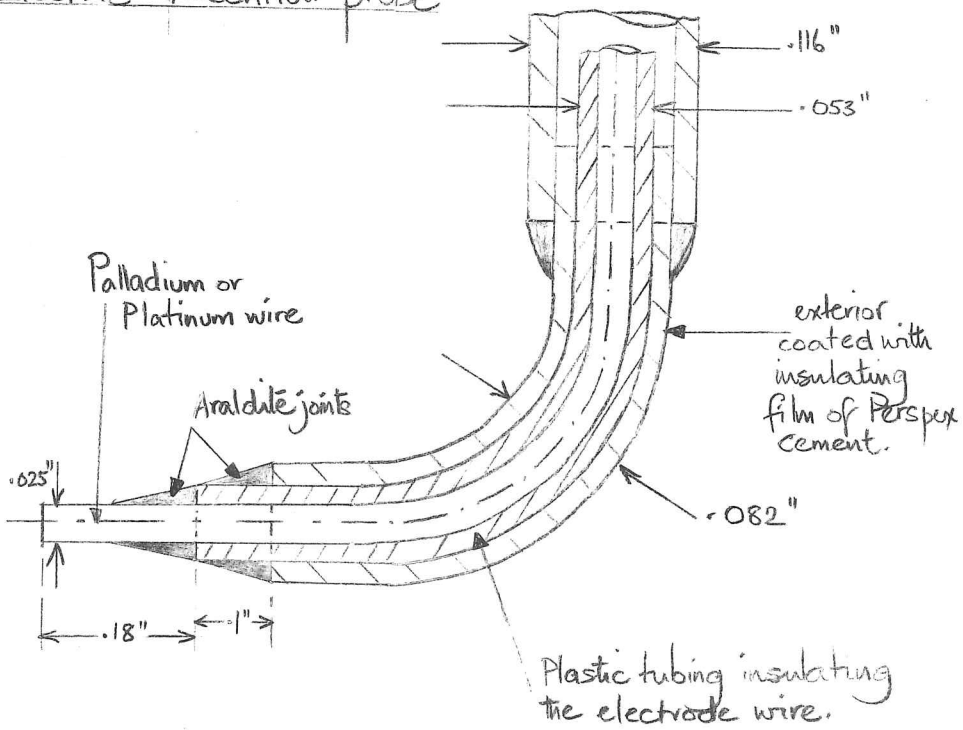

Fig 7.2 Pitot and electric Potential probe.

However the advantage of Pyrex tubing is that it does not require insulation from the conducting material inside the probe. We could either choose to have mercury inside the probe as our conducting region or we could use an electric wire. The advantage of the wire is that it can be made to protude from the end of the probe and thus present a small area to the flow. We chose to use Palladium and Platinum wires, the thermoelectric potential of these wires being close to that of mercury; we did not try out the method of Lecocq (1964) who used Platinum wires coated with sodium, which, apparently, reduced the thermoelectric potential difference between the wire and the mercury to zero.

The final design is shown in fig.7.2(a). Note the two diameters of stainless stell tubing used; the use of flexible plastic tubing as the insulator between the steel tubing and the wire, and the coating of the exterior of the probe with a thin layer of non-conducting Perspex cement.

We now consider the various regions of the flow between the discs, as described theoretically in §3.3.3, in order to predict the kind of errors to be expected.

Region (4)

In this region the current density is uniform and the velocity is zero so that, if the probe is at right angles to the current, i.e. $\gamma = 0$, from our symmetry result of §4.3.2, no error would be induced. However, as we have explained, the probe could always be at right angles to the plane $\Theta = \pi/2$, so that we could expect some error due to blocking the currents. Then the error in ϕ compared to $\Delta\phi$, the potential of the disc is easily seen to be $O(d/a)$, where d is the probe diameter. (There is another possible source of error caused by a local velocity, $\underset{\sim}{v}'$, induced by the displaced currents; then the $\underset{\sim}{v}' \times \underset{\sim}{B}_0$ electric field could affect ϕ_m, the measured value of ϕ, but in the region (1) $\underset{\sim}{B}_0$ is parallel to $\nabla\phi_\infty$ and it may be seen that no error can result from $\underset{\sim}{v}' \times \underset{\sim}{B}_0$).

Region (1)

In this region, where severe velocity and potential gradients exist and the approximate relation

$$-\frac{\partial \phi}{\partial r} + v_\theta B_0 \simeq 0 \qquad 7.2.1.$$

holds true we can use the result (4.3.8) to estimate the order of magnitude of the error between Φ and ϕ_m. Changing the notation of §4.3.2 we have:

$$\Phi_m \simeq \phi + k d^2 B_0 \partial v_\theta / \partial r . \qquad 7.2.2.$$

where from §4.3.2 we can assume k to be a positive constant of order unity. (In our analysis we assumed $R_d \gg 1$ where R is the Reynolds number based on the probe diameter, and that the flow was independent of R_d. However if R_d is low enough the flow is dependent on R_d and then k in (7.2.2) becomes a function of v_θ). For the purpose of this approximate argument we also assume that the probe is pointing into the flow, i.e. $z \cong a$, otherwise the error in (7.2.2) might be proportional to v_θ as well as dv_θ/dr.

Using (7.2.1), (7.2.2.) becomes,

$$\Phi_m \simeq \phi + k d^2 \partial^2 \phi / \partial r^2 . \qquad 7.2.3.$$

Two main results stem from this. If we consider a very simplified expression to represent the fall of ϕ through the regions (1), say $\phi = 1 - erf(\bar{\rho}')$ where $\bar{\rho}' = (r-b)/aM^{-\frac{1}{2}}$, then we can first see that $\partial \phi_m / \partial r$ has two maxima one for $\bar{\rho}' < 0$ and one for $\bar{\rho}' > 0$, and secondly that if k is low enough, the maximum value of $\partial \phi_m / \partial \bar{\rho}'$ is less than that of $\partial \phi_m / \partial \bar{\rho}'$

As is obvious if (7.2.3) is written in terms of $\bar{\rho}'$, i.e.

$$\Phi_m = \phi + k \frac{d^2}{a^2} M \frac{\partial^2 \phi}{\partial \bar{\rho}'^2} , \qquad 7.2.4.$$

the condition for the error term to be negligible is that $\frac{d^2}{a^2} M \ll 1$. From (7.2.4) we also see that, if $Rd \to \infty$, $\phi_m \propto \phi$ or I, the current passing between the electrodes, whereas, if the flow over the probe is sensitive to variations in R_d, Φ_m would not be proportional to ϕ or I. If the error term is appreciable, it follows that, even if ϕ is a function of $\bar{\rho}'$ at a particular value of $\int$, ϕ_m is not. Since the potential measured by a probe is the mean of the potential across the face of its tip, a circle of .025" in diamter, to calculate the error we had to average $\frac{\partial^2 \phi}{\partial r^2}$ or $\frac{\partial v_\theta}{\partial r}$ across the probe face.

Finally we note that we could either calculate ϕ purely from ϕ_m by integrating (7.2.4) or we could use the results of the pitot tube readings v_θ as well as the readings of ϕ_m to calculate ϕ from (7.2.2).

7.2.4. Pitot tubes.

The considerations leading to the design of the pitot tube were very similar to those leading to the design of the e.p. probe, the only difference being that the probe should not have too small an internal diameter because of the need to reduce the time for taking a reading of pressure. Again we used various sizes of stainless steel non-magnetic tubing for the probe, each tube fitting inside the other. The tube was coated with Perspex cement in order to minimise the effects of the probe on the electric fields; however this was not really necessary as the contact resistance of stainless steel is so large as to render it effectively non-conducting. The final design of pitot tube is shown in figure 7.2(b).

From the theory of chapter 4 and the experimental results of East we expected that the MHD probe errors could be calculated from the formula:

$$p_o = p_s + \frac{1}{2}\rho v_\theta^2 \left(1 + \alpha \frac{\sigma B_o^2 d}{\rho v_\theta}\right), \qquad 7.2.5.$$

where p_o and p_s are the total and static pressure respectively. It turned out that $N = \frac{\sigma B_o^2 d}{\rho v_\theta}$ was about unity so that higher order terms in the expansion should have been used. However, the results of East gave $\alpha = .39$ and our own results of chapter 8 gave $\alpha \simeq .4$ for values of N of O(1), so we assumed $\alpha = .4$ in our calculations of velocity.

The other source of error to be expected was caused by measuring velocity in a shear flow the length scale of which was comparable with the diameter of the pitot tube. However we show in §8.2 that using a pitot tube to measure the velocity of a plane Poiseuille flow in a duct, the width of which is only four times that of the tube, leads to negligible errors over the central half, but appreciable errors ($\sim 50\%$) when the probe touches the wall. Therefore in a free shear flow such as this we do not expect errors in velocity greater than 10% due to this effect.

We decided to measure the velocity induced in the region (1) by means of a pitot tube only, the pressure in the pitot tube being measured relative to the pressure at a tapping in the wall of the duct, p_w. The static pressure was not measured in the layer, even though there was a small static pressure gradient through the layer due to the rotating flow. However we were able to calculate this pressure gradient using the equation

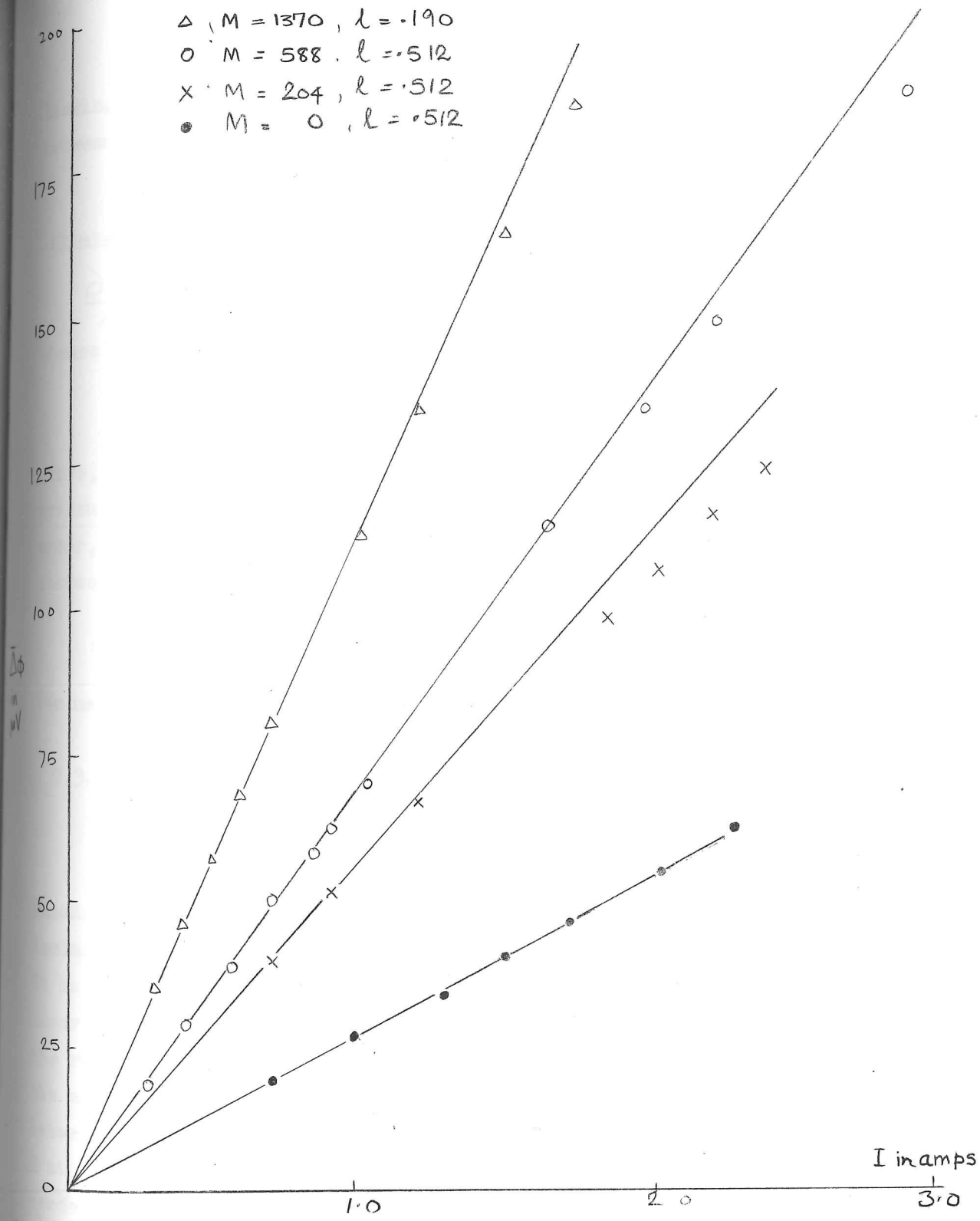

Fig 73. Potential between the discs, $\Delta\phi$, against current, I, at various M.

$$\frac{\partial p_s}{\partial r} = \frac{\rho v_\theta^2}{r}. \qquad 7.2.6.$$

Leaving the error in p_o for the moment, we have the usual relation between p_o and p_s, the total and static pressures, i.e.

$$P_o = P_s + \tfrac{1}{2}\rho v_\theta^2. \qquad 7.2.7.$$

Eliminating p_s from (7.2.6) and (7.2.7) we have:

$$\frac{\partial P_o}{\partial r} = + \frac{\rho v_\theta^2}{r} + \frac{\rho}{2}\frac{\partial v_\theta^2}{\partial r},$$

whence:

$$v_\theta^2 = \frac{2}{\rho r^2}\int_\infty^r \left(r^2 \frac{\partial P_o}{\partial r}\right) dr. \qquad 7.2.8.$$

Thus, by only measuring p_o, we could calculate v_θ. Since the static pressure effect is $O(\delta/b)(\ll 1)$, we could approximately allow for the MHD error, which was greater than the static pressure effect, by using successive approximations to calculate v_θ, viz

$$v_{\theta_n} = \left(\frac{2}{\rho r^2}\int_\infty^r \left(r^2 \frac{\partial P_o}{\partial r}\right) dr\right) \Big/ \left(1 + \frac{4\sigma B_o^2 d}{\rho v_{\theta_{n-1}}}\right). \qquad 7.2.9.$$

(We needed to use two iterations at the most in our calculations).

7.3. Experimental results.

7.3.1. Electric potential measurements.

Since the aim of the experiments was to reproduce conditions examined in the theory of §3.3.3 we first had to establish that a laminar flow regime existed in which the secondary flow was negligible. It is clear from the equations of motion that when the secondary flow occurs, i.e. a flow occurs with a radial component of velocity driven by the radial pressure gradient, $(\rho v_\theta^2/r)$, the relationship between $\overline{\Delta\phi}$, the mean potential between the discs, and I, the total current flowing between the discs, would become non-linear. Thus, by measuring $\overline{\Delta\phi}$ against I at a given value of M, we were able to find out how low the current I needed to be for us to achieve the required flow. Fig.(73) shows the $\overline{\Delta\phi}$ -I curves for the two apparatus at various values of M. (For the second apparatus we have doubled the potential between the discs and the

Fig 14 ϕ against I for two values of M, at a fixed position of probe: $r/b = .127$ $\zeta = .754$

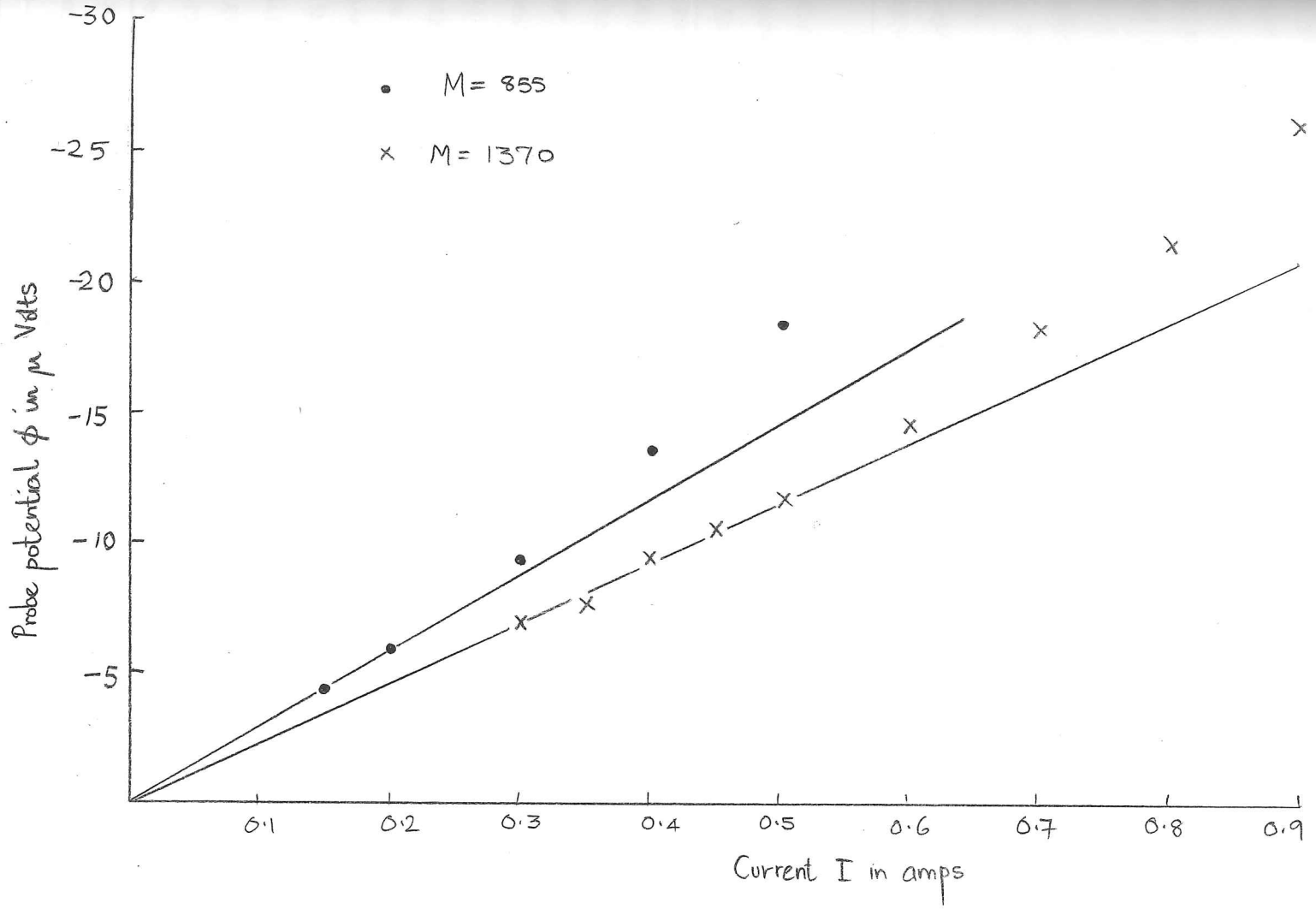

wall). Note that, in the range of I considered, $\overline{\Delta\phi} \propto I$ when $M = 0$ and that, when $M \neq 0$, the curve of $\overline{\Delta\phi}$ against I is a straight line for I sufficiently low, but as I increases the curve ceases to be a straight line indicating the onset of secondary flow. There are two curves for the first apparatus (two discs, $\ell = .512$) taken at $M = 588$ and $M = 204$. Note that the value of I at which the flow becomes unstable is higher when M is higher, thus indicating that an increased magnetic field tends to suppress the secondary flow. This may be explained by the fact that, since the velocity, v_θ is proportional to $(IM^{-\frac{1}{2}})$, the ratio of inertial forces inducing the secondary flow to the viscous forces restraining, being proportional to v_θ, decreases as M increases for a given value of I. However a more detailed discussion of the onset of secondary flow is impossible without knowing the form of the secondary flow distribution, which at the present time is obscure.

We continued this investigation of the onset of secondary flow by examining the relation between ϕ, the difference in potential between that measured by the electric potential probe and that on the line $z = 0$, and the current I, the second apparatus (one-disc) being used. The probe was placed at a radius of $1.27b$ and a value of $\zeta = -.95$, i.e. in the region (1), so that any secondary flow effects could be markedly demonstrated. As is shown in fig.7.4 the curve becomes non-linear at a much lower value of I for the same value of M than in the $\overline{\Delta\phi} - I$ curve for the second apparatus, shown in fig.7.3. There may be three explanations for this; the first is that the $\overline{\Delta\phi} - I$ curve is simply curving away from the straight line curve gradually and there is no definite point at which the curve ceases to be linear; the second is that the probe itself induces a local secondary flow which has no appreciable effect on the $\overline{\Delta\phi}$-I curve; the third is that the errors in the probe created this non-linearity as predicted in §7.2.2. However, since the Reynolds number of the probe, R, was greater than 100 for the values of I considered, and since the velocity distribution round the probe does not vary greatly with the Reynolds number in this range, it seems unlikely that this non-linearity is due to the probe error. Also, when the secondary flow occurs the radial velocity will tend to thicken the region (1). For a given value of I this reduces the current density in region (4) and thence reduces $\overline{\Delta\phi}$

Fig 7.5 Variation of resistance between the electrodes with M.
(R/R_∞ against $1/(\ell M^{1/2})$)

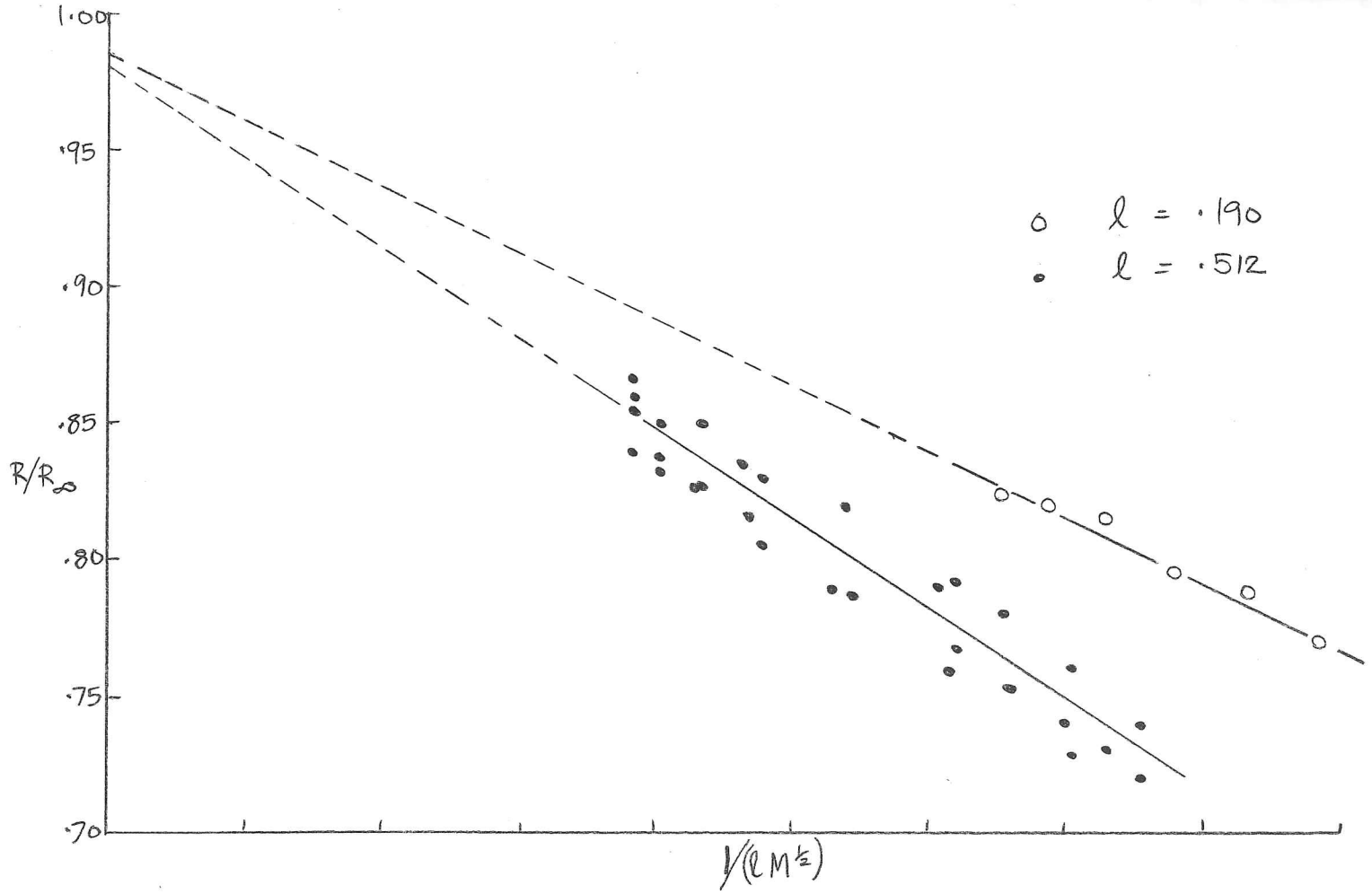

as we see in fig.7.3. However as the region (1) thickens, the potential gradients fall and therefore if the probe's position is at a radius greater than that of the disc $|\phi|$ rises and where less, falls. This explains why, when the $\phi - I$ curves in fig.7.4 become non-linear, $|\phi|$ rises. The last and most practical point to notice in these figs. 7.3 and 7.4 is that the values of ϕ and $\overline{\Delta\phi}$ in the regime are always below $100\,\mu V$ and often below $10\,\mu V$ in the regions (1). Since the potentiometer only measured to $1\,\mu V$ it follows that the random errors to be expected are sometimes as much as 10%.

Having found the values of I below which it was necessary to operate at to avoid secondary flow, we then measured the variation of $R = \overline{\Delta\phi}$ with M, for the two apparatus. We showed theoretically in §3.3.3 that whatever the distribution of current density across the electrodes, as $M \to \infty$,

$$R \to R_\infty, (=2a/\pi\sigma b^2) .$$

We also demonstrated physically why we could expect R/R_∞ to be a linear function of $(\ell M^{\frac{1}{2}})^{-1}$ when $M \gg 1$. Therefore, in presenting our experimental results in fig.7.5 we plotted R/R_∞ against $(\ell M^{\frac{1}{2}})^{-1}$ for the two electrode configurations in which ℓ = .512 and .190 respectively. We draw three main conclusions from these two sets of results. The first is that R/R_∞ is indeed a linear function of $M^{-\frac{1}{2}}$. The second is that, to within 2%, i.e. well within the experimental error, $R/R_\infty = 1.00$ when the lines of R/R_∞ against $(\ell M^{\frac{1}{2}})^{-1}$ are extrapolated to the point where $M = \infty$, and the third is that the slopes of the two lines are different being within 60% and 20% of the value of the slope found theoretically by assuming a constant current distribution across the electrodes (see §3.3.3). We take up this point in §7.3.3 after discussing the detailed results of the probes.

Having demonstrated that some of the external characteristics of the behaviour were approximately as predicted theoretically, we then examined the internal flow structure. In our theoretical discussion of §3.3.3 we first postulated the existence of various separate regions and then made various deductions about them some of which we have been able to verify experimentally. In the central region between the electrodes, region (4), we concluded that when $M \gg 1$ the velocity is zero and that

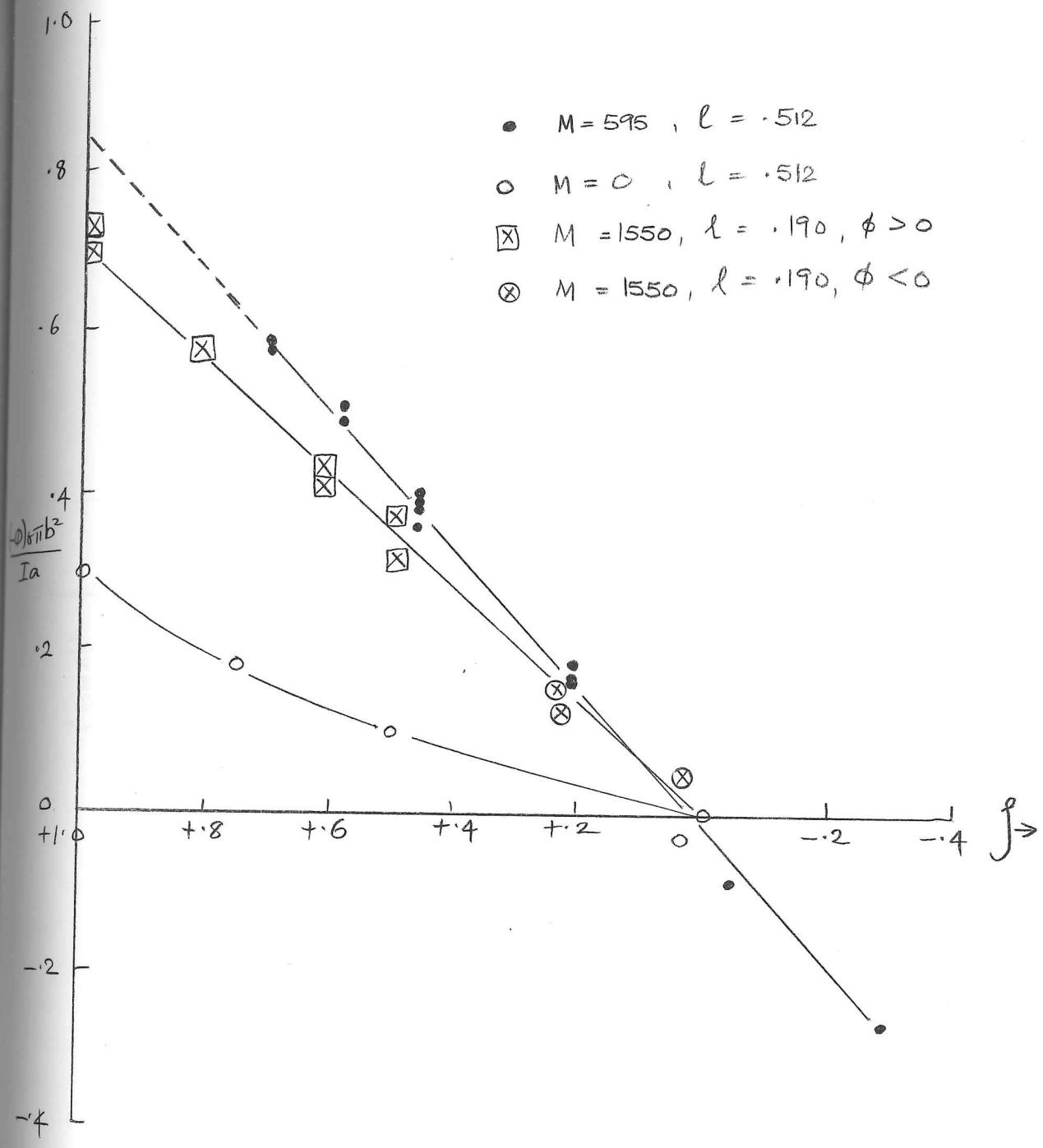

Fig 7.6 Variation of potential, $\frac{(-\phi)6\pi b^2}{Ia}$, along the centre line of the electrodes when $M \gg 1$ and $M = 0$

Fig 1. 2. Graphs of potential $(\phi)\sigma\pi b^2/Ia$ against radius $(r-b)/b$, when $M=0$

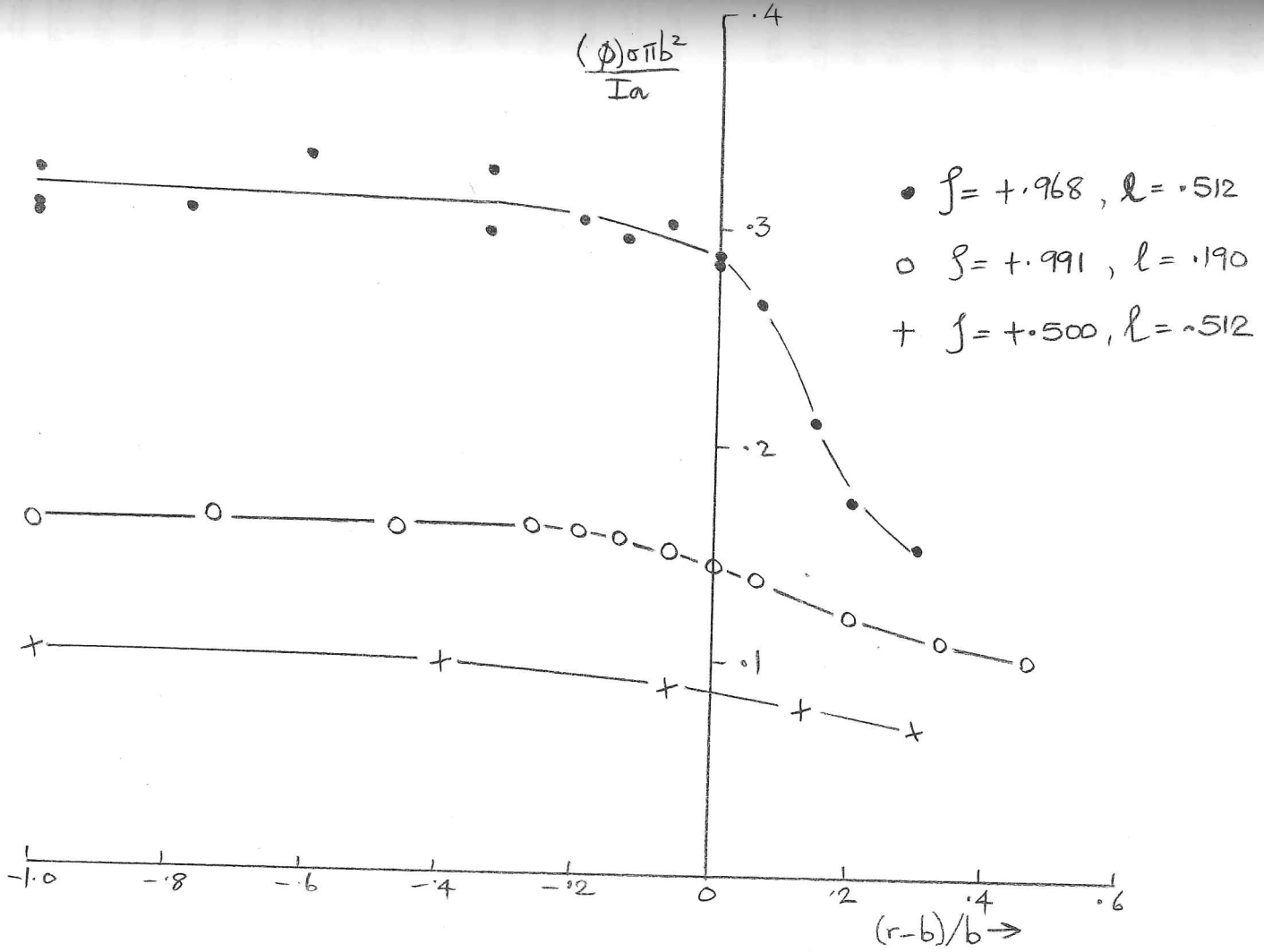

the current density and electric field is uniform, provided the current density is uniform on the electrodes in this region, as, for example, on perfectly conducting electrodes. In fig.7.6 we have plotted $(-\phi)\pi\sigma b^2/aI$ against $\int$ along the centre line ($r = 0$) when $M = 0$ and $M \gg 1$, since $(-\phi)\pi\sigma b^2/aI = \phi/\phi_\infty$ where ϕ_∞ is the value of ϕ on the disc when $M = \infty$ at the same value of I. This figure shows that, when $M = 0$, the current density j_z is lower at $\int = 0$ than at $\int = 1$ because of the spreading of the current lines, and that when $M \gg 1$ the curves become straight lines indicating that the current distribution is uniform in this region and that therefore the spreading is eliminated. The slopes of the two straight lines are different because the R/R_∞ against $1/(\ell M^{\frac{1}{2}})$ curves have different slopes; however, when $M \to \infty$, the lines should merge, cutting the ordinate at $(-\phi)\sigma b^2\pi/Ia = 1.0$. We should note that the potential measurements in this region were only likely to be in error to order (d/a), ie. less than 4%, due to MHD effects, (§7.2.2), but the random errors were about 5%.

We now consider the results of the radial traverses of the electric probes in the region (1). Fig.7.7 shows the results of a potential traverse when $M = 0$, which acts as a reference with which to compare those when $M \gg 1$. We then made three sets of measurements of ϕ in the first apparatus, i.e. the two discs, when $\int = .294$ and $M = 175$, 330 and 610. (The notation we use is the same as that of fig.3.8, I being positive when parallel to the magnetic field). In fig.7.8(a) we have plotted the results in the form of one graph of $(-\phi)\sigma\pi b\ell/I$ against $(r-b)/aM^{\frac{1}{2}}$, $(\equiv \rho' M^{-\frac{1}{2}})^*$, in order to show firstly that the thickness of the region (1) is unquestionably of order $(aM^{-\frac{1}{2}})$ and secondly to show that the distribution of ϕ and therefore v_θ is similar for different values of M in these layers. We have drawn the best line through the experimental points, because they show only a small systematic departure from this line. We could perhaps say that the best line through the points for $M = 175$ would have a greater slope than the curve drawn, which would be expected from (7.2.4). However, considering the randomness of many of the errors involved, the curves do not indicate any large scale departure from similarity except where $(r-b)/(aM^{-\frac{1}{2}}) < -3$, when the values of $(-\phi)$ are lower for the lower values of M. This result is to be

(a) $\frac{(-\Phi)\sigma\pi b^2}{Ia}$ against $\frac{(r-b)M^{\frac{1}{2}}}{a}$, $l = \cdot 502$, $\zeta = +\cdot 706$

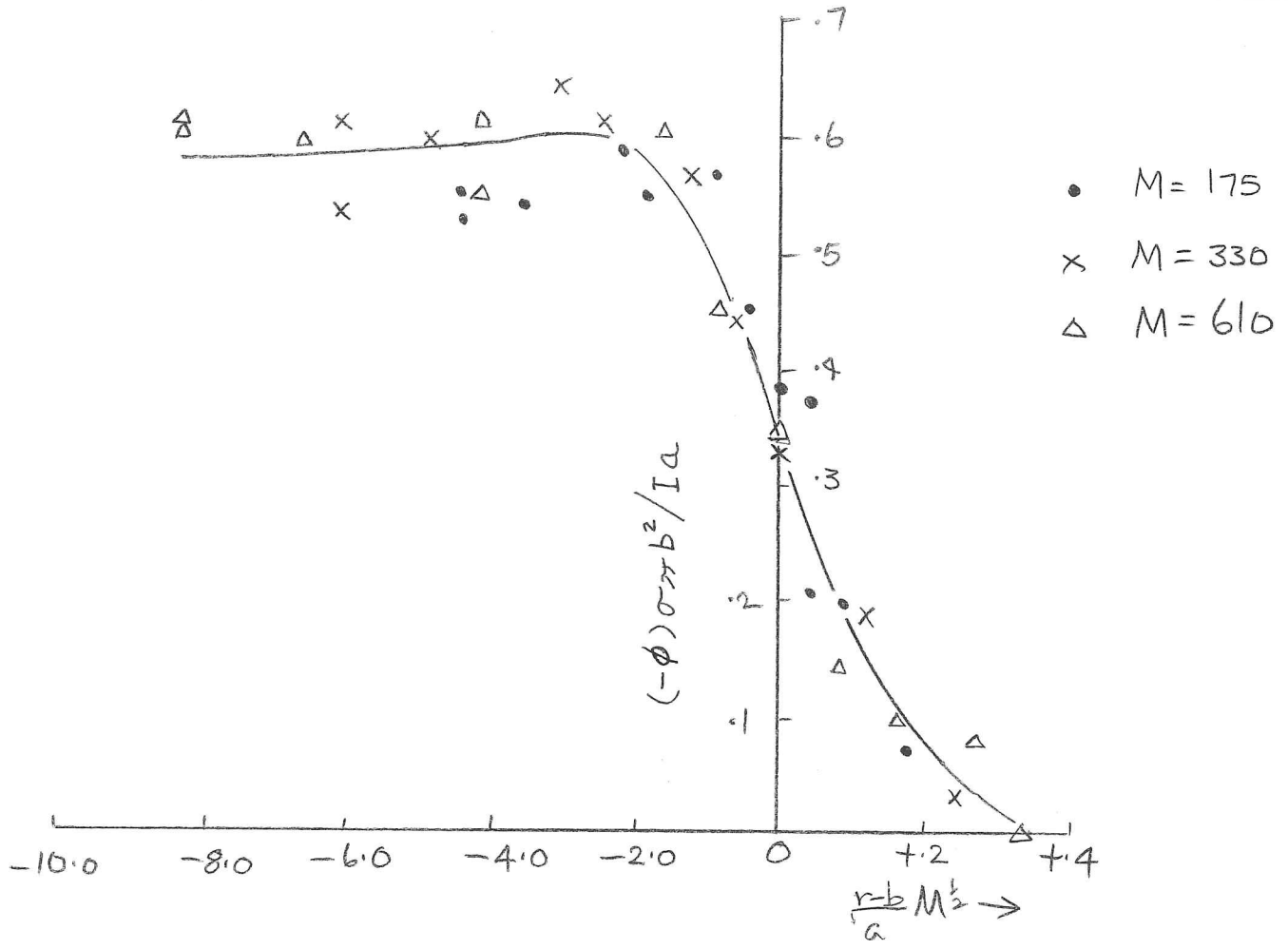

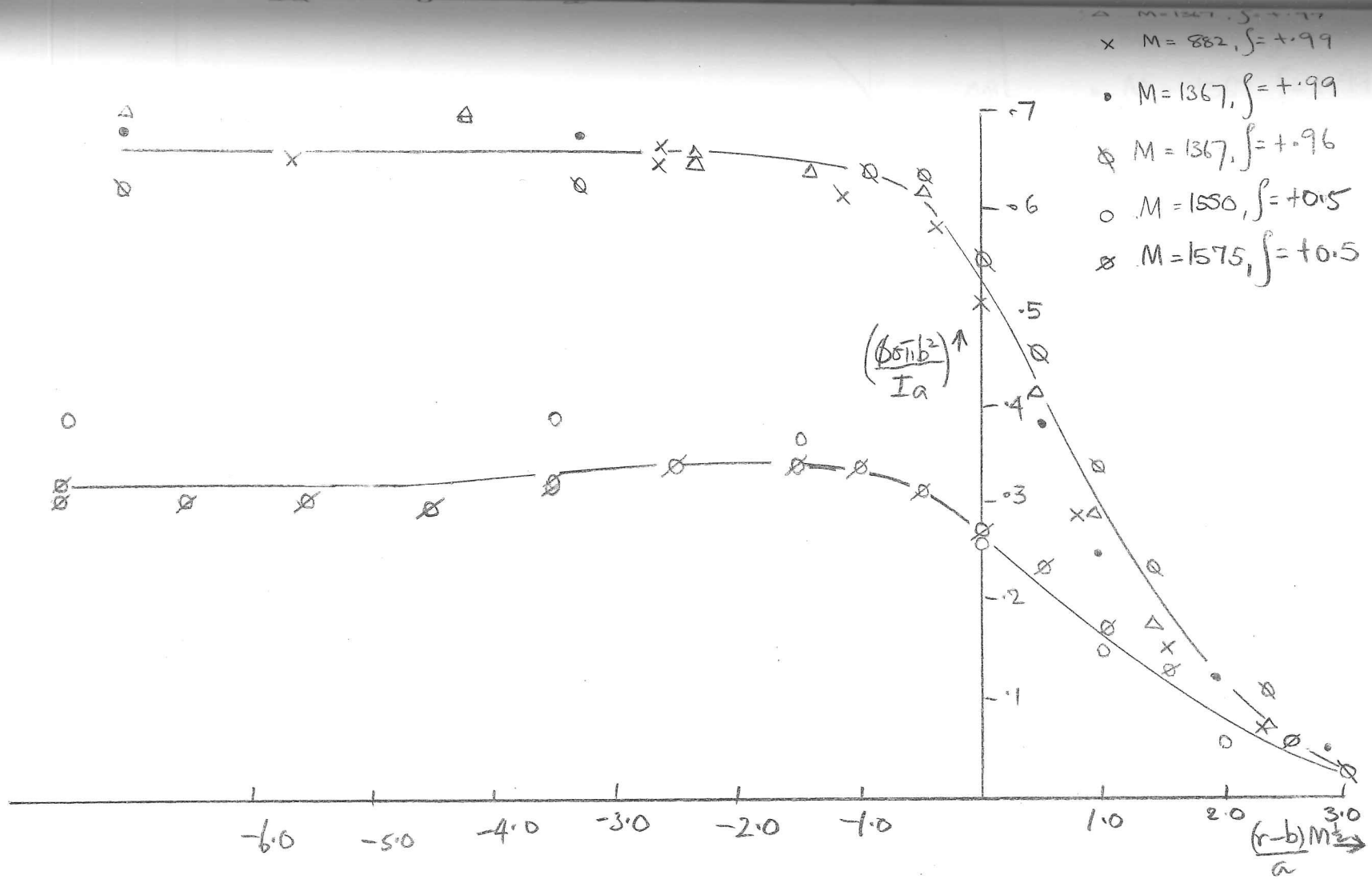
M = 882, ∫ = +.99
M = 1367, ∫ = +.99
M = 1367, ∫ = +.96
M = 1550, ∫ = +0.5
M = 1575, ∫ = +0.5
(Φ₀₁₁b²/Ia)
.7
.6
.5
.4
.3
.2
.1
-6.0
-5.0
-4.0
-3.0
-2.0
-1.0
1.0
2.0
3.0
(r-b)M^½/a

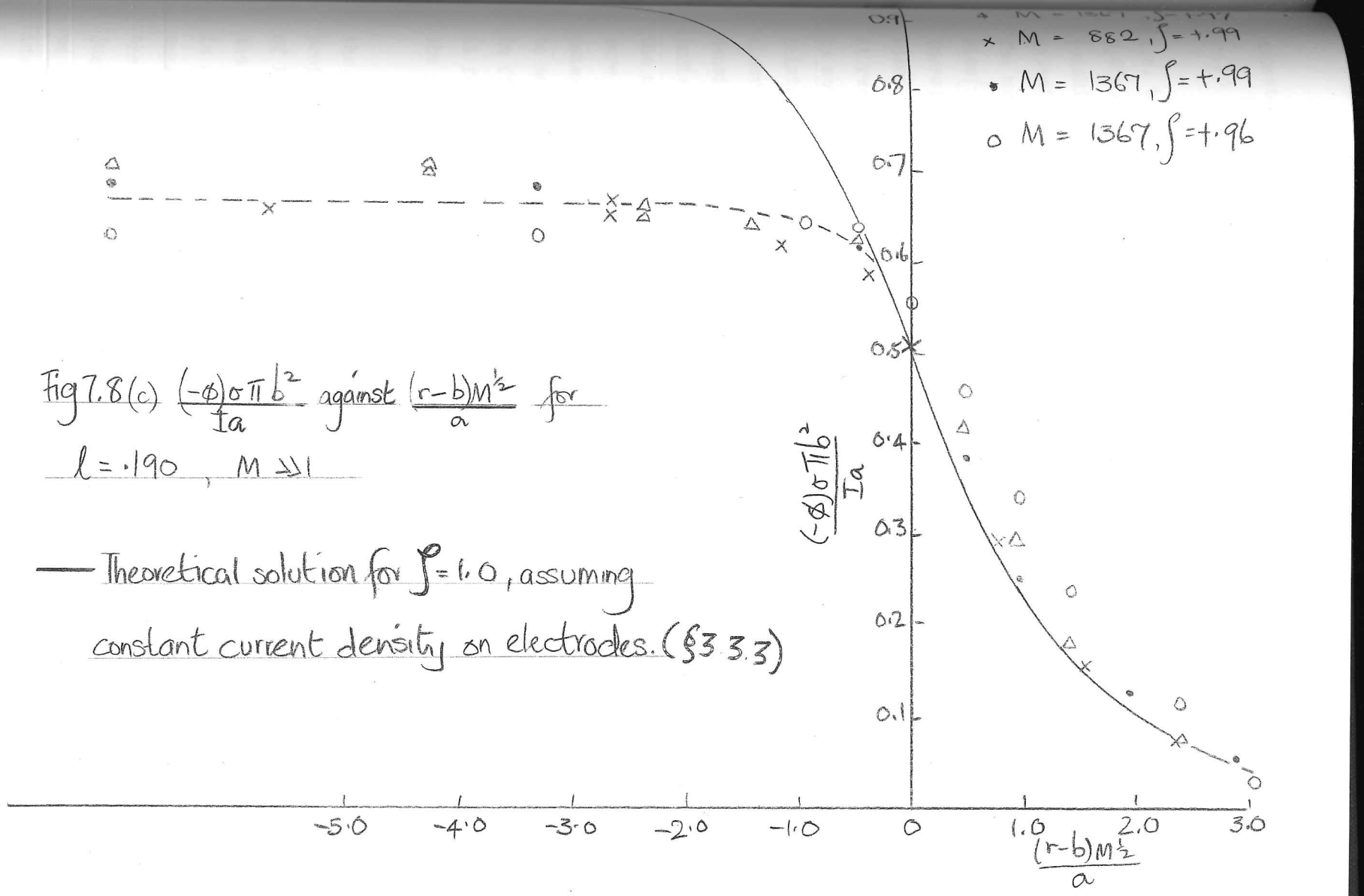

Fig 7.8(c) $\frac{(-\phi)\sigma\pi b^2}{Ia}$ against $\frac{(r-b)M^{\frac{1}{2}}}{a}$ for

$l = .190$, $M \gg 1$

— Theoretical solution for $\int = 1.0$, assuming constant current density on electrodes. (§3.3.3)

expected since in the central region, (4), as we have already noted, $(-\phi) \sigma b^2 / aI$ varies linearly with $M^{-\frac{1}{2}}$, $(-\phi)$ increasing as M increases.

The results shown in fig.7.8(b) were taken in the second apparatus i.e. the disc and wall, and were plotted in the same way as those in fig. 7.8(a). In this case we have some results taken with the probe just touching the wall or very close to it, $\delta < .043$, there being no detectable difference due to moving the probe very slightly near the wall. The most interesting point about these results is that near the edge of the disc $(-\phi)$ and, what is more, the distance in which this drop occurs is $O(aM^{-\frac{1}{2}})$. Therefore the potential on the electrodes cannot be considered as resembling that on perfectly conducting electrodes, the question of whether it resembles that on electrodes emitting current at a constant density is settled by reference to fig.7.8(c) where we compare the experimental points with the potential profile produced by such an electrode. The discrepancy for $r < b$ clearly shows why the assumption of a constant current density is erroneous, but the comparatively good agfeement for $r > b$ indicates, perhaps, that in this region the profile is less sensitive to the current distribution on the electrode. Note that if the electrodes were perfectly conducting, the probe would have recorded a constant potential across the electrode, at least to O(d/a). The second point to notice is that the profiles of ϕ for all the values of δ, examined in figs.7.8(a) and 7.8(b) are functions of $(r-b)/(aM^{-\frac{1}{2}})$, and therefore it follows from our argument in §3.3.3 that the current distribution on the electrodes near their edges was a function of $\left((r-b)/aM^{\frac{1}{2}}\right)$.

It is interesting that the thickness of the layers are approximately the same in all cases, being about $6\, aM^{-\frac{1}{2}}$. This may indicate why the profiles are not completely similar and why the slopes of the two curves of R/R_∞ against $(\ell M^{\frac{1}{2}})^{-1}$ are different in fig. (7.5), since if $\delta \simeq 6aM^{-\frac{1}{2}}$ the ratio of the thickness of the layers to the radius of the electrodes is $\delta/b = 6(\ell M^{+\frac{1}{2}})^{-1}$. For the maximum value of M in the first apparatus $\delta/b = .46$ and in the second apparatus $\delta/b = .78$. Therefore the approximation we made in § 3.3 that $\partial/\partial\rho \gg \frac{1}{\rho}$ is not really justifiable in analysing our experimental situation, and consequently we do not expect that the curves of R/R_∞ against $(\ell M^{\frac{1}{2}})^{-1}$ to be identical for the two apparatus. Neither do we expect the ϕ profiles

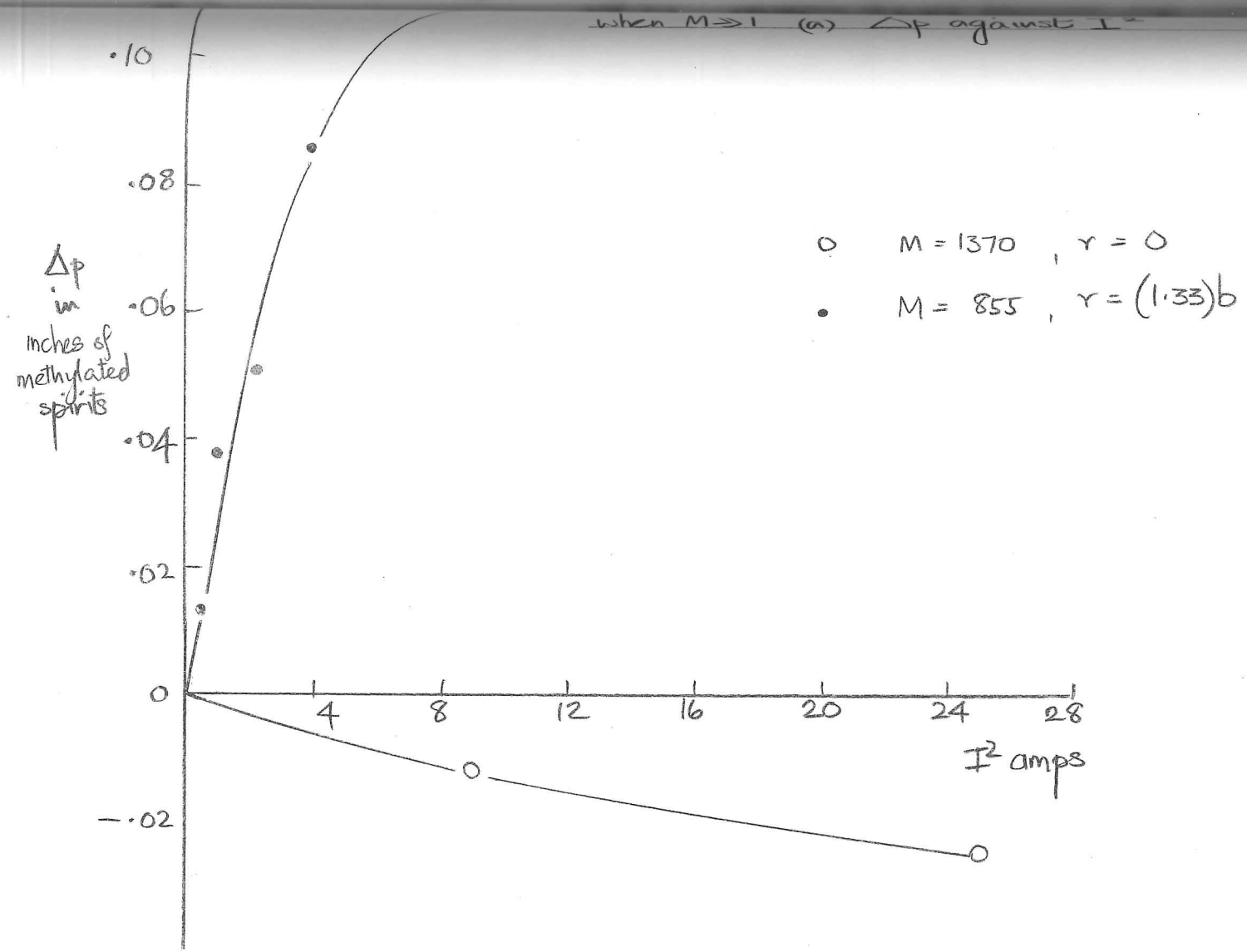
when M⇒1 (a) Δp against I²
·10
·08
·06
·04
·02
0
−·02
Δp in inches of methylated spirits
4
8
12
16
20
24
28
I² amps
M = 1370 , r = 0
M = 855 , r = (1·33)b

Fig 74 (b) Δp against I^2, $J^2 = 1$, $r/b = 1.267$

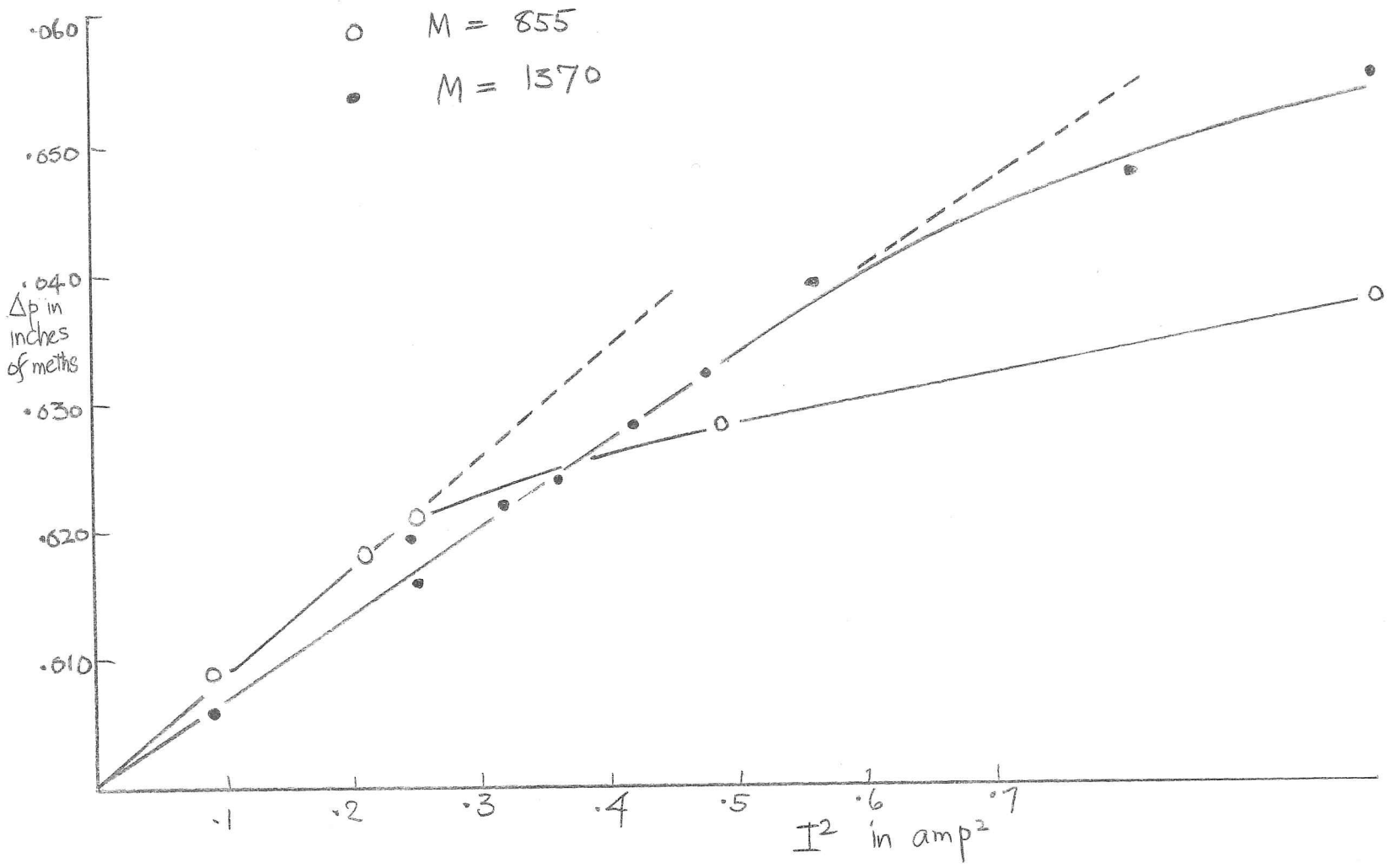

to be the same, even if they had been measured at the same value of ρ.

7.3.2. Pitot tube measurements.

As with the electric potential probes, when we began to use the pitot probe we first checked that we were measuring a velocity low enough to be in the required flow regime. With the pitot tube we also had to ensure that the measured velocity was high enough for $(p_o - p_s)$ to be proportional to the square of the velocity v_θ. Since in the flow regime examined in §3.3. v_θ is proportional to I and since it follows from (7.2.7) that p_o is proportional to v_θ^2, if the MHD error is negligible, we had to find the values of I for which $\Delta p_1 = p_o - p_w$, was proportional to I^2 where p_w is the pressure at the tapping on the wall.

In fig.7.9(a) we plot Δp against I^2 when r = 0, M = 1370, and when r = 1.33b, M = 855, these and all subsequent readings being taken in the second apparatus, i.e. $\ell = .190$. Note that when r = 0, $\Delta p < 0$ since $v_\theta = 0$ and the static pressure is below that outside the discs due to the radial pressure gradient. When r = 1.33b, $\Delta p > 0$ showing that in region (1) the rise in total pressure is greater than the fall in static pressure, which is, of course, to be expected. The interesting point about these two curves is how they show that the static pressure in the centre is less sensitive to the onset of secondary flow than the pressure recorded in the flow region (1). The other interesting fact we found when investigating the onset of the secondary flow was that, as the current was raised, initially the flow was steady, but when $I \simeq 5$ amps a steady oscillation developed with a period of about 2 seconds, which was easily observable on the manometer by the rise and fall of the meniscus. This indicates that, as I increases, an unsteady flow occurs rather than a stronger secondary flow, as in the experiments of Lehnert (1955).

Realising that the most critical region for examining the onset of secondary flow was region (1), we then measured Δp at two values of M when r = (1.267)b. The results, plotted in fig.7.9(b), show firstly that the velocity decreases as M increases for given I, as is to be expected from the theory of § 3.3.3. Secondly they show that the onset of secondary flow is suppressed as M increases, which is the same conclusion

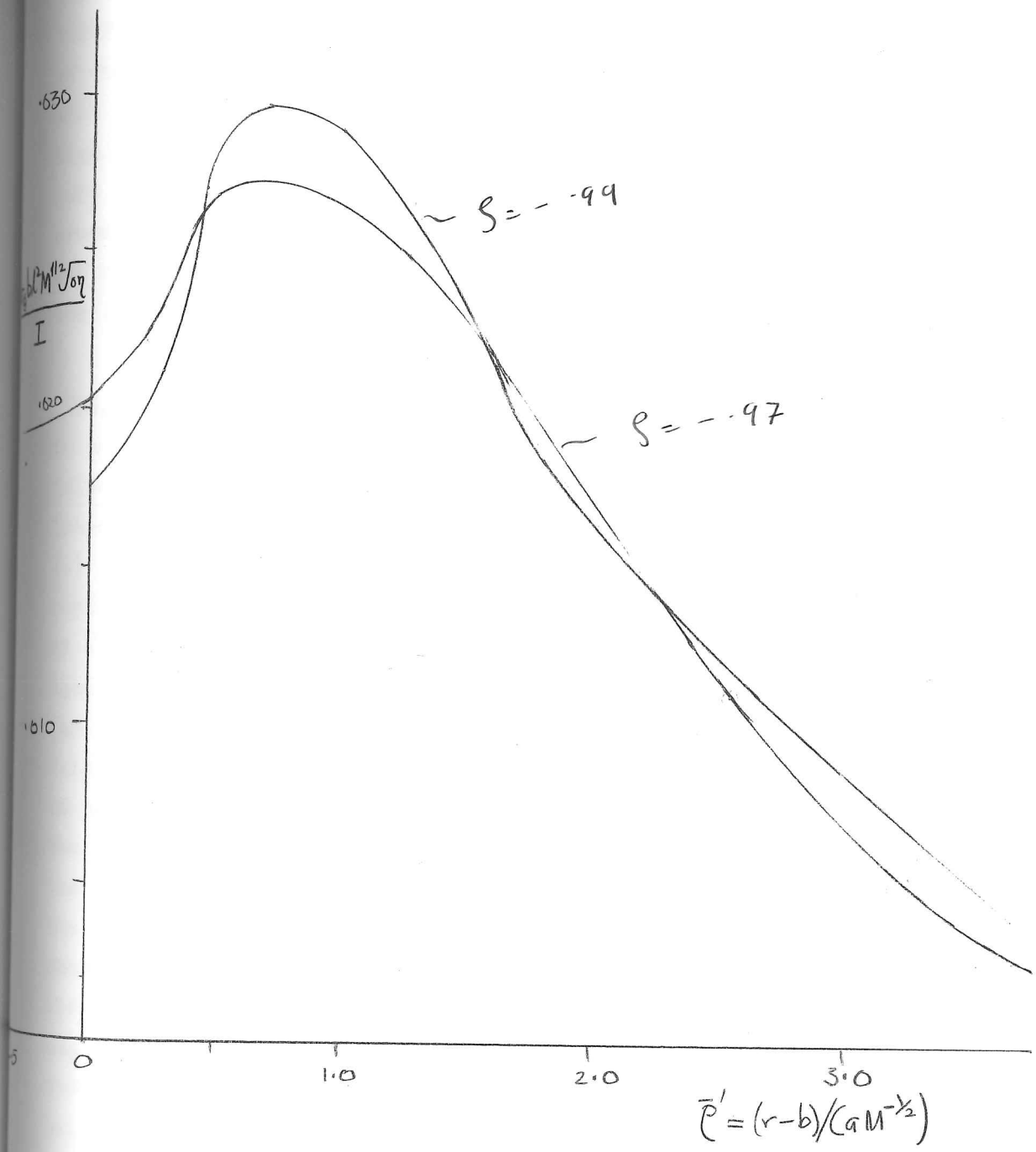

Fig 7.10 The variation of velocity with radius in (1).

$v_\theta b l^2 M^{\frac{1}{2}}\sqrt{\sigma\eta}\,/\,I$ against $(r-b)/(aM^{-\frac{1}{2}})$; $M = 1365$, $I = \cdot 7A$

that we reached in examining the electric potential measurements; thirdly to operate in the required regime we needed to measure pressures of the order of .030" meths which are about as low as can be measured with any degree of repeatability. This meant we had to operate at high values of M, with the associated disadvantage of using the pitot tube when the thickness of region (1) was least. Fourthly we have to presume that though the MHD probe error for these values of I is $\sim 0.5\Delta p$ the random errors preclude any conclusion as to the exact linearity of the $\Delta p - I^2$ relation.

We measured the radial distribution of Δp at $\int = .991$ and $\int = .972$, at only one value of M, 1370, since we could not lower M enough to obtain appreciably different yet repeatable readings and at only one value of I, .7 amps. From the radial distribution of Δp we calculated v_θ using the relations (7.2.9). Since Δp is positive in region (1) and negative in (4) it is zero on the boundary between these two regions and consequently it is impossible to calculate the velocity there at all accurately. We have plotted $\left[(v_\theta) b l^2 M^{1/2} \sqrt{\sigma\eta}/I\right]$ against $\left((r-b)(a M^{-1/2})\right)$ in fig. 7.10 so that if a suitable theory can be developed it may be compared with these results. We note that the velocity is greatest nearest the wall which is predictable since the jump in potential across the layer is greatest when ϕ is greatest, i.e. near the disc. Also note that, as r <u>decreases</u>, v_θ <u>decreases</u> more sharply near the wall, which is to be expected since, if the wall is highly conducting, the current must leave the electrode at right angles, thus reducting the shear stress and consequently the velocity at the wall. We may note that the Hartmann boundary layer here was so thin, .001" thick, as to be negligible. We compared the values of v_θ against our only available theory, namely derived from the assumption of a constant current distribution on the electrodes to see whether the values obtained were of the right order and found that at $\int = -.99$, $r = b$, the theoretical value at a current of .7 amps was 3.09 cm/sec, whereas that found experimentally was 2.40 cm/sec: at $\int = -.97$, $r = b$, the theoretical and experimental values were 2.85 and 2.65 respectively. Note that the experimental values are <u>lower</u> than the theoretical, which is to be expected since the maximum velocity induced by the theoretical current distribution

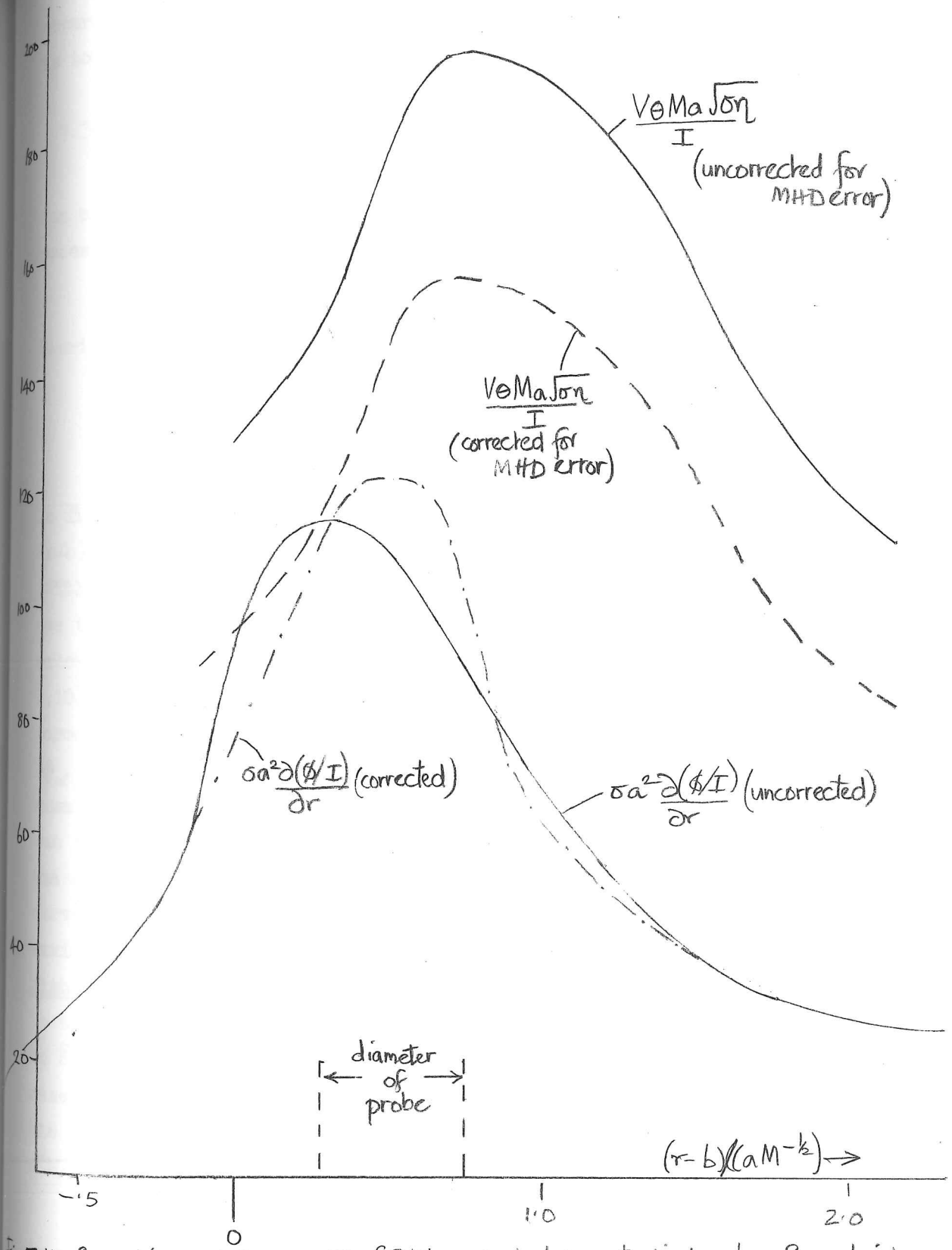

Fig 7.11. Comparison of the results of Pitot and electric potential probes for velocity
($\beta = .993$ $M = 1367$)

occurs at r = b, whereas the experimental maximum occurs at r > b, which is to be expected with highly conducting electrodes.

7.3.3. Discussion.

Having calculated the velocity from the pitot tube readings, we can now compare these values found with those caluclated from the electric potential distribution, using the relation,

$$-\frac{\partial \phi}{\partial r} + v_\theta B_o = 0 \qquad 3.3.24.$$

Rewriting this in a non-dimensional form we have:

$$\left(-\frac{v_\theta Ma \sqrt{\sigma\eta}}{I}\right) = -\frac{\sigma a^2 \partial(\phi/I)}{\partial r} \qquad 7.3.1.$$

In fig.7.11 we have plotted $\sigma a^2 \partial(\phi/I)/\partial r$ and $(v_\theta Ma\sqrt{\sigma\eta}/I)$ against $(r-b)aM^{-\frac{1}{2}}$, using the uncorrected readings of the e.p. and pitot probe. (With the latter we have corrected for the static pressure gradient). We see that a discrepancy of >100% exists between the two curves. We then calculated $(v_\theta Ma\sqrt{\sigma\eta})/I$ using the formula (7.2.9), (as we did for fig. 7.10), and thence calculated the mean value of $kd^2 \frac{\partial^2}{\partial r^2}\left[Ma\, v_\theta \sqrt{\sigma\eta}/I\right]$ across the probe face in order to use the correction formula (7.2.2) for ϕ_m. (We took $k = \frac{1}{4}$ being the value for the two-dimensional probe examined in §4.3). We note that though $d^2M/a^2 \simeq .1$, since $\partial^2 v_\theta/\partial r^2$ was so great the correction was large enough to reduce the difference in the maxima to about 30%. We also note that the maximum of the uncorrected curve of the potential gradient is at a lower value of r than the velocity maximum and that, with the correction applied, the maximum moves to a higher value of r. We note that this displacement is approximately equal to the diameter of the probe. See fig.7.11. This effect was predicted in §7.2.2 for an 'erf' potential profile, which we saw in fig.7.8(c) resembles our experimental curve. (We may note that the criterion for the e.p. probe error to be negligible, i.e. $d^2M/a^2 \ll 1$, was not satisfied; $d^2M/a^2 = .105$).

The main reason for the difference in these two corrected curves is probably that the experimental situation did not sufficiently satisfy the condition that $\partial/\partial r \gg 1/r$ and that therefore the radial currents were

sufficiently large to make (3.3.24) a poor approximation.

In conclusion we believe that these experiments have convincingly demonstrated the following qualitative flow phenomena predicted by Moffatt (1964) and further discussed in chapter 3.

(i) The 'channelling' of current between the two circular electrodes.

(ii) The existence of thin layers joining the disc edges of the circular electrodes. We have observed that in these layers a velocity is induced, which, when $M \gg 1$, decreases as M increases and that these layers become thinner as M increases.

(iii) The dependence on the magnetic field of the potential distribution across the electrodes, due to the finite conductivity of the electrodes.

The main quantitative results are:

(i) That when $M \gg 1$, the resistance between the two discs $R = \Delta\phi/I$ was found to vary with M according to the formula

$$R/R_\infty = 1 - k/M^{\frac{1}{2}},$$

where k is a constant depending on the geometry of the electrodes. This result was predicted on analytical and physical grounds in §3.3.3.

(ii) The potential, ϕ, in the regions (1) was found to vary with the radius r at a given value of ζ according to the formula:

$$\frac{\phi \sigma \pi b^2}{Ia} = P\left((r-b)/(aM^{-\frac{1}{2}})\right)$$

The function P varies with the disc geometry and the value of ζ : it is independent of M when $M \gg 1$. We conclude from this that the thickness of the region (1) was $O(aM^{-\frac{1}{2}})$.

(iii) From the previous result, using the theory of §3.3.3 we conclude that the current distribution on the electrodes was a function of $\left[(r-b)(aM^{-\frac{1}{2}})\right]$ near the edge of the discs. In the centre of the discs the current distribution was constant.

(iv) The value of k (see result (i)), for the second apparatus ($\ell = .190$), was 1.22, whereas that calculated assuming a constant current distribution is 1.064 - a difference of 20%. The values of v_θ found from pitot tube readings at $r = b$ were within 25% of values calculated from the same theory. The distribution of ϕ for $r < b$ did not compare well

with the theoretical profile, but did agree to within 15% for $r > b$. Most noticeable though was that the shape of the two curves was very similar, indicating perhaps that the potential profiles for $r > b$ are not very sensitive to the current distribution on the electrode. Therefore we conclude that the constant current distribution theory provides a rough estimate for the values to be expected experimentally, particularly for $r > b$.

(v) The calculations of velocity in the region (1) deduced from Pitot probe measurements were between 100% and 40 % higher than those made from electric probe measurements, when no corrections were applied for MHD probe errors. After applying such corrections we found that the difference between the two sets of measurements were reduces to between 30% and 150%; also the value of r at the maximum of the e.p. readings became closer to that of the pitot readings. Thus we concluded that our error corrections were of some value, particularly that to the e.p. probe which has never been used before. However, the large discrepancy remaining between the results demonstrates how little we understand the probes. (Some of the discrepancy may be due to the flows not satisfying the conditions of the asymptotic theory, by which we compared the results of the probes).

8. Experiments in rectangular ducts.

8.1. Introduction

8.1.1. Aims.

The aims of our experiments in rectangular ducts were twofold.

Firstly we wanted to use Pitot and electric potential probes in stable, laminar flows which are well understood in order to measure the errors caused by MHD effects, such as those discussed in chapter 4, and those caused by using the probes in regions where the probe size is comparable with the distance in which large changes in velocity or potential occur.

Secondly we wanted to use our probes to investigate the flow in a duct whose walls perpendicular to the magnetic field (BB) are highly conducting and whose walls parallel to the magnetic field (AA) are non-conducting, i.e. that flow examined in §2.4 and in our paper, Hunt (1965). In particular we wanted to confirm the existence of the salient features of the flows found in our analysis and to investigate the manner in which these flows become unstable.

8.1.2. Previous work

We mentioned the work of East (1964), Moreau (1966) and Lecocq (1964) on Pitot tubes in chapter 4. Other experiments with Pitot tubes in magnetic fields have been performed by Sachs (1965) and Branover & Lielausis (1961) on measuring velocity profiles of turbulent flows in narrow rectangular channels. As far as we are aware there have been no experiments to measure velocity profiles of laminar MHD flows, for the very good reason that such a task is difficult and, of course, one's measurements can be compared with the theory. Therefore the work described in this chapter is the first attempt into this field. Furthermore we describe the results of electric probe measurements and, where possible, compare these results with those of the Pitot tubes. (Although Lecocq used both types of probe he did not compare the results of the two probes).

Alty (1966) has already examined experimentally the duct flow we analysed, Hunt (1965), by means of pressure and potential measurements on the walls of the duct, his results agreed very well with the theory as described in §2.5.3. However, as the Reynolds number, R, of his flows increased the flow ceases to be laminar and exhibited certain interesting effects; these effects could not be examined further by external measurements, but only by probe measurements. Thus the work of §8.4 is a continuation of Alty's work.

8.1.3. Summary

In §8.2 we describe experiments to examine the flow in a narrow, .116" x $2\frac{3}{8}$", duct with non-conducting walls using two Pitot tubes, one with a circular tip of diameter .028" and the other with an oval tip (.012" x .062"). The Pitot tubes were supported in the thin duct from a wider circular duct, 1" in diameter. The main conclusions we drew were:

(a) At the junction between such a thin duct and a wide duct, the exit effects are very much stronger, i.e. affect the flow further upstream, the greater the magnetic field applied perpendicular to the thin duct. As a result we were only able to use the Pitot tubes at zero or low values of M, the Hartmann number based on the half width of the duct.

(b) When M = o, Pitot tubes of diameter even up to $\frac{1}{4}$ of the duct width can measure the velocity to within 7%, the experimental error in our case, when the probe is more than one diameter or thickness away from the wall.

(c) When M = 2.36 and M = 5.03 we measured the velocity profile across the duct and found that the agreement between the theoretical curve and experimental results was about 7% when M = 2.36 for the wide probe and better than this for the narrow probe. The results at M = 5.03 were poor on account of the greater exit effects. These are the first measurements known to us of the velocity profile in laminar Hartmann flow.

In §8.3 we describe experiments on the flow in a .6" x 3.01" duct, 32" long, made of non-conducting material, and placed inside the 66" duct described in chapter 6. We first investigated the MHD error on three kinds of Pitot tube for values of $N(=\sigma B_o^2 d/\rho U_\infty)$ up to about 3. The flow in this duct was less steady than in the $\frac{1}{8}$" duct, but despite the random errors in the manometer readings, two main conclusions emerged. First the Pitot error did not increase linearly with U_∞ or as the square of B_o as predicted by the formula

$$P_o = p_s + \tfrac{1}{2}\rho U_\infty^2 (1+\alpha N) \qquad 8.1.1.$$

where p_o and p_s are the dynamic and static pressures. This was to be expected since $N \ll 1$ was not satisfied, the requirement for the theoretical validity of the condition (8.1.1); however it was interesting that the error was

less than that predicted by (8.1.1) as N increased. Secondly, using α as a crude measure of the probe error, we found that if N was based on the length D_p, = 4 x (cross-section area/perimeter) of the probe tip, α was greatest ($\simeq 1.0$) for a flattened tube in which the width parallel to the magnetic field, a_p, = .012" and the width perpendicular to the magnetic field, b_p = .062"; it was smaller for a circular tube ($\alpha \simeq .4$) and least ($\alpha \simeq .2$) for a flattened tube in which a_p = .073", b_p = .024". This effect was a qualitative confirmation of the result predicted in §4.2.

We also used electric probes in this duct. We first measured the electric field in the core, finding good agreement with the theoretical value for laminar flow (< 1.5%) when M = 140, 247 but poorer agreement ($\sim$7%) at M = 418. In the boundary layer on the walls parallel to the magnetic field (AA) the experimental measurements differed markedly from the theoretical values, by about 50% for M = 247. However the difference decreased as M increased, indicating that as $M \to \infty$ the agreement with the asymptotic theory would improve.

In §8.4 we describe experiments in our main 66" duct, whose walls perpendicular to the magnetic field, BB, are highly conducting and walls AA are non-conducting, the dimensions being 2.486" x 3.010". We only examined the flow at $R < 1000$ and M = 943. Our measurements of static pressure, ΔP , showed that the flow ceased to be laminar at $R \lesssim 70$ and for $R > 500$ settled into a well defined second regime in which $\Delta P \propto R$ and $\Delta P/R$ was about 2.6 times its laminar flow value. The flow was very unsteady for $500 > R > 70$. Measurements of velocity in the boundary layer on the walls BB were below the values predicted by the laminar theory (Hunt, 1965), yet the velocity profile exhibited qualitatively the main features of the theoretical laminar flow, namely a large velocity close to the wall, a negative velocity in the outer part of the boundary layer and a core velocity less than the maximum velocity in the core. The electric potential measurements taken relative to the wall AA were also below the theoretical, both in the core and the boundary layer; however they indicated clearly the width of the boundary layer and the important fact that $\underset{\sim}{E} = 0$ in the core in the second flow regime. Comparing these results of static pressure, Pitot pressure, and the potential measured by the e.p. probe we were able to provide an order of

magnitude explanation for the curious second flow regime, in which secondary flows are likely to occur.

These experiments and those of chapter 7 have shown that, despite their limitations which need thorough prior investigation, Pitot and e.p. probes enable us to investigate flows not amenable to theoretical analysis and increase our understanding of those flows. We cannot, yet, place great confidence in the quantitative deductions made from their measurements. Clearly further work is necessary.

These experiments have also shown that the main 66" duct can be used for investigating other duct flows as well as that examined in §8.4, thus indicating its versatility. The other important fact proved by these experiments is that it does not leak!

(a) Side view (not to scale)

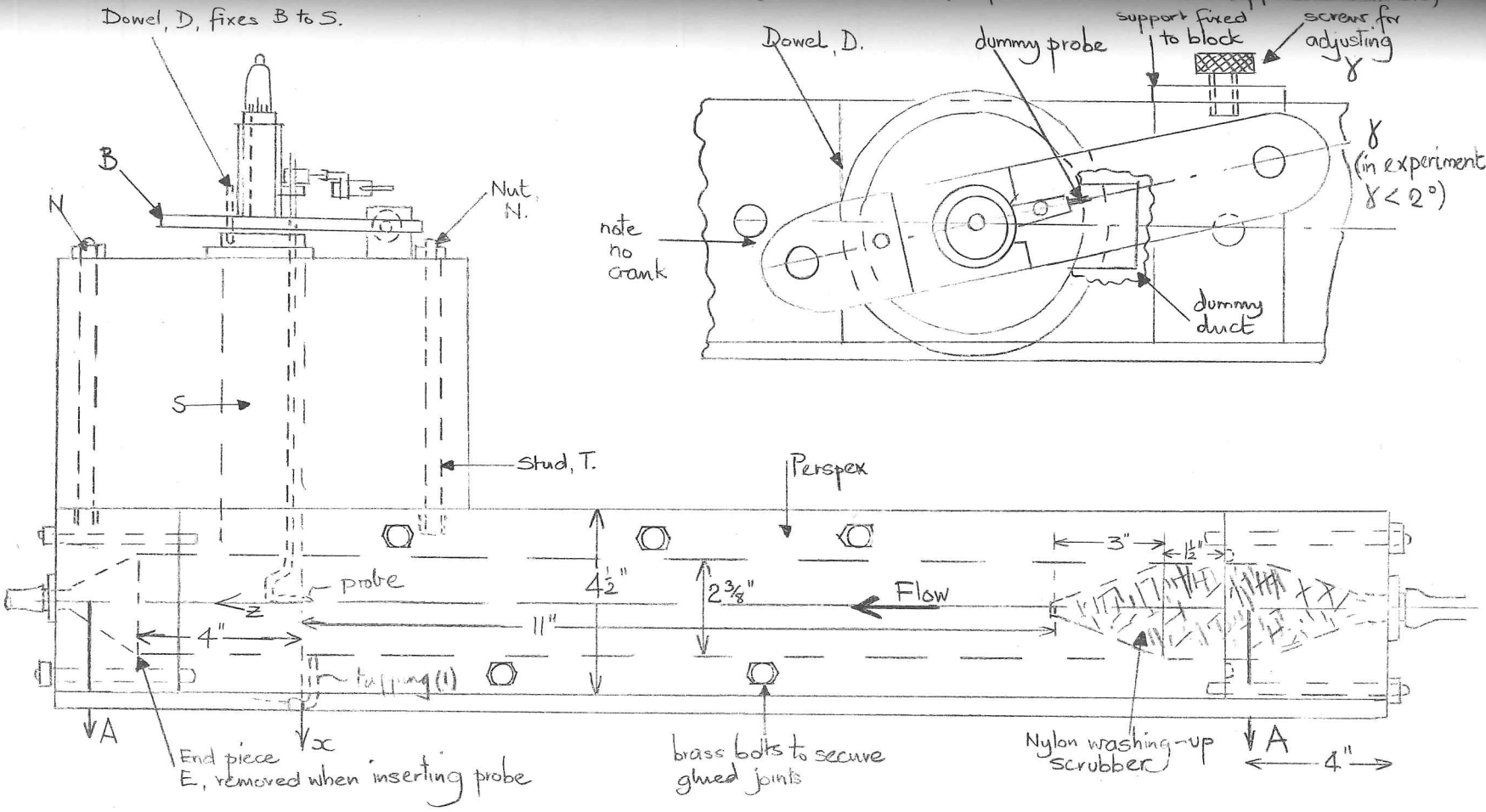

(b) Plan view of probe mechanism (approx ½ full scale)

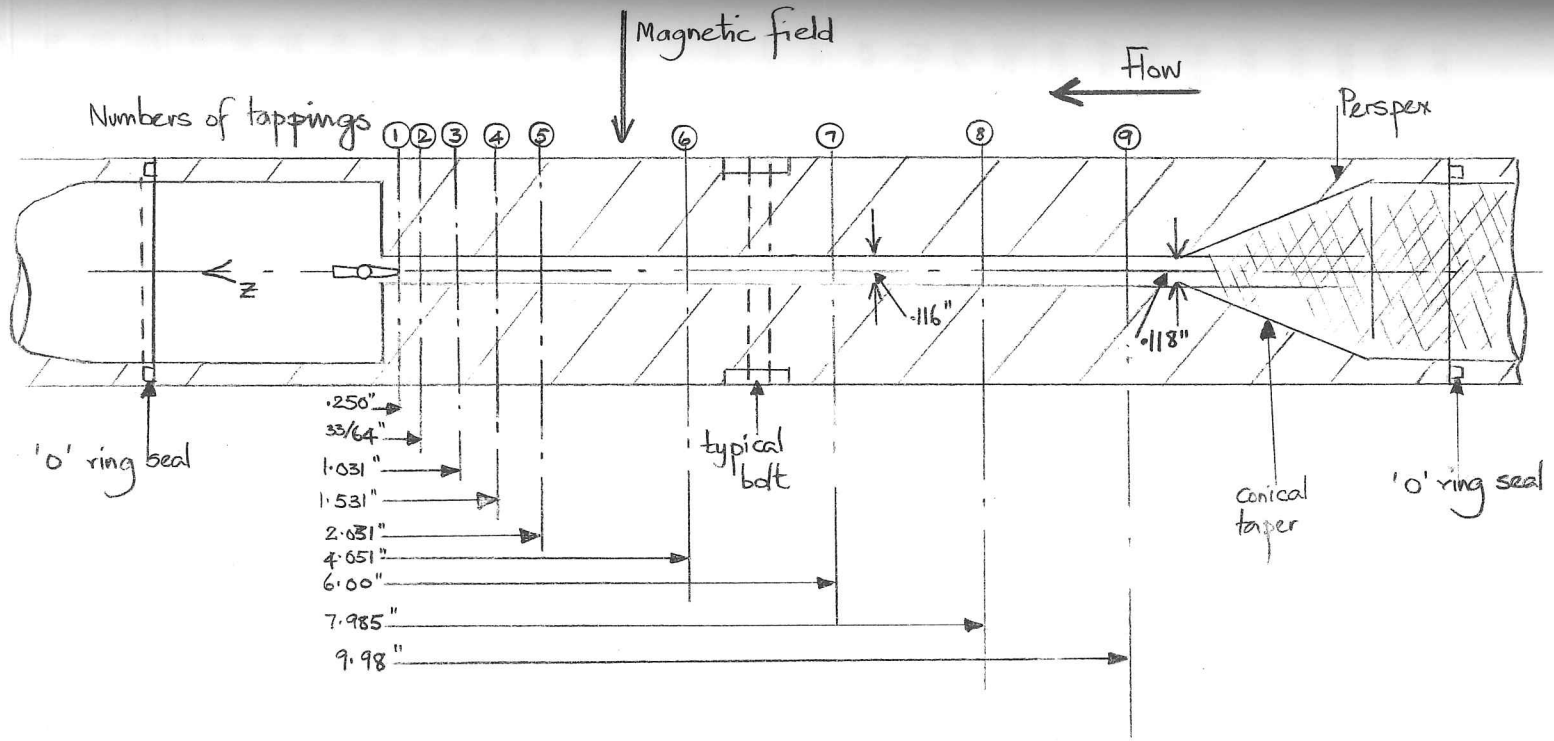
Magnetic field
Flow
Perspex
Numbers of tappings
1
2
3
4
5
6
7
8
9
N
.116"
.118"
.250"
33/64"
1.031"
1.531"
2.031"
4.051"
6.00"
7.985"
9.98"
'O' ring seal
typical bolt
conical taper
'O' ring seal

8.2. $\frac{1}{8}$" x $2\frac{3}{8}$" duct; non-conducting walls.

8.2.1. Apparatus.

The purpose of our first experiment on the use of probes in rectangular ducts was mainly to examine the errors caused by using a Pitot tube in a shear flow. We found that most text books on this subject merely recommended using Pitot tubes whose diameters were much less than the distance in which the velocity changed appreciably or else gave a very crude factor for measuring the displacement effect e.g. Rosenhead (1963) p.620. In air or water flow, if the velocity profile is required very near the wall, hotwire anemometers, Preston tubes, or heat transfer measurements may be used; all such measurements would be very complicated and uncertain in MHD flows.

Duct. As a result of these considerations we designed a rectangular duct with dimensions $\frac{1}{8}$"(= 2a) and $2\frac{3}{8}$"(= 2b), in section, to be used with Pitot tubes of diameter (d) up to .028", i.e. $d < .48a$. In order to avoid blocking the channel with the stem of the Pitot we decided to increase the duct width downstream of the Pitot tip. The duct, as constructed, is shown in fig.8.1. It was made up from various pieces of 'Perspex' being glued and bolted together. Its length was sufficient to enable us to measure fully developed flows and a settling chamber was constructed upstream of the slot. To reduce any unsteadiness, this gap was filled with a nylon washing-up scrubber. The pressure tappings were constructed by the same method as those of the 66" duct described in chapter 6.

Probes. The Pitot tubes were constructed to point sufficiently far upstream into the narrow portion of the duct (the slot) as to avoid any effects caused by the duct widening and the blocking of the flow by the probe stem. The first Pitot was constructed so that its tip would be protuding $\frac{1}{4}$" ($\simeq 4a$) into the slot, since we believed that with or without a magnetic field the exit effect would be negligible this far into the flow. (How wrong we were is shown in §8.2.2.). This was constructed in a similar way to that described in §7.2.3, namely by the fitting together of different stainless steel tubes; the tube at its tip being .028" o.d., .0155" i.d. (See fig.8.2a). The second Pitot had a

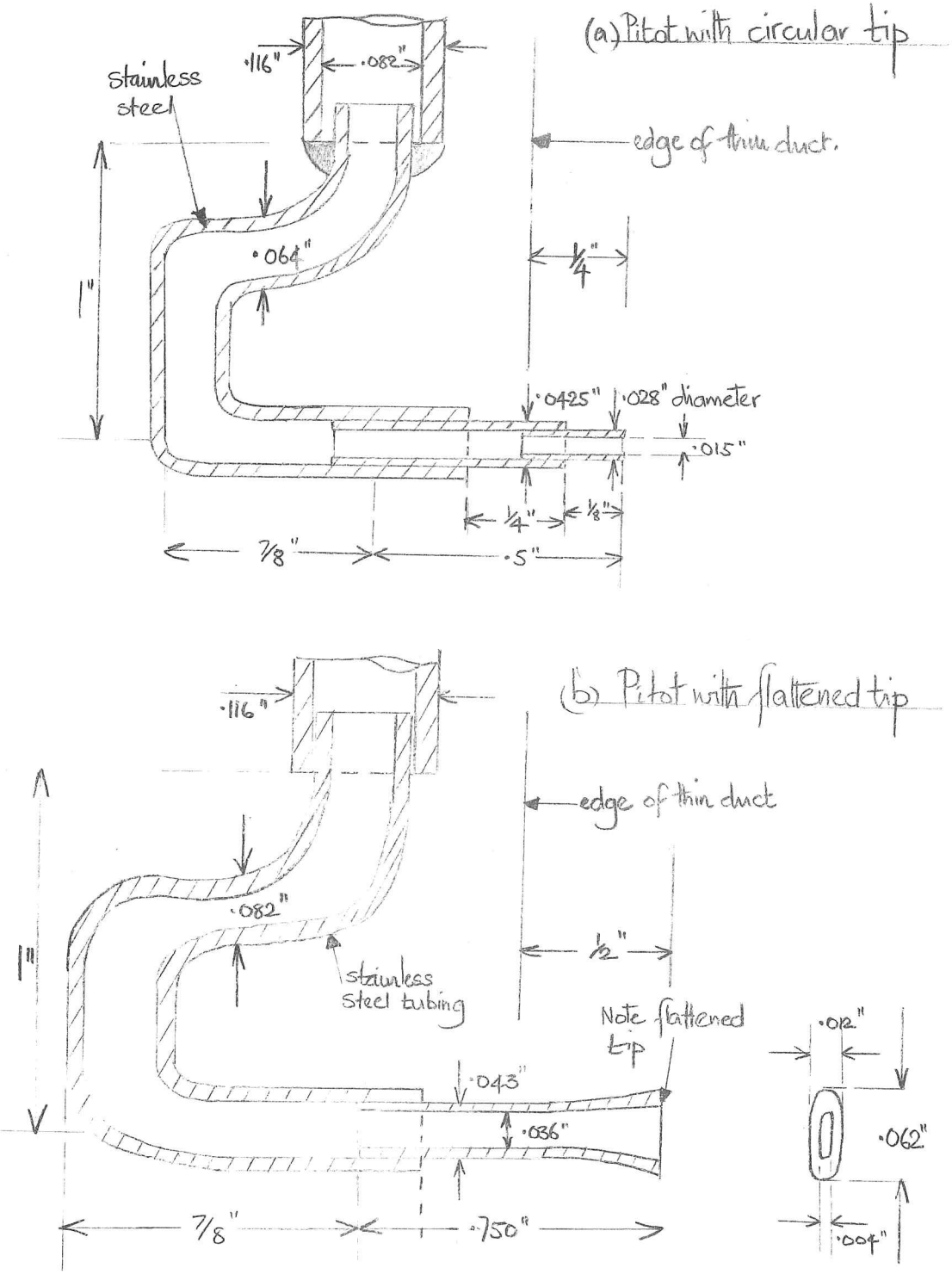

Fig 8.2 Pitot tubes used in duct I

different tip, being a .042" o.d. tube which was drilled out until its i.d. was .036" and then flattened until its external width was .012", (see fig.8.2b). We used the Pitots uninsulated and insulated, but found no difference in their behaviour.

Probe mechanism. The probe mechanism was not used in quite the same way as described in §6.4. Instead of using the cranks to maintain the crank-bar B (see fig.8.1a) parallel to the duct axis, we removed the cranks and fixed the crank-bar rigidly to the spindle, S, by means of a dowel, D. Then turning S moved the dummy probe across the duct, but altered its orientation, γ, relative to the duct axis; since $\gamma < 2^{\circ}$ for this thin duct the effect of varying γ on the Pitot was negligible. The spindle S was turned by pushing the crank-bar B with a screw adjustment attached to the probe block; see fig.8.1(b).

With this design of duct, it was very difficult fitting the probe mechanism and probe onto the duct. To do this the studs, T, retaining the probe block had to be removed and the probe block very gingerly manoeuvred onto the duct to avoid knocking the probe; (the probe was fitted in the probe mechanism outside the duct). To ensure correct alignment of the dummy duct and that the probe had not been knocked, we removed the end piece, E, and looked into the duct.

The details of the duct measurements and the various conversion factors for calculations of the experimental results are given in table 8.1.

8.2.2. Static pressure measurements.

Since this was the first experiment in which we had used the flow circuit described in §6.5, we ought to mention the procedure involved. Because the static pressure reading on the manometer between any two tappings or between a tapping and the Pitot when there was no flow, (the zero reading), tended to vary it was necessary to take this zero reading as often as possible, otherwise interpolating over a long time between two zero readings led to large errors in calculating the pressure differences. (In the electrically driven flows this did not create any problem as the flow was started by turning a switch). A typical series

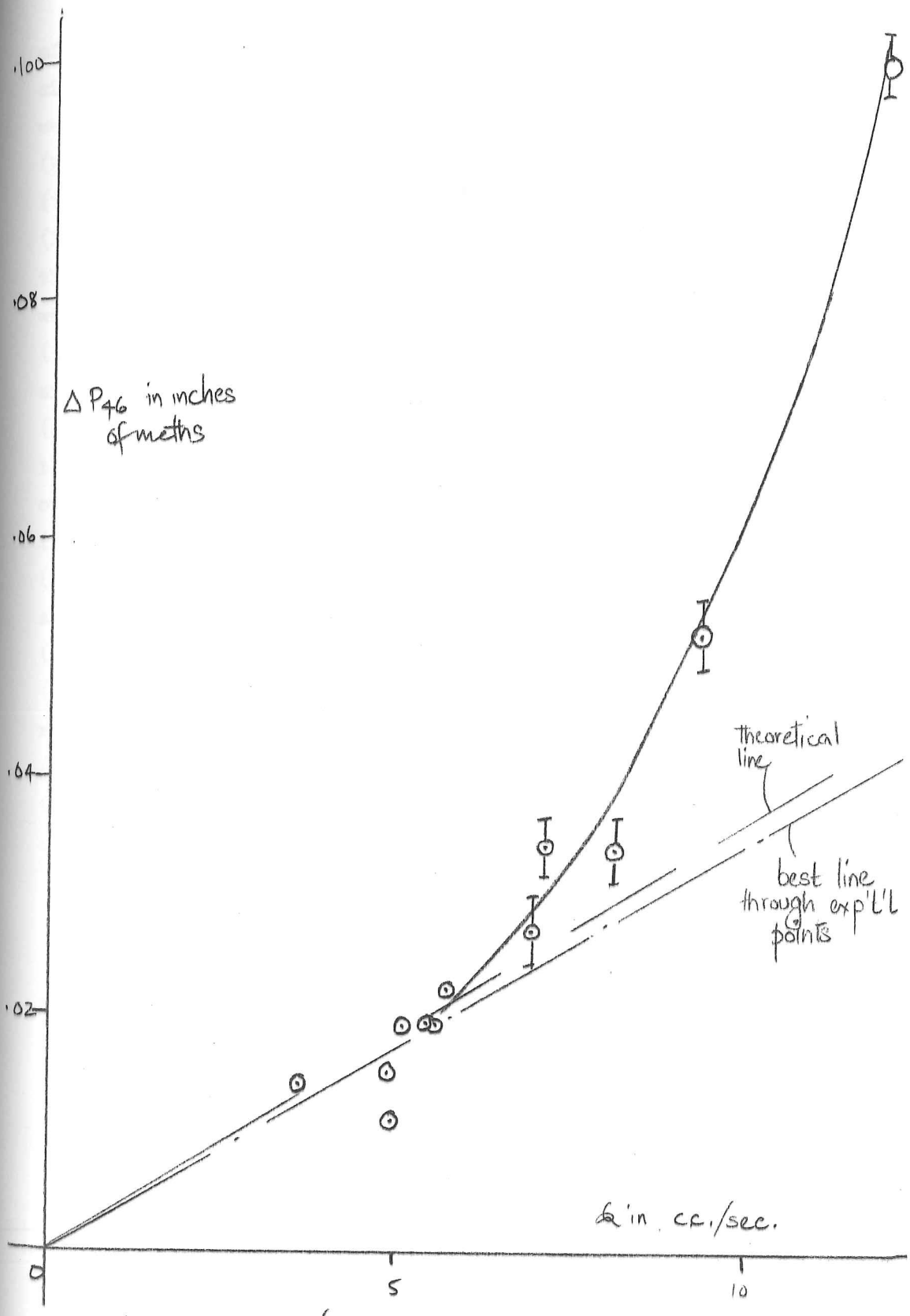

Fig 8.3 Pressure drop (ΔP_{46}) near the end of the duct against flowrate Q.

of readings would be taken in the following way. We assume the flow circuit has been filled such that there is mercury either side of the weir in the lower weir tank and that all the taps have been closed. (We refer to fig.6.6).

(1) Take zero reading on manometer.

(2) Open taps (4), (5) and (7). This does not lead to a flow from the upper weir tank u.w.t. to the l.w.t. since the pump seals the flow when it is stationary.

(3) Turn on pump at desired flow rate. This makes the mercury circulate between the l.w.t. and u.w.t., returning via the overflow pipe.

(4) Open tap (1) and regulate throttle valve. Flow now starts through the duct, settling down very quickly. We ensure that the pump is operating fast enough for there to be some flow through the overflow pipe.

(5) Take manometer reading.

(6) Take potentiometer readings of voltage across the flowmeter and the shunt in the magnet supply circuit.

(7) Re-check manometer reading.

(8) Take one or two more readings at differing flow rates, by regulating the throttle valve and the pump.

(9) Turn off tap (1). This stops the flow in the duct.

(10) Turn off pump. There may be some leakage back through the pump so we also close (7).

(11) Take zero reading on manometer.

The first measurements we made in this duct were static pressure readings between tappings (4) and (6), Δ_{46}. (See fig.8.1c), the Pitot being in position in the duct and M = 0. Our results, which are plotted in fig.8.3, showed that ΔP_{46} was proportional to Q only when Q < 7 cc/sec. This surprised us since the flow was fully developed and we could not believe that the effect of the Pitot tube was so great. However, in the linear regime we calculated the mean value of $\Delta P_{46}/Q$, (see table 8.2), and found that it differed from the theoretical value for plane Poiseuille flow by 1.5% with a standard deviation, s.d., of 8%. At these very low flow rates our pressure differences were difficult to measure and this was the cause of the randomness of the readings. (The more readings we took the more consistent the mean value).

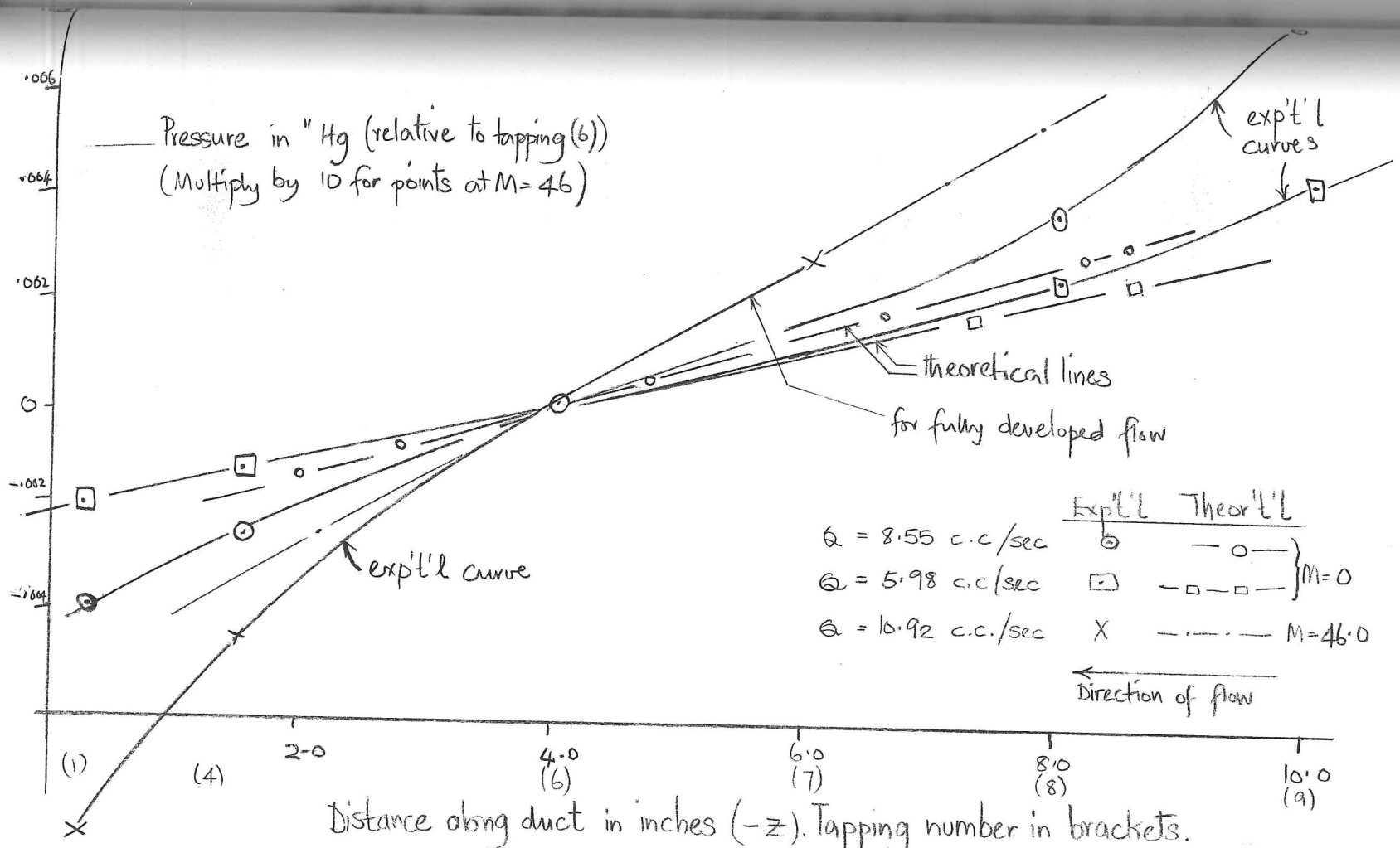

Distance along duct in inches (-z). Tapping number in brackets.

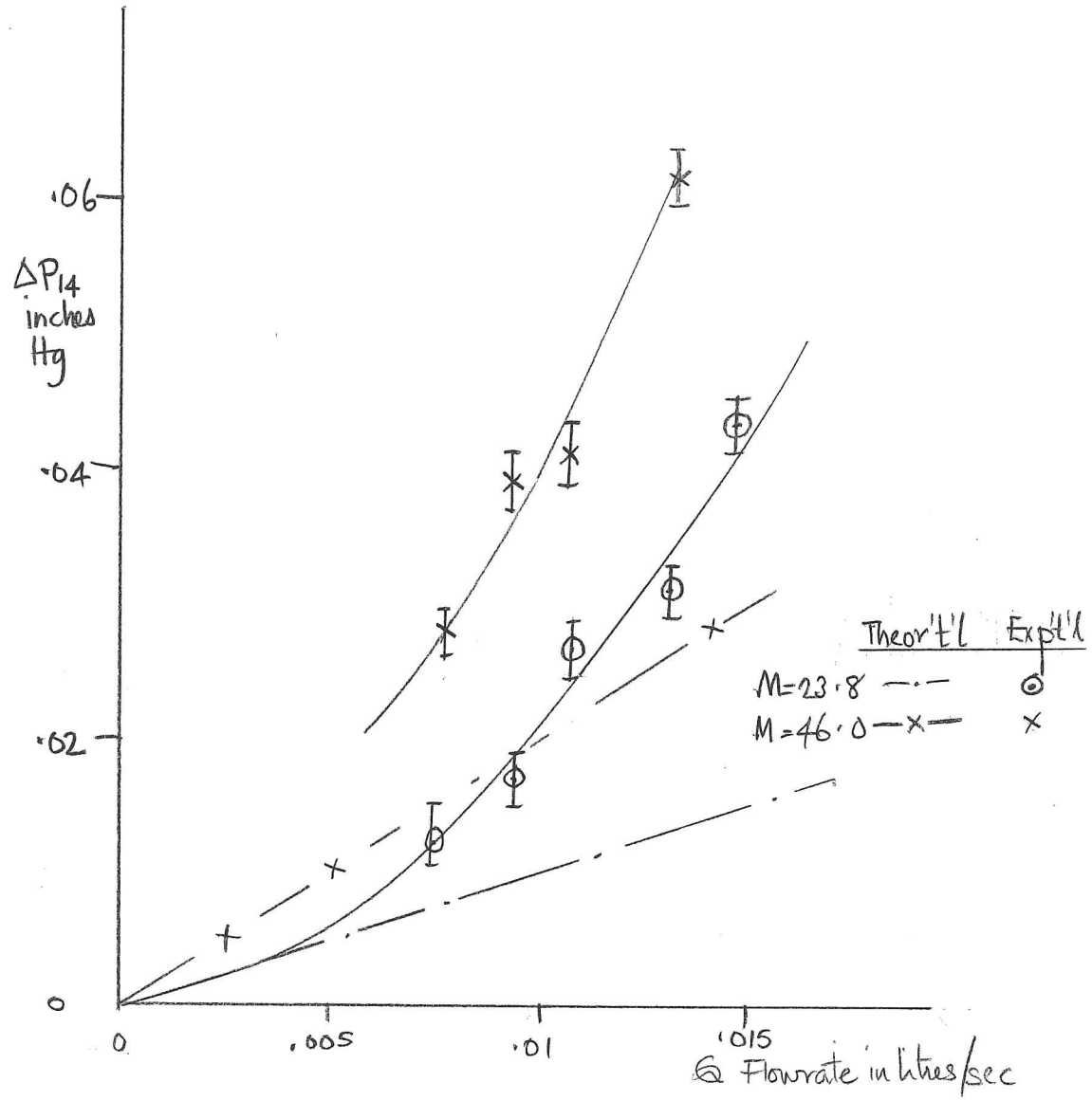

Fig 8.5 Variation of pressure drop (ΔP_{14}) with flow rate (Q) near the end of the duct when $M \gg 1$.

That the cause of the non-linearity was an exit or Pitot effect is shown better by fig.8.4 where the pressure differences between various tappings along the duct are plotted. When Q = 6 cc/sec, the pressure gradient is the same as that of plane Poiseuille flow near the exit but not at the entrance; it is interesting to note that the theoretical (i.e) entry length = Ra/20 = 1.4" when Q = 6 cc/sec, whereas we find that the 1.4" from the end of the duct dp/dz is 80% greater than its final value. When Q = 8.55 cc/sec, we see how the pressure gradient is least in the centre of the duct, thus confirming our hypothesis.

We then measured ΔP_{14} as a function of Q (fig.8.5) when M = 23.8 and M = 46.0 and found, to our surprise, that the $\Delta P_{14} - Q$ relation was not linear for the same values of Q as the $\Delta P_{46} - Q$ relation was linear. The entry length, of course, in this situation was much less; the obvious conclusion was that the exit length was greater. Again the $\Delta P - z$ curve confirms this view. We see in fig.8.4 that when M = 46.0, dp/dz agrees with the theoretical value for fully developed flow when $(-z) > 4"$, but diverges from this value very sharply as $(-z) \rightarrow 0$. We believe that the explanation of this effect is quite simple and should have been forseen.

If, when $M \gg 1$, the flow had changed suddenly from that of conventional Hartamnn flow in the narrow part of the duct to uniform flow in the wide part, it would have meant that the current in the slot would have returned from x = b to x = -b via the high resistance Hartmann layers on the walls. Instead of doing this the current near the end of the slot could return via the low resistance path of the wide part of the duct where v_z and E_x are much lower. Thus, the wide part of the duct effectively short circuited the Hartmann flow at the exit of the slot causing $(-j_x)$ in the core to be greater and producing a component of current $-j_z$ for $x > 0$ and $+j_z$ for $x < 0$. Clearly the effect of the short circuiting would be greatest when M was greatest, and would diminish towards the entrance of the slot, i.e. (-z) increasing. (We refer to this hypothesis later).

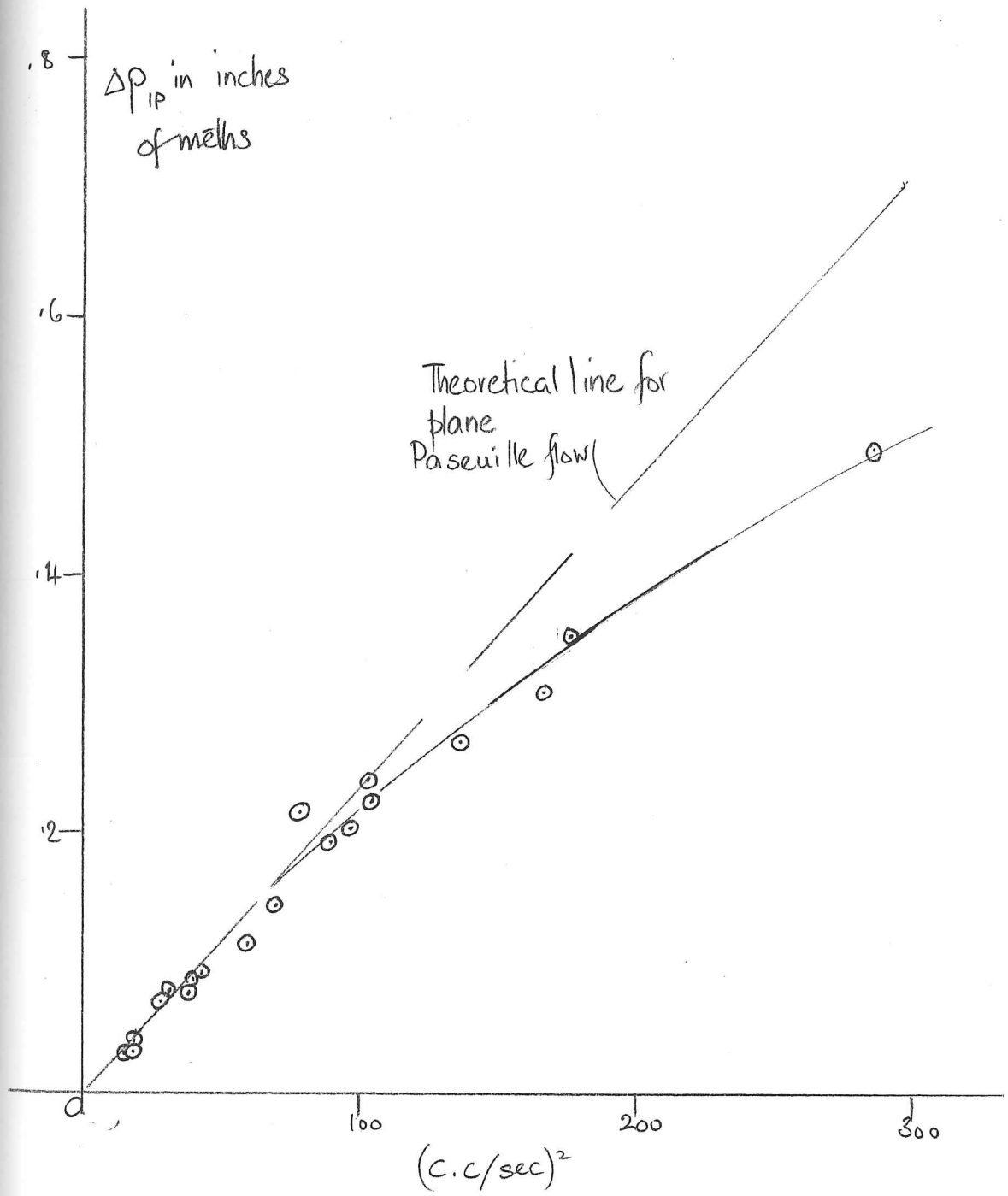

Fig 8.6 Graph of Pitot pressure (in inches of meths) (ΔP_{IP}) against (flow rate)², Q^2, when M = 0 and probe is in centre of the duct.

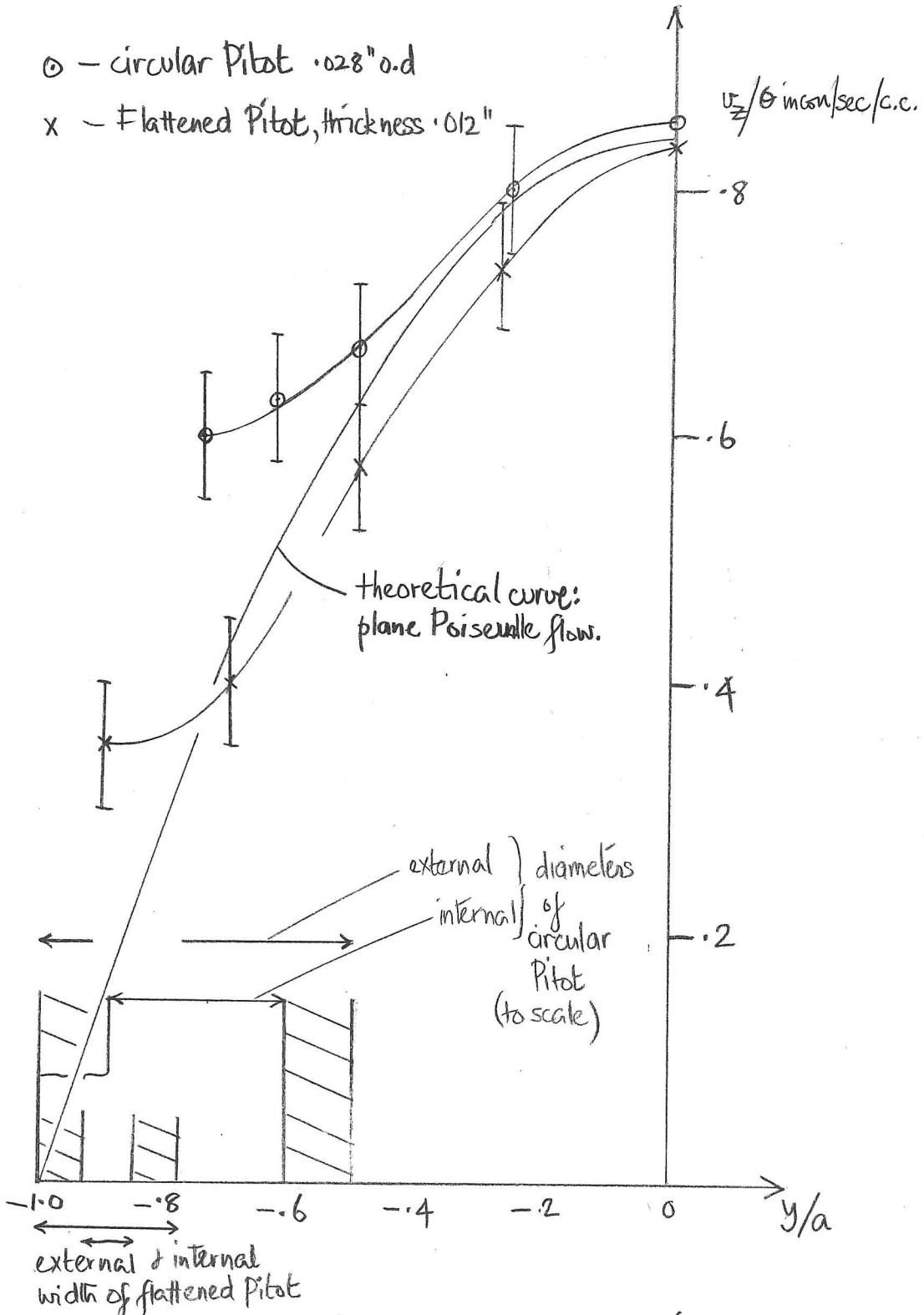

Fig 8.7. Measured velocity profiles in ⅛" x 2⅜" duct when M = 0. (Circular & flattened Pitot tubes.)

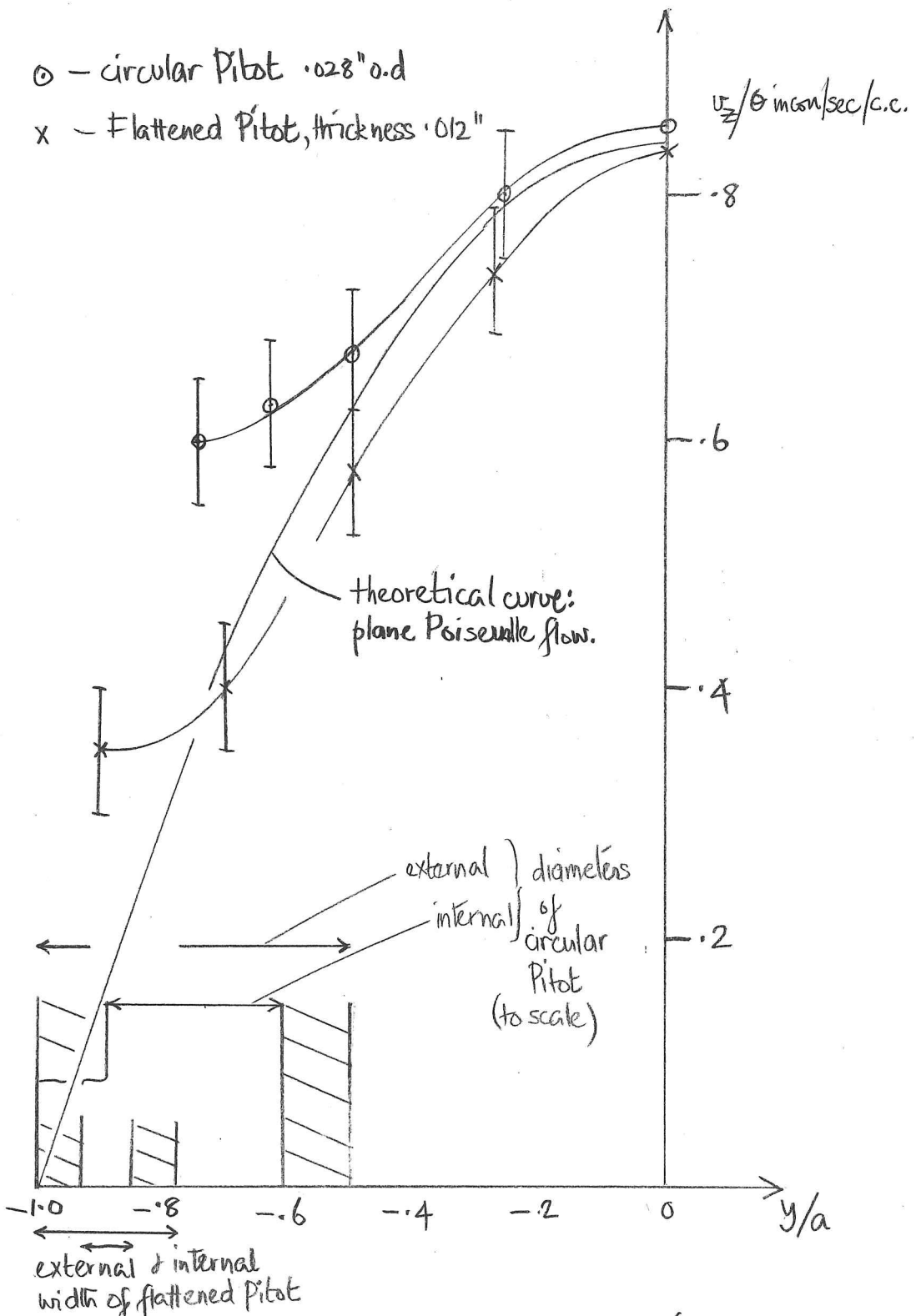

Fig 8.7. Measured velocity profiles in ⅛" x 2⅜" duct when M = 0. (Circular & flattened Pitot tubes.)

8.2.3. Pitot tube measurements

We first measured the pressure difference between tapping (1) and the Pitot tube, Δp_{1p}, when M = 0 at y = x = 0, z = $-\frac{1}{4}$". We noticed that the lag in the Pitot reading was much greater than that of the static pressure so that, since the flow over the weirs was not very steady, these readings were more prone to random error than those between two static pressure tappings.

We measured Δp_{1p} as a function of Q^2, since if the flow was fully developed $\Delta p_{1p} \propto Q^2$. Our results, which are plotted in fig.8.6, show that $\Delta p_{1p} \propto Q^2$ for $Q < \sim 7$ cc/sec and for Q greater than this Δp_{1p} falls below the theoretical line. Whether this was due to the velocity profile changing or due to some static pressure gradient is uncertain. (We did not have time to investigate further). In table 8.3 we have calculated the mean value of $\Delta p_{1p}/Q^2$ and $\sqrt{\Delta p_{1p}}/Q$, for Q < 7 cc/sec, comparing them to the values for plane Poiseuille flow. We again found that the agreement was well within the standard deviation, so that we could assume that the mean of a few measurements of Δp_{1p} would be accurate to within these limits.

We then measured Δp_{1p} against Q at various values of y, ($< (a-d)$) for Q < 7cc/sec and thence calculated v_z/Q. From our results, which are plotted in fig.8.7, we draw two tentative conclusions; first, the blocking effects of the Pitot are negligible, and second, that to within the experimental error the Pitot may be relied upon to measure velocity near a wall provided it is further than one diameter from the wall. To test these ideas, particularly the second, we then constructed a second, thinner Pitot, already described in §8.2.1. After measuring Δp_{1p} against Q, (table 8.4) and finding a similar order of agreement as with the first Pitot, we measured the velocity at points across the duct. (Fig.8.7). The measured velocities again follow the theoretical curve, differing by less than the experimental error for $(a-y) < d$, which confirms our conclusion mentioned above. The reason why the points all fall below the theoretical curve in the second case as compared to falling above in the first is obscure. Despite the possible random errors, it certainly seems a significant difference.

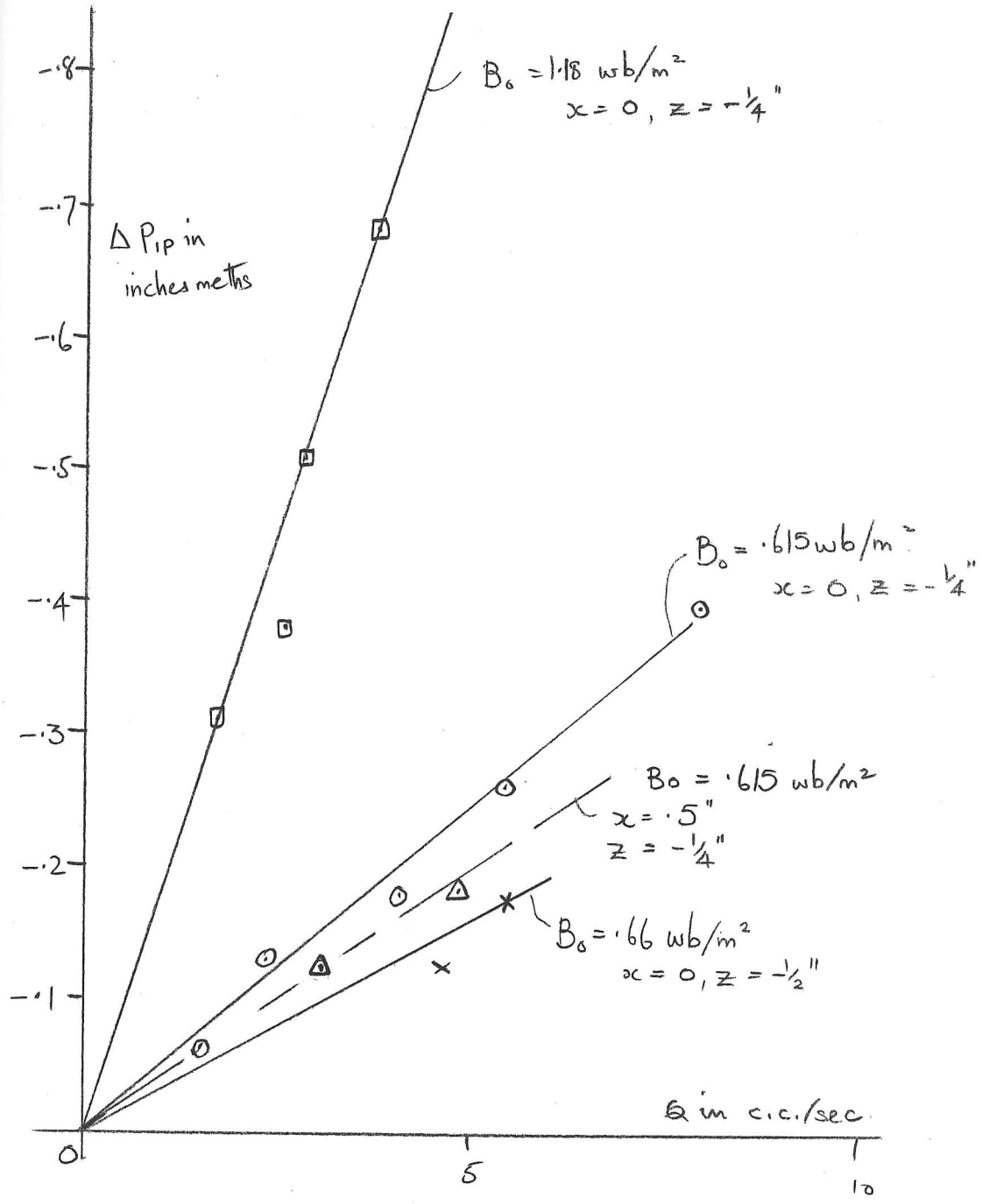

Fig 8.8 Graph showing negative pressure registered by Pitot when $M \gg 1$.

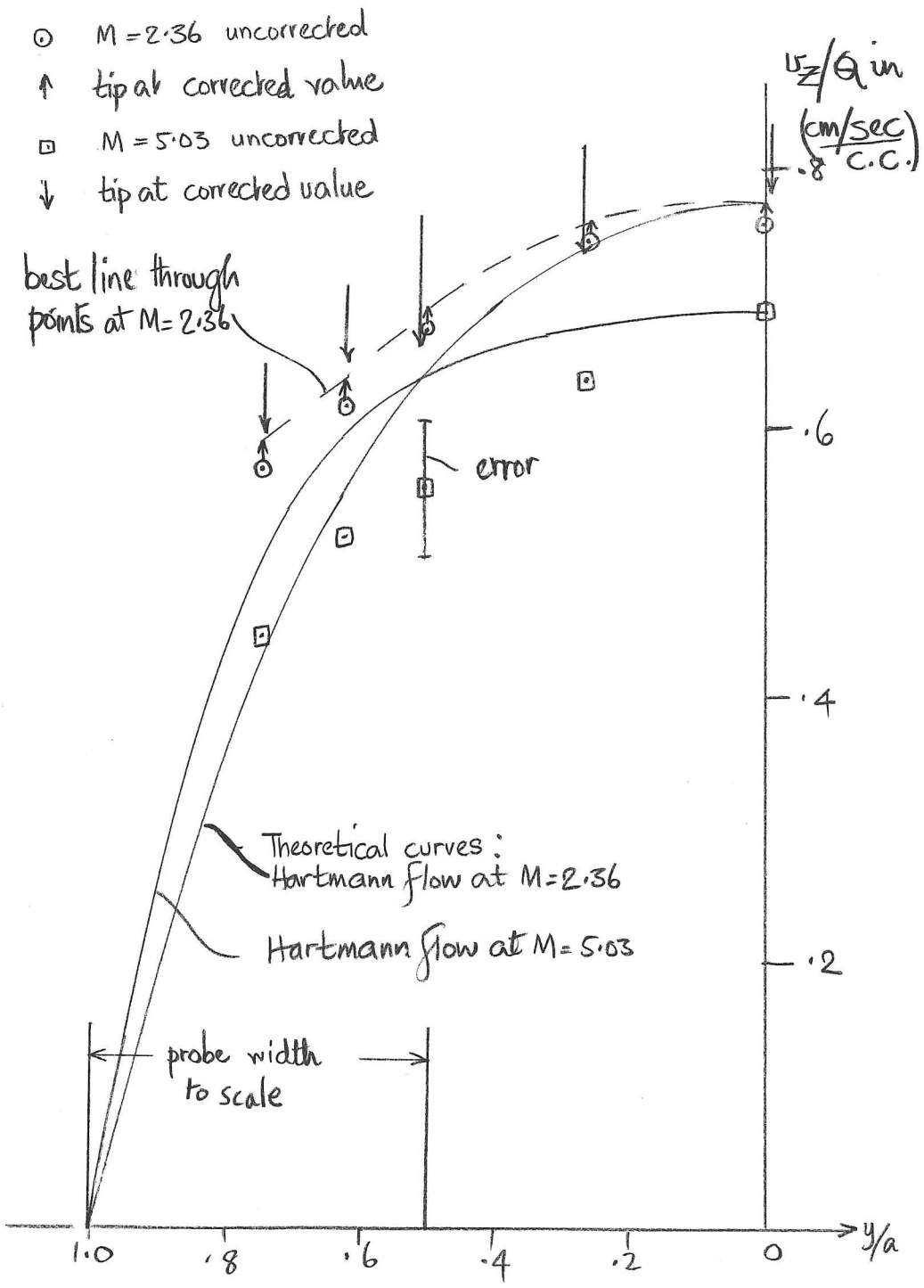

Fig 8.9 Measured velocity profiles when M = 2·36, 5·03. Circular Pitot tube

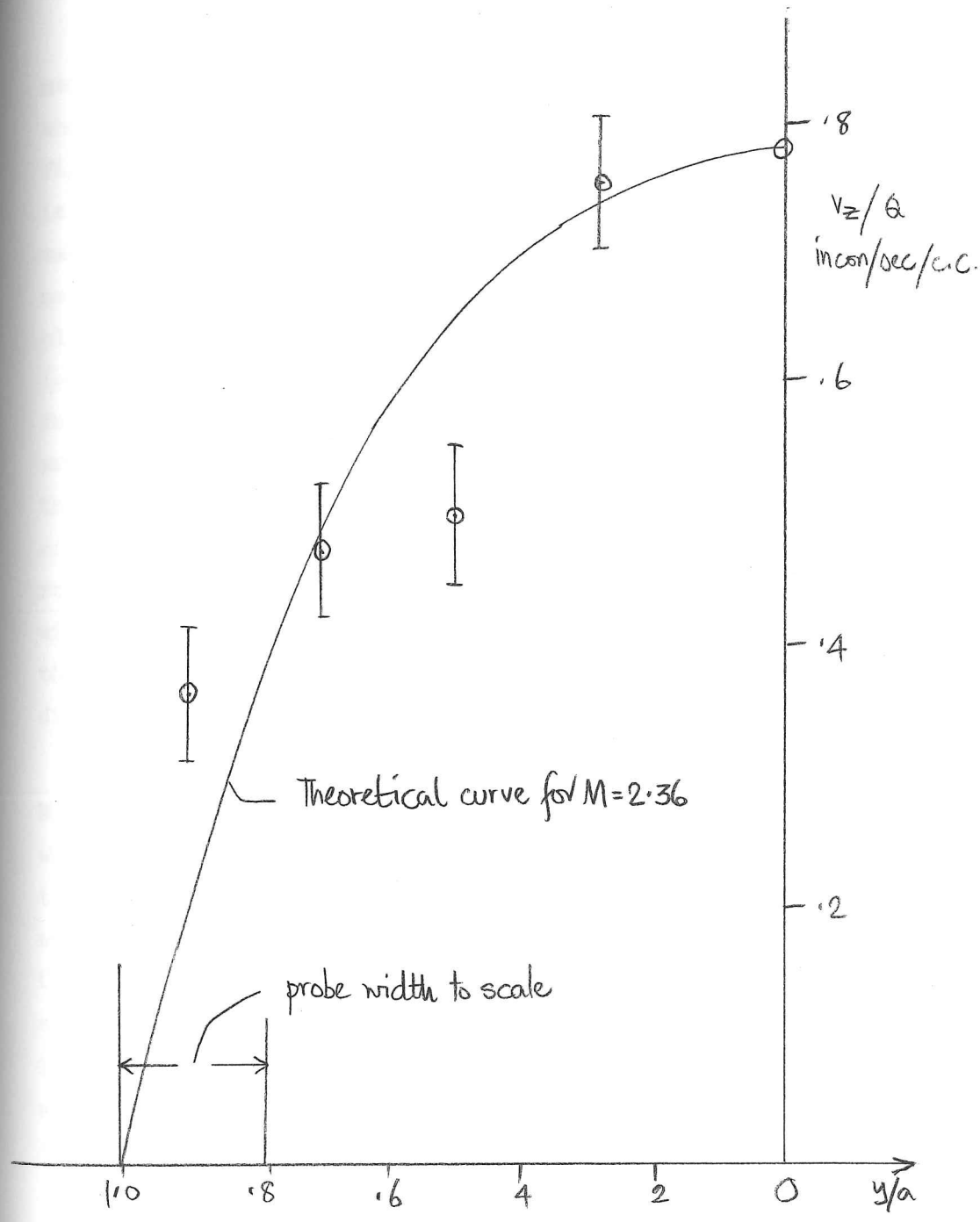

Fig 8.10 Measured velocity profile when M = 2·36 — flattened Pitot tube

Since the exit effects were worse for the static pressure measurements when $M \gg 1$ than when $M = 0$, we expected a similar effect when using Pitot tubes. This was, indeed, the case as is shown by fig.8.8 where Δp_{ip} is plotted against Q. We see first that Δp_{ip} is negative and second that Δp_{ip} varies approximately as $B_o^2 Q$ at the same value of x and z. This result would confirm our hypothesis that near exit of the slot when $M \gg 1$, large currents circulate in the x-z plane, since the presence of j_z leads to a vertical pressure gradient $(-j_z B_o)$, which would produce a negative pressure in the Pitot. To further test this idea, we measured Δp_{ip} at x = .5" and found, as would be expected on our hypothesis, that $(-\Delta p_{ip})$ was reduced. That the effect diminishes as (-z) increases is verified by the measurements of Δp_{ip} taken by the thin Pitot at $z = -\frac{1}{2}$"; we see that $(-\Delta p_{ip})$ is reduced. After first using an uninsulated Pitot, we coated the Pitot with non-conducting Perspex cement, but found no difference. We note that the MHD errors of chapter 4 would lead to a positive Δp_{ip} and so diminish the negative pressure.

We then decided to measure two velocity profiles at M = 2.36 and M = 5.03, using the MHD correction factor $-\Delta P_{ip} \simeq 170 B_o^2 Q$, where B_o is measured in wb/m^2, Q in litres/sec, and ΔP_{ip} in inches of meths. We found that, at these low values of M, Δp_{ip} was approximately proportional to Q^2 so that we could compare our results with the theoretical Hartmann flow profile. Our results, (fig.8.9), show how even at these low values of M the correction factors are appreciable and how unreliable the results are, inconsequence. However, the results for M = 2.36 when $a - y > d$ agree with the theoretical to within the experimental error and certainly demonstrated the flattening of the velocity profile.

Our results with the thin probe are better, fig.8.10 and three out of the four points (each taken from a graph of ΔP_{ip} against Q^2) for $a - y > d$ agree very closely. Poor as the results of figs.8.9 and 8.10 are, they are the first measurements, we know, of velocity profiles in Hartmann flow.

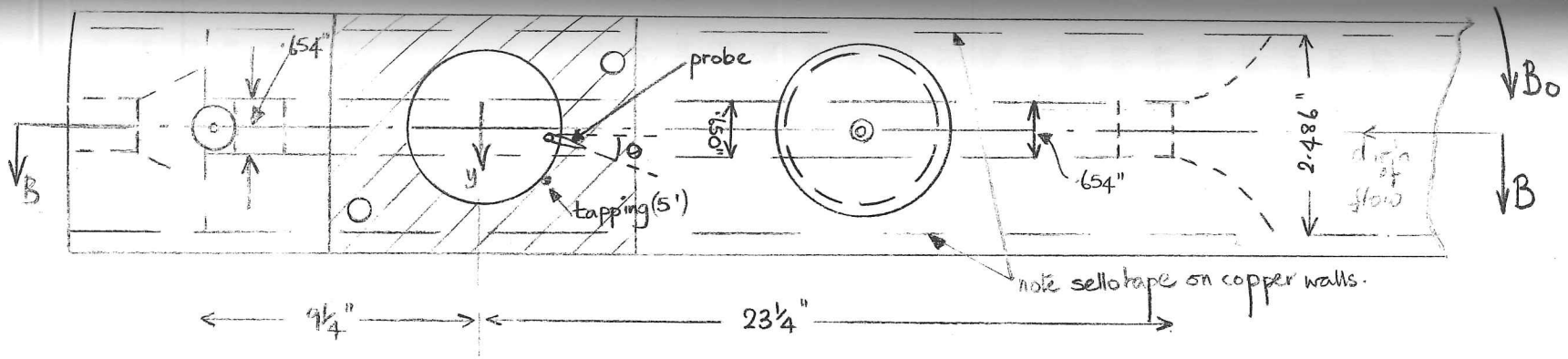

(b) Cross-section BB

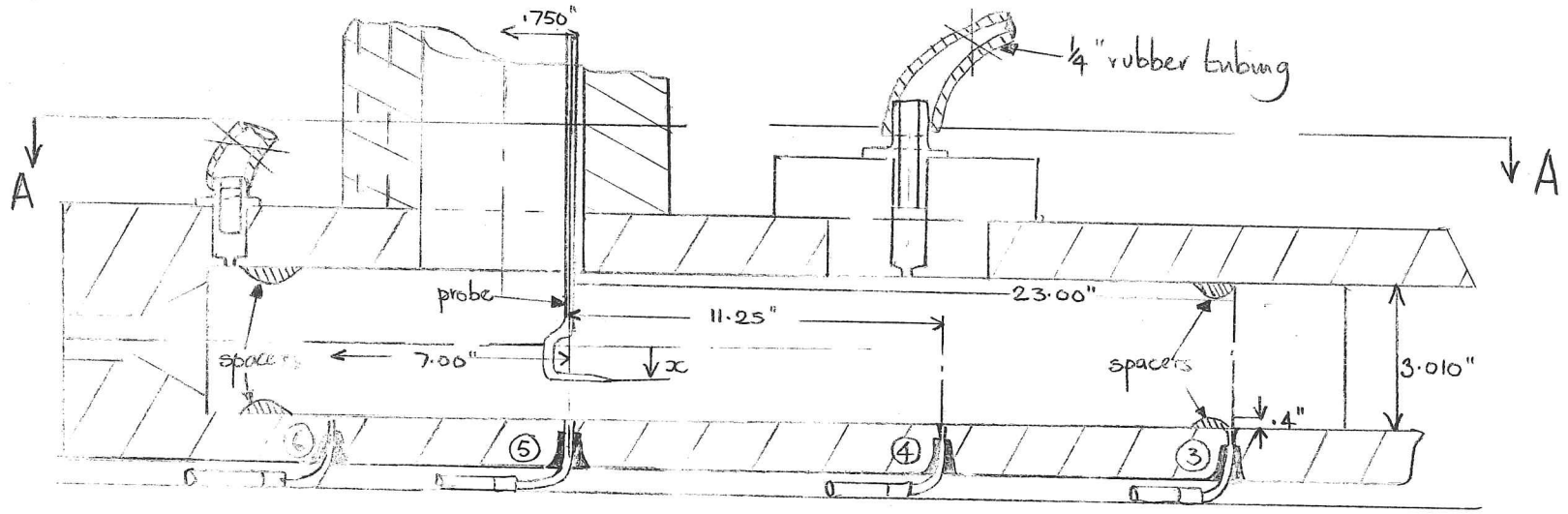

8.3. .6" x 3" duct: non-conducting walls.

8.3.1. Apparatus

The main purpose of the experiments in this duct was to investigate the Pitot and e.p. probe errors when the interaction parameter base on the probe diameter, N, was $O(1)$, since the experiments which had been designed for this purpose in the $\frac{1}{8}$" duct failed when $M \gg 1$. We needed a duct with non-conducting walls, (so that $\underset{\sim}{E} \neq 0$ in the core), sufficiently narrow for reasonably accurate readings of Pitot pressure at attainable flowrates, and yet wide enough for the probe not to block the flow.

Duct. We decided to make a duct .6" x 3.01" in section and place it inside the main 66" duct so that we could use the probe mechanism easily. The internal duct, which was made of 'Perspex', is shown in fig.8.11. Its length was $32\frac{1}{2}$", with a rounded entry; the probe mechanism was 9" from the end to avoid any exit effects which would be smaller with this duct anyway. The internal duct fitted into the main duct sufficiently snugly for the leakage between its walls and those of the main duct to be negligible. Even with the little leakage there was, we felt that short circuits could only be eliminated by covering the copper walls of the duct with sellotape. The only questionable feature of its design were the 'spacers', shown in section in fig.8.11(b), which were needed to keep the two walls apart. According to the entry length calculations of Shercliff (1956), the effects of these 'spacers' near the probes would be negligible at high field strengths.

We might mention that the successful construction and use of this inner duct demonstrated the versatility of the 66" duct.

Probes. One of the aims of these experiments was to see if the shape of a probe affected its MHD error in order to verify, at least qualitatively, our theoretical conclusions of §4.2. We had already constructed a circular and a flattened Pitot, whose dimension parallel to the magnetic field, a_p, (=.012") was very much less than that perpendicular, b_p, (=.062"), so now we constructed one with a_p = .073" and b_p = .024", (fig.8.12a); the reason we increased its size was to reduce the lag of the Pitot reading

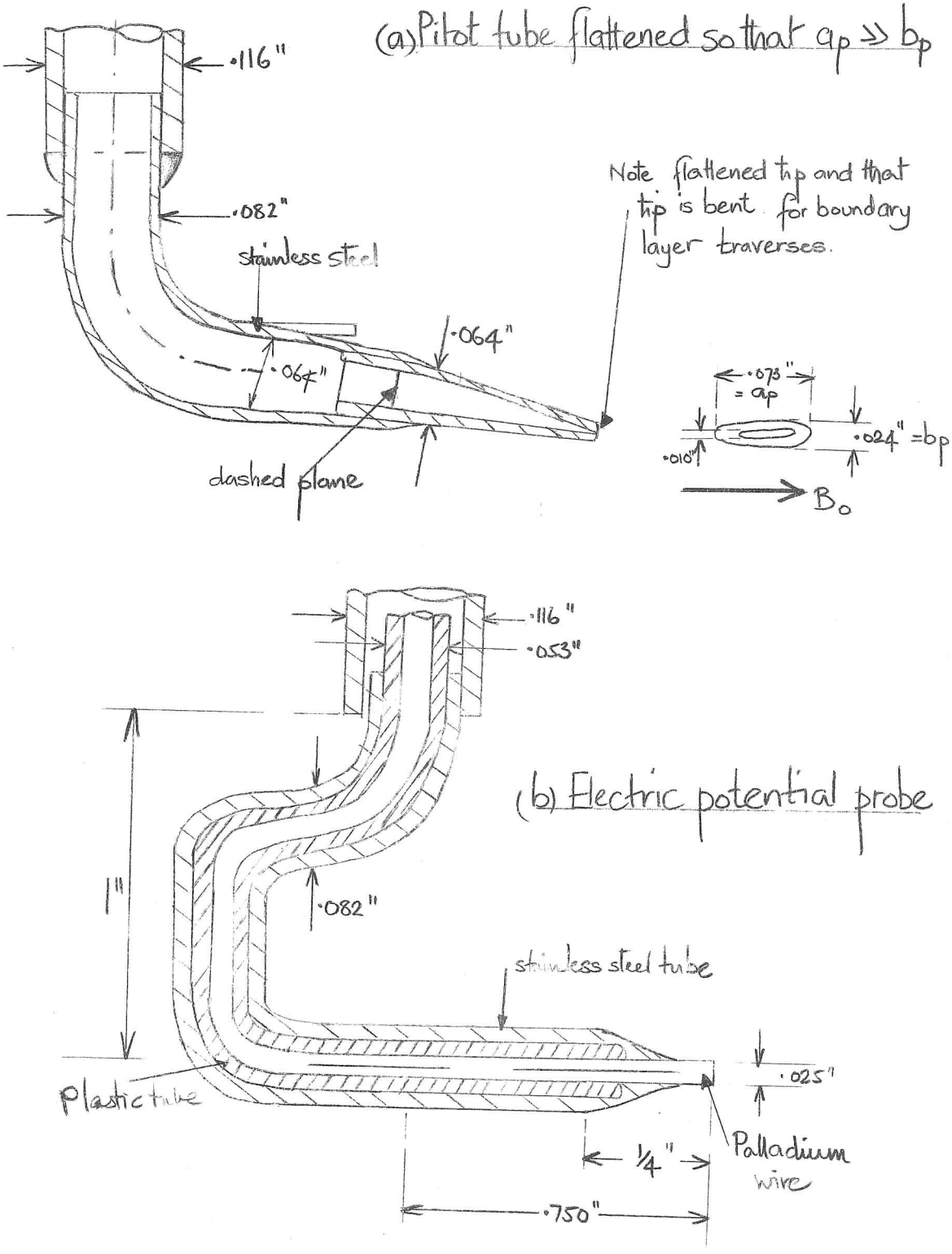

Fig 8.12 Pitot and e.p. probes used in duct II

relative to the static pressure reading, which was even more important in this duct where the flow was considerably less steady than in the $\frac{1}{8}$" duct.

As an electric potential probe we used one already constructed for the $\frac{1}{8}$" duct. We used it in preference to that constructed for the electrically driven flows because the flow at its tip would be less affected by the stem in this design. (Fig.8.12b).

8.3.2. Static pressure measurements.

We first made static pressure measurements, when M $\simeq$ 135, between tappings (4) and (5). We found that measurements of Δp_{54} were not the same as those of $(-\Delta p_{45})$. (The notation refers to the way in which the pressure tappings are connected to the manometer, either tapping (4) or (5) could be connected to the micrometer side of the manometer, if (4), we measure Δp_{54} and if (5), Δp_{45}). Whether this was caused by the manometer or some spurious connection we are not sure. However the results were repeatable and the mean of Δp_{54} and $(-\Delta p_{45})$ was found to agree closely with the theoretical value, as shown in table 8.6. We found the flow in this duct more unstable than in the $\frac{1}{8}$" duct; though the flow was laminar the pressure was all the time oscillating. This may partly have been caused by the fact that there was little constriction between the duct and the l.w.t, where the flow over the weir was not steady, so that though the flowrate, as measured the flowmeter, was very steady, the static pressure level in the duct was fluctuating. On account of the different lag in the leads necessarily led to random errors.

8.3.3. Pitot tube measurements.

The first readings were made with the circular Pitot used in the $\frac{1}{8}$" duct (still insulated). The pitot tip was $\frac{3}{4}$" upstream of the pressure tapping so that, in calculating the velocity, we had to allow for the static pressure drop, Δp_s. We first measured Δp_{sp} against V, the flow-meter reading, when M = 135. The results are tabulated in Table 8.7(a); the difference, Δ , between the theoretical value of Δp , $= \Delta p_0 + \Delta p_s$,

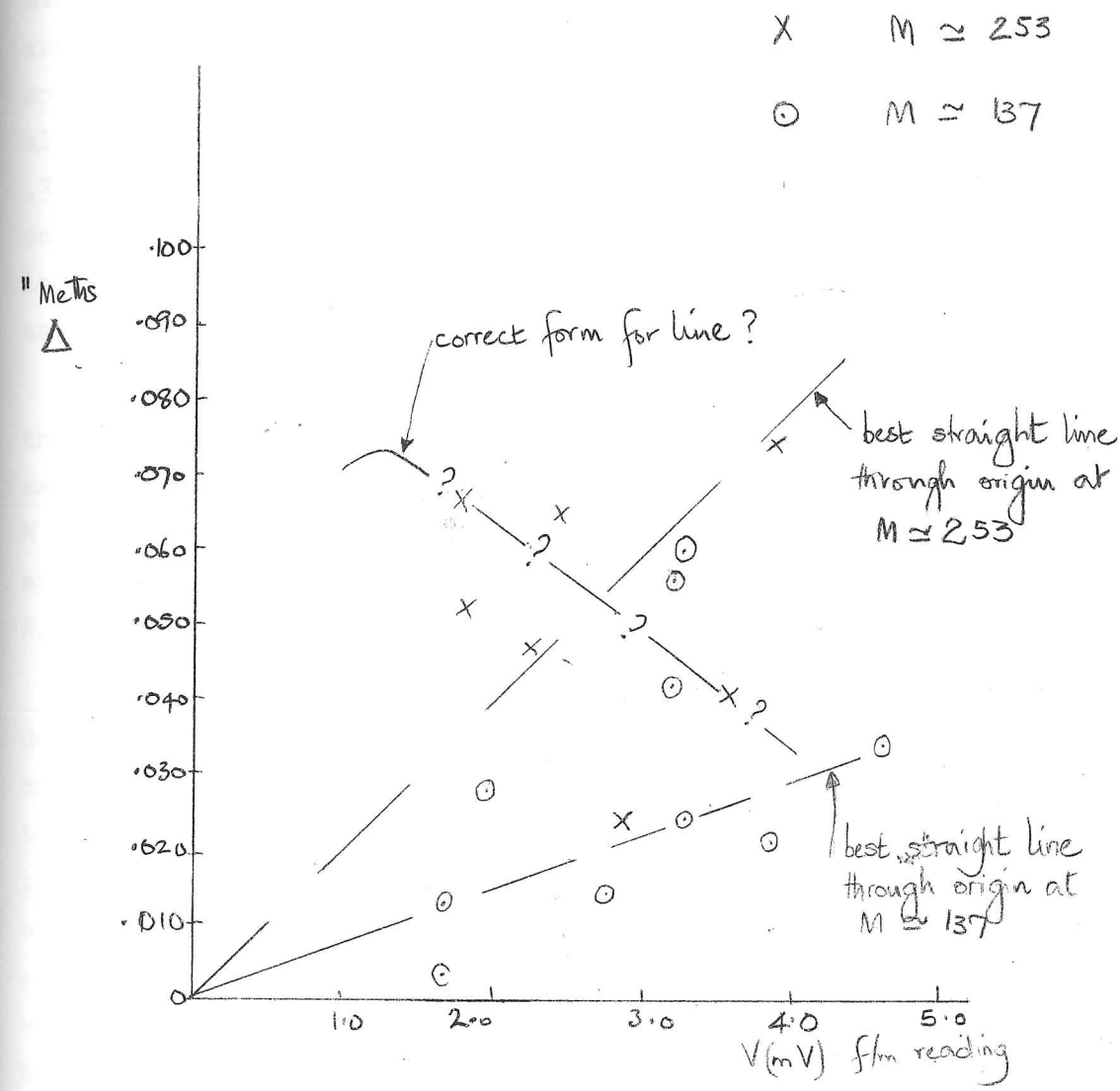

Fig 8.13 Variation of Pitot tube error with flow rate

when M = 253 and 137

($\Delta P_o = \frac{v_{core}^2}{2g} \times \rho_{Hg}/\rho_{melt}$, v_{core} being calculated from Q and M), and ΔP_{SP}. Since ΔP_{SP} was subject to random errors of at least $\pm$ .010", Δ was subject to the same errors and since $|\Delta| < |\Delta P_{SP}|$ the percentage errors are large. This explains why the values of $\alpha = \frac{\Delta}{\Delta P_o \times N}$, have so much scatter. It is interesting that the mean value of $\alpha = .38$, albeit with a standard deviation of $\pm$ .4, whereas East (1964) found $\alpha =$ .39 for a similar Pitot tube. Also note that the mean value of N = .8, so that the basic assumption that $N \ll 1$, was not satisfied. Owing to the scatter of the results we cannot tell if $\Delta \sim Q + C_1/Q$, or $\Delta \sim Q + C_1/Q + C_2/Q^2$, as would be the case higher order terms in N were appreciable.

We then used the Pitot, already described in fig.7.2, to see if the Pitot lag was reduced by such a design of tube. There was only a small improvement. We used the tube to measure ΔP_{SP} against V when M = 257 and found that the mean value of α = .49, but since α noticeably decreased as V increased the result has little meaning (See table. 8.7(b)). Clearly in this case the higher order terms were appreciable.

We used the thin Pitot tube which had been used already in the $\frac{1}{8}$" duct, (fig.8.2.(b)), to see if its MHD error would be greater than that of the circular Pitot. The measurements of ΔP_{SP} were even more subject to random error on account of the longer lag of this tube. The results, tabulated in table 8.8 and plotted in fig.8.13, show the variation of Δ and α with V for $M \simeq 137$ and for $M \simeq 253$. We see, firstly that the general increase of Δ with V is more discernible when $M \simeq 137$ than when $M \simeq 253$. In the latter case, the points do not really indicate any pattern at all, on account of the random errors. We have hesitantly drawn on fig.8.13 a line which might represent the variation of Δ caused by the second and higher order terms in the expansion in N of the pitot error. However, if we merely regard α as a crude measure of the pitot error these results demonstrate one important fact, namely that the MHD error is greater with this kind of probe. If N is based on D_p = 4 x (area)/(perimeter) of the probe tip (i.e. 4 x hydraulic mean diameter) then α is somewhere between 3 and 4 times greater for this probe than for a circular probe. It is puzzling that the error we find is 5 times greater than that predicted by the theory of §4.2. We have no explanation for this.

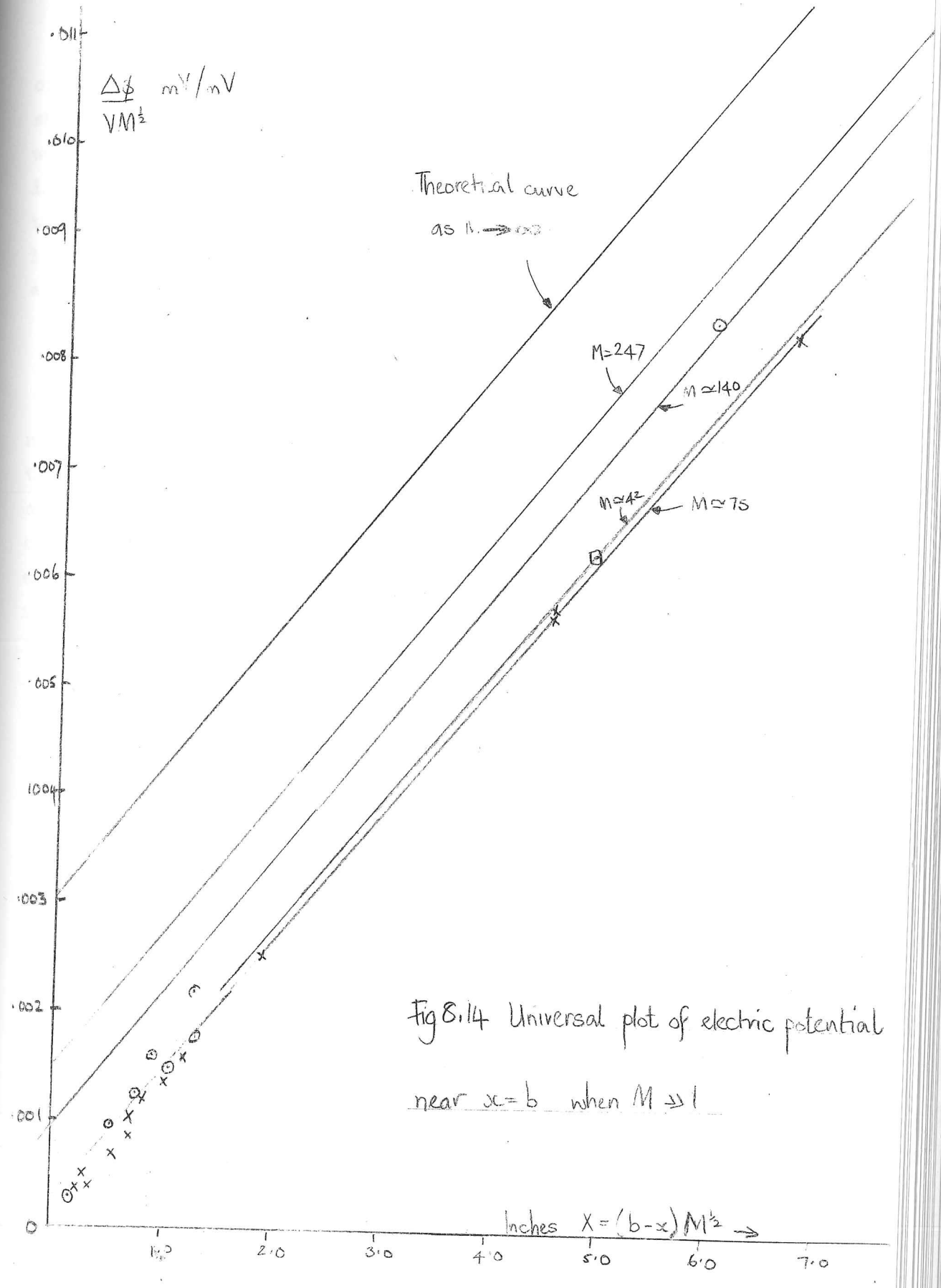

Fig 8.14 Universal plot of electric potential near $x = b$ when $M \gg 1$

Encouraged by this confirmation of our theoretical prediction of §4.2 we then examined the MHD error in a Pitot tube for which $a_p >> b_p$ shown in fig.8.12(a). The results are tabulated in table 8.9 whence we see that α is not appreciably below that of a circular tube, when N is based on D_p. The tube used had a ratio of a_p/b_p of 3 compared to the ratio of b_p/a_p in the former Pitot tube of .5. It would be interesting to investigate in more detail how this ratio affects the MHD error.

8.3.4. Electric potential measurements.

Before describing our measurements we first note that we could not form an adequate loop of wire in the magnet gap to compensate for the flux linked by the circuit between the lead to the tapping (5) and the electric probe so that our reading of potential was subject to oscillations caused by small variations in the magnetic field. (We could not, using the 66" duct which just fitted into the magnet, use the method of Shercliff (1955) which would have entailed having the tapping lead leave the magnet gap in the same plane perpendicular to the pole faces as the probe).

As a reference for the probe potential we measured the difference between the electric potential of the probe, ϕ_p , and that of tapping (5), ϕ_5, $\Delta\phi_{5p} = \phi_p - \phi_5$. We have to confess that we were not measuring the potential at (5) but at (5'), a fact only discovered after the apparatus had been dismantled. Therefore we refer to $\Delta\phi_{5'p}$. In the boundary layer traverses we measured ϕ_p relative to ϕ_4 , the potential tapping of tapping (4). Then we refer to $\Delta\phi_{4'p}$. Since we could not find any difference between $\Delta\phi_{4p}$ and $\Delta\phi_{5'p}$ we only refer to $\Delta\phi$.

We first examined the variation of $\Delta\phi$ with Q and found that over the flowrates and magnetic field strengths available $\Delta\phi \propto Q$. In the core we measured the difference in $\Delta\phi$ / V measured at x = .003 and x = .753 for values of M = 41.8, 140 and 247 and found satisfacory agreement with the theory of laminar flow in a rectangular duct, using Shercliff's (1953) theory. Clearly no systematic MHD error was discernible from these results which, of course, was to be expected from the

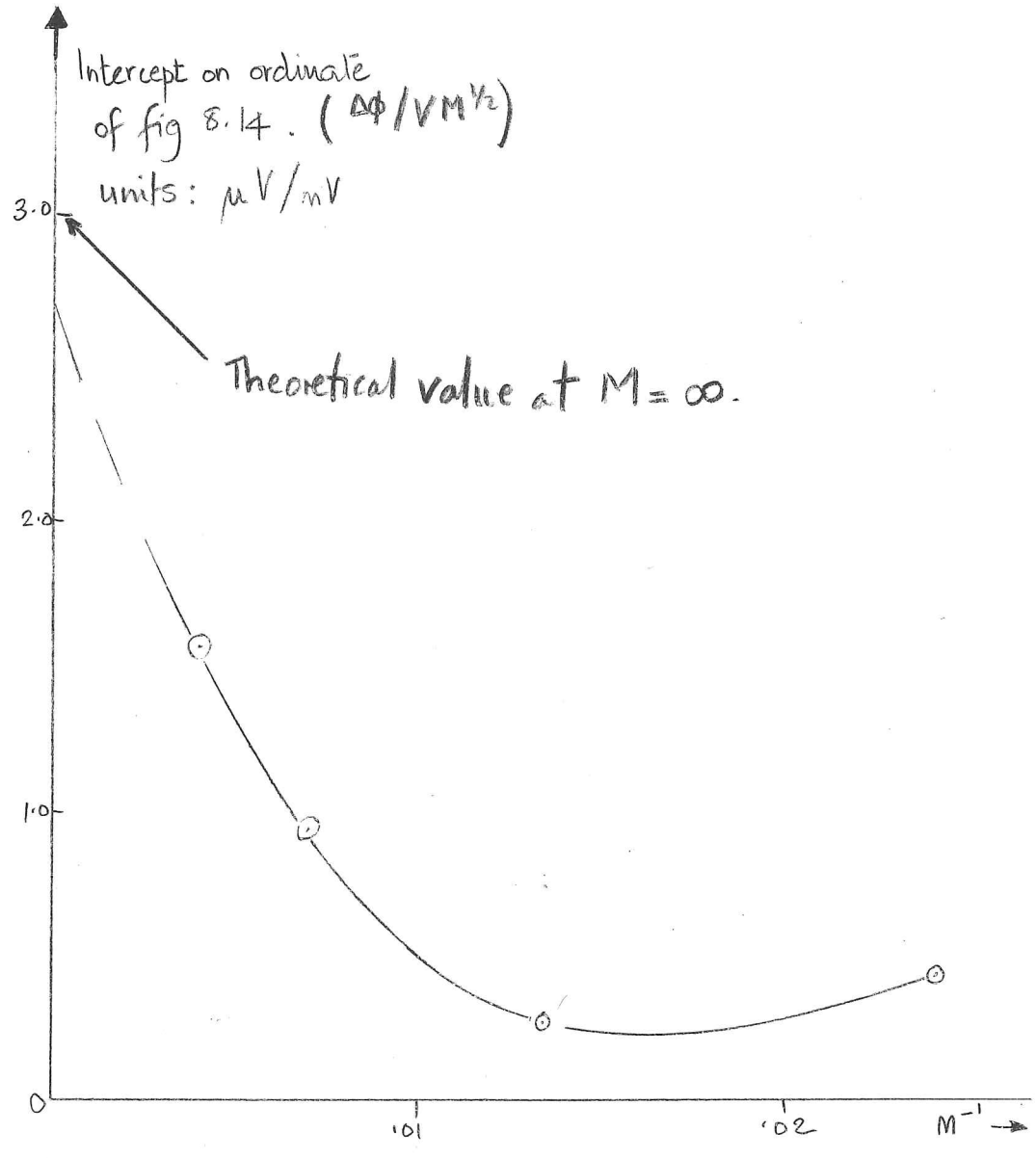

Fig 8.15 Variation of potential drop in boundary layer with M^{-1}

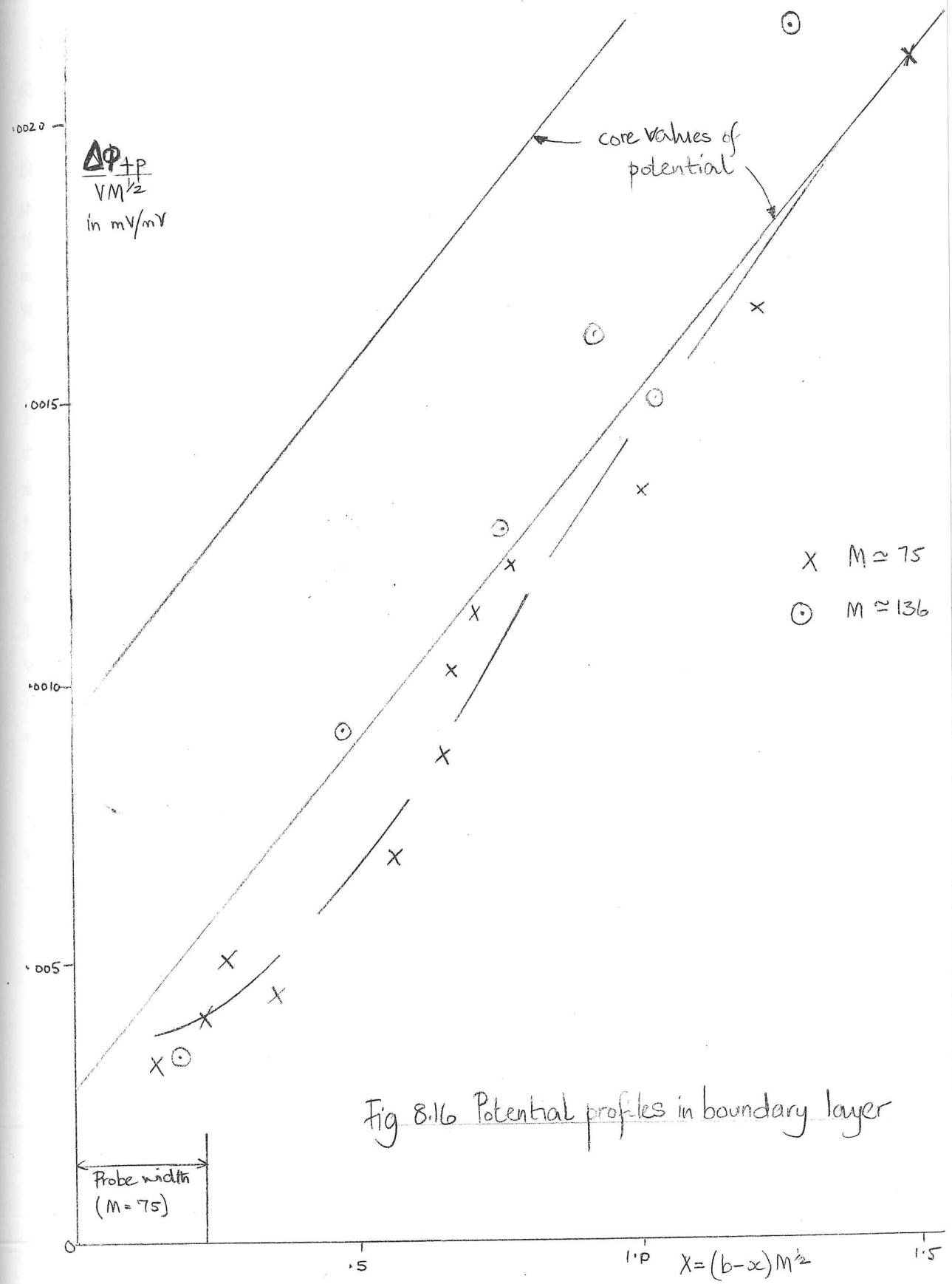

Fig 8.16 Potential profiles in boundary layer

symmetry arguments of §4.3. (Table 8.10).

It was when we compared the actual value of $\Delta\phi/V$ with the theory that curious discrepancies occurred. In fig.8.14. we have plotted $\Delta\phi/VM^{1/2}$ against $X = (b - x)/aM^{-\frac{1}{2}}$, (It may be deduced from the theory of Shercliff (1953) that to $O(M^{-1})$, in the boundary layer on the walls parallel to the magnetic field AA, $\Delta\phi_{sp}/B_0 M^{-1/2} Q = f_1(X)$. Whence, in our flow, $\Delta\phi/M^{1/2}V = f_2(X)$, since $\Delta\phi_{4p}$ is measured relative to the mid point of the wall AA. It also follows that if $\Delta\phi_c$ is the value of $\Delta\phi$ on the wall, x = b, if the electric field in the boundary layer were the same as that in the core, then $\Delta\phi_c/M^{1/2}V = .003$ mV/mV in our duct). Fig.8.14 shows how the slopes of all the lines for the core flow are the same and equal to that of the theoretical line. (We have used the data taken at x = .003 and x = 753, to calculate some of the lines), However the intercepts on the ordinate, I, of the various lines differ, all falling below the theoretical value. To see whether, as $M \to \infty$, the value of I tends to the theoretical value we drew fig.8.15. It shows, very roughly, that we can expect I to be between 2.5 and 3.2 as $M \to \infty$. However with the theoretical error only of $O(M^{-1})$ it is hard to see why such a discrepancy exists when M = 247.

Little further insight into this curious result was afforded by the traverse of the e.p. probe in the boundary layer, fig.8.16. (We measured $\Delta\phi_{4p}$ here to avoid blocking effects). These readings were very difficult to take since $\Delta\phi_{4p}$ was very low and the random errors proportionately large. We note that in our plot the points <u>should</u>, if they were to agree with the results of the asymptotic theory, all fall on the same curve. Clearly they do not. The errors in this experiment cannot be ascribed to the probe itself as in the electrically driven flows on account of the relatively small size of the probe. They may be due to the flow not being as fully developed as it should be, e.g. the 1/e entry length criterion when $M \gg 1$ of Shercliff (1956) was only just satisfied when M = 42. Of one thing we feel sure, that these discrepancies cannot be explained by the fact that we were measuring relative to (5') or (4) rather than (5). We regret there was not more time to spend on these experiments. They ought to be repeated.

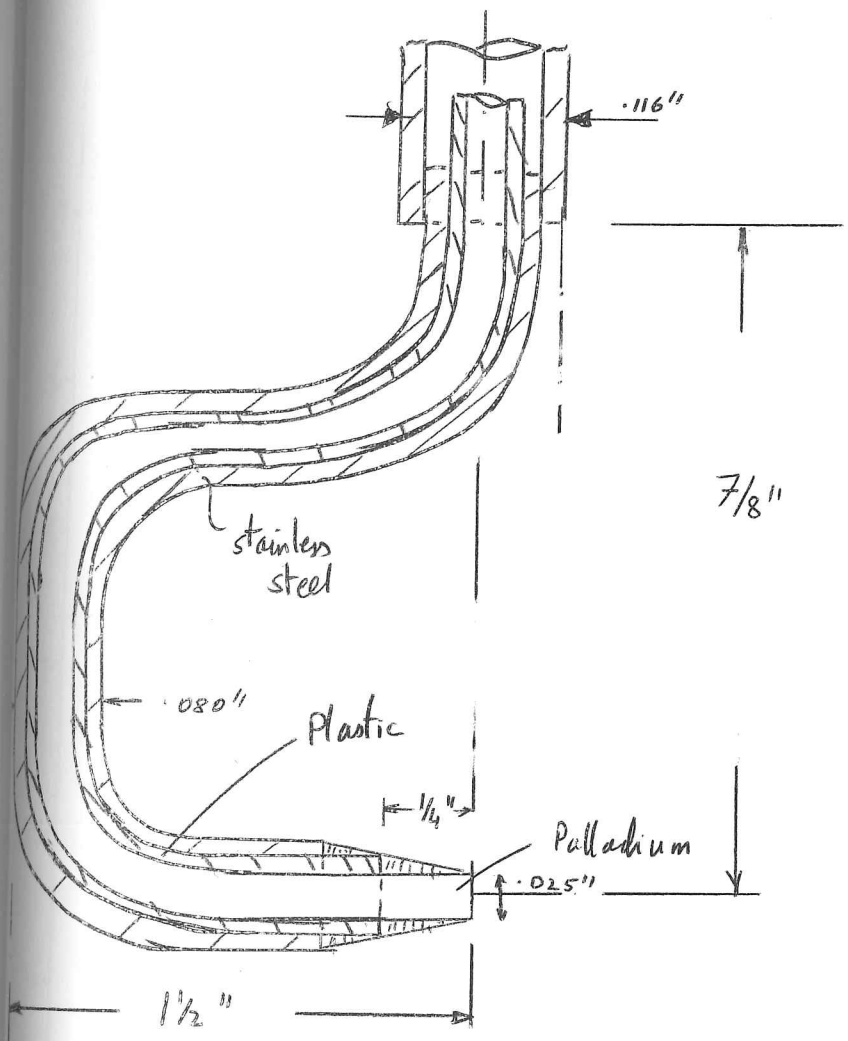

Fig 8.17 E.p. probe for 2.5" x 3" duct III

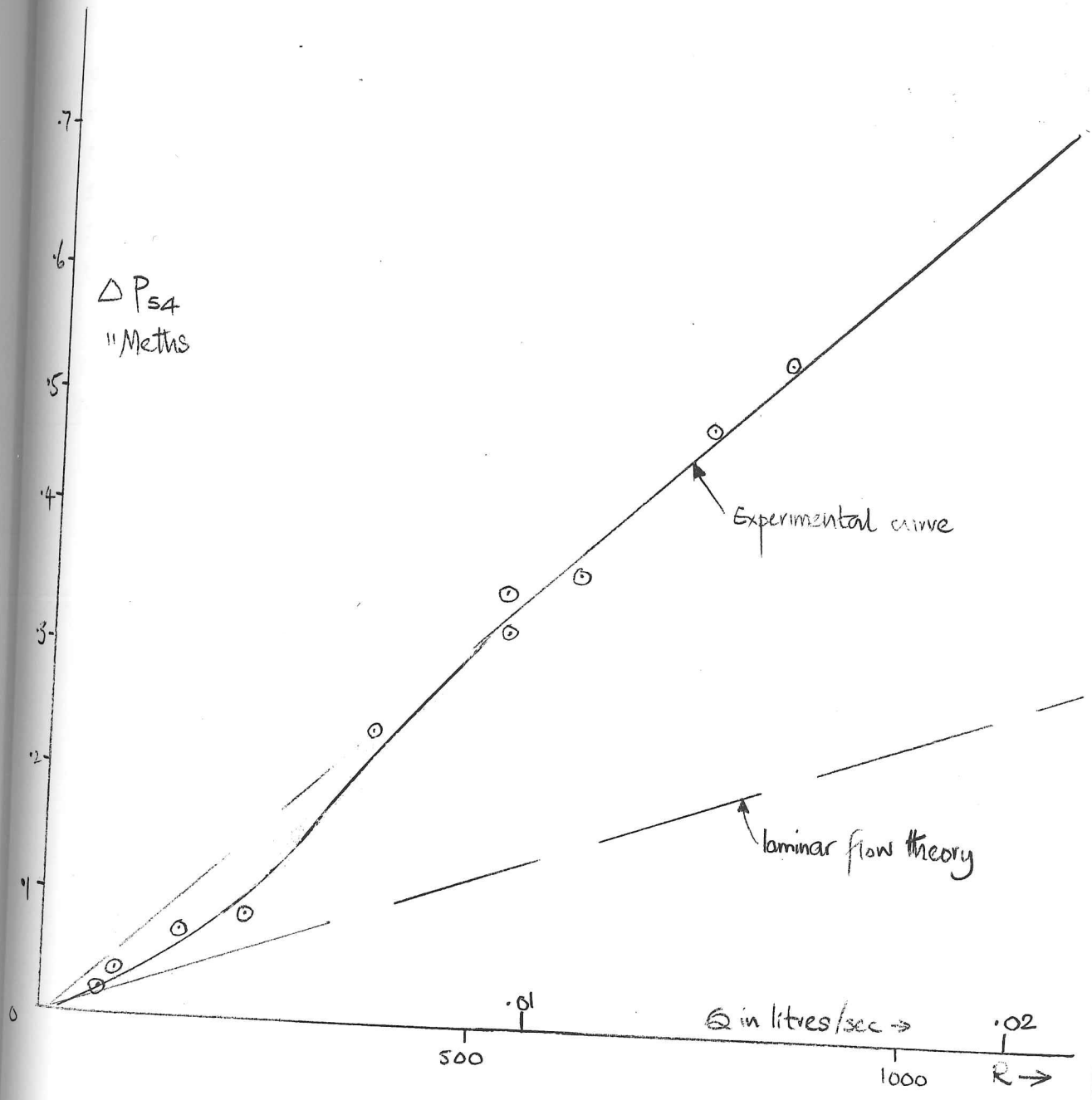

Fig 8.18 Static pressure drop in 2½" x 3" duct ; M = 943

8.4. $2\frac{1}{2}$" x 3" duct; conducting and non-conducting walls.

8.4.1. Apparatus.

In this experiment we hoped to use our probes to examine the curious flows predicted by our theory of §2.4 and Hunt (1965) and to continue the investigation of Alty (1966) into the instability of the flows. As was intended in the design we could use the main 66" duct for this purpose with the copper walls exposed to the mercury. (See fig.6.1). To reduce the copper-mercury contact resistance we left the duct full of mercury for 3 days.

The only new probe used in these experiments was an electric potential probe which was designed to minimise the effect on the flow near the tapping (5), the Probe is shown in fig.8.17.

The basic data of the apparatus are presented in table 8.1.

8.4.2. Static pressure measurements.

We first measured the static pressure between tappings (4) and (5), Δp_{45}, as a function of Q when M = 943. We assumed that the flow was fully developed since the entry length, given by $(a\ R/M^2)$ was much less than the duct width. Also Alty (1966) had shown that for higher values of R and lower values of M the flow was fully developed in a very short distance. Our results, along with the theoretical line, are plotted in fig.8.18.

In taking the readings it was noticeable that the flow was very much less steady when $R < 500$ than for $R > 500$, when the readings were very reproducible. This would seem to relate to the curious kink in the graph when $R < 500$. It is pertinent to note that Alty found that his Δp against R curve touched the theoretical laminar flow curve at $R \simeq 1000$, gradually moving away from it as R increased. The difference may be caused by the fact that our curve was taken at M = 943, as compared to Alty's value of 228; however we showed in §2.4.3 that the critical Reynolds number is theoretically independent of M as $M \to \infty$, so this is an unlikely explanation. A more plausible one is that his flow circuit produced a more smoother flow than ours thus causing a smoother and later transition to the second flow regime we seem to find,

Fig 8.19 Velocity profiles in the boundary layer at $x = b$ ($M = 945$)

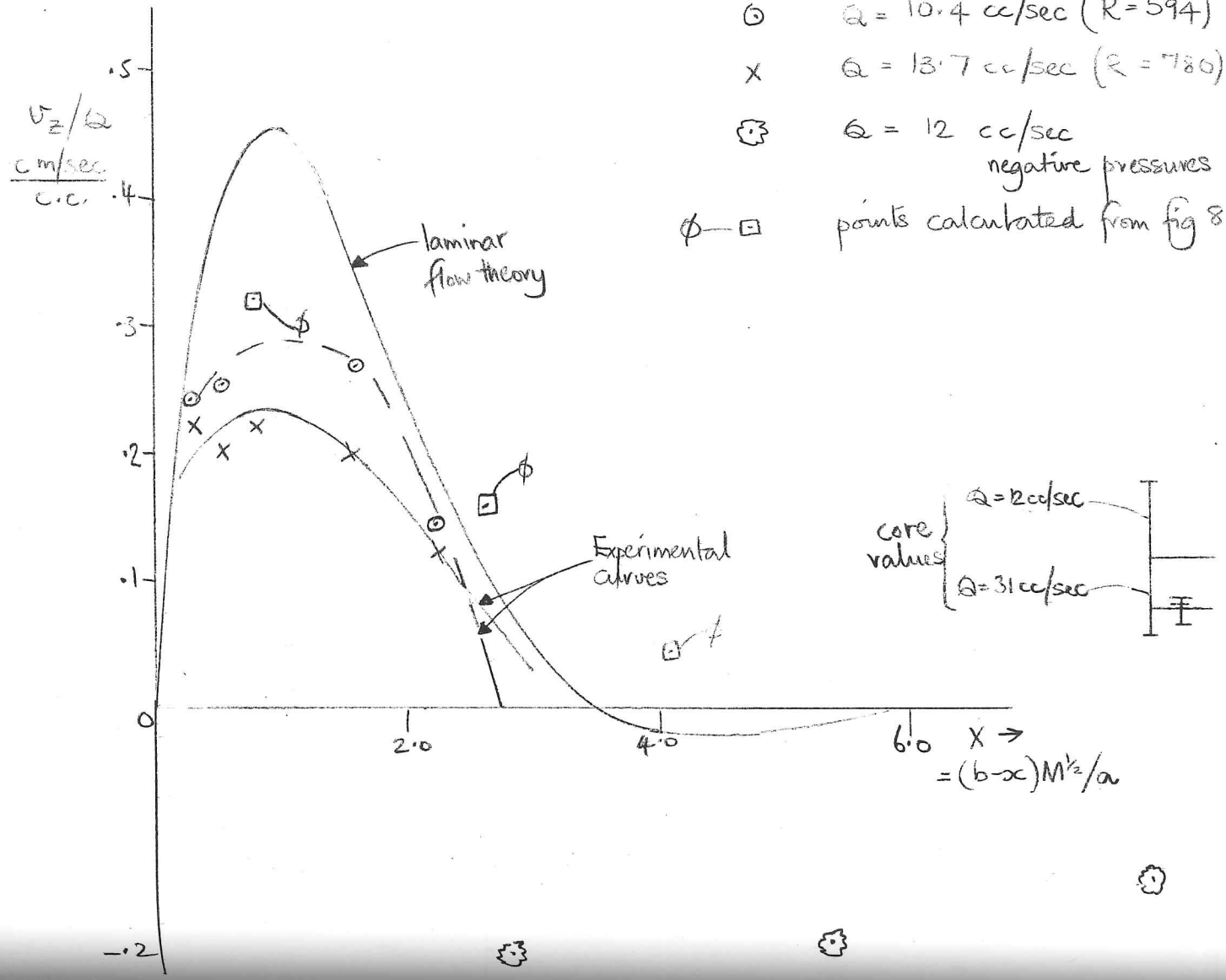

arguing by analogy with non-MHD flows.

Thus our readings indicate that the minimum critical Reynolds number for M = 943 is < 70 and that for $R > 500$, a stable, but not laminar second flow regime is set up. (This second flow regime, if fully developed, cannot be completely laminar because there is only one laminar, fully developed flow as shown by our uniqueness theorem of §2.3). We also note that this second flow regime is still basically laminar because ΔP is proportional to Q and not Q^2. We refer to this again in §8.4.5.

8.4.3. Pitot tube measurements.

We used the flat Pitot tube ($a_p = .073"$, $b_p = .024"$) of fig. 8.12(a) to investigate the boundary layer on the lower non-conducting wall parallel to the magnetic field at y = o. Realising that the flow would be rather unstable we attempted to measure ΔP_{s-p} within a small range of Q so as to plot v_z/Q at one or two particular values of Q. It was exceedingly difficult taking the readings on account of the unsteadiness of the flow and the lag between the Pitot and static reading. Our results are tabulated in table 8.12 and plotted in fig.8.19. Note, firstly that we computed v_z by using the result of §8.3 in taking α to be .4, when N was based on b_p. Second, we assumed the pressure to be constant across the duct. Thirdly, since the Pitot was placed $\frac{3}{4}"$ downstream of the tapping (5) we used the static pressure drop measurements to calculate ΔP_s, the static pressure drop between (5) and the probe. Fourthly, where the velocity was clearly negative and the readings even more unsteady, we have plotted the apparent values of $-v_z$ on fig. 8.19, merely to indicate the presence of such backflow.

The results of these readings indicate; first, that the existence of the general features of the flow predicted by our theory was confirmed; a large velocity close to the wall in the boundary, a negative velocity and a core velocity less than the maximum boundary layer velocity: second, that the form of the velocity profile varied as Q varied, the lower value of Q leading to values of v_z/Q closer to the theoretical near

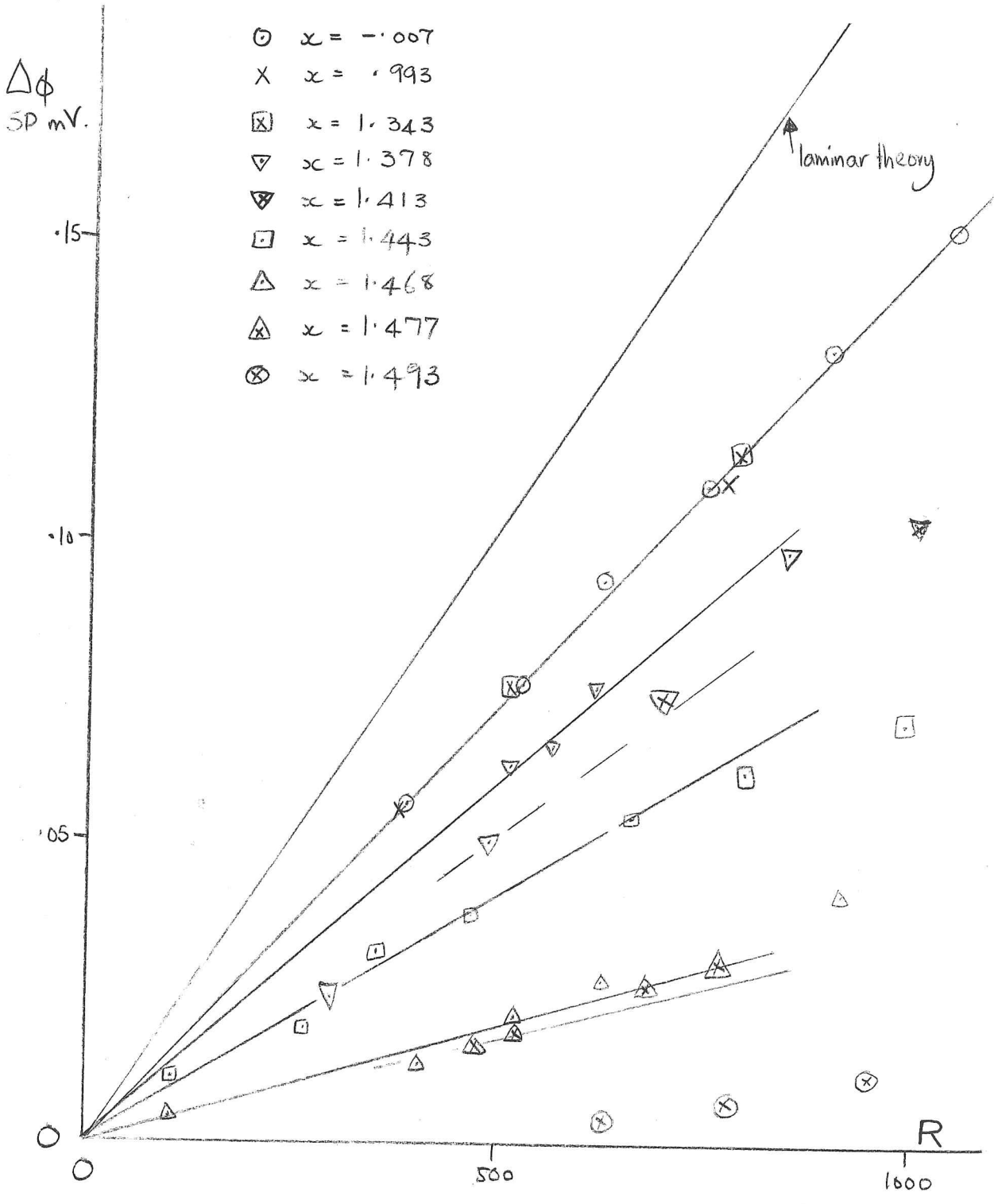

fig 8.20 Variation of potential with flow rate in $2\frac{1}{2}$" × 3" duct ; M = 943

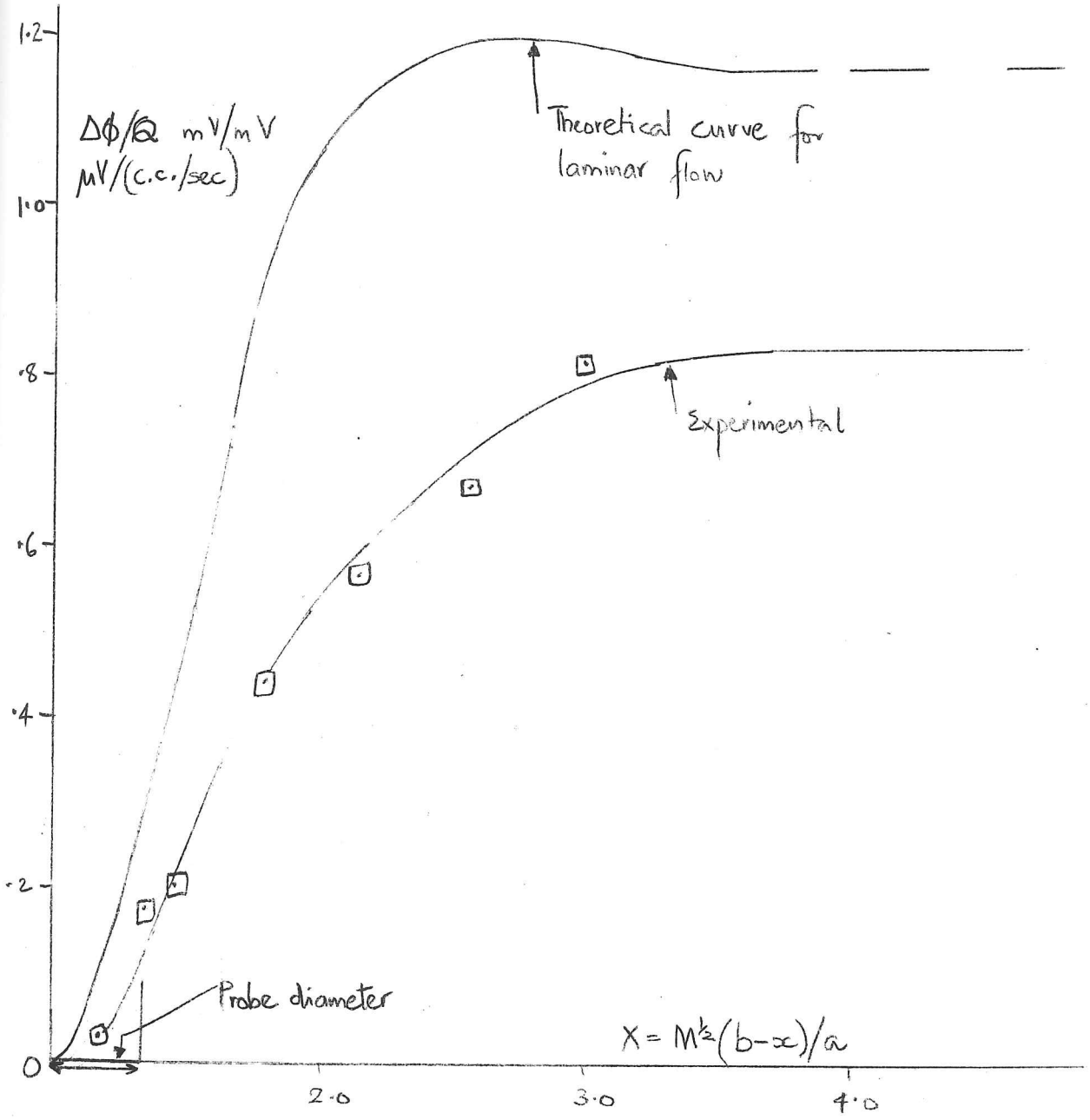

Fig 8.21 Potential profile in boundary layer at $x = b$:

$M = 943$

the wall: third, that the velocity shear at the wall was apparently greater when the flow was unstable; this effect would be expected from the static pressure measurements, but the readings here are uncertain because the probe was so close to the wall; fourth, that the apparent values of velocity in the core were between 50 and 70 times as great as the theoretical value for laminar flow. (More about this later).

8.4.4. Potential probe measurements.

We only had time to measure the potential on the line $y = o$, and we only measured the potential relative to the tapping (5) after assuming that the potential between the probe and the copper wall was negligible when $x = y = o$. Note that the probe was vertically above the tapping (5). We measured $\Delta\phi_{sp}$ as a function of Q at various values of x, for M = 943, the results being plotted in fig.8.20. These measurements were all prone to the same difficulty in taking them as those of §8.3.4, namely the probe-tapping circuit linked flux and consequently $\Delta\phi_{sp}$ was subject to random fluctuations. Over and above these fluctuations we could discern a noticeable difference between the steadiness of the readings, being much steadier in the core ($x < 1.35$) than in the boundary layer.

The main results of fig.8.20 are these. (i) The relation between $\Delta\phi_{sp}$ and Q is linear in the core for $R < 1000$, the highest value measured. (ii) The electric field in the core is zero since all the points fall on the same $\Delta\phi_{sp}$ - Q curve. (iii) In the boundary layer $\Delta\phi_{sp}$ is only proportional to Q if Q is sufficiently low. It was difficult to determine how low owing to the randomness of the readings.

Taking the best straight lines through those points which might reasonably be estimated to be in the linear regime, at the various values of x we plotted $\Delta\phi_{sp}/Q$ against $X = (b-x)/(aM^{-\frac{1}{2}})$ in order to compare the theoretical laminar profile with the experimental one. (See Fig. 8.21) First, we notice that the experimental curve falls below the theoretical for all values of X and second we note that the experimental curve does not have a maximum, unlike the theoretical curve, where it occurs because $v \simeq 0$ at this point in the laminar theory.

We may observe from the fact that $E_x = 0$ in the core, that the

copper walls had a negligible resistance and therefore the conditions of the flow were as intended.

8.4.4. Discussion

Our aim here is to provide a plausible explanation for the differences between the results for ΔP_{3-4}, (hereafter ΔP), v_z/Q, and $\Delta\phi_{5-0}/Q$ and those predicted by the laminar theory. We start from the incontrovertible fact that $E_x = E_y = 0$ in the core in both the situations, hereinafter denoted by the suffices 2 and 1 respectively; furthermore, the velocity is uniform in the core in both cases and therefore, $dp/dz = -\sigma v_z B_0^2$ and

$$\frac{\Delta P_2}{\Delta P_1} = \frac{(v_{core})_2}{(v_{core})_1} \qquad 8.4.1.$$

Now we see from fig.8.18 that $\Delta P_3 \simeq 2.6\ \Delta P_1$, whence

$$(v_{core})_2 = 2.6 (v_{core})_1 \qquad 8.4.2.$$

But in fig 8.19 we see that

$$(v_{core})_2 \simeq 50 (v_{core})_1 \qquad 8.4.3.$$

Thus some discrepancy needs to be explained.

We see from the Pitot and e.p. probe traverses in the boundary layers that the 'turbulent' boundary layer thickness is not greater than the laminar. Therefore we can still make the approximation in the boundary layer:

$$-d\phi/dx - v_z B_0 = 0, \qquad 8.4.4.$$

with an error of order $(v_c/v_{b.l.})$, the suffices referring to the core and boundary layer respectively. From (8.4.4) it follows that $\Delta\phi_c = B_0 \int_0^\infty v_z\, d(b-x) = B_0 Q_{b.l.}$ where $Q_{b.l.}$ is the volume flow rate in the boundary layer. Now in laminar flow (Hunt, 1965), $Q = Q_{b.l.} + Q_c$ where $Q_c \simeq \frac{3.336}{aM^{1/2}} Q_{b.l.}$. Now in our flow we found that $\left(\frac{\Delta\phi_c}{Q}\right)_2 = .7 \left(\frac{\Delta\phi_c}{Q}\right)_1$, whence from the conservation of flow it follows that:

$$(Q_c)_2 \simeq (Q_c)_1 + .3 (Q_{b.l.})_1 \simeq Q_{c_1} \left(1 + \frac{.3 \times 31}{4}\right)$$

for our duct when M = 943. Thus:

$$\frac{(Q_c)_2}{(Q_c)_1} = \frac{(v_c)_2}{(v_c)_1} \simeq 3.3 \qquad 8.4.5.$$

which is in better agreement with (8.4.2) than is (8.4.3).

We believe that the explanation for (8.4.3) is that a pressure gradient $\partial p/\partial x$ (< 0) exists in the centre of the duct near the wall $x = b$. This pressure gradient may be caused by turbulent secondary flow which impells fluid <u>from</u> places where the shearing stress is greatest and <u>towards</u> places where it is least, to paraphrase Prandtl (1952), p.149; such a flow would induce a velocity v_x (> 0) and thus a pressure gradient $(\partial p/\partial x) < 0$; Q.E.D.

This apparently convincing argument has two main flaws: (1) Why is Δp_{sp} proportional to Q in the second flow regime, if this regime is dominated by secondary flows? (2) Is the reason for the discrepancy between Alty's results and our's simply due to the greater unsteadiness of our flow? or does the value of M matter? We have to leave these questions unanswered.

We note that it follows from (8.4.4) that we can calculate v_z in the boundary from the potential profile. In fig.8.19 we have plotted 3 points by measuring the slope of the $\Delta\phi_{sp}/Q$ against X curve of fig.8.21. The agreement between these values and those measured by the Pitot tube is quite good ($\sim 5\%$) near the wall but is poor as X increases.

We conclude by observing that these measurements of static pressure, dynamic head and electric potential, taken together can be correlated and they show how the use of Pitot and e.p. probes enables us to increase our understanding of very complex, unsteady flows.

9. Conclusions.

Summaries of the work described in this thesis are to be found at the beginning of each chapter. In this chapter we mention some possible lines for further research which arise out of our work and some improvements which might be made on our experimental apparatus.

The most important development of the theoretical work on MHD duct flows described in chapter 2 should be the extension of the analysis to compressible flows. We believe that such a development is not only possible, but of practical use. The reasons for our belief were set out in Hunt (1966,b); however the outline calculations of that paper will obviously have to be worked out in greater detail before these calculations are taken seriously by the designers of MHD generators. There are still some interesting aspects of laminar duct flows to be analysed, e.g. the boundary layers on the walls parallel to the magnetic field in the diverging ducts considered in §2.7., or the flow in a duct with a sudden change in cross sectional area, (not the sudden change in the rate of change we examined).

Clearly the theory of Pitot and electric potential probes of chapter 4 is very inadequate. The theory will only advance when we understand the flow over bodies placed in various kinds of flow with the magnetic fields at various orientations. This aspect of MHD theory has been pooh-poohed in the past (by Professor Shercliff in particular) as being entirely academic; the study of Pitot tubes is definitely not academic and therefore this practical application may stimulate further theoretical work on the MHD flow over bodies. Also, with the advent of the use of MHD probes, we can now investigate the flow over bodies in ducts experimentally, e.g. Tsinober et al, (1963), which should provide another stimulus to this theory and, most important, a check on it.

As regards the possible uses of MHD probes, the number of flows which we cannot analyse and which need investigating are limitless. However, it is more important to concentrate on flows about which we have some theoretical understanding. One such is the onset of turbulence

in narrow channels; this type of flow has mainly been examined by external pressure measurements, and upon these a huge body of semi-empirical theory is built. This theory badly needs verification by internal probe measurements. Also this particular flow is technologically the most important and, we feel, the one where most effort should be concentrated.

Our flow circuit is subject to many serious defects which must be eliminated if more accurate measurements are to be made. First, our choice of pump was disastrous; the flow it produced was not smooth and the trouble caused by the wearing down of the pipes in it produced more spilling of mercury than ever a small leak from a centrifugal pump would cause. Having seen the flow circuits of Moreau and Lecocq, we feel sure that, if a circuit with two free surfaces is to be used, a centrifugal pump is quite satisfactory. However, from the published accounts of the flow rigs at Riga, it is not clear whether the Russians, who use closed circuits with electromagnetic pumps, achieve more or less steady flows than those using centrifugal pumps. This point must be resolved before any satisfactory measurements are to be made on the onset of instability in MHD flows. Another point to be resolved concerns the best design of weirs for use with mercury. The one we designed seemed to induce an unsteady flow over them, perhaps because they were circular in shape. Some experiments should be done to find that design of weir which uses the least amount of mercury and yet produces a steady flow over it.

References.

Abbas, S. (1966) — Ph.D.Thesis. University College, London.

Ahlstrom, H.G. (1964). — Experiments on the upstream wake in magneto-fluid-dynamics. J.Fluid.Mech. 15, 205.

Alty, C.J.N. (1966). — 'Magnetohydrodynamic duct flow'. Ph.D. Thesis Cambridge University.

Berezin, D.A. (1963). — Stable motion of an electrically conducting fluid in a rectangular tube in the presence of a transverse magnetic field. Z.Prikl.Mekh.Tekh.Fiz.No.3, 155. (National Lending Library Translation).

Baylis, J.A. (1966). — Ph.D.Thesis. Cambridge University.

Bornhorst, W.J. (1965). — MHD effect in open-channel flow. A.I.A.A.J. p.1181. June.

Braginskii, S.I. (1960). — Magnetohydrodynamics of weakly conducting liquids. Sov.Phys(JEPT). 10, 1005.

Branover, G.G. et al.(1966). — Review of MHD duct flows. Magn.gidro.din. No.3, 3-21.

Branover, G.G. & Lielausis, O. — Effect of a transverse magnetic field on the internal structure and hydraulics resistance in turbulent flows of liquid metals. Izv.Akad.Nauk.Latv.No.1. 1961. 59-66. English Transl. -TT-TO-61-281 US Air force.

Chandrasekhar, S. (1961). — 'Hydrodynamic and hydromagnetic stability'. (Oxford U.P.).

Chang, C.C. and Lundgren, T.S. (1961). — 'Duct flow in magnetohydrodynamics'. Z.Angew.Math, Phys. 12, 100.

Chang, C.C. and Yen.J.T.(1962). — Magnetohydrodynamic channel flow as influenced by wall conductance. Z.Angew.Math.Phys, 13, 266.

Chiang, D. (1965). — Magnetohydrodynamic flow in a rectangular duct with perfectly conducting electrodes. Ph.D. thesis. Univ.Minnesota, Minneapolis, Minnesota.

Childress, S (1963). The effect of a strong magnetic field on two dimensional flows of a conducting fluid J. Fluid Mech 15, 429.

Drazin, P.G. (1960). Stability of parallel flow in a parallel magnetic field at small magnetic Reynolds numbers. J.Fluid Mech. 8, 130.

East, D. (1964). 'The Pitot tube in magnetohydrodynamics'. Ph.D. Thesis, Masachussetts Inst. Technology.

Hains, F.D. (1965). Stability diagrams for magnetogas-dynamic channel flow. Phys.Fluids. p.2014.

Hale, F.J. & Kerrebrock, J. L. (1964) A.I.A.A. J. 2, 461.

Hasimoto, H. (1960). Steady longitudinal motion of a cylinder in a conducting fluid. J.Fluid Mech. 8, 61.

Heiser, W. (1964). Influence of Magnetic fields upon separation AIAA 2, 2217.

Hughes, W.F. & Young, F.J. (1966) The Electromagnetodynamics of Fluids, J. Wiley & Sons.

Hunt, J.C.R., (1965). Magnetohydrodyanic flow in rectangular ducts, J.Fluid.Mech. 21, 577.

Hunt, J.C.R. and Stewartson, K. (1965), Magnetohydrodynamic flow in rectangular ducts, II. J.Fluid Mech. 23, 563.

Hunt, J.C.R. (1966,a). On the stability of plane parallel flows with parallel magnetic fields. Proc.Roy.Soc.A, 293, 342. (1966).

Hunt, J.C.R. (1966,b). On some fluid dynamic effects in large-scale MHD generators, Proc.Symp. on MHD Elec.Power.Gen. Salzburg, 1966.

Hunt, J.C.R. (1966,c). Remarks on the use of Pitot tubes in compressible flows. Proc.Int.Symp. on MHD Elec.Power Gen. Salzburg, 1966.

Hunt, J.C.R. & Leibovich, S. (1967). Magnetohydrodynamic flow in channels of variable cross-section with strong transverse magnetic fields. J.Fluid Mech. Accepted for publication.

Hunt, J.C.R. & Williams, W.E. (1967).
Some electrically driven flows in magnetohydrodynamics. I: Theory. to be published.

Kerrebrock, J.L. (1961)
J. Aero/Space Sci. 28, 631.

Lecocq, P. (1964).
Contribution to the study of frictional loss and velocity profiles in turbulent flows in Magnetohydrodynamics. Ph.D. Thesis, Toulouse.

Lock, R.C. (1955).
The stability of the flow of an electrically conducting fluid between planes under a transverse magnetic field.
Proc.Roy.Soc.A, 233, 105.

Ludford, (1961).
The effect of a very strong magnetic cross-field on on the steady motion through a slightly conducting fluid.
J.Fluid Mech. 10, 141.

Ludford, G.S.S. & Singh, M.P. (1963).
Motion of a non-conducting sphere through a conducting fluid in a magnetic field.
Proc.Camb. Phil.Soc. 59, 615.

Ludford (1963).
Hydromagnetic stagnation-point flow for small R_m.
Z.A.M.M., 43, 9.

Lundgren, T.S. & Atabek, S.H. & Chang, C.C. (1961).
Transient magnetohydrodynamic duct flow.
Phys.Fluids 4, 1006.

Michael, D.H. (1953).
The stability of plane parallel flows of electrically conducting fluids.
Proc.Camb.Phil.Soc. 49, 166.

Milne-Thompson, (1962).
Theoretical Hydrodynamics. (Macmillan)

Moffatt, H.K. (1964).
Electrically driven steady flows in magnetohydrodynamics.
Proc. 11th Int.Cong.Appl.Mech. Munich. September, 1964.

Moreau, R. (1963).
Experimental rig of the Fluid Mechanics Laboratory of the University of Grenoble.
Compte. Rend. Acad. Sci. 256, 5052.

Moreau, R. (1964).
The effect of a transverse magnetic field on separation.
Compt.Rend.Acad.Sci. 258, 1732.

Moreau, R. (1966). An experimental study of the similarity of the profiles of excess velocity in confined jets in the presence of a transverse magnetic field. Compte.Rend.Acad.Sci. 262, 259.

Prandtl. L. (1952). Fluid Dynamics. (Blackie).

Resler, E.J. & Sears, W.R. (1958) J. Aero/Space Sci. 25, 235.

Rosenhead, L. (1963). Laminar Boundary Layers. (Oxford Univ.P.).

Sachs, S. 'MHD entry lengths as determined by Pitot tube velocity profile measurements' S.B.Thesis. Dept.Mech.Eng. MIT. 1965.

Shercliff, J.A. (1953). Steady motion of conducting fluids in pipes under transverse magnetic fields. Proc.Camb.Phil.Soc. 49, 136.

Shercliff, J.A. (1955). Problems in MHD. Ph.D. Thesis. Camb.Univ.

Shercliff J.A. (1956) Entry of conducting and non-conducting fluids in pipes, Proc.Camb.Phil.Soc. 52, 573.

Shercliff, J.A. (1962). The theory of electromagnetic flow measurement. Cambridge Univ.P.

Shercliff, J.A. (1965). A textbook of magnetohydrodynamics. Oxford: Pergamon Press.

Squire, H.B. (1933). On the stability for three-dimensional disturbances of viscous fluid flow between parallel walls. Proc.Roy.Soc., A. 142, 621.

Stuart, J.T. (1954). On the stability of viscous flow between parallel planes in the presence of a coplanar magnetic field. Proc.Roy.Soc.A, 221, 189.

Stewartson, K. (1960). On the motion of a non-conducting body through a perfectly conducting fluid. J.Fluid Mech. 8, 82.

Sutton, G.W. & Carlson, A.W. (1961) J. Fluid Mech. 11, 121.

Tani, I. (1962). Steady flow of conducting fluids in channels under transverse magnetic fields with consideration of Hall effect. J.Aero.Sci. 29, 287.

Tarasov, Y. A. (1960) Sov.Phys.JETP, 10, 1209.

Tatsumi, T. (1962) Magnetofluid-dynamic stability and turbulence. Progr.Theor.Phys.Suppl. 24, 156.

Taylor, J.B. & Wesson, J.A. (1965) End losses from a theta pinch. Nucl.Fus. 5, 159.

Tsinober, A, (1963). Questions of the effect of a magnetic field on the flow past bodies. Vopr.Magn.Gridro. 3; 49-88. (Akad.Nauk.Latv SSR, Riga).

Tsinober, A., Shtern. A., & Shcherbinin, E. (1963). On the separation of a magnetohydrodynamic boundary layer. Izv.Akad.Nauk, Latvia SSR no.12, 49.

Uflyand, Y.S. (1961). Flow of a conducting fluid in a rectangular channel in a transverse magnetic field. Sov.Phys. - Tech.Phys. 5, 1191.

Uflyand, Y.S. (1962). Certain questions in the unsteady flow of a conducting fluid through a tube of constant cross-section in a transverse magnetic field. Sov.Phys. - Tech.Phys, 6, 1031.

Velikhov, E.P. (1959) The stability of plane Poiseuille flow of an ideally conducting fluid in a longitudinal magnetic field. Sov.Phys.JETP 9, 848.

Waechte, T. (1966). Ph.D. Thesis, Cambridge University.

Wooler, P.T. (1961) Instability of flow between parallel planes with a coplanar magnetic field. Phys.Fluids, 4, 24.

Yakubenko, A.Ye. Certain problems concerning the movement of a conducting fluid in a plane channel. Zh.Prikl.Mech.Tech.Fiz.No.6, 1963. JASA Transl. F-241, Sept. 1964.

Table 8.1. Basic data for $\frac{1}{8}$" x $2\frac{3}{8}$" duct (I).

Cross-section dimensions: $2a = .116"$, $2b = 2.375"$.

Properties of mercury (MKS units):

	15^0	25^0
ρ	13.56×10^3	13.5×10^3
$\tilde{\eta}$	1.58×10^{-3}	1.52×10^{-3}
σ	1.048×10^6	1.034×10^6
Density of meths, ρ_M	$.820 \times 10^3$	$.812 \times 10^3$

(This data is also used in tables 8.5 and 8.11)

Reynolds number, $R = \left(\frac{Q}{4ab}\right) \rho a/\tilde{\eta}$ $= 73\ Q$ at 20^0c.

(Q is the flow rate in cc./sec).

Hartmann number, $M = B_0 a(\sigma/\tilde{\eta})^{\frac{1}{2}} = B_0 \times 38.7$ at 20^0c.

Flowmeter calibration, $Q = 3.42 \times V$ (B_0 in wb/m^2).

(Q in cc/sec; V is the flow meter reading in mVolts).

Pressure gradients in fully developed laminar flow:

$M = 0$, $\partial p/\partial z = -\frac{3\tilde{\eta} Q}{4a^3 b}$ (ignore effects of walls at $x = \pm b$)

whence $dh/dz = -1.47Q$, (Q in litres/sec, dh/dz in inches of meths per inch of duct, h being manometer reading. We omit subsequent calculations of dh/dz, since they follow from this one).

$M \neq 0$; $\partial p/\partial z = \frac{-MQ\tilde{\eta}}{4a^3 b(\tanh M - 1/M)}$

Velocity profiles in fully developed laminar flow:

$M = 0$, $v_z = \frac{3Q}{8ab}\left(1 - y^2/a^2\right)$

whence $\sqrt{\Delta P_f}/Q = .0484\left(1 - y^2/a^2\right)$

(Q in cc/sec, ΔP_f in inches of meths).

$M \neq 0$, $v_z = \frac{Q}{4ab} M \left(\frac{1 - \cosh(My/a)/\cosh M}{M - \tanh M}\right)$

Table 8.2. Static pressure drop in duct I when M = 0.

Q (c.c./sec)	$\Delta P_{46}/Q$ (inches of meths/cc/sec).
3.62.	3.86
4.82	3.13
5.10	3.56.
5.38	3.74
5.47	3.38
5.57	3.42
Mean	= 3.59 standard deviation (s.d)=.28
Theoretical Value	= 3.64

Table 8.3. Pitot tube readings in duct I when M = 0; circular tip.

Q (c.c/sec)	$\Delta P_{1P}/Q^2$ "melts/(c.c/sec)^2	$\sqrt{\Delta P_{1P}}/Q$
3.32	3.18×10^{-3}	5.64×10^{-2}
4.00	2.00	4.47
4.14	2.06	4.53
4.41	2.51	5.01
5.30	2.64	5.14
5.51	2.66	5.16
6.15	2.12	4.60
6.25	2.28	4.78
6.50	2.37	4.87
Mean	$= 2.42 \times 10^{-3}$	4.91×10^{-2}
s.d.	$= .35 \times 10^{-3}$	$.30 \times 10^{-2}$
(i.e. 14.5% of mean)		(i.e. 6.1% of mean)
Theoretical Value	$= 2.34 \times 10^{-3}$	4.84×10^{-2}

Note: (1) $Q < 7$ c.c./sec so that flow is in linear regime.

(2) the square root of the mean value of $\Delta P_{1P}/Q^2$, $\overline{\Delta P_{1P}/Q^2}$ is 4.92 and so very close to the mean value of $\sqrt{\Delta P_{1P}}/Q$, $\overline{\sqrt{\Delta P_{1P}}/Q}$. Thus to calculate $\overline{\sqrt{\Delta P_{1P}}/Q}$, we can calculate $\overline{\Delta P_{1P}/Q^2}$ and then take its square root - a much simpler process.

Table 8.4. Pitot tube readings in duct I when M = 0: flat-ended tip.

Q (c.c/sec)	$\Delta P_{ip}/Q$ "metres/(c.c/sec)"
3.00	2.26×10^{-3}
3.49	2.49
4.10	2.31
4.41	2.32
4.62	2.53
5.10	2.62
5.51	2.23
8.35	2.23

Mean value = 2.37

s.d. = .14 (6% of mean)

Theoretical Value = 2.34.

Table 8.5. Basic data for .6" x.3" duct (II).

Cross-section dimensions; 2a = .600", 2b = 3.010".

Distance between probe and duct entry = 22"

Calibration of flowmeter (Mark II). Q = 13V;

(Q in c.c/sec, V in mV).

Maximum flowrate .06 litres/sec.

Reynolds number, R, = 57.2Q

Hartmann number, $M = B_o \times 213.3$ (at 20°c),

Theoretical pressure gradient for laminar, fully developed flow:

$M = 0 \quad \frac{dh}{dz} = -6.64 \times 10^{-6} Q$

$M \gg 1 \quad \frac{\partial p}{\partial z} = \frac{\tilde{\eta} M Q}{4a^3 b}\left(1 - \frac{852a}{b M^{1/2}} - \frac{1}{M} + \right)^{-1},$

$\frac{dh}{dz} = \frac{2.885 \times 10^{-5} \, VM}{(1 - .184 M^{-1/2} - M^{-1})},$

using the result of Shercliff (1953).

Entry length (l) when $M \gg 1$:

$l = aR/M$. (Shercliff (1956)).

Hence, since l = 20", $R/M \leq 62$ for fully developed flow in our duct.

Pitot tube measurements in the core when $M \gg 1$:

$$\Delta P_{5p} = \Delta P_0(1+\alpha N) + \Delta P_s = \Delta + \Delta P_0(\alpha N)$$

where $\Delta = \Delta P_0 + \Delta P_s$, $\Delta P_0 = \frac{1}{2}\rho v_c^2 = \frac{1}{2}\rho Q^2/\left(4ab(1-.184M^{-1/2}-M^{-1})\right)^2$,
$N = \sigma B_0^2(d, a_p, b_p)/\rho v_c$, ($d$ is used for Pitot tubes with circular tips, and the smallest value of a_p or b_p is used for flattened tips.).

α is an arbitrary constant to be measured, and

$$\Delta P_s = -\frac{\Delta z_{5p}\eta^{\sim} M Q}{4a^3 b(1-.184M^{-1/2}-M^{-1})}$$

where Δz_{5p} is the axial distance between the tapping (5) and the Pitot tip measured in the +z direction.

Electric potential probe measurements:

If $\Delta\phi$ is the potential difference between the probe tip and the tapping (5) at y=0, x = b = 1.505", then in the core when $M \gg 1$, the laminar flow theory is that

$$\frac{\Delta\phi}{\Delta x} = v_c B_0(1-M^{-1}) = \frac{Q(1-M^{-1})B_0}{4ab(1-.184M^{-1/2}-M^{-1})}$$

whence $\Delta\phi = 2.62\times10^{-4} B_0 \Delta x V\left(1-.184M^{-1/2}+O(M^{-3/2})\right)$

In the boundary layer on the wall at x = b,

$$\frac{\partial(\Delta\phi_c)}{\partial x} - \frac{\partial(\Delta\phi)}{\partial x} = B_0(v_c - v)\left(1+O(M^{-1})\right)$$

where $\Delta\phi_c$ is the core value of $\Delta\phi$. Using the result of Shercliff (1953),

$$(\Delta\phi_c)_{y=0} = \frac{6.4\times10^{-5} B_0 M^{-1/2} V}{(1-.184M^{-1/2})}.$$

Table 8.6. Static pressure drop in duct II when M 135.

V mv	M	$(\Delta P_{54}/MV)$ "meth/mv	V mv	M	$(-\Delta P_{45}/MV)$
1.99	134	2.99×10^{-4}	1.42	134	3.66×10^{-4}
2.28	134	2.92	1.89	139	3.69
2.33	135	2.83	2.39	135	3.40
2.97	133	3.00	2.46	138	3.51
3.70	134	3.00	2.92	134	3.62

Table 8.6 (cont).

V	M	V	M ($-\Delta P_{45}/MV$)
		2.96	135 3.25
		4.02	135 3.72

Mean 2.95×10^{-4} at 16°c Mean 3.55×10^{-4} at 17°c

with temp. correction. 3.12×10^{-4} at 20°c with temp. correction. 3.57 at 20°c

Average of both 3.35×10^{-4} at 20°c

Theoretical value 3.32×10^{-4} .

Table 8.7. Pitot tube errors in duct II. (circular tips).

(a) tip dimensions: .028" o.d. .0155" i.d. (fig.8.2)

M	V mV	ΔP_{SP} "metts	ΔP_0	ΔP_S	Δ	N	α
134	1.77	.012	.0130	.0050	-.0061	1.18	-.39
135	2.78	.033	.0198	.0066	.007	.91	.39
135	2.42	.050	.0223	.0070	.021	.88	1.07
133	2.44	.041	.0227	.0069	.011	.85	.57
135	2.82	.026	.0304	.0082	-.013	.75	-.55
135	2.84	.065	.0308	.0083	.024	.74	1.05
135	2.86	.049	.0304	.0082	.010	.75	.44
135	3.14	.077	.0377	.0091	.030	.68	1.18
134	3.44	.046	.0450	.0098	-.009.	.61	-.32

Mean value of α, $\bar{\alpha}$, = .38, s.d. = .4

Mean value of N = .82

(b) tip dimensions: .034" o.d., .020" i.d.

M	V						
256	1.95	.049	.0145	.0105	.045	4.54	.68
258	2.60	.058	.0258	.0141	.046	3.40	.52
257	3.35	.077	.0428	.0181	.052	2.65	.46
257	3.35	.058	.0428.	.0181	.033	2.65	.29

$\bar{\alpha}$ = .49

Table 8.8. Pitot tube errors in duct II. (flattened tip, $a_p \ll b_p$).

(a) external tip dimensions .012" x .062" (fig.7.2b); $M \simeq 137$.

M	V mv	ΔP_{stp} "melts	ΔP_o	ΔP_s	Δ "melts	N	α
139	1.67	.027	.0111	.0034	.013	.57	2.1
139	1.68	.017	.0112	.0051	.003	.57	.5
135	1.96	.048	.0146	.0057	.028	.46	4.2
139	2.75	.053	.0302	.0084	.014	.35	1.3
135	2.77	.026	.0293	.0080	-.011	.32	-1.2
139	3.16	.088	.0398	.0097	.042	.30	3.5
134	3.20	.105	.0390	.0093	.057	.28	5.2
135	3.26	.074	.0405	.0095	.024	.28	2.1
135	3.27	.110	.0408	.0095	.060	.28	5.2
139	3.57	.055	.0508	.0109	-.007	.27	-.5

$\overline{\alpha} = 2.0$

s.d. = .6

If N is based on D_p (= 4 x area/perimeter of tip cross section), the mean value of α, $\overline{\alpha}_{D_p} = 1.2$.

(b) same Pitot tube: $M \simeq 251$.

M	V	ΔP_{stp}	ΔP_o	ΔP_s	Δ	N	α
255	1.78	.089	.0125	.0098	.067	1.79	3.0
254	1.81	.075	.0129	.010	.052	1.76	2.3
253	2.25	.079	.0200	.012	.047	1.42	1.7
251	2.43	.092	.0233	.0134	.065	1.31	2.1
251	2.84	.084	.0318	.0157	.036	1.12	1.01
255	2.84	.062	.0318	.0157	.012	1.12	.34
253	3.18	.129	.0398	.018	.061	1.00	1.5
254	3.57	.111	.0501	.0197	.041	.89	.92
248	3.92	.157	.0607	.0217	.075	.82	1.5

$\overline{\alpha} = 1.6$

s.d. = .25

Table 8.9. Pitot tube error in duct II (flattened tip, $a_p >> b_p$)

Tip dimension. .073" x .024"; M ~253 (Fig.8.12a).

M	V	Δp_{stf}	Δp_o	Δp_s	Δ	N	α
252	2.71	.055	.0280	.0145	.042	2.34	.64
255	2.85	.047	.031	.0153	.031	2.66	.38
253	3.38	.055	.0435	.0181	.030	1.88	.37
253	3.55	.060	.048	.0190	.031	1.79	.36
253	3.92	.065	.0585	.0210	.027	1.62	.29

With N based on b_p, $\overline{\alpha} = .40$

With N based on D_p, $\overline{\alpha}_{D_p} = .24$

Table 8.10. Electric potential measurements in core flow of duct II.

x inches	B_o wb/m^2	M	$\Delta\phi/V$ mV/mV	$(\Delta\phi/V)_{x=0} - (\Delta\phi/V)_{x=.75}$ mV/mV	Theoretical value.
.003 .753	.196	41.8	.780 ± .006 .403 "	.377 ± .012	.396
.003 .753	.655	140	.271 ± .01 .1415 "	.130 ± .003	.1305
.003 .753	1.160	247	.478 ± .001 .250 ± .002	.227 ± .003	.2305

Note (1) the values of $\Delta\phi/V$ are mean values deriving from several readings of $\Delta\phi$ at various values of V.

(2) The probe used is that shown in fig.8.12(a).

Table 8.11. Basic data of 2½" x 3" duct (III).

Cross-section dimensions: 2a = 2.486", 2b = 3.010".

Positions of tappings relative to (5) in +z direction: (1) -46"; (2) -44.5"; (3) -23"; (4) -11.25"; (5).0; (6) 7".

Reynolds number, R = 1930 x V = 148.5 Q; where Q is in c.c/sec. and V is in mV.

Hartmann number, M = 820 B_o, where B_o is in wb/m^2.

Flowmeter calibration; Q = 13.0 V.

Pressure gradient in fully developed laminar flow (Hunt, 1965):

$$\frac{\partial p}{\partial z} = -\frac{Q\tilde{n}}{4a^3 b}\left(\frac{.3a}{bM^{3/2}} + \frac{1}{M^2} + \cdots\right)^{-1}$$

whence $$dh/dz = .57 \times 10^{-7} V M^{3/2} / \left(1 + \frac{4.02}{M^{1/2}}\right)$$

The theoretical velocity and potential profiles in the boundary layer at x = b may be found from (Hunt, 1965). In the core the potential relative to tapping (5) (x = b, y = o) is theoretically:

$$\Delta\phi = \frac{.149 \times 10^{-3} B_0 V}{\left(1 + 4.02/M^{1/2}\right)}$$

To calculate v_z from ΔP_{5p} we use the experimental value of dh/dz to find ΔP_s and the value of α for the MHD correction factor of the flattened Pitot tube from the table 8.9., i.e. .4, so that

$$\Delta P_{5p} = \tfrac{1}{2}\rho v_z^2\left(1 + \alpha\frac{\sigma B_0^2 b_p}{\rho v_z}\right) + \Delta P_s$$

Thence we calculate v_z. Note that $\Delta P_s < 0$ since the probe tip in this case is .750" downstream of tapping (5).

Table 8.12. Pitot readings in duct III: M = 943.

Tip dimensions .073" x .024".

b-z in inches	V mV	ΔP_{5p}	ΔP_s	$\Delta P_{5p} + \Delta P_s$	ΔP_o Ref·05	ΔP_o V=·8	v' cm/sec	v	v/Q (cm/sec) (c.f. col) at V=·8 & 1·05
·014	·830	·018	·025	·043		·043	3·58	2·53	·243
	1·29	·028	·040	·068	·055		4·06	3·04	·222
	1·76	·067	·054	·121					
·024	·73	·035	·023	·058					
	·78	·007	·024	·031		·045	3·67	2·63	·253
	1·04	·020	·052	·048	·048		3·80	2·76	·201
·039	1·06	·022	·033	·055	·055		4·06	3·04	·222
	1·44	·028	·045	·073					
·064	·690	·015	·021	·036					
	·850	·030	·026	·056					
	·870	·025	·027	·052		·050	3·87	2·83	·272
	1·15	·010	·065	045	·048		3·80	2·76	·202
	1·58	-·005	049	·044					

Table 8·12 (cont)

b-x	V	ΔP_{ST}	ΔP_S	$\Delta P_{ST} + \Delta P_S$	ΔP_0 V≈1·05	ΔP_0 V≈·8	v'	v	v/Q	
·089	·77	-·004	·024	·020		·020	2·45	1·50	·144	
	·88	-·005	·027	·022						
	·9	-·013	·028	·015						
	1·06	-·015	·033	·018	·018		2·32	1·37	·124	
	1·30	-·034	·040	·006						
	1·49	-·010	·046	·036						
·114	·65	-·051	·016	-·035						
	·95	-·022	·029	·007		·014	(-2·05)		(-·2)	
	1·44	-·065	·044	·021						
·214	·93	-·045	·029	-·016			(-2·14)		(-·18)	
·314	·93	-·035	·029	-·006			(-1·8)		(-·13)	
·614	·93	-·010	·029	·019			2·38	1·44	·12	← V=·93
(cone)	2·41	-·075	·110	·045			3·67	2·63	·08	← V=2·41

id Mech. (1965), vol. 21, part 4, pp. 577–590
d in Great Britain

Magnetohydrodynamic flow in rectangular ducts

By J. C. R. HUNT

Central Electricity Research Laboratories, Leatherhead*

(Received 27 July 1964)

paper presents an analysis of laminar motion of a conducting liquid in a ngular duct under a uniform transverse magnetic field. The effects of the having conducting walls are investigated. Exact solutions are obtained wo cases, (i) perfectly conducting walls perpendicular to the field and thin of arbitrary conductivity parallel to the field, and (ii) non-conducting walls llel to the field and thin walls of arbitrary conductivity perpendicular to ield.

e boundary layers on the walls parallel to the field are studied in case (i) it is found that at high Hartmann number (M), large positive and negative ities of order MV_c are induced, where V_c is the velocity of the core. It is sted that contrary to previous assumptions the magnetic field may in cases have a destabilizing effect on flow in ducts.

Introduction

e design of magnetohydrodynamic generators, pumps and accelerators ires an understanding of the flows of conducting fluids in rectangular s with finitely conducting walls under transverse magnetic fields. At the nt time even the case of uniformly conducting incompressible laminar with no variation in the flow direction has not been fully analyzed. In this r we confine ourselves to problems of this type alone. The main character- s of such flows that need to be known are:

) the volumetric flow rate q through the duct for given pressure gradient magnetic field;

) the potential difference between electrodes placed in the walls;

) the stability of the flow.

hree exact solutions have been found for incompressible laminar flows ucts with transverse magnetic fields:

) rectangular ducts with non-conducting walls and the field perpendicular ne side (Shercliff 1953);

) rectangular ducts with perfectly conducting walls (Chang & Lundgren ; Uflyand 1961);

) circular pipes with non-conducting walls (e.g. Gold 1962 and Fabri & trunck 1960).

pproximate methods have been developed for the physically interesting

* Seconded to the Department of Engineering Science, University of Warwick.

case of flows at high Hartmann number, M. For a rectangular duct with non-
conducting walls Shercliff (1953) developed an approximate method for analysing
the boundary layers on the walls parallel to the field and thence deduced q
and the potential distributions round the walls. By ignoring the reduction in
flow rate due to the boundary layers, he then found a first approximation for q
in a duct of any cross-section, which was later extended to the case of ducts
with thin walls of any conductivity by Chang & Lundgren (1961). Sakao (1962)
used a variational method to find a second-order approximation for q in circular
pipes.

In finding the overall features of the flow at high M, approximate methods
are often best since the exact solutions are in the form of infinite series whose
rate of convergence *decreases* for higher values of M. It is possible, however, to
compare the expressions for q at high M obtained by the two methods. The only
case hitherto of the approximate expression for q at high M agreeing with that
derived from the exact solution is that of flow in a rectangular duct with non-
conducting walls (Williams 1963). In the same paper, using some lengthy mathe-
matics, Williams deduced an expression for q at high M from Chang & Lund-
gren's result for flow in a rectangular channel with perfectly conducting walls.
The asymptotic form of the exact solution for circular pipe flow at high M
provides an expression for q which differs from Shercliff's (1962*a*) and Sakao's
(1962) approximate expressions by a term due to the velocity defect in the bound-
ary layers.

No satisfactory approximate or exact solutions exist for the most important
practical case of a rectangular duct with conducting walls parallel to the field
and non-conducting walls perpendicular to the field. Some observations on this
problem have been made by Shercliff (1962*b*, page 16) and by Braginskii (1960).
Grinberg (1961, 1962) has attempted an exact analysis using a Green's function
method but his result is incomplete. We have not been able to solve this problem
but we have solved exactly two other classes of problem of flow in a rectangular
duct, in which the duct has (i) perfectly conducting walls at right angles to the
field and thin walls of arbitrary conductivity parallel to the field, and (ii) non-
conducting walls parallel to the field and thin walls of arbitrary conductivity
perpendicular to the field. These exact solutions are in the form of infinite
series whose rate of convergence *increases* for higher values of M. In this paper
we examine the asymptotic form of these solutions at high M and draw some
interesting physical conclusions, the main one being that a magnetic field may
have a destabilizing influence on the flow in a duct.

2. Formulation of the problem

We consider the steady flow of an incompressible conducting fluid driven by a
pressure gradient along a rectangular duct under an imposed transverse magnetic
field. We assume that the walls of the duct are thin and finitely conducting.
We postulate no secondary flow and no variation in duct cross-section or
magnetic field. Consequently all conditions except pressure are constant along
the duct.

Relative to the axes defined in figure 1, the equations describing such magneto-
hydrodynamic duct flows are:

$$j_x = \sigma(-\partial\phi/\partial x - v_z B_0), \quad j_y = \sigma(-\partial\phi/\partial y), \tag{1}$$

$$\partial j_x/\partial x + \partial j_y/\partial y = 0, \tag{2}$$

$$j_x = \partial H_z/\partial y, \quad j_y = -\partial H_z/\partial x, \tag{3}$$

$$0 = -\frac{\partial p}{\partial z} + j_x B_0 + \tilde{\eta}\left(\frac{\partial^2}{\partial x^2} + \frac{\partial^2}{\partial y^2}\right) v_z. \tag{4}$$

and j_y are the current components; ϕ is the electric potential; H_z is the induced
which may also be considered as a current stream function; B_0 is the flux
ity of the imposed magnetic field; v_z is the velocity; $\sigma, \tilde{\eta}, \partial p/\partial z$ are con-
vity, viscosity and pressure gradient respectively. Let $2a$, and $2b$ be the
hs of the sides of the channel (see figure 1).

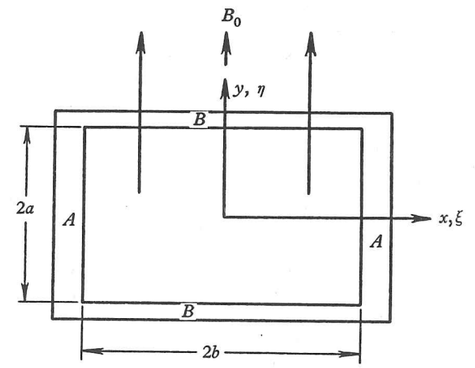

IGURE 1. Cross-section of a rectangular duct with magnetic field in y-direction.
The walls AA lie at $x = \pm b$ and BB at $y = \pm a$.

e equations are usually re-written to give two coupled second-order partial
ential equations in H_z and v_z,

$$0 = -\frac{\partial p}{\partial z} + B_0\frac{\partial H_z}{\partial y} + \tilde{\eta}\left(\frac{\partial^2}{\partial x^2} + \frac{\partial^2}{\partial y^2}\right) v_z \tag{5}$$

$$0 = B_0\frac{\partial v_z}{\partial x} + \frac{1}{\sigma}\left(\frac{\partial^2}{\partial x^2} + \frac{\partial^2}{\partial y^2}\right) H_z. \tag{6}$$

and H_z are normalized in terms of $(\partial p/\partial z)$, a, σ and $\tilde{\eta}$, (5) and (6) become

$$\frac{\partial^2 V}{\partial \xi^2} + \frac{\partial^2 V}{\partial \eta^2} + M\frac{\partial H}{\partial \eta} = -1, \tag{7}$$

$$\frac{\partial^2 H}{\partial \xi^2} + \frac{\partial^2 H}{\partial \eta^2} + M\frac{\partial V}{\partial \eta} = 0, \tag{8}$$

$$V = v_z\tilde{\eta}\Big/\left(-\frac{\partial p}{\partial z}\right)a^2; \quad H = H_z(\tilde{\eta})^{\frac{1}{2}}\Big/\left(-\frac{\partial p}{\partial z}\right)a^2\sigma^{\frac{1}{2}};$$

$$M = aB_0(\sigma/\tilde{\eta})^{\frac{1}{2}}; \quad \xi = x/a; \ \eta = y/a.$$

Also let $$\Phi = \phi\,(\sigma\tilde{\eta})^{\frac{1}{2}}\Big/\left(-\frac{\partial p}{\partial z}\right)a^2 \quad \text{and} \quad l = b/a.$$

We follow Shercliff (1956) in the specification of boundary conditions on H at a thin bounding wall. If $\partial H/\partial n$ is the normalized inward normal gradient of H at the wall, the condition satisfied by H at the wall is

$$\partial H/\partial n = \sigma a H/\sigma_w w,$$

where σ_w is the conductivity of the wall and w its thickness ($w \ll a$). If $d = \sigma_w w/\sigma a$, the boundary condition for H is

$$\partial H/\partial n = H/d.$$

The boundary condition on V, of course, is that it should vanish at the walls.

In §§3 and 4 we consider the following two cases, defined with reference to figure 1:

case I rectangular duct with walls BB perfectly conducting and walls AA of arbitrary conductivity;

case II rectangular duct with walls AA non-conducting and walls BB of arbitrary conductivity.

3. Case I

In this case walls BB are perfectly conducting, $d_B = \infty$, and walls AA have arbitrary conductivity d_A. The boundary conditions on V and H are:

$$\left.\begin{aligned} &\text{at} \quad \eta = \pm 1, \quad V = 0 \quad \text{and} \quad \partial H/\partial \eta = 0, \\ \text{and} \quad &\text{at} \quad \xi = \pm l, \quad V = 0 \quad \text{and} \quad \partial H/\partial \xi = \mp H/d_A. \end{aligned}\right\} \tag{10}$$

We can satisfy the boundary conditions on $\eta = \pm 1$ by expressing V and 1 as Fourier series in η, with the coefficients functions of ξ,

$$V = \sum_{j=0}^{\infty} v_j(\xi)\cos\alpha_j\eta; \quad H = \sum_{j=0}^{\infty} h_j(\xi)\sin\alpha_j\eta; \quad 1 = \sum_{j=0}^{\infty} a_j\cos\alpha_j\eta,$$

where $\alpha_j = (j+\frac{1}{2})\pi$ and $a_j = 2(-1)^j/\alpha_j$. Substituting these expansions for V and H into (7) and (8) leads to two ordinary differential equations for v_j and h_j

$$v_j'' - \alpha_j^2 v_j + M\alpha_j h_j = -a_j,$$

and

$$h_j'' - a_j^2 h_j - M\alpha_j v_j = 0.$$

The solutions of these equations which satisfy the boundary conditions on $\xi = \pm l$ are

$$v_j = \frac{a_j}{\alpha_j^2+M^2}\left[1 - \frac{([1-iM/\alpha_j]\cosh r_{2j}l + d_A r_{2j}\sinh r_{2j}l)\cosh r_{1j}\xi}{K_j} - \frac{([1+iM/\alpha_j]\cosh r_{1j}l + d_A r_{1j}\sinh r_{1j}l)\cosh r_{2j}\xi}{K_j}\right], \tag{11}$$

$$h_j = \frac{a_j}{\alpha_j^2+M^2}\left[-\left(\frac{M}{\alpha_j}\right) + \frac{([i+M/\alpha_j]\cosh r_{2j}l + id_A r_{2j}\sinh r_{2j}l)\cosh r_{1j}\xi}{K_j} - \frac{([i-M/\alpha_j]\cosh r_{1j}l + id_A r_{1j}\sinh r_{1j}l)\cosh r_{2j}\xi}{K_j}\right], \tag{12}$$

where

$$r_{1j}, r_{2j} = (\alpha_j^2 \pm iM\alpha_j)^{\frac{1}{2}}$$

and

$$K_j = 2\cosh r_{1j}l\cosh r_{2j}l + d_A[r_{2j}\sinh r_{2j}l\cosh r_{1j}l + r_{ij}\sinh r_{ij}l\cosh r_{2j}l].$$

r_{1j} and r_{2j} may be split into their real and imaginary parts, namely,

$$r_{1j}, r_{2j} = \beta_j \pm i\gamma_j,$$

where

$$\beta_j, \gamma_j = (\tfrac{1}{2}\alpha_j)^{\frac{1}{2}}[\pm\alpha_j + (\alpha_j^2+M^2)^{\frac{1}{2}}]^{\frac{1}{2}}.$$

and

$$K_j = \cosh 2\beta_j l + \cos 2\gamma_j l + d_A(\beta_j\sinh 2\beta_j l - \gamma_j \sin 2\gamma_j l).$$

The final result for V and H is

$$V = \sum_{j=0}^{\infty} \frac{2(-1)^j\cos\alpha_j\eta}{\alpha_j(\alpha_j^2+M^2)}\left[1 - \frac{C_j(\xi) - M/\alpha_j D_j(\xi)}{K_j} - \frac{d_A[\beta_j E_j(\xi) - \gamma_j F_j(\xi)]}{K_j}\right], \tag{13}$$

$$B = \sum_{j=0}^{\infty} \frac{2(-1)^j\sin\alpha_j\eta}{\alpha_j(\alpha_j^2+M^2)}\left[-\left(\frac{M}{\alpha_j}\right) + \frac{M/\alpha_j C_j(\xi) + D_j(\xi)}{K_j} + \frac{d_A[\gamma_j E_j(\xi) + \beta_j F_j(\xi)]}{K_j}\right], \tag{14}$$

where

$$\begin{aligned} C_j(\xi) &= \cos\gamma_j(l-\xi)\cosh\beta_j(l+\xi) + \cos\gamma_j(l+\xi)\cosh\beta_j(l-\xi), \\ D_j(\xi) &= \sin\gamma_j(l-\xi)\sinh\beta_j(l+\xi) + \sin\gamma_j(l+\xi)\sinh\beta_j(l-\xi), \\ E_j(\xi) &= \cos\gamma_j(l-\xi)\sinh\beta_j(l+\xi) + \cos\gamma_j(l+\xi)\sinh\beta_j(l-\xi), \\ F_j(\xi) &= \sin\gamma_j(l-\xi)\cosh\beta_j(l+\xi) + \sin\gamma_j(l+\xi)\cosh\beta_j(l-\xi). \end{aligned}$$

The non-dimensional volumetric flow rate, Q, is defined by

$$Q = \int_{-1}^{+1}\int_{-l}^{+l} V\,d\eta\,d\xi,$$

and, from (17),

$$Q = \sum_{j=0}^{\infty} \frac{8}{a_j^2(\alpha_j^2+M^2)}\left[l - \frac{(\beta_j - M\gamma_j/\alpha_j)\sinh 2\beta_j l + (\gamma_j + M\beta_j/\alpha_j)\sin 2\gamma_j l}{(\beta_j^2+\gamma_j^2)K_j} - \frac{\alpha_j d_A(\cosh 2\beta_j l - \cos 2\beta_j l)}{(\alpha_j^2+M^2)^{\frac{1}{2}}K_j}\right]. \tag{15}$$

Note that the terms independent of ξ in the expressions for V and H are the Fourier expansions of the Hartmann solution and also that, as $d_A \to \infty$, the solutions become identical to those obtained for rectangular ducts with perfectly conducting walls by Uflyand (1961) and Chang & Lundgren (1961).

At high Hartmann numbers the fluid tends to move at a constant velocity, the core velocity, in the centre of the duct with the velocity gradients confined to thin Hartmann layers on the walls BB. If the non-dimensional core velocity is V_c then $V_c \sim 1/M^2$ as $M \to \infty$. The current density is also constant in the core. The Hartmann layers are well understood, but the boundary layers on the walls AA are less well understood and need examination.

We consider the boundary layer on the wall $\xi = -l$ at high Hartmann number and make the following approximations:

$$M \to \infty, \quad \beta_j, \gamma_j \sim (\tfrac{1}{2}\alpha_j M)^{\frac{1}{2}}(1 \pm O(1/M)\ldots) \sim \lambda_j, \quad \text{where} \quad \lambda_j = (\tfrac{1}{2}\alpha_j M)^{\frac{1}{2}},$$

hence

$$K_j \sim \tfrac{1}{2}[\exp\{2(\tfrac{1}{2}\alpha_j M)^{\frac{1}{2}}l\}](1 + d_A(\tfrac{1}{2}\alpha_j M)^{\frac{1}{2}})(1+O(1/M))$$

~~$\sim \exp\frac{1}{2}[(2\lambda_j l)(1+d_A\lambda_j)]$.~~

$\sim \frac{1}{2}(1+d_A\lambda_j)\exp(2\lambda_j l)$.

For clarity we take the two cases of $d_A = 0$ and $d_A = \infty$ and consider the V, H, and Φ profiles in the boundary layer. If $\xi' = \xi + l$ and $\Phi = 0$ at $\eta = \pm 1$, then for $d_A = 0$, as $M \to \infty$,

$$V \sim \sum_{j=0}^{\infty} \frac{2(-1)^j \cos \alpha_j \eta}{M^2 \alpha_j} [1 - \exp(-\lambda_j \xi') \{\cos(\lambda_j \xi') - M/\alpha_j \sin(\lambda_j \xi')\}], \tag{16}$$

$$H \sim \sum_{j=0}^{\infty} \frac{2(-1)^j \sin \alpha_j \eta}{M^2 \alpha_j} [-(M/\alpha_j) + \exp(-\lambda_j \xi') \{(M/\alpha_j) \cos(\lambda_j \xi') + \sin(\lambda_j \xi')\}], \tag{17}$$

$$\Phi \sim \sum_{j=0}^{\infty} \frac{2(-1)^j \cos \alpha_j \eta}{M^2 \alpha_j^2} [\{M^{\frac{3}{2}}/(2\alpha_j)^{\frac{1}{2}}\} \exp(-\lambda_j \xi') \{\cos(\lambda_j \xi') + \sin(\lambda_j \xi')\}], \tag{18}$$

and for $d_A = \infty$, as $M \to \infty$,

$$V \sim \sum_{j=0}^{\infty} \frac{2(-1)^j \cos \alpha_j \eta}{M^2 \alpha_j} [1 - \exp(-\lambda_j \xi') \{\cos(\lambda_j \xi') - \sin(\lambda_j \xi')\}], \tag{19}$$

$$H \sim \sum_{j=0}^{\infty} \frac{2(-1)^j \sin \alpha_j \eta}{M^2 \alpha_j} [-(M/\alpha_j) + \exp(-\lambda_j \xi') \{\cos(\lambda_j \xi') + \sin(\lambda_j \xi')\}], \tag{20}$$

$$\Phi = \sum_{j=0}^{\infty} \frac{2(-1)^j \cos \alpha_j \eta}{\alpha_j^2 M^2} [2\lambda_j \exp(-\lambda_j \xi') \sin(\lambda_j \xi')]. \tag{21}$$

In contrast with the exact solutions for rectangular and circular pipes with non-conducting walls, the higher terms in these series decrease exponentially and therefore it is a good approximation to consider the first few terms only. Hence we see that the V, H, and Φ boundary layer profiles approximately have the form of exponentially damped sine waves, the thickness of the layers being $O(M^{-\frac{1}{2}})$. In figures 2 and 3 velocity profiles when $d_A = 0$ are plotted for various values of η at $M = 100$ and for various values of M at $\eta = 0$. In figure 4, the velocity profiles when $d_a = \infty$ are plotted for various values of η at *arbitrary* M, provided $M \gg 1$. Here the abscissa $M^{\frac{1}{2}}\xi'$ provides a universal plot, when $M \gg 1$. Note that in all cases $V/V_c \to 1$ as $\xi' \to \infty$.

The dramatic effect on the flow of varying the conductivity of the walls AA is seen by comparing figures 3 and 4. When $d_A = \infty$ (figure 4) the maximum velocity in the boundary layer A is greater than the core velocity though of the same order; but when $d_A = 0$ (figure 3), the maximum velocity is $O(M)V_c$ and the minimum velocity is *negative* provided M is high enough. We can deduce from (16) that the maximum velocity tends to $0{\cdot}25\,MV_c$ as $M \to \infty$, while the minimum velocity becomes locally negative for $M > 89$ and tends to $-0{\cdot}011\,MV_c$ as $M \to \infty$. The physical reason for the effect on the flow of varying d_A when $M \gg 1$ may be seen from equation (13) which shows that the form of the velocity profile depends on $d_A M^{\frac{1}{2}}$, the ratio of the conductance of the wall to that of the boundary layer on the wall A. Thus when $d_A M^{\frac{1}{2}} \gg 1$ the currents return to the walls BB through the walls AA and when $d_A M^{\frac{1}{2}} \ll 1$ the currents return to the walls BB through the boundary layers on walls AA. These effects are shown in figures 5*a* and *b*. In the first case the $\mathbf{j} \times \mathbf{B}$ drag force remains almost as high in the

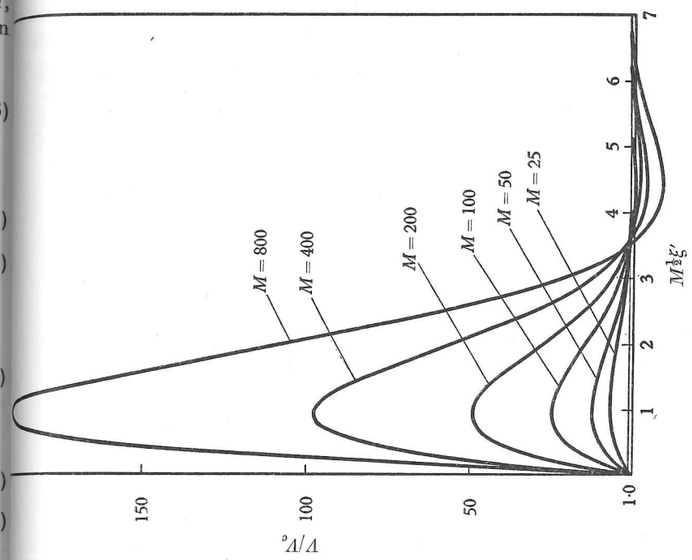

FIGURE 3. I: $d_A = 0$. Graph of V/V_c against $\sqrt{M}\xi'$ at $\eta = 0$ in the boundary layer on $\xi = -l$ for various values of $M(\gg 1)$.

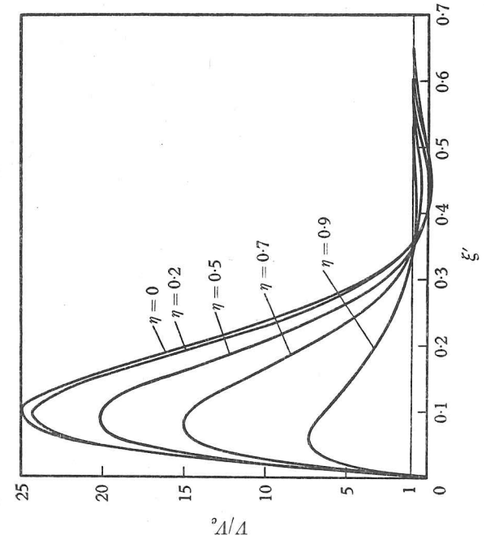

FIGURE 2. Case I: $d_A = 0$, $M = 100$. Graph of V/V_c against ξ' in the boundary layer on $\xi = -l$ for various values of η.

boundary layer as it is in the core and in the second case the $\mathbf{j}\times\mathbf{B}$ drag force decreases to zero at the walls, which explains why the velocities in the boundary layer are much less when $d_A = \infty$ than when $d_A = 0$. The reason for the large positive and negative velocities when $d_A = 0$ is difficult to explain simply, but it appears that relative to its value in the core, the $\mathbf{j}\times\mathbf{B}$ force *increases* at the outer edge of the boundary layer, where the negative velocity occurs, before it *decreases* near the wall, where the large positive velocities occur.

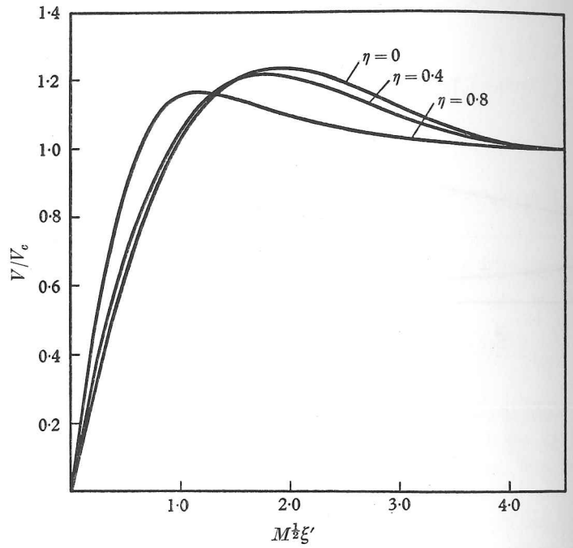

FIGURE 4. Case I: $d_A = \infty$. Graph of V/V_c against $\sqrt{M}\xi'$ in the boundary layer at $\xi = -l$ for various values of η at any value of M, provided $M \gg 1$.

Figures 2 and 4 show how little variation in velocity there is in the η-direction as compared with the ξ' direction which is to be expected since the magnetic field tends to damp only the vorticity perpendicular to it.

Williams has worked out an asymptotic expansion for Q when $d_A = \infty$ as $M \to \infty$ in terms of $1/M$. It is possible to use a simpler method than he used to derive the same result and this same method may also be used for any value of d_A.

We consider the expression for Q in equation (15) as $M \to \infty$ and make the same approximations as in equations (16) to (21). As $M \to \infty$, $M\gamma_j/\alpha_j \simeq M\lambda_j/\alpha_j$ and $\beta_j \simeq \lambda_j$, where $\lambda_j \simeq (\frac{1}{2}\alpha_j M)^{\frac{1}{2}}$. Hence for low values of j, such that $\alpha_j \gg M$, $M\gamma_j/\alpha_j \gg \beta_j$. Also, as $M \to \infty$, $\cosh 2\beta_j l \simeq \sinh 2\beta_j l \simeq \frac{1}{2}\exp(2l\lambda_j)$ and hence $\cosh 2\beta_j l \gg \cos 2\beta_j l$ and $\sinh 2\beta_j l \gg \sin 2\gamma_j l$. Therefore from equation (15) as $M \to \infty$

$$Q \sim \sum_{j=0}^{\infty} \frac{8}{\alpha_j^2(\alpha_j^2+M^2)}\left\{l + \frac{(M\lambda_j/\alpha_j)\,\frac{1}{2}\{\exp(2l\lambda_j)\}}{2\lambda_j^2\,\frac{1}{2}[\{\exp(2l\lambda_j)\}(1+d_A\lambda_j)]} - \frac{\alpha_j d_A\,\frac{1}{2}\{\exp(2l\lambda_j)\}}{(\alpha_j^2+M^2)^{\frac{1}{2}}\,\frac{1}{2}[\{\exp(2l\lambda_j)\}(1+d_A\lambda_j)]}\right\},$$

hence,

$$Q \sim \sum_{j=0}^{\infty} \frac{8}{\alpha_j^2(\alpha_j^2+M^2)}\left\{l + \frac{M^{\frac{3}{2}}(2\alpha_j)^{-\frac{1}{2}} - d_A\alpha_j^2}{M\alpha_j\{1+d_A(\frac{1}{2}\alpha_j M)^{\frac{1}{2}}\}}\right\}. \tag{22}$$

first term in this expression represents the velocity flux due to Hartmann between the planes $\eta = \pm 1$, while the second term is the change due to the dary layers on the walls AA. Note that the form of the second term depends

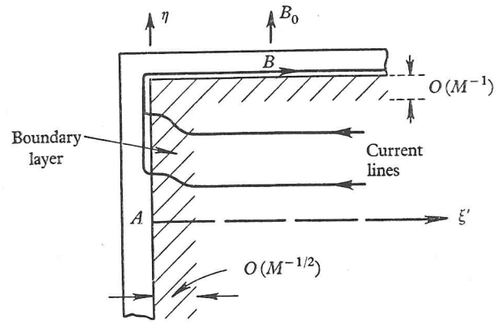

(a)

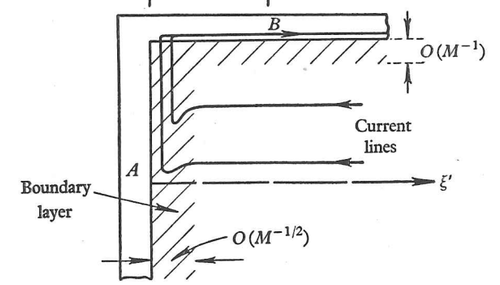

(b)

RE 5(a). Cross-section of the duct when $d_A = \infty$ and $d_B = \infty$ ($M \gg 1$). (Not to (b) Cross-section of the duct when $d_A = 0$ and $d_B = \infty$ ($M \gg 1$). (Not to scale.)

he value of $d_A/M^{\frac{1}{2}}$, the ratio of the conductance of the wall to that of the dary layer. If $d_A = \infty$,

$$Q \sim \frac{4l}{M^2}\left(1-\frac{1}{M}\right) - \sum_{j=0}^{\infty}\frac{8\sqrt{2}}{M^{\frac{1}{2}}\alpha_j^{\frac{3}{2}}} \simeq \frac{4l}{M^2}\left(1-\frac{1}{M}\right) - \frac{32}{M^{\frac{1}{2}}\pi^{\frac{3}{2}}}\sum_{j=0}^{\infty}\frac{1}{(2_j+1)^{\frac{3}{2}}},$$

summing the series leads to

$$Q \sim \frac{4l}{M^2}\left(1-\frac{1}{M}-\frac{2{\cdot}40}{lM^{\frac{3}{2}}}+O\left(\frac{1}{M^2}\right)\right).$$

Hence the mean velocity

$$\bar{v}_z \sim \frac{(-\partial p/\partial z)\,a^2}{\eta M^2}\left(1-\frac{1}{M}-\frac{2{\cdot}40a}{bM^{\frac{3}{2}}}\right). \qquad (2$$

In the exact expression derived by Williams the coefficient of the third term w
2·43.

If $d=0$,

$$Q \sim \frac{4l}{M^2}\left(1-\frac{1}{M}\right)+\sum_{j=0}^{\infty}\frac{64}{M^{\frac{3}{2}}(2_j+1)^{\frac{7}{2}}}$$
$$\sim \frac{1{\cdot}20}{M^{\frac{3}{2}}}+\frac{4l}{M^2}+O\left(\frac{1}{M^{\frac{5}{2}}}\right).$$

Hence the mean velocity

$$\bar{v}_z \sim \frac{(-\partial p/\partial z)\,a^2}{\eta}\left\{\frac{a}{b}\frac{0{\cdot}30}{M^{\frac{3}{2}}}+\frac{1}{M^2}+\frac{a}{b}O\left(\frac{1}{M^{\frac{5}{2}}}\right)\right\}. \qquad (2$$

These results further demonstrate the interesting physical effects due to th
conducting walls. From (23) we see that the velocity deficiency in the boundar
layers on AA, i.e.

$$\int_{-1}^{+1}\int_{-l}^{+l}(V_c-V)\,d\eta\,d\xi,$$

is $O(M^{-\frac{7}{2}})$, when all the walls are perfectly conducting, i.e. $d_A=\infty$. This is le
than that in the case of the rectangular duct with non-conducting walls whe
it is $O(M^{-\frac{3}{2}})$ (Shercliff 1953). The reduced velocity deficiency is due to the velocit
in the boundary layers showing an overshoot; relative to its value in the co
the velocity first decreases, then increases above its value in the core, and finall
decreases to zero at the wall. In fact there are an infinite number of fluctuatio
in the velocity profile between the overshoot, just referred to, and the core, b
they are sufficiently small for us to ignore them (see figure 4). Note that in bot
these cases the thickness of the boundary layers is $O(M^{-\frac{1}{2}})$.

When $d_A=0$ the velocity 'deficiency', as defined above, is negative and w
find that for a reasonably square duct ($a/b \gg M^{-\frac{1}{2}}$) most of the flow (equation (24
is *in the boundary layers* on AA. If the boundary layer has thickness $O(M^{-}$
and the velocity in the boundary layer is $O(MV_c)=O(M^{-1})$ then the velocit
flux through the boundary layer is $O(M^{-\frac{3}{2}})$ as compared with $O(M^{-2})$ for the tot
velocity flux in the core. A practical consequence of this would be that, whatev
the value of d_A, for a given pressure gradient a system of thin insulating baffl
placed parallel to AA at a distance $O(aM^{-\frac{1}{2}})$ apart would promote a great
volume flow rate by creating more boundary layers. The explanation is that th
dominant retarding force on the core flow is electro-magnetic rather than viscou
and the baffles will reduce the currents and hence also the electromagnetic retar
ing force. Provided the baffles are at least $O(aM^{-\frac{1}{2}})$ apart, the decrease in electr
magnetic drag will be greater than the increase in viscous drag.

4. Case II

In this case walls AA are non-conducting, $d_A=0$, and walls BB have arbitra
conductivity, d_B. The boundary conditions on V and H are

$$\left.\begin{aligned}&\text{at } \eta=\pm 1, \quad V=0, \quad \partial H/\partial\eta=\mp H/d_B,\\ \text{and}\quad &\text{at } \xi=\pm l, \quad V=0, \quad H=0.\end{aligned}\right\} \qquad (2$$

satisfy the boundary conditions on $\xi=\pm l$ by expressing V and H as
r series in ξ, with coefficients functions of η,

$$V=\sum_{k=0}^{\infty}v_k(\eta)\cos\alpha_k\xi, \quad H=\sum_{k=0}^{\infty}h_k(\eta)\cos\alpha_k\xi, \qquad 1=\sum_{k=0}^{\infty}a_k\cos\alpha_k\xi,$$
$$\alpha_k=(k+\tfrac{1}{2})\frac{\pi}{l} \quad \text{and} \quad a_k=\frac{2(-1)^k}{\alpha_k l}.$$

ituting these values for V and H into (7) and (8) again leads to two
ry differential equations for v_k and h_k

$$v_k''-\alpha_k^2 v_k+Mh_k'=-a_k,$$
$$b_k''-\alpha_k^2 b_k+Mv_k'=0.$$

olutions of these equations which satisfy the boundary conditions (25)
e some formidable algebra. The results are

$$\frac{2(-1)^k\cos\alpha_k\xi}{l\alpha_k^3}\left[1-\frac{(1+\tanh r_{2k}/d_B r_{2k})\cosh r_{1k}\eta}{(\cosh r_{1k})\,(M^2+4\alpha_k^2)^{\frac{1}{2}}/r_{2k}+\sinh(r_{1k}+r_{2k})/d_B r_{2k}\cosh r_{2k}}\right.$$
$$\left.-\frac{(1+\tanh r_{1k}/d_B r_{1k})\cosh r_{2k}\eta}{(\cosh r_{2k})\,(M^2+4\alpha_k^2)^{\frac{1}{2}}/r_{1k}+\sinh(r_{1k}+r_{2k})/d_B r_{1k}\cosh r_{1k}}\right], \qquad (26)$$

$$\frac{2(-1)^k\cos\alpha_k\xi}{l\alpha_k^3}\left[\frac{(1+\tanh r_{2k}/d_B r_{2k})\sinh r_{1k}\eta}{(\cosh r_{1k})\,(M^2+4\alpha_k^2)^{\frac{1}{2}}/r_{2k}+\sinh(r_{1k}+r_{2k})/d_B r_{2k}\cosh r_{1k}}\right.$$
$$\left.-\frac{(1+\tanh r_{1k}/d_B r_{1k})\sinh r_{2k}\eta}{(\cosh r_{2k})\,(M^2+4\alpha_k^2)^{\frac{1}{2}}/r_{1k}+\sinh(r_{1k}+r_{2k})/d_B r_{1k}\cosh r_{1k}}\right], \qquad (27)$$

$r_{1k}, r_{2k}=\frac{1}{2}(\pm M+\{M^2+4\alpha_k^2\}^{\frac{1}{2}})$.
en $d_B=0$ then all the walls are non-conducting which is the case analyzed
ercliff (1953). Putting $d_B=0$ in the above formulae and adding V to H
Shercliff's result (equation (15) in his paper).
en $d_B=\infty$ the duct is the same as that analyzed in §3 when $d_A=0$. It
be desirable to check that the two solutions were the same but this proves
lt, since to examine the above solutions near $\xi=\pm l$ the higher harmonics
expansions of V and H have to be considered. It would be easier to check
he expressions for Q derived from the two solutions are the same. Using
when $d_B=\infty$, gives

$$Q=\int_{-1}^{+1}\int_{-l}^{+l}V\,d\eta\,d\xi=\sum_{k=0}^{\infty}\frac{8}{l\alpha_k^4}[1+r_{2k}\tanh r_{1k}/r_{1k}(M^2+4\alpha_k^2)^{\frac{1}{2}}$$
$$-r_{1k}\tanh r_{2k}/r_{2k}\,(M^2+4\alpha_k^2)^{\frac{1}{2}}]. \qquad (28)$$

ay expand this expression in terms of $1/M$ as $M\to\infty$, using the methods of
ams (1963) and it is easily seen that the leading term is $O(M^{-\frac{3}{2}})$ in agreement
the previous result (24). The significance of this term has already been
ssed in §3.
om (26) we may see that V and Q depend on $d_B M$, the ratio of the conduc-

tance of the walls BB to that of the boundary layers on BB. Decreasing d_B m
makes the current induced in the core return through the Hartmann layers o
BB and hence reduces the electro-magnetic drag on the flow. This in turn damp
out the sinusoidal form of the boundary layers on AA and for some finite d_I
no negative velocities will be induced in these layers.

In examining the case when the walls are non-conducting, Shercliff firs
derived the exact solution for $(V+B)$, but found that this solution gave littl
information about the boundary layers at $\xi = \pm l$ owing to the slow convergenc
of the series. Then by assuming that, in the boundary layers on $\xi = \pm l$,

$$\frac{\partial^2(V+B)}{\partial\eta^2} \ll \frac{\partial^2(V+B)}{\partial\xi^2},$$

he found a self-similar solution for $(V+B)$. Thence he was able to work out th
velocity deficiency in the boundary layer. Shercliff's method is not applicabl
to cases other than $d_B = 0$ and $d_A = 0$; no other type of self-similar solutio
has yet been found.

5. Conclusion

Though this study is far from complete, it does indicate the need for furthe
theoretical and experimental study of MHD flows in ducts with conducting wall
First, it is not difficult in a mercury experiment to raise M to values greate
than 100, and the effects predicted by the theory should be observable.

Secondly, the stability of the boundary layers on the walls AA in the presen
of excess velocity and reversed flow needs theoretical examination. The analys
of the steady-state duct flow problem does not depend on the value of th
Reynolds number R or the magnetic Reynolds number R_m, but the stability
such a flow depends on R, R_m, and M. In most practical situations $R_m \ll$
and we can ignore the Alfvén wave motions associated with $R_m \gg 1$. Whe
$R_m \gg 1$ the stability analysis depends only on R and M. Lock (1955) has analyze
the stability of Hartmann flow and found that in realistic cases the magneti
field stabilizes the flow by its effect on the equilibrium velocity profile and n
by inhibiting the growth of small disturbances, since this is dominated by viscou
effects. We can then make some qualitative predictions about the stability
the flows studied above, based on our knowledge of the stability of boundar
layers when there is no magnetic field.

Let us examine the stability of the boundary layers on the walls AA in a du
with perfectly conducting walls perpendicular to the field and insulating wal
parallel to the field ($d_A = 0, d_B = \infty$). As $M \to \infty$, there is an increasing number
points of inflexion in the velocity profile which indicates that the higher M the low
the Reynolds number at which the flow in the boundary layers becomes unstab
(figure 3). The degree to which the magnetic field is likely to be destabilizi
depends also on the shape of the duct. If $a/b \ll M^{-\frac{1}{2}}$, a very thin duct with wal
AA much shorter than walls BB, the mean velocity in the duct closely approach
the core velocity and most of the flow is in the core. (For $a/b \ll M^{-\frac{1}{2}}$ most of t
flow is in the boundary layers on AA (§3)). Then the mean velocity in the boun

yers on the walls AA is $O(M)\,\bar{v}_z$, and since the thickness of these boundary
s is $O(aM^{-\frac{1}{2}})$, the Reynolds number of the boundary layer

$$R_{\text{b.l.}} = O(aM^{\frac{1}{2}})\,\bar{v}_z/\nu,$$

e ν is the kinematic viscosity. Hence

$$R_{\text{b.l.}} \simeq O(M^{\frac{1}{2}})\,R, \tag{29}$$

e R is the overall Reynolds number of the flow in the duct ($R = \bar{v}_z a/\nu$).
s, for given R, $R_{\text{b.l.}}$ increases with M; hence the critical overall Reynolds
ber at which the boundary layer becomes unstable is reduced by increasing
Note, however, that away from the remote walls AA the flow would be very
le.

ow consider an approximately square duct with $a/b = O(1)$. We see from
tion (24) that in this case most of the flow is in the boundary layers on AA.
mean velocity in the boundary layers on AA is $O(M)\,v_c$, where v_c is the core
city, and since the thickness of these boundary layers is $O(aM^{-\frac{1}{2}})$, the overall
n velocity is given by

$$v_z \simeq O[(Mv_c \times a^2M^{-\frac{1}{2}} + v_c \times ab)/ab] \simeq O[M^{\frac{1}{2}}v_c a/b].$$

ce if $a/b = O[1]$, $R \simeq O[M^{\frac{1}{2}}av_c/\nu]$ and since $R_{\text{b.l.}} \simeq O[M^{\frac{1}{2}}av_c/\nu]$,

$$R \simeq R_{\text{b.l.}}. \tag{30}$$

s for this type of duct for given R, $R_{\text{b.l.}}$ does not increase with M. Comparing
and (30) indicates that the thinner the duct the more the magnetic field
ls to destabilize the flows in the boundary layers on AA.

is important to realize that the forms of the velocity profiles are functions
and not R. Thus velocity overshoot and reversed flow can occur in the bound-
layers on AA at arbitrarily small Reynolds number. We cannot assume,
efore, that these boundary layers are always unstable as $M \to \infty$: they will
ably be stable at sufficiently small Reynolds numbers, whatever the value
f.

hen the walls of the duct are all perfectly conducting ($d_A = d_B = \infty$) the
city profile of the boundary layers also contains points of inflexion (figure 4)
hence raising M reduces the Reynolds number at which these boundary
rs become unstable. But in this case for $M \gg 1$ the velocity in the boundary
rs on AA is of the same order as the core velocity and since the boundary
r thickness is $O(aM^{-\frac{1}{2}})$,

$$R_{\text{b.l.}} = O(M^{-\frac{1}{2}})\,R.$$

ovided $a/b < M^{\frac{1}{2}}$ the shape of the duct does not matter.) Therefore in contrast
he former case ($d_A = 0$; $d_B = \infty$), raising M at given R may first tend to *de-*
ilize the flow in the boundary layers on AA and then to *stabilize* it.

he only tentative conclusion we can draw from this qualitative analysis
hat, for flow in a rectangular duct with conducting walls, the value of the
rall Reynolds number at which the boundary layers on walls AA become
table decreases as the Hartmann number increases. This may be contrasted

to the case of flow in a plane channel where it has been shown, both theoretically and experimentally, that the magnetic field *stabilizes* the flow.

Thirdly, we have only discussed flows in ducts whose walls are either perfect conductors of insulators and it would be of interest to study the cases where the walls have finite conductivity. When all the walls are non-conducting and $M \gg 1$, the velocity profile in the boundary layers on the walls AA has no point of inflexion and the flow in such a duct is probably stabilized by the magnetic field. Hence it is likely that uniformly lowering the conductivity of the wall will tend to stabilize the flows in the boundary layers. And lastly we have not considered contact resistance, though it would not be difficult to include it in the analysis.

I should like to express by thanks to Dr J. A. Shercliff for the help he has given me and for the interest he has shown in this work.

The work has been carried out under the sponsorship of the Central Electricity Research Laboratories, and is published by permission of the Central Electricity Generating Board.

REFERENCES

Braginskii, S. I. 1960 *Sov. Phys. J.E.T.P.* **10**, 1005.
Chang, C. C. & Lundgren, T. S. 1961 *Z. angew. Math. Phys.* **12**, 100.
Fabri, J. & Siestrunck, R. 1960 *Bull. Assoc. Tech. Marit. Aero.* no. 60, 333.
Gold, R. A. 1962 *J. Fluid Mech.* **13**, 505.
Grinberg, G. A. 1961 *Appl. Math. Mech.* (*Prik. Mat. Mek.*), **25**, 1536.
Grinberg, G. A. 1962 *Appl. Math. Mech.* (*Prik. Mat. Mek.*), **26**, 106.
Lock, R. C. 1955 *Proc. Roy. Soc.* A, **233**, 105.
Sakao, F. 1962 *J. Aero Space Sci.* **29**, 246.
Shercliff, J. A. 1953 *Proc. Camb. Phil. Soc.* **49**, 136.
Shercliff, J. A. 1956 *J. Fluid Mech.* **1**, 644.
Shercliff, J. A. 1962*a* *J. Fluid Mech.* **13**, 513.
Shercliff, J. A. 1962*b* *The Theory of Electromagnetic Flow Measurement.* Cambridge University Press.
Uflyand, Y. S. 1961 *Sov. Phys.-Tech. Phys.* **5**, 1194.
Williams, W. E. 1963 *J. Fluid Mech.* **16**, 262.

id Mech. (1965), *vol.* 23, *part* 3, *pp.* 563–581
d in Great Britain

Magnetohydrodynamic flow in rectangular ducts. II

By J. C. R. HUNT
Central Electricity Research Laboratories, Leatherhead*
AND K. STEWARTSON
Department of Mathematics, University College London

(Received 26 April 1965)

paper is an extension of an earlier paper by Hunt (1965) on laminar motion conducting liquid in a rectangular duct under a uniform transverse magnetic The effects of the duct having conducting walls are further explored; is case the duct considered has perfectly conducting walls parallel to the and non-conducting walls perpendicular to the field. A solution is obtained igh Hartmann numbers by analysing the boundary layers on the walls. solution involves an integral equation of a standard form.
is found that in this case, unlike the cases studied in the earlier paper, velocity profiles in the boundary layers are monotonically decreasing. effect of an external electrical circuit is examined, although it is found that es not influence the form of the velocity profiles.

Introduction

he fully-developed laminar flow of uniformly conducting and incompressible s through ducts under the action of a transverse magnetic field is attracting iderable interest at the present time, mainly for two reasons.

rst, magnetohydrodynamic generators, pumps and accelerators are devices actical importance in which conducting fluids are passed through transverse netic fields. The analysis of the flow in these devices is formidable for one have to take into account the variable conductivity and density of the fluid, plicated potential drops between the electrodes and the fluid and the fact the flow is usually turbulent. In order to make progress in the understanding e phenomena therefore, considerable simplification is necessary which may various forms, e.g. (*a*) an assumption of slug flow (Neuringer & Migotsky), (*b*) a reduction of the problem to one-dimensional gas dynamics (Resler ars 1958), (*c*) a two-dimensional analysis of the development of the laminar ndary layer on the walls in the direction of the flow (Kerrebrock 1961; & Kerrebrock 1964), (*d*) a two-dimensional analysis of the flow down the assuming that it is inviscid (Sutton & Carlson 1961), or (*e*) the form used in present paper, two-dimensional analysis of the flow variation across the assuming that it is laminar, fully developed and that there is no variation id properties throughout the duct. These various idealizations are comple-

* Seconded to: School of Engineering Science, University of Warwick, Coventry.

mentary in that they each extract some of the basic physical ideas, and collec-
tively it is hoped that they will prove useful in interpreting more complicated
physical situations.

Secondly, this theory of duct flows can be tested in laboratory experiments
with liquid metals. The uncertainty in the experimental results can be reduced
to below 1 %, and consequently these experiments provide critical tests for the
theory, in marked contrast with the majority of magneto-fluid dynamic ex-
periments.

Since most magnetohydrodynamic generators and pumps have a rectangular
cross-section, we shall confine ourselves to examining rectangular ducts. Exact
solutions have been obtained for laminar flows of uniformly conducting incom-
pressible fluids through rectangular ducts with thin conducting walls under
transverse magnetic fields by Chang & Lundgren (1961), Uflyand (1961) and
Hunt (1965). Chang & Lundgren and Uflyand analysed the case in which all the
walls were perfectly conducting. Hunt analysed (i) the case in which the walls
perpendicular to the field (walls BB, in figure 1) were perfectly conducting and
those parallel to the magnetic field (walls AA) were thin and of arbitrary con-
ductivity, and (ii) the case in which the walls BB were thin and of arbitrary
conductivity and the walls AA were non-conducting. Thus he included the pre-
vious author's analysis as a special case of (i). Hunt also examined the form of the
solutions for large M, where M is the Hartmann number, and found that varying
the conductivity of the walls AA dramatically altered the form of the velocity
profile in the boundary layers on walls AA and also the velocity flux through them.
When the walls AA are non-conducting and the walls BB perfectly conducting, he
found that large positive and negative velocities of order Mv_c are induced, where
v_c is the velocity of the core. This fact indicates that the magnetic field may de-
stabilize the flow in certain types of duct. It is this effect of the conductivity
of the walls on the flow which gives the problem its physical interest and suggests
the need for solving the outstanding problems.

In ducts of most practical value the walls AA are conducting and the walls
BB are non-conducting; this case is not included in any of those examined by
Hunt and at present no complete analytic solution is available. Grinberg
(1961, 1962) has, however, reduced the problem to the solution of an integral
equation, whose kernel is the Green's function for the problem and involves a
double infinite series of Bessel funtions. When the Hartmann number M is
large, only the leading terms of this series need be retained and he was then
able to solve the simpler equation. In order to determine the current and
velocity distribution and the mass flux down the tubes, however, further numeri-
cal work needs to be done. In this paper we approach the problem of the flow
at high Hartmann numbers using a boundary-layer technique which has the
advantage that the analysis is more transparent and it is easier to form a physical
picture of the properties of the magnetic and velocity fields. Expressions are
obtained for the leading terms in the expansion of the flux through the duct in
descending powers of $M^{\frac{1}{2}}$. Also diagrams and a graph are displayed showing
representative velocity and magnetic fields in the neighbourhood of the walls A
where their structure is complicated.

ually the walls AA are electrically connected and either the duct supplies
nt to a load or a potential difference is placed across the walls AA to drive
low. We show that if the walls AA are sufficiently highly conducting, the
nal electric circuit has no effect on the mathematical problem and that it is
rial calculation to work out its effect on the flow parameters. Some examples
ternal circuits are given. In comparing the cases where the walls AA are
ucting and the walls BB are non-conducting and where all the walls are
ucting we find as before, that the conductivity of the walls has a marked
t on the flow in the boundary layers on the walls AA; we also find that in
cases the conductivity of the walls *in the corners* is important since the
nt distribution in the corners affects the rest of the flow in the boundary

The formulation of the problem and the basic solution

e consider the steady flow of an incompressible conducting fluid driven by a
ure gradient along a rectangular duct under an imposed transverse magnetic
We assume that no secondary flow is generated and that there is no varia-
either in the duct cross-section or in the imposed magnetic field, with dis-
z along the duct. It is also postulated that any external circuit connected
conducting walls of the duct is continuous and unvarying in the streamwise
tion. (This condition may be relaxed if the conductivity is sufficiently
l.) Thus all physical quantities except pressure are independent of z. Relative
axes defined in figure 1, the equations describing such flows are:

$$j_x = \sigma\left(-\frac{\partial\phi}{\partial x} - v_z B_0\right), \quad j_y = \sigma\left(-\frac{\partial\phi}{\partial y}\right), \tag{2.1}$$

$$\frac{\partial j_x}{\partial x} + \frac{\partial j_y}{\partial y} = 0, \quad j_x = \frac{\partial H_z}{\partial y}, \quad j_y = -\frac{\partial H_z}{\partial x}, \tag{2.2}$$

$$0 = -\partial p/\partial z + j_x B_0 + \bar{\mu}\left(\frac{\partial^2 v_z}{\partial x^2} + \frac{\partial^2 v_z}{\partial y^2}\right). \tag{2.3}$$

j_x, j_y are the components of the current, ϕ is the electric potential, H_z
induced field and may also be regarded as a current stream function, B_0
flux density of the imposed magnetic field, v_z is the velocity, σ the conduc-
$\bar{\mu}$ the viscosity and $\partial p/\partial z$ the pressure gradient which is a constant. The
tions can be re-written to give two coupled second-order partial differential
tions in H_z and v_z, viz.

$$\bar{\mu}\left(\frac{\partial^2 v_z}{\partial x^2} + \frac{\partial^2 v_z}{\partial y^2}\right) + B_0\frac{\partial H_z}{\partial y} - \frac{\partial p}{\partial z} = 0, \tag{2.4}$$

$$\frac{1}{\sigma}\left(\frac{\partial^2 H_z}{\partial x^2} + \frac{\partial^2 H_z}{\partial y^2}\right) + B_0\frac{\partial v_z}{\partial y} = 0. \tag{2.5}$$

take the lengths of the sides of the channel to be $2a$ and $2b$ (see figure 1)
suppose that the sides $y = \pm a$ (BB) are non-conducting, while the sides
$\pm b$ (AA) are perfectly conducting. It follows that the boundary conditions

$$v_z = 0, \quad \partial H_z/\partial x = 0 \quad \text{when} \quad y = \pm a, \tag{2.6}$$

$$v_z = 0, \quad \partial H_z/\partial x = 0 \quad \text{when} \quad x = \pm b. \tag{2.7}$$

Thus on the walls $y = \pm a$, H_z is independent of x and consequently we can modif
(2.6) to

$$v_z = 0, \quad H_z = H_1 \quad \text{when} \quad y = a; \quad v_z = 0, \quad H_z = H_2 \quad \text{when} \quad y = -a, \quad (2.8$$

where H_1, H_2 are constants. The net current I leaving and entering the walls A,
per unit length of the duct is simply related to H_1, H_2:

$$I = \int_{-a}^{a} j_x dy|_{x=b} = H_1 - H_2. \quad (2.9$$

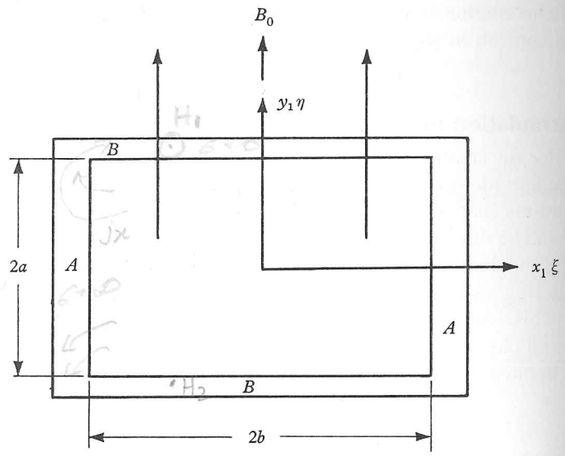

FIGURE 1. Cross-section of a rectangular duct with the magnetic field in the y-direction. The walls AA lie at $x = \pm b$ and BB at $y = \pm a$.

The governing equations and boundary conditions may now be reduced to non-dimensional form by writing

$$\xi = x/a, \quad \eta = y/a, \quad M = aB_0(\sigma/\mu)^{\frac{1}{2}}, \quad (2.10$$

$$-\frac{\partial p}{\partial z} + \frac{B_0}{2a}(H_1 - H_2) = P, \quad (2.11$$

$$v_z = \frac{a^2 P}{\mu} v(\xi, \eta), \quad H_z = \tfrac{1}{2}(H_1 + H_2) + \tfrac{1}{2}(H_1 - H_2)\eta + aP(\sigma/\mu)^{\frac{1}{2}} h(\xi, \eta). \quad (2.12$$

The equations satisfied by v, h are

$$\frac{\partial^2 v}{\partial \xi^2} + \frac{\partial^2 v}{\partial \eta^2} + M\frac{\partial h}{\partial \eta} = -1, \quad \frac{\partial^2 h}{\partial \xi^2} + \frac{\partial^2 h}{\partial \eta^2} + M\frac{\partial v}{\partial \eta} = 0, \quad (2.1$$

subject to $\quad v = 0, \quad h = 0 \quad \text{when} \quad \eta = \pm 1,$

and $\quad v = 0, \quad \partial h/\partial \xi = 0 \quad \text{when} \quad \xi = \pm b/a = \pm c. \quad (2.1$

We are particularly interested in the properties of the solution when $M \gg$
and to find them we proceed by a heuristic argument, relying for justificatio

e consistency of the results. For large M the interior of the duct may be
ded into five parts, as indicated in figure 2. These are:
The core region consisting of the majority of the interior but excluding
eighbourhoods of the walls.
The primary or Hartmann layers, of thickness $O(M^{-1})$, near the walls
± 1 but excluding the regions distant $O(M^{-\frac{1}{2}})$ from the side walls $\xi = \pm c$. We
he word primary for these boundary layers to emphasize their control of the
in the core (a) and to distinguish them from (c).

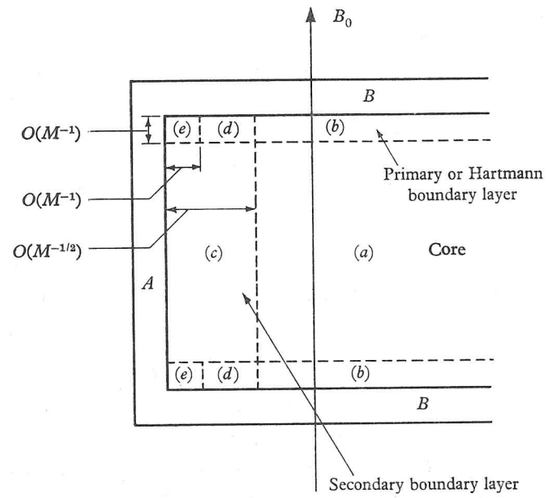

FIGURE 2. Cross-section of the duct showing the various regions of flow when $M \gg 1$ (not to scale).

The secondary boundary layers, of thickness $O(M^{-\frac{1}{2}})$, near the walls
$\pm c$, so called because they are determined from the core flow and the primary
dary layers but do not exert a decisive control on them in return.
Those parts of the primary boundary layers at a distance $O(M^{-\frac{1}{2}})$ but
$^{-1}$ from the side walls $\xi = \pm c$.
Those parts of the interior of the duct within a distance $O(M^{-1})$ of the four
ers.
f these regions (e) is of the least importance and the most difficult to treat
n M is large; we shall discuss it only by order of magnitude arguments.
other regions can, however, be discussed in detail as follows.

2.1. *Core flow* (a)

e this region extends over almost the whole duct it follows that $\partial/\partial\xi$, $\partial/\partial\eta$
$O(1)$. Further, from the boundary conditions and differential equations h
t be odd and v even in η. Anticipating that v and h are of the same order of
nitude we then have from (2.13) that

$$h = h_0 \equiv -\eta/M, \quad v = v_c \equiv g(\xi)/M, \quad (2.15)$$

where $g(\xi)$ is a function of ξ to be determined, and terms of order M^{-2} have bee neglected.

2.2. *The primary boundary layer* (*b*) *near* $\eta = 1$

The core solution (2.15) fails to satisfy the bundary conditions at the walls an in particular at $\eta = \pm 1$. Consequently there must be boundary layers near thes walls to make the necessary adjustments in v and h and, since they are *ex hypc thesis* thin, in them

$$\partial/\partial\eta \gg \partial/\partial\xi. \tag{2.16}$$

Writing

$$v = v_c + v_p, \quad h = h_c + h_p, \tag{2.17}$$

and concentrating attention on the boundary layer near $\eta = 1$, v_p and h_p satisf

$$\frac{\partial^2 v_p}{\partial\eta^2} + M\frac{\partial h_p}{\partial\eta} = 0, \quad \frac{\partial^2 h_p}{\partial\eta^2} + M\frac{\partial v_p}{\partial\eta} = 0 \tag{2.18}$$

in virtue of (2.16) together with the boundary conditions

$$h_p = 1/M, \quad v_p = -g(\xi)/M \quad \text{at} \quad \eta = 1, \quad |\xi| < c, \tag{2.19a}$$

and

$$v_p \to 0, \quad h_p \to 0 \tag{2.19b}$$

on leaving the immediate neighbourhood of $\eta = 1$. A consistent solution of (2.18 satisfying (2.19) is only possible if

$$g(\xi) \equiv 1 \tag{2.20}$$

and then

$$v_p = -\frac{1}{M}e^{-M(1-\eta)}, \quad h_p = \frac{1}{M}e^{-M(1-\eta)}. \tag{2.21}$$

Thus the core velocity is determined by the condition for the existence of th primary boundary layer and, as anticipated in (2.15), is of the same order c magnitude as the induced magnetic field. Further the thickness of the primar boundary layer is $O(M^{-1})$, and the associated defect in velocity flux is

$$-\int_{-c}^{+c} d\xi \int_0^\infty v_p \frac{dY}{M} = 2c/M^2, \tag{2.22}$$

where $Y = (1-\eta)M$. The primary boundary layer near $\eta = -1$ may be treate by a parallel argument but we do not need to deal with it explicitly here since is known to be even and h to be odd in η.

2.3. *The secondary boundary layer* (*c*) *near* $\xi = c$

The core solution is now fully known and does not satisfy the boundary conditio at $\xi = \pm c$. Consequently there must be boundary layers near these walls, t make the necessary adjustments in v and h and, since they are *ex hypothes* thin, in them

$$\partial/\partial\xi \gg \partial/\partial\eta. \tag{2.23}$$

Writing

$$v = v_c + v_s, \quad h = h_c + h_s, \tag{2.24}$$

and concentrating attention on the boundary layer near $\xi = c$, v_s and h_s satisfy

$$\frac{\partial^2 v_s}{\partial\xi^2} + M\frac{\partial h_s}{\partial\eta} = 0, \quad \frac{\partial^2 h_s}{\partial\xi^2} + M\frac{\partial v_s}{\partial\eta} = 0 \tag{2.25}$$

rtue of (2.23), together with the boundary conditions

$$\partial h_s/\partial\xi = 0, \quad v_s = -1/M \quad \text{at} \quad \xi = c, \quad |\eta| \leqslant 1, \tag{2.26a}$$

$$h_s \to 0, \; v_s \to 0 \tag{2.26b}$$

aving the immediate neighbourhood of $\xi = 1$. These obvious boundary con- ns are, however, insufficient to solve the differential equations (2.25) pletely. In addition we must know something about v_s, h_s at a station or ons of η. In the same way that region (*b*) provides the additional information etermine region (*a*), the regions (*d*) provide the extra boundary conditions ed here. We shall anticipate the discussion of regions (*d*) here and state the itions

$$v_s + h_s \to 0 \quad \text{as} \quad \eta \to 1, \quad v_s - h_s \to 0 \quad \text{as} \quad \eta \to -1, \tag{2.27}$$

ring the reader to (2.52) below for their justification.

order to solve (2.25) it is convenient to write

$$h_s = \alpha(\eta)/M \quad \text{at} \quad \xi = c, \tag{2.28}$$

h means that, in effect, we are specifying the current distribution on the walls Further write

$$X = v_s + h_s, \tag{2.29}$$

hen, since v_s is even and h_s is odd in η, we have

$$v_s = \tfrac{1}{2}[x(\eta) + X(-\eta)], \quad h_s = \tfrac{1}{2}[X(\eta) - X(-\eta)]. \tag{2.30}$$

X satisfies

$$\frac{\partial^2 X}{\partial\xi^2} + M\frac{\partial X}{\partial\eta} = 0, \tag{2.31}$$

the boundary conditions (2.26) and (2.28) become

$$X = \frac{1-\alpha(\eta)}{M}, \quad \frac{\partial}{\partial\xi}[X(\eta) - X(-\eta)] = 0 \quad \text{when} \quad \xi = c, \tag{2.32}$$

0 on leaving the vicinity of $\xi = c$, and $X = 0$ at $\eta = 1$. Leaving the con- n on $\partial X/\partial\xi$ on one side for the moment the general solution for X is

$$X = -\frac{1}{M}\operatorname{erfc}\frac{(c-\xi)M^{\frac{1}{2}}}{2(1-\eta)^{\frac{1}{2}}} + \frac{c-\xi}{2(\pi M)^{\frac{1}{2}}}\int_\eta^1 \frac{\alpha(\eta_1)\,d\eta_1}{(\eta_1-\eta)^{\frac{3}{2}}}\exp\left\{-\frac{M(c-\xi)^2}{4(\eta_1-\eta)}\right\}. \tag{2.33}$$

atisfy the condition on $\partial X/\partial\xi$, it follows on differentiating (2.33) with respect and setting $\xi = c$ that

$$\int_\eta^1 \frac{\alpha'(\eta_1)\,d\eta_1}{(\eta_1-\eta)^{\frac{1}{2}}} - \frac{\alpha(1)-1}{(1-\eta)^{\frac{1}{2}}} = \int_{-1}^\eta \frac{\alpha'(\eta_1)\,d\eta_1}{(\eta-\eta_1)^{\frac{1}{2}}} + \frac{\alpha(-1)+1}{(1-\eta)^{\frac{1}{2}}}. \tag{2.34}$$

s the problem has been reduced to finding the value of $\alpha(\eta)$ which leads to nstant electric potential on the walls AA.

he equation (2.34) may be cast into a recognizable form by writing

$$\alpha(\eta) = 1 - A(\eta)(1+\eta)^{\frac{1}{2}}. \tag{2.35}$$

iplying it by $(\zeta-\eta)^{-\frac{1}{2}}$ and integrating from -1 to ζ with respect to η:

$$A(\zeta) - \frac{1}{\pi}\int_{-1}^{+1} \frac{A(\eta)\,d\eta}{\eta-\zeta} = +\frac{2}{(\zeta+1)^{\frac{1}{2}}}. \tag{2.36}$$

This equation has a known solution (Rott & Cheng 1954) for a general right
hand side, which reduces in our case to

$$\alpha(\eta) = 1 - \frac{8(1-\eta^2)^{\frac{1}{4}}}{\pi(1+\eta)} \int_1^\infty \frac{s^2\,ds}{(s^4+\psi)\,(s^4-1)^{\frac{1}{2}}}, \tag{2.37}$$

where $\psi = (1-\eta)/(1+\eta)$. Thus α may be expressed in terms of a hypergeometri
function. In particular when $\eta \approx 1$, ψ is small and

$$\alpha(\eta) = 1 - \frac{(1-\eta^2)^{\frac{1}{4}}}{\pi^{\frac{1}{2}}} \frac{(-\frac{1}{4})!}{(\frac{1}{4})!} + O(1-\eta^2)^{\frac{5}{4}}. \tag{2.38}$$

$\alpha \to 0$ as $\eta \to 0$ and α is of course an odd function of η. Knowing $\alpha(\eta)$ we ca
calculate X, v_s and h_s from (2.33) and (2.32).

In an earlier paper by one of us (Hunt 1965) it was shown that, if the wall
$\xi = \pm c$ are non-conducting and the walls $\eta = \pm 1$ perfect conductors, then th
velocity in the secondary boundary layers is an order of magnitude greater tha
the core velocity and contains an infinite number of reversals of sign. If all fou
walls are perfect conductors, then the velocity also oscillates an infinite numbe
of times in the secondary boundary layer, although in this case there are n
reversals of sign and the velocity is of the same order of magnitude as in the core
It is of interest therefore to examine the nature of the boundary-layer flow in th
present problem. At large distances (in terms of $(c-\xi)\,M^{\frac{1}{2}}$) from the wall $\xi = c$
the structure of the boundary layer in X is given by the behaviour of α nea
$\eta = 1$. From (2.38) $1-\alpha \sim (1-\eta)^{\frac{1}{4}}$ as $\eta \to 1-$ and hence, from the similarit
solution of (2.31) satisfying

$$X = 0 \text{ at } \eta = 1, \quad X \to 0 \text{ as } \xi \to -\infty, \quad X \sim (1-\eta)^{\frac{1}{4}} \text{ at } \xi = c,$$

we find that when $(c-\xi)\,M^{\frac{1}{2}}$ is large

$$X \sim \frac{(1-\eta)^{\frac{3}{4}}}{M^2(c-\xi)^3} \exp\left\{-\frac{M/(c-\xi)^2}{4(1-\eta)}\right\}, \tag{2.39}$$

so that the number of oscillations in v is at most finite. A graph of v as a functio
of $M^{\frac{1}{2}}(c-\xi)$ for $\eta = 0$ is given in figure 3 and shows that in fact v never change
sign. Lines of constant h are shown schematically in figure (5).

In order to calculate the overall velocity flux, we have to work out the flu
deficits due to the boundary layers. Since h is an odd function of η, the flu
deficit due to the secondary boundary layer is given by

$$-\int_{-1}^{+1} d\eta \int_0^\infty \frac{d\bar{\xi}}{M^{\frac{1}{2}}} v_s = -\int_{-1}^{+1} d\eta \int_0^\infty \frac{d\bar{\xi}}{M^{\frac{1}{2}}} X,$$

where

$$\bar{\xi} = (c-\xi)\,M^{\frac{1}{2}}.$$

From (2.31)

$$-\int_0^\infty \frac{d\bar{\xi}}{M^{\frac{1}{2}}} X = \frac{1}{M(M\pi)^{\frac{1}{2}}} \int_\eta^1 \frac{(1-\alpha(\eta_1))\,d\eta_1}{(\eta_1-\eta)^{\frac{1}{2}}},$$

so that the flux deficit is

$$\frac{2}{M(M\pi)^{\frac{1}{2}}} \int_{-1}^{+1} [1-\alpha(\eta)]\,[1+\eta]^{\frac{1}{2}}\,d\eta.$$

ubstituting from (2.41) into (2.42) we obtain, after formal manipulation,

$$\frac{(-\frac{1}{4})!}{(+\frac{1}{4})!} \frac{2^{\frac{1}{2}}}{M^{\frac{3}{2}}} \tag{2.43}$$

he flux deficit due to this boundary layer.

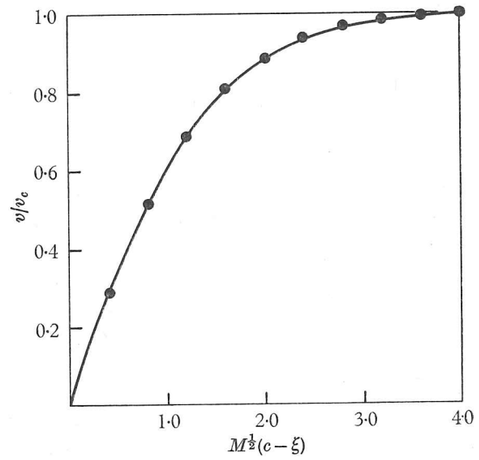

URE 3. Graph of v/v_c against $M^{\frac{1}{2}}(c-\xi)$ at $\eta = 0$ in the boundary layer at $\xi = c$. The value of M is arbitrary, provided $M \gg 1$.

2.4. *Primary boundary layer (d) near the corner $\xi = c$, $\eta = 1$*

ing

$$v = v_c + v_p + v_s, \quad h = h_c + h_p + h_s, \tag{2.44}$$

atisfy the governing differential equations provided we can neglect terms
$^{-2})$. The boundary conditions on the walls $\xi = c$ and $\eta = 1$ are also satisfied,
ided we can neglect exponentially small terms and provided we exclude the
hbourhood of the corner $\xi = c$, $\eta = 1$. Specifically the conditions are not
sfied when $\xi = c$ and $\eta = 1 - O(M^{-1})$ and when $\eta = 1$ and $\xi = c - O(M^{-\frac{1}{2}})$.
the second of these with which we are concerned here and we shall briefly
to the other in §2.5. If instead of (2.44) we write

$$v = v_c + v_p + v_s + v_{p_1}, \quad h = h_c + h_p + h_s + h_{p_1}, \tag{2.45}$$

re v_{p_1}, h_{p_1} satisfy the same differential equations as v, h, then, on the wall
1, we must have

$$v_{p_1} + v_s = 0, \quad h_s + h_{p_1} = 0. \tag{2.46}$$

hough the values of v_s, h_s on the wall $\eta = 1$ vary rapidly with ξ, the scale is
h larger than the scale of the primary boundary layer, $O(M^{-\frac{1}{2}})$ compared with
$^{-1})$, and hence we are justified in assuming that v_{p_1}, h_{p_1} satisfy the condition
$\gg \partial/\partial\xi$, whence

$$v_{p_1} = -v_s(\xi, 1)\,e^{-M(1-\eta)}, \quad h_{p_1} = -h_s(\xi, 1)\,e^{-M(1-\eta)}. \tag{2.47}$$

It follows that a consistent solution is only possible if

$$v_s(\xi, 1) + h_s(\xi, 1) = 0, \tag{2.48}$$

as assumed earlier in (2.27). The other condition in (2.27) follows from a parallel argument for the wall $\eta = -1$. It is noted that, if the wall $\eta = 1$ is a perfect conductor, $v = 0$, $\partial h/\partial\eta = 0$ there, and a parallel argument shows that the condition satisfied by v_s, h_s at $\eta = 1$ is then

$$v_s(\xi, 1) = 0. \tag{2.49}$$

2.5. *The corner* $\xi = 0$, $\eta = 1$

The assumptions leading to the primary boundary layer (d) and the secondary boundary layer (c) fail when both $1-\xi$ and $1-\eta$ are $O(M^{-1})$, i.e. in region (e). No simplification in the governing equations is possible therefore in this region. However its effect on the flux is small, being of the order of the maximum velocity multiplied by the area, i.e. $O(M^{-3})$, and consequently we have not attempted to elucidate its properties.

The leading terms in the asymptotic expansion for the flux of fluid through the tube when M is large may now be written down

$$\iint_{\text{duct}} v\,d\xi\,d\eta = \frac{4c}{M} - \frac{(-\frac{1}{4})!}{(+\frac{1}{4})!}\frac{2^{\frac{3}{2}}}{M^{\frac{3}{2}}} - \frac{4c}{M^2} + O(M^{-\frac{5}{2}}). \tag{2.50}$$

The term $O(M^{-\frac{5}{2}})$ arises partly from the neglect of $\partial^2 v/\partial\eta^2, \partial^2 h/\partial\eta^2$ in the secondary boundary layer and partly from the deficit due to the primary boundary layer (d). In principle it can be calculated using the methods of this paper but we have not done so.

3. Practical implications

In § 2 it was shown that, whatever the value of I, the net current leaving and entering the duct, the problem of calculating the velocity and current distributions could be reduced to the solution of two differential equations with a single set of boundary conditions. It follows that the velocity *distribution* is always the same, though the *magnitude* of the velocity depends on the values of I, J and $\partial p/\partial z$. It follows from (2.12) that the distribution of current density does vary with the external circuits, but in a simple manner: j_y varies in magnitude but its distribution does not change: j_x has two constituents one of which, j_{x_1}, is constant throughout the duct, but varies with I, and is given by

$$j_{x_1} = \tfrac{1}{2}(H_1 - H_2)/a;$$

the other, j_{x_2}, whose *distribution* is always the same but whose *magnitude* varies is given by

$$j_{x_2} = \frac{\sigma^{\frac{1}{2}} a P}{(\bar{\mu})^{\frac{1}{2}}}\frac{\partial H_z}{\partial y},$$

where $P = B_0 I/2a - \partial p/\partial z$.

In § 2 we also found the velocity and current distributions and a relation between $Q, \partial p/\partial z, I$ and M. In this section we use this information to examine the effect of electrically connecting the walls AA for the various practical applications of the duct.

The type of duct whose walls BB are non-conducting and walls AA are perfectly conducting has many applications. Shercliff (1965) has recorded how a duct for which $b \gg a$ acts as a pump, flowmeter, generator or brake depending on the value of $-E_x/B_0 V_m$, where E_x is the electric field in the core and V_m the mean velocity; $V_m = V_c(1 - 1/M)$. If $b \sim a$ and the effects of the walls AA are considered, a new parameter has to be defined. In interpreting experiments or designing equipment the following five parameters are of most interest: Q, $\partial p/\partial z$, B_0, I, and $\Delta\phi$, the electric potential difference between the walls AA defined by

$$\Delta\phi = \phi_{x=b} - \phi_{x=-b}. \tag{3.1}$$

Usually we are given three of these parameters and we wish to find the other two in terms of these, e.g. in designing an electromagnetic pump we would want to calculate I and $\Delta\phi$, given Q, $\partial p/\partial z$, B_0, and the fluid properties.

To find $\Delta\phi$ integrate equation (2.1) from $x = -b$ to $x = b$ and from $y = -a$ to $y = a$, which leads to

$$-\Delta\phi = \frac{b}{a\sigma} I + \frac{B_0 Q}{2a}. \tag{3.2}$$

This equation shows that to an external electric circuit the duct is equivalent to a e.m.f. $U_i = \frac{1}{2}B_0 Q/a$ in series with a resistance $R_i = b/a\sigma$. The replacement of a cell in a d.c. electric circuit by an e.m.f. and a resistance is familiar to electrical engineers as Thevenin's theorem. By the same theorem any linear external circuit may be regarded as a resistance R_e and an e.m.f. U_e. Hence, in the general case $\Delta\phi$, $\partial p/\partial z$, Q, M and I may be calculated from the following relations:

$$\Delta\phi = -U_i - R_i I = U_e + R_e I,$$

$$\Delta\phi = -\tfrac{1}{2}B_0 Q/a - (b/\sigma a)\, I = U_e + R_e I, \tag{3.3}$$

$$Q = f(\tfrac{1}{2}B_0 I/a - \partial p/\partial z, M). \tag{3.4}$$

In § 2 we calculated the function (3.4). See (2.50), which may be re-written as

$$Q = \left(\frac{B_0 I}{2a} - \frac{\partial p}{\partial z}\right)\frac{4a^3 b}{\bar{\mu} M}\left(1 - \frac{0{\cdot}956a}{bM^{\frac{1}{2}}} - \frac{1}{M} - \ldots\right). \tag{3.5}$$

We now examine three special cases.

3.1. *Open-circuit case*

If the duct is on open circuit, $I = 0$. In this case the duct is a flowmeter. It follows from (3.5) that

$$Q = \frac{(-\partial p/\partial z)\, 4a^3 b}{\bar{\mu} M}\left(1 - \frac{0{\cdot}956a}{bM^{\frac{1}{2}}} - \frac{1}{M} - \frac{a}{b}O(M^{-\frac{3}{2}})\right), \tag{3.6}$$

and from (3.3) that

$$\Delta\phi = -\tfrac{1}{2}B_0 Q/a. \tag{3.7}$$

This fact has been noted many times before (see Shercliff 1962, p. 16).

3.2. *Short-circuit case*

In this case the walls AA are joined by a circuit of zero resistance ($R_e = U_e = 0$) and consequently $\Delta\phi = 0$. This device is an electromagnetic brake or generator or short-circuit.

Equation (3.3) becomes,

$$0 = \frac{2bI}{\sigma} + B_0 Q,$$

and hence (3.5) becomes

$$Q = \left(-\frac{B_0^2 Q\sigma}{4ab} - \frac{\partial p}{\partial z}\right)\frac{4a^3 b}{\bar{\mu}M}\left(1 - \frac{0{\cdot}956a}{bM^{\frac{1}{2}}} - \frac{1}{M}\cdots\right). \tag{3.}$$

It follows that

$$Q = \frac{(-\partial p/\partial z)\,4a^3 b}{\bar{\mu}M^2}\left[\frac{1 - \dfrac{0{\cdot}956a}{bM^{\frac{1}{2}}} - \dfrac{1}{M}\cdots}{1 - \dfrac{0{\cdot}956a}{bM^{\frac{1}{2}}} - O(M^{-\frac{3}{2}})}\right],$$

and re-arranging

$$Q = \frac{(-\partial p/\partial z)\,4a^3 b}{\bar{\mu}M^2}\left[1 - \frac{1}{M} - O(M^{-\frac{3}{2}})\right]. \tag{3.}$$

Though the form of the $Q - \partial p/\partial z$ relation is different in this case from the ope circuit case, the velocity flux deficit due to the secondary boundary layers as proportion of the flux through the core is the same, since the velocity distributio is unaffected by external connexions. There is no term of order $(M^{-\frac{1}{2}})$ in t bracket, as one might expect, because the core velocity V_c is given by

$$V_c = \frac{(-\partial p/\partial z)\,a^2}{\bar{\mu}M^2}\left(1 + \frac{0{\cdot}956a}{bM^{\frac{1}{2}}} + O(M^{-1})\right). \tag{3.1}$$

Thus the flow in the core is not the same as that for flow in a duct whose wal are all perfectly conducting. In that case

$$V_c = \frac{(-\partial p/\partial z)\,a^2}{\bar{\mu}M^2}.$$

This difference is explained by the fact that in the latter case $E_x = 0$ in the cor whereas in the former case, even though $\Delta\phi = 0$, $E_x \neq 0$ in the core because the defect of $\mathbf{v} \times \mathbf{B}$ in the secondary boundary layers.

3·3. *Purely electrically driven case*

When the pressure gradient is zero and the flow is electrically driven by th potential difference across the walls AA, the device is a limiting form of MH pump. Since $\partial p/\partial z = 0$, equation (3.5) becomes

$$Q = \frac{\frac{1}{2}B_0 I a^2 b}{\bar{\mu}M}\left(1 - \frac{a}{b}\frac{0{\cdot}956}{M^{\frac{1}{2}}} - \frac{1}{M} + \cdots\right). \tag{3.1}$$

Combining this result with (3.2) leads to

$$Q = -\frac{2a\Delta\phi}{B_0}\left[1 - \frac{1}{M} - O\left(\frac{a}{bM^{\frac{3}{2}}}\right)\right]. \tag{3.1}$$

In the two previous cases either I or $\Delta\phi$ is zero, whereas in this case we can obta a useful relation between I and $\Delta\phi$ by dividing (3.12) by (3.11),

$$\frac{\Delta\phi}{I} = -\frac{Mb}{a\sigma}\left[1 - \frac{0{\cdot}956a}{bM^{\frac{1}{2}}} - O\left(\frac{a}{bM^{\frac{3}{2}}}\right)\right]. \tag{3.1}$$

is interesting to note that in the core $j_x = 0$ since $\partial p/\partial z = 0$. All the current the primary and secondary boundary layers (see figure 5 (b)).

om an examination of these three special cases it follows that the para- r which describes the particular application of a duct for which $b \sim a$ is $\Delta\phi/B_0 Q$ as opposed to $-E_x/B_0 V_m$ in a duct for which $b \gg a$.

Discussion

§2, we analysed the flow through ducts whose walls AA were perfectly ducting and walls BB were non-conducting. The flow was assumed to be lami- incompressible, uniformly conducting, and fully developed; also the Hart- n number (M) was assumed to be large. In §3, we showed how the results of nalysis could be used for ducts with various electrical connexions between alls AA. In this section we compare the previous results with those obtained ther types of duct and we show how some of the effects of the conductivity e walls on the flow may be interpreted physically.

r a duct whose walls AA are perfectly conducting and walls BB are non- ducting, we have been able to analyse the flow only for very large Hartmann ber. For our purposes this is no great disadvantage since a solution at high sufficient to illustrate the essential physical features of the flow and also it ite usual in liquid metal experiments to have M greater than 100. In this ssion we shall concentrate on flows with $M \gg 1$.

high M, provided the conductivity of each of the walls BB is constant along ength, the value of the conductivity of each of the walls BB does not affect *form* of the velocity profile away from the walls AA. The velocity is constant pt in the narrow primary or Hartmann boundary layers on $y = \pm a$. How- the *magnitude* of the velocity in the core depends on the conductivity of alls BB as well as on the pressure gradient and any external electrical circuit nected between the walls AA.

hough boundary layers are also found on the walls AA as $M \to \infty$, their changes considerably with the conductivity of the duct walls. It is these ndary boundary layers which have been little understood hitherto. The e main characteristics of these boundary layers are the velocity profile, current distribution and the velocity flux deficit, as defined in (2.40). It not seem possible to provide convincing explanations for the shape of the city profiles, *a priori*, but it is possible to provide a physical explanation the current distribution and velocity flux deficit and thence to explain the e of the velocity profile.

et us now compare the flows in two types of rectangular duct:

ase (i) Perfectly conducting walls all around.

(ii) Walls AA perfectly conducting and walls BB non-conducting.

ase (i) the velocity profile in the secondary boundary layers has the form damped sine wave and the velocity flux is given by

$$Q = \frac{(-\partial p/\partial z)\,4a^3 b}{\bar{\mu}M^2}\left[1 - \frac{1}{M} - \frac{2{\cdot}43a}{bM^{\frac{3}{2}}} + \cdots\right],$$

so that the flux deficit is $O(M^{-\frac{3}{2}})$ times the flux in the core (see Hunt 1965) in case (ii) the velocity in the secondary boundary layers monotonically decrease to zero at the wall, and the flux deficit is $O(M^{-\frac{1}{2}})$ times the core velocity (see § 2 These values of flux deficit were obtained by mathematical rather than physica arguments. To show that the difference in flux deficit between cases (i) and (i is explicable physically, we now give arguments by which the orders of magn tude of the flux deficits are estimated.

4.1. *All the walls are perfectly conducting—case (i)*

We consider the secondary boundary layer on the wall A at $x = -b$ (see figure 4 Let

$$j_x = j_c + j_p + j_s, \tag{4.1}$$

$$v_z = v_c + v_p + v_s, \tag{4.2}$$

where, as before, the suffices c, p and s refer to the core, primary and secondar boundary layers, respectively.

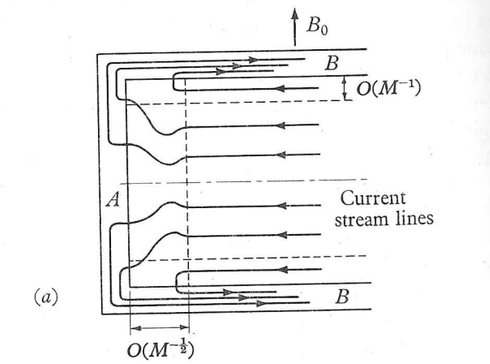

FIGURE 4. Cross-section of the duct when all the walls are perfectly conducting. ($M \gg$ not to scale). (*a*) Shows the actual current streamlines. (*b*) Shows the core, primary a secondary current streamlines.

aking the usual assumption that in the boundary layer on walls AA

$$\partial/\partial x \gg \partial/\partial y, \quad \text{for} \quad (a-y) \gg aM^{-1},$$

tion (2.3) leads to

$$0 = -\frac{\partial p}{\partial z} + (j_c + j_s) B_0 + \bar{\mu} \frac{\partial^2}{\partial x^2}(v_c + v_s). \tag{4.3}$$

e $j_c B_0 = \partial p/\partial z$ and $\partial v_c/\partial x = 0$, (4.3) becomes

$$0 = j_s B_0 + \bar{\mu} \frac{\partial^2 v_s}{\partial x^2}. \tag{4.4}$$

the thickness of the boundary layer be δ, then

$$\frac{\partial^2 v_s}{\partial x^2} = -O\left(\frac{v_c}{\delta^2}\right) \quad \text{and} \quad j_s = O\left(\frac{\bar{\mu} v_c}{B_0 \delta^2}\right). \tag{4.5}$$

low since the current in the core enters the wall A, $E_x|_{x=-b} = O(j_c/\sigma)$. Since = 0 at $y = \pm a$, $\partial E_x/\partial y = O(-j_c/a\sigma)$ for $y > 0$. But

$$\partial E_y/\partial x = O(j_y/\sigma\delta) \quad \text{and} \quad \partial E_x/\partial y = \partial E_y/\partial x,$$

hence $j_c/a = -O(j_y/\delta)$. But $\partial j_y/\partial y = -\partial j_s/\partial x$ since $\partial j_c/\partial x = 0$. Hence

$$j_s/\delta = O(j_y/a) = O\,(-j_c\delta/a^2)$$

$$j_s = -O(\delta^2 j_c/a^2). \tag{4.6}$$

rom equations (4.5) and (4.6) we have,

$$\bar{\mu} v_c/\delta^2 = O(-\delta^2 B_0 j_c/a^2). \tag{4.7}$$

e $E_x = 0$ in the core, $\qquad B_0 v_c = -j_c/\sigma.$ (4.8)

bining (4.7) and (4.8) we deduce that

$$\delta = O(aM^{-\frac{1}{2}}). \tag{4.9}$$

sing (4.9) we now have an expression for j_s:

$$j_s = O(\bar{\mu} M v_c/a^2 B_0). \tag{4.10}$$

consider $\oint E.d\mathbf{l}$ taken round the path $PQRS$ on figure 4(*b*). Since $E_y = 0$ he core and along PS, and $E_x = 0$ along RS,

$$\oint_{PQRS} \mathbf{E}.d\mathbf{l} = \int_p^Q E_x d_x.$$

in steady flow $\oint \mathbf{E}.d\mathbf{l} = 0$. Therefore $\int_p^Q E_x d_x = 0$, and hence

$$\int_0^\delta \frac{(j_c + j_s)}{\sigma}\, dx + B_0 \int_0^\delta (v_c + v_s)\, dx = 0.$$

But from (4.8), $j_c/\sigma + B_0 v_c = 0$. Then, using (4.10) and assuming that j_s is mainly positive so that $\int_0^\delta j_s dx = O(\delta j_s)$,

$$\int_0^\delta v_s dx = -O\left(\frac{\bar{\mu} M v_c \delta}{\sigma a^2 B_0^2}\right),$$

and

$$\int_{-a}^{a}\int_0^\delta v_s dx dy = -O(v_c a^2/M^{\frac{3}{2}}). \tag{4.11}$$

Hence the ratio of the flux deficit due to the secondary boundary layer to the flux in the core is $O[M^{-\frac{3}{2}}]$, in agreement with the exact analysis.

4.2. *Walls AA perfectly conducting and walls BB non-conducting—case (ii)*

The notation is the same as for case (i). We can then proceed to equation (4.5) as before. In this case the walls BB are non-conducting and consequently

$$\int_{-a}^{+a} j_x dy = I$$

is a constant for all values of x (see figure 5).

Therefore all the secondary current j_s leaving the wall A will have to return at the corners via the region (d) on wall B. If $j_s = j_s'$ in region (d), then, for condition (4.12) to be satisfied,

$$j_s' a/M = O(-a j_s),$$

and hence

$$j_s' = O(-M j_s). \tag{4.12}$$

We can deduce the value of j_s' from the equation of motion in region (d). If $v_s = v_s'$ in this region, then

$$0 = -\partial p/\partial z + (j_c + j_p + j_s')\, B_0 + \bar{\mu}\frac{\partial^2}{\partial y^2}(v_c + v_p + v_s').$$

The boundary conditions on v_s are (i) $v_s' = v_s = -0(v_c)$ in the main part of the secondary boundary, layer, i.e. region (c), and (ii) $v_s = 0$ on $y = \pm a$. Since the thickness of this layer is $O(M^{-1})$,

$$j_s' = -O\left(\frac{\bar{\mu}}{B_0}\frac{v_c}{(a/M)^2}\right). \tag{4.13}$$

Hence, from (4.12),

$$j_s = +O\left(\frac{\bar{\mu}}{B_0} M v_c/a^2\right). \tag{4.14}$$

But, from (4.5),

$$j_s = O\left(\frac{\bar{\mu}}{B_0} v_c/\delta^2\right),$$

and therefore

$$\delta = O(aM^{-\frac{1}{2}}).$$

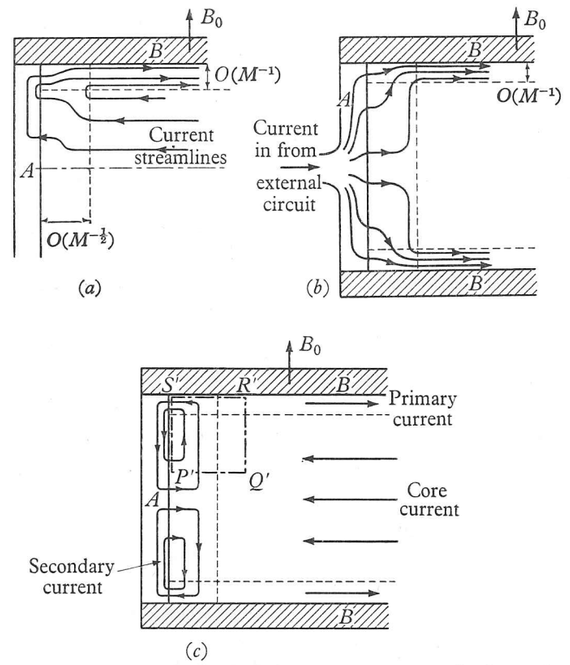

URE 5. Cross-section of the duct when the walls AA are perfectly conducting and the s BB are non-conducting ($M \gg 1$, not to scale). (a) Shows the current streamlines n the duct is on open circuit. (b) Shows the current streamlines when the flow is en by a potential difference between the walls AA. (The current in the walls AA is rn schematically.) (c) Shows the core, primary and secondary currents when the duct n open circuit.

Now consider $\oint \mathbf{E}.d\mathbf{l}$ round $P'Q'R'S'$, where P' S' are on the wall A, R' is the wall B outside the secondary boundary layer and Q' is in the core (figure)). Since $E_y = 0$ in the core and along the wall A,

$$\int_{S'}^{R'} E_x d_x = \int_{P'}^{Q'} E_x d_x, \quad \text{since} \quad \oint \mathbf{E}.d\mathbf{l} = 0.$$

w

$$\int_{S'}^{R'} E_x d_x = \int_0^\delta \frac{j_s'}{\sigma} dx,$$

l

$$\int_{P'}^{Q'} E_x d_x = \int_0^\delta \frac{j_s}{\sigma} dx + B_0 \int_0^\delta v_s d_x.\dagger$$

king the same assumption as for case (i), that $\int_0^\delta j_s' dx = O(\delta j_s')$ we have

$$\int_0^\delta \int_{-a}^{a} v_s dx dy = -O(v_c a^2/M^{\frac{1}{2}}).$$

† Thus $\int_0^\delta E_x dx \neq 0$ in this case, whereas $\int_0^\delta E_x dx = 0$ in case (i). The consequences this were discussed in § 3.

Hence the flux deficit due to the secondary boundary layer is $O(M^{-\frac{1}{2}})$ times the flux in the core.

We see from these order-of-magnitude arguments that the form of the boundary layer on the walls AA is best explained in terms of the secondary currents induced in these layers, much in the same way as the Hartmann layer may be explained by the decrease in current in the boundary layer relative to that in the core. In both these types of boundary layer the current is less than its value in the core because of the reduced $\mathbf{v}\times\mathbf{B}$ induced electric field and consequently the electromagnetic $\mathbf{j}\times\mathbf{B}$ force can decrease in the layer relative to its value in the core to the same extent that the viscous stress increases. If this were not so the boundary layers would grow or diminish. A comparison of cases (i) and (ii) shows that the value of the secondary currents relative to the core current can differ by an order of magnitude.

In case (i), $j_s = -O(j_c M^{-1})$.
In case (ii), open circuit, $j_s = -O(j_c)$.
In case (ii), closed circuit, $j_s = -O(j_c M^{-1})$.

Yet expressed as a fraction of v_c, the values of j_s are of the same order in both cases. This is necessary for the balancing of viscous and electromagnetic forces in the boundary layer. We make this observation because the approximation made by Kerrebrock (1961) and others that the current is constant through the secondary boundary layer, i.e. $j_s = 0$, even though j_s is a very small fraction of j_c, will lead to results which may over-estimate the rate of growth of boundary layers on the walls AA.

The order-of-magnitude arguments also show how the conductivity of the walls affects the secondary currents which in turn affect the velocity distribution in the duct. In case (ii) when the walls BB are non-conducting, the secondary currents circulate in the duct and walls AA; they leave the walls AA in region (c) and return through the Hartmann layer on walls BB, region (d). This is similar to the way in which the core currents return through the Hartmann boundary layers when the walls BB are non-conducting (figure 5(c)). In case (i), when the walls BB are perfectly conducting, the secondary currents mainly return to the wall AA via the walls BB. Owing to the oscillatory nature of the boundary layer in this case, some currents circulate solely in the duct and walls BB (see figure 4(b)). Thus in case (ii), because the secondary current has to return through a narrow layer of thickness $O(M^{-1})$ on walls BB, the resistance of the current path is *higher* than in case (i); hence the secondary current, relative to the core velocity, is *lower*. This means that the viscous stresses in the secondary boundary layer are less in case (ii) than case (i). Since v_s has to rise from $-v_c$ to 0 as $M^{\frac{1}{2}}(x+\ldots)$ increases from 0 to ∞, then the *lower* $\partial^2 v_s/\partial x^2$ and $\partial v_s/\partial x$ are, the *greater* will be $\int_0^\infty v_s\,dx$, i.e. the flux deficit. As we have already noted, in case (i), the flux deficit in the secondary boundary layer relative to the flux in the core is $O(M^{-1})$ times as small as the flux deficit in case (ii). We see now that the explanation lies in the influence on the secondary currents of the conductivity of the walls BB in the corner regions.

This may be illustrated further by comparing case (i) and case (ii) when the walls AA are short-circuited. The $Q-\partial p/\partial z$ relation in these two cases are both of the form

$$Q = \frac{(-\partial p/\partial z)\,4a^3 b}{\mu M^2}\left(1-\frac{1}{M}-\frac{a}{b}O(M^{-\frac{3}{2}})\ldots\right)$$

although the velocity profiles are very different (see §3). If we were to alter the duct of case (ii) and make the walls BB conducting for a distance $O(aM^{-\frac{1}{2}})$ near the corners, then we would not alter the $Q-\partial p/\partial z$ relation but we would change the velocity profile, the core velocity from

$$\frac{(-\partial p/\partial z)\,a^2}{\mu M^2}\left[1+\frac{0{\cdot}956a}{bM^{\frac{1}{2}}}\right] \quad \text{to} \quad \frac{(-\partial p/\partial z)\,a^2}{\mu M^2},$$

and the ratio of the flux deficit due to the secondary boundary layers to the flux in the core from $O(M^{-\frac{1}{2}})$ to $O(M^{-\frac{3}{2}})$. The reason is that the extra pieces of conductor would increase the secondary currents and hence reduce the flux deficit and potential difference across the secondary boundary layer. The value of the core velocity would be reduced, but the form of the core and primary layer profile would of course be unaltered.

We have stated already that we can give no good reasons, *a priori*, for the shape of the velocity profile in the secondary boundary layers; all we can do is deduce the shape from the flux deficit. In cases (ii) and (iii) the flux deficit is $O(aM^{-\frac{1}{2}})$. Since the thickness of the secondary boundary layers is $O(aM^{-\frac{1}{2}})$, there is no reason to expect that the velocity does not uniformly decrease from its value in the core to zero at the walls. In case (i) the flux deficit is $O(M^{-\frac{3}{2}})$ but the boundary layer thickness is still $O(M^{-\frac{1}{2}})$. This explains why the velocity in the boundary layer must be greater than its value in the core over part of the boundary layer. The velocity profiles for case (i) are given by Hunt (1965).

We are grateful to Prof. J. A. Shercliff for his helpful advice and criticism during the preparation of this paper. J. C. R. H. is able to publish this work by permission of the Central Electricity Generating Board.

REFERENCES

ANG, C. C. & LUNDGREN, T. S. 1961 *Z. angew. Math. Phys.* **12**, 100.
INBERG, G. A. 1961 *Appl. Math. and Mech.* (*PMM*), **25**, 1536.
INBERG, G. A. 1962 *Appl. Math. and Mech.* (*PMM*), **26**, 106.
LE, F. J. & KERREBROCK, J. L. 1964 *AIAA J.* **2**, 461.
NT, J. C. R. 1965 *J. Fluid Mech.* **21**, 577.
ERREBROCK, J. L. 1961 *J. Aero/Space Sci.* **28**, 631.
URINGER, J. L. & MIGOTSKY, E. 1963 *Phys. Fluids*, **6**, 1164.
SLER, E. J. & SEARS, W. R. 1958 *J. Aero. Sci.* **25**, 235.
TT, N. & CHENG, H. K. 1954 *J. Rat. Mech. and Anal.* **3**, 357.
ERCLIFF, J. A. 1962 *The Theory of Electromagnetic Flow Measurement.* Cambridge University Press.
ERCLIFF, J. A. 1965 *A Textbook of Magnetohydrodynamics.* Oxford: Pergamon Press.
TTON, G. W. & CARLSON, A. W. 1961 *J. Fluid Mech.* **11**, 121.
LYAND, Y. S. 1961 *Sov. Phys. Tech. Phys.* **5**, 1194.

Reprinted without change of pagination from the
Proceedings of the Royal Society, A, *volume* 293, *pp.* 342–358, 1966

the stability of parallel flows with parallel magnetic fields

By J. C. R. Hunt†
Central Electricity Research Laboratories, Leatherhead

(*Communicated by K. Stewartson, F.R.S.—Received* 15 *November* 1965)

The first part of the paper is a physical discussion of the way in which a magnetic field affects the stability of a fluid in motion. Particular emphasis is given to how the magnetic field affects the interaction of the disturbance with the mean motion.

The second part is an analysis of the stability of plane parallel flows of fluids with finite viscosity and conductivity under the action of uniform parallel magnetic fields. We show that, in general, three-dimensional disturbances are the most unstable, thus disagreeing with the conclusion of Michael (1953) and Stuart (1954). We show how results obtained for two-dimensional disturbances can be used to calculate the most unstable three-dimensional disturbances and thence we prove that a parallel magnetic field can never completely stabilize a parallel flow.

1. Introduction

e stability of a fluid system is determined by the rate of growth or decay of turbances in any of its components, e.g. velocity, pressure, temperature, or gnetic field. Though there are exceptional cases, a perturbation of one component ally causes perturbations in the others, so that if one type of disturbance is stable, in general all types are. Let us consider mechanical disturbances, as being mmon to all types of fluid systems. The forces which determine their rate of wth or decay may be considered as falling into two main groups which are tinct though interdependent. The *first* consists of the forces acting on the disturnce directly, e.g. viscous, electromagnetic, or surface tension, and the *second* sists of the forces due to the interaction of the disturbance with the fluid system, centrifugal forces in rotating flows. (This is merely putting into words the uations for the forces acting on a small disturbance which contain terms indedent and dependent on values of the components of the undisturbed fluid stem.) The effect of a magnetic field on the stability of various fluid systems is ilar in the sense that the electromagnetic forces acting on the disturbances ectly are similar but the forces due to the interaction of the disturbance and the in fluid system are different in different fluid systems. Most explanations of the ect of a magnetic field on the stability of magnetohydrodynamic (m.h.d.) flows e similar to those of its effects on the stability of static situations, being given in rms of the fluid moving through or 'freezing' to the field lines (see, for example, andrasekhar 1961). This type of explanation does not demonstrate the essential fferences between the effects of a magnetic field on the stability of dynamic and atic situations and is especially weak in dynamic situations where it only shows w the magnetic field affects the first group of forces and not the second.

In § 2 of this paper we discuss the stability of m.h.d. flows from a different physical int of view so as to demonstrate the effect of the magnetic field on the second oup of forces as well as the first. We first examine the currents induced by a

† Seconded to School of Engineering Science, University of Warwick, Coventry.

disturbance, pointing out the important difference between electromagnetic and mechanical disturbances, and then examine the electromagnetic $\mathbf{j}\times\mathbf{B}$ force. By considering the rotationality of the $\mathbf{j}\times\mathbf{B}$ force we find under what conditions the magnetic field affects the forces acting on the disturbance. We then consider the different ways in which a small disturbance interacts with a mean flow and how the value of R_m, the magnetic Reynolds number, affects this interaction.

For the rest of the paper we concentrate on the stability of plane parallel flows for fluids with finite viscosity and conductivity, uniform properties, and no free surfaces. We prove that, when a uniform magnetic field is parallel to the flow and sufficiently large, the wavenumber vector of the most unstable disturbance is not in general parallel to the flow, i.e. it is a three-dimensional disturbance. We then interpret this result physically using the concepts of § 2. Our result invalidates the conclusion of Michael (1953) and Stuart (1954) who asserted that the wavenumber vector of the most unstable disturbance was parallel to the flow, i.e. a two-dimensional disturbance. Using this erroneous assumption, Stuart (1954), Velikhov (1959) and Tarasov (1960) examined the stability of plane Poiseuille flow with a parallel magnetic field. Drazin (1960) has examined some general aspects of the stabilizing influence of a parallel magnetic field on a plane parallel flow, also considering only two-dimensional disturbances. Wooler (1961) has examined the stability of a plane parallel flow when $R_m \ll 1$ and when the magnetic field lies in the plane of the flow but is not parallel to it. He found that three-dimensional disturbances can be the most unstable; however, he did not point out that, even when the magnetic field is parallel to the flow, three-dimensional disturbances can still be the most unstable. For all values of R_m we show how results obtained for two-dimensional disturbances can be modified to take into account three-dimensional disturbances and thence draw some general conclusions about the stabilizing influence of a parallel magnetic field on a plane parallel flow. In particular we prove that a parallel magnetic field can never completely stabilize a flow, i.e. stabilize it for all values of the Reynolds number.

2. Physical aspects of the stability of m.h.d. flows

2·1. We shall only be interested in the stability of incompressible fluids with uniform conductivity, density and viscosity. Then the relevant equations of magneto-hydrodynamics are

$$\rho \mathrm{D}u/\mathrm{D}t = -\nabla p + \mathbf{j}\times\mathbf{B} + \eta\nabla^2\mathbf{u}, \tag{2·1}$$

$$\mathbf{j} = \sigma(\mathbf{E}+\mathbf{u}\times\mathbf{B}), \tag{2·2}$$

$$\mathbf{j} = (1/\mu)\nabla\times\mathbf{B}, \tag{2·3}$$

$$\nabla\times\mathbf{E} = -\partial\mathbf{B}/\partial t, \tag{2·4}$$

$$\nabla.\mathbf{u} = 0, \tag{2·5}$$

$$\nabla.\mathbf{B} = 0, \tag{2·6}$$

where $\mathbf{u}$ is velocity, p pressure, $\mathbf{j}$ current density, $\mathbf{B}$ magnetic flux density, $\mathbf{E}$ electric field, and μ magnetic permeability, ρ density, η viscosity, and σ conductivity; the latter four quantities are all constant.

ow consider a steady flow whose velocity vector is $\mathbf{U}(x,y,z)$ and vorticity vector (x,y,z). Let this steady flow be perturbed such that the velocity vector is now

$$\mathbf{U}(x,y,z)+(\mathbf{u}(x,y,z,t),$$

the vorticity vector is

$$\boldsymbol{\Omega}(x,y,z)+\boldsymbol{\omega}(x,y,z,t).$$

ssume $|\mathbf{u}| \ll |\mathbf{U}|$ and $|\boldsymbol{\omega}| \ll |\boldsymbol{\Omega}|$.

he magnetic field consists of a steady component, $\mathbf{B}_0(x,y,z)$ and an unsteady ponent, $\mathbf{b}(x,y,z,t)$. Let the steady current associated with $\mathbf{B}_0$ be $\mathbf{J}_0(x,y,z)$ and perturbation current associated with $\mathbf{b}$ be $\mathbf{j}(x,y,z,t)$. Assume $|\mathbf{b}| \ll |\mathbf{B}_0|$, $|\mathbf{J}_0|$.

o examine the stability of the mean flow $\mathbf{U}$ under the action of the magnetic $\mathbf{B}_0$, we examine the behaviour with time of the disturbances of the velocity, nd of the magnetic field, $\mathbf{b}$. We first consider the generation of electric currents the growth of $\mathbf{b}$.

2. If we eliminate the mean values, Ohm's law, i.e. (2·2), for the disturbance mes:

$$\mathbf{j} = \sigma(\mathbf{E}+\mathbf{u}\times\mathbf{B}_0+\mathbf{U}\times\mathbf{b}), \tag{2·7}$$

ignore the second-order term $\mathbf{u}\times\mathbf{b}$. Taking the curl of (2·7) and using (2·4) to we have:

$$\frac{\partial\mathbf{b}}{\partial t}+(\mathbf{U}.\nabla)\mathbf{b} = (\mathbf{b}.\nabla)\mathbf{U}+\nabla\times(\mathbf{u}\times\mathbf{B}_0)+\frac{1}{\mu\sigma}\nabla^2\mathbf{b}. \tag{2·8}$$

he terms in (2·7) may be described physically as follows: the perturbation city $\mathbf{u}$ and the main magnetic field $\mathbf{B}_0$ induce a current $\mathbf{j}_1$ which produces its own netic field $\mathbf{b}_1$, which with the mean flow $\mathbf{U}$ induces extra currents, $\mathbf{j}_2$. These ents, $\mathbf{j}_2$, flow in such a direction that their own magnetic field, $\mathbf{b}_2$, acts in the osite direction to $\mathbf{b}_1$, by Lenz's law. $\mathbf{j}_2$ is modified by the growth of its own netic field $\mathbf{b}_2$, since $\mathbf{j}_2$ is induced by the mean flow $\mathbf{U}$ and the combined induced netic fields $(\mathbf{b}_1+\mathbf{b}_2)$. The relative directions of $\mathbf{j}_2$ and $\mathbf{j}_1$ depend on the geometry he mean flow and the magnetic field.

$\mathbf{j}_2$, $\mathbf{b}_1$ and $\mathbf{b}_2$ may be found from the following equations which derive from) and (2·8):

$$\frac{\partial\mathbf{b}_1}{\partial t}-\nabla\times(\mathbf{u}\times\mathbf{B}_0) = -\frac{1}{\sigma}(\nabla\times\mathbf{j}_1) = \frac{1}{\mu\sigma}\nabla^2\mathbf{b}_1,$$

$$\frac{\partial\mathbf{b}_2}{\partial t}-\nabla\times(\mathbf{U}\times(\mathbf{b}_1+\mathbf{b}_2)) = -\frac{1}{\sigma}(\nabla\times\mathbf{j}_2) = \frac{1}{\mu\sigma}\nabla^2\mathbf{b}_2,$$

$$\mathbf{j} = \mathbf{j}_1+\mathbf{j}_2,$$

$$\mathbf{b} = \mathbf{b}_1+\mathbf{b}_2.$$

en $R_m(=\overline{U}l\mu\sigma) \ll 1$, where $\overline{U}$ is a characteristic velocity of the mean flow and l characteristic length, for disturbances of interest $\partial\mathbf{b}/\partial t$ is much smaller than other terms in the above equations and we can then deduce the ratio of $\mathbf{j}_1$ to $\mathbf{j}_2$ crude order of magnitude argument, from the above equations.

$$|\mathbf{b}_1| \sim O[|\mathbf{j}_1|\,l\mu],$$

$$|\mathbf{j}_2| \sim O[\sigma|\overline{U}|\,|\mathbf{b}_1+\mathbf{b}_2|],$$

$$|\mathbf{b}_2| \sim O[|\mathbf{j}_2|\,l\mu].$$

Therefore when $R_m \ll 1$, $|\mathbf{j}_2| \sim O[\sigma\mu l|\,\overline{U}\,||\mathbf{j}_1|]$, and

$$|\mathbf{j}_2|/|\mathbf{j}_1| \sim O[R_m]. \tag{2·9}$$

Thus when $R_m \ll 1$, e.g. in a laboratory experiment with mercury, $|\mathbf{j}_2| \ll |\mathbf{j}_1|$ and t a good approximation, Ohm's law becomes

$$\mathbf{j} = \sigma(\mathbf{E} + \mathbf{u} \times \mathbf{B}_0). \tag{2·10}$$

This approximation, which can be justified by more refined arguments in particular problem, is used in all stability analyses when $R_m \ll 1$ (see § 3). Fron equation (2·8) we can find out under what circumstances currents will be induced b a perturbation velocity, $\mathbf{u}$. If $\mathbf{u}$ and $\mathbf{B}_0$ satisfy the condition

$$\nabla \times (\mathbf{u} \times \mathbf{B}_0) = 0, \tag{2·11}$$

equation (2·8) becomes:

$$\frac{\partial \mathbf{b}}{\partial t} + (\mathbf{U}.\nabla)\,\mathbf{b} = (\mathbf{b}.\nabla)\,\mathbf{U} + \frac{1}{\mu\sigma}\nabla^2\mathbf{b}. \tag{2·12}$$

The disturbances in the velocity and in the magnetic field are coupled. A distur bance of one leads to a disturbance of the other and an m.h.d. flow can be mad unstable by either type of disturbance. Equation (2·12) is interesting in that it doe not include the perturbation velocity $\mathbf{u}$, but only the mean velocity $\mathbf{U}$. It show how a disturbance in the magnetic field, $\mathbf{b}$, can develop by its interaction with th mean velocity, $\mathbf{U}$, without being affected by $\mathbf{u}$, provided $\mathbf{u}$ satisfies (2·11).

For $\mathbf{b}$ and $\mathbf{U}$ not to induce any currents they must satisfy the conditions

$$\nabla \times (\mathbf{U} \times \mathbf{b}) = 0. \tag{2·13}$$

We now deduce three sets of conditions each of which is a sufficient condition fo there to be no growth of $\mathbf{b}$ or $\mathbf{j}$.

(i) If conditions (2·11) and (2·13) are satisfied simultaneously equation (2·12 becomes

$$\frac{\partial \mathbf{b}}{\partial t} = \frac{1}{\mu\sigma}\nabla^2\mathbf{b};$$

which shows that any stray magnetic field will simply decay due to ohmi dissipation.

(ii) Consider the development of a small velocity $\mathbf{u}$ when condition (2·11) i satisfied and let us postulate that at some time $t = 0$, when the perturbation velocity $\mathbf{u}$ is generated there are no perturbation currents, j, in the fluid or in the region surrounding the fluid. It follows from (2·3) and (2·6) that $\nabla^2\mathbf{b} = 0$.

If, also, $\mathbf{b} \to 0$ as $x, y, z \to \infty$ then $\mathbf{b} = 0$ everywhere. Then from the form of th equation (2·12), whatever the distribution of $\mathbf{U}$ or the value of R_m, the only solutio for the equation when $t > 0$ is

$$\mathbf{b} = 0.$$

Hence if condition (2·11) is satisfied and if $\mathbf{j} = 0$ when $t = 0$, for all $t > 0$,

$$\mathbf{j} = 0.$$

(iii) Most studies of the stability of m.h.d. flows use 'normal mode' analyses, wit

$$\mathbf{u}, \mathbf{b} \sim \exp[\mathrm{i}(\alpha x - \sigma t)].$$

hen the condition that $\mathbf{b} = 0$ everywhere when $t = 0$ is not satisfied since the se of $\mathbf{b}$ varies with position. (For a particular example, see § 3). Therefore even .11) is satisfied, in general $\mathbf{j} \neq 0$ for $t > 0$. However, if $R_m \ll 1$ we can usually re $\partial\mathbf{b}/\partial t$ and using the result (2·10) we obtain the good approximation to (2·8)

$$O = \nabla \times (\mathbf{u} \times \mathbf{B}_0) + (1/\mu\sigma)\nabla^2\mathbf{b}.\dagger$$

$\times (\mathbf{u} \times \mathbf{B}_0) = 0$, this becomes $(1/\mu\sigma)\nabla^2\mathbf{b} = 0$. Then if $\mathbf{b} = 0$ on the boundaries, $= 0$ throughout the fluid. Thus it is only when condition (2·11) is satisfied, $R_m \ll 1$ $\mathbf{b} = 0$ on the boundaries, that we can say $\mathbf{j} = 0$ whatever the initial conditions. he physical justification of this reasoning is that if curl $(\mathbf{u} \times \mathbf{B}_0) = 0$, the change ux of the *main* magnetic field, $\mathbf{B}_0$, linked by a fluid loop due to the *perturbed* ion, is zero and thereby no perturbation currents are induced. If a stray magnetic d, $\mathbf{b}$, exists, the change of flux of $\mathbf{b}$ linked by a fluid particle due to the *mean* ion is not necessarily zero, and hence perturbation currents can be induced ther or not curl $(\mathbf{u} \times \mathbf{B}_0) = 0$. Clearly, if curl $(\mathbf{b} \times \mathbf{U}) = 0$, then this latter source urrents also vanishes.

3. A magnetic field can only affect the velocity of a disturbance by means of the tromagnetic body force $\mathbf{j} \times \mathbf{B}$, which occurs in the equation of motion (2·1). rly, if $\mathbf{j} = 0$, the magnetic field has no effect on a disturbance. However, even if $\neq 0$, the $\mathbf{j} \times \mathbf{B}$ force does not necessarily produce any change in the motion of the urbance. Shercliff (1965) has discussed how the $\mathbf{j} \times \mathbf{B}$ term in the equation of ion (2·1) only changes the velocity distribution of an incompressible flow when rotational, i.e. curl $(\mathbf{j} \times \mathbf{B}) \neq 0$, assuming the fluid has no free surfaces and has stant density. To examine the effect of curl $(\mathbf{j} \times \mathbf{B})$ on the disturbance we con- r the curl of (2·1) ignoring second-order quantities:

$$\rho\left[\frac{\mathrm{D}\boldsymbol{\omega}}{\mathrm{D}t} + (\mathbf{u}.\nabla)\,\boldsymbol{\Omega} - (\boldsymbol{\Omega}.\nabla)\,\mathbf{u} - (\boldsymbol{\omega}.\nabla)\,\mathbf{U}\right]$$
$$= (\mathbf{B}_0.\nabla)\,\mathbf{j} + (\mathbf{b}.\nabla)\,\mathbf{J}_0 - (\mathbf{J}_0.\nabla)\,\mathbf{b} - (\mathbf{j}.\nabla)\,\mathbf{B}_0 + \eta\nabla^2\boldsymbol{\omega}. \tag{2·14}$$

hus it follows that the rate of growth or decay of the vorticity of the disturbance ot affected by the magnetic field if

$$(\mathbf{B}_0.\nabla)\,\mathbf{j} + (\mathbf{b}.\nabla)\,\mathbf{J}_0 - (\mathbf{J}_0.\nabla)\mathbf{b} - (\mathbf{j}.\nabla)\,\mathbf{B}_0 = 0. \tag{2·15}$$

We are mainly interested in situations where $\mathbf{B}_0$ is constant in space and does not y with time. Then $\mathbf{J}_0 = 0$ and (2·11) becomes

$$(\mathbf{B}_0.\nabla)\,\mathbf{u} = 0, \tag{2·16}$$

(2·15) becomes

$$(\mathbf{B}_0.\nabla)\,\mathbf{j} = 0. \tag{2·17}$$

he important difference between conditions (2·16) and (2·17) is that (2·16) only ends on the disturbance velocity $\mathbf{u}$ and the magnetic field $\mathbf{B}_0$ whereas, since $\mathbf{j}$

† This approximation should be justified, *a posteriori*, in each case it is used. It is justifiable many cases for the disturbances which are most unstable, e.g. in Plane Poiseuille flow. very high frequency disturbances, which are highly damped and stable we could not ore $\partial\mathbf{b}/\partial t$.

depends on **U** as well as **u**, (2·17) depends on the mean velocity, **U**, as well as th disturbance velocity, **u**. However, when $R_m \ll 1$, we have shown that

$$\mathbf{j} = \sigma(\mathbf{E} + \mathbf{u} \times \mathbf{B}_0), \tag{2·18}$$

so that one can then ignore the effects of **b** and the mean flow, **U**.

In deducing (2·17) we assumed $\mathbf{J}_0 = 0$. If, however, $R_m \ll 1$ and a uniform magneti field $\mathbf{B}_1$ is produced outside the region of flow and induces currents $\mathbf{J}_0$ by means o the mean flow **U**, the field due to $\mathbf{J}_0$, $\mathbf{B}_2$ is very small compared to $\mathbf{B}_1$ (Shercliff 1965) i.e. $|\mathbf{B}_2| \ll |\mathbf{B}_1|$, where

$$\mathbf{B}_0 = \mathbf{B}_1 + \mathbf{B}_2 \quad \text{and} \quad \mathbf{J}_0 = (1/\mu)\nabla \times \mathbf{B}_2.$$

Then it follows that the terms on the right-hand side of (2·14), $(\mathbf{b}.\nabla)\mathbf{J}_0$, $(\mathbf{J}_0.\nabla)\mathbf{b}$ $(\mathbf{j}.\nabla)\mathbf{B}_0$ are much smaller than $(\mathbf{B}_0.\nabla)\mathbf{j}$. Thus if $(\mathbf{B}_0.\nabla)\mathbf{j} = 0$ it may be a goo approximation to say that the magnetic field has no effect on a disturbance even i $\mathbf{J}_0 \neq 0$, provided $R_m \ll 1$. However, this approximation would need careful investi gation in any particular problem and would have to be justified, *a posteriori*.

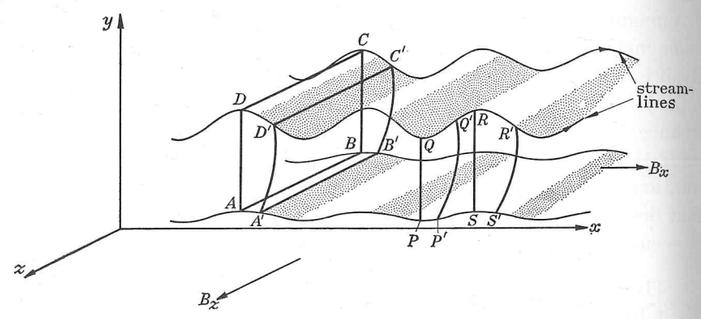

FIGURE 1. A typical disturbance travelling in the direction Ox. The effect of the magneti field on the disturbance is seen by examining the change of flux linked by the fluid circuit $ABCD$ and $PQRS$ with the imposed magnetic fields B_x and B_z. (The induced magneti fields and currents are not shown.)

Let us now consider a particular example to demonstrate the physical meaning o the conditions we have derived for the magnetic field to affect a disturbance, (2·16 and (2·17). Consider a simple two-dimensional disturbance of the type

$$\mathbf{u} = [u(y)\exp[\mathrm{i}(\alpha x - \sigma t)],\ v(y)\exp[\mathrm{i}(\alpha x - \sigma t)],\ 0],$$

imposed upon a mean flow in the x direction, as shown in figure 1. The disturbanc moves in the Ox direction, and its amplitude varies in the Oy direction. At certain time, t, a circuit drawn in the fluid lies on the points $ABCD$. At a later tim $t + \Delta t$ the particles on the circuit have reached $A'B'C'D'$.

If $\mathbf{B}_0 = (B_x, 0, 0)$ the flux linked by the fluid circuit has changed in the time Δt and consequently currents are induced in the z direction. The currents which ar induced will affect the flow because j_z varies with x and hence $(\mathbf{j} \times \mathbf{B}_0)$ is rotational, i.e.

$$\operatorname{curl}(\mathbf{j} \times \mathbf{B}_0) = \left(B_x . \frac{\partial}{\partial x}\right) j_z \neq 0.$$

$\mathbf{B}_0 = (0, 0, B_z)$ the flux linked by the fluid circuit $ABCD$ is zero and does not ge with time. But now consider another fluid circuit $PQRS$ at right angles to former one. Then, since the flow is incompressible, the area enclosed by this uit is constant and so the flux linked by the field B_z remains constant. Hence, ided there is no disturbance to the magnetic field, **b**, there are no induced ents, $(B_z\partial/\partial z)\mathbf{u} = 0$, and therefore B_z does not affect such a flow. Thus a orm magnetic field does not affect a two-dimensional disturbance, if it is llel to the vorticity of the disturbance.

We now consider the mode of interaction between the mean flow and the distur- ce. This discussion is speculative since there have been few previous attempts iscuss this aspect of the problem physically. We will only consider here the ation where *all* the energy of the disturbance comes from the mean flow.

et us first consider plane parallel flows with parallel magnetic fields. When there magnetic field such a flow is able to feed energy into a disturbance by means he Reynolds, or inertial, stresses $(-\rho\overline{u_x u_y})$. Viscosity does not affect this inter- ion directly, but by the stresses it induces it is able to change the disturbance cities, and hence the Reynolds stresses. Thus, indirectly, viscous action can e a flow stable or unstable. The electromagnetic force due to the current $\mathbf{j}_1$, i.e. $\mathbf{B}_0$, can act in a similar way, as shown by Drazin (1960). The main difference ween these two types of damping forces is that the electromagnetic damping of sturbance depends on its direction relative to $\mathbf{B}_0$, i.e. it is anisotropic. Drazin did differentiate between $\mathbf{j}_1$ and $\mathbf{j}_2$, since he was only interested in the case of $R_m \ll 1$, n $\mathbf{j}_2$ is negligible. When $R_m \ll 1$ so that effects due to $\mathbf{j}_2$ are negligible, Drazin wed that if $\mathbf{B}_0$ is sufficiently great the dissipative forces due to $\mathbf{j}_1 \times \mathbf{B}_0$ are so ng that at a given finite value of the Reynolds number any plane parallel flow be stabilized by a parallel magnetic field. (We show in § 3 that this result is not nged by considering three-dimensional disturbances).

In other flows where the destabilizing agents are inertial forces, surface tension, vity, etc., and where the action of viscosity is primarily to reduce the rate of wth of disturbances, then when $R_m \ll 1$ the effect of a magnetic field, i.e. the $\times \mathbf{B}_0$ force, is also damping. Examples of this effect to be found in Chandrasekhar's k, are Couette flow between rotating cylinders and capillary instability of jets. us by means of the currents $\mathbf{j}_1$, the energy of the disturbance is dissipated, but velocity distribution of the disturbance may be altered in such a way that the turbance can grow more rapidly.

We have already described how the currents $\mathbf{j}_2$ are induced by the perturbation gnetic field $\mathbf{b}_1$ and the mean flow **U**. By means of these currents, $\mathbf{j}_2$, the mean w can feed energy into the perturbation field **b** and by means of the $\mathbf{j}_2 \times \mathbf{B}_0$ force an feed energy into the perturbation velocity, **u**. Thus the current, $\mathbf{j}_2$, leads to th the electromagnetic and mechanical energy being transferred *electromagneti- lly*† as distinct from the *mechanical* or *inertial* way it is transferred when the turbance and the mean flow exchange energy by inertial stresses. An important

† This mechanism may also be interpreted as the interaction of the mean flow with the gnetic shear stresses $(b_x b_y/\mu)$. See, for instance, the equation for the energy of a small turbance in a plane parallel flow deduced by Stuart (1954).

difference between these two methods of energy transfer is that the former is long range and the latter short range, i.e. a small localized disturbance can exchange energy electromagnetically with a part of the mean flow some distance from it.

When $R_m \ll 1$, $|\mathbf{j}_2| \ll |\mathbf{j}_1|$ (equation (2·9)), and consequently the main means of energy transfer between the disturbance and the mean flow is *mechanical*. As R_m increases $\mathbf{j}_2$ and $\mathbf{b}_2$ increase and the means of energy transfer between the main flow and the disturbance is as much electromagnetic as mechanical.

In the presence of a magnetic field some of the kinetic energy of a *mechanical* disturbance is converted to electrical and magnetic energy. This energy is both dissipated as Joule heating and stored in electric and magnetic fields. The energy which is stored can change back into mechanical energy. This alternation between mechanical and electromagnetic energy provides the mechanism for a disturbance to *propagate* along the field lines as Alfvén waves. At the present time there is little physical understanding of how this mechanism affects the stability of flows, especially since the normal mode analysis does not reveal much about how a disturbance propagates. Velikov (1959) has shown that when $R_m \to \infty$ and $R \to \infty$ a magnetic field can stabilize all two-dimensional disturbances in a plane flow parallel to it if

$$A = \frac{B_0}{\sqrt{(\mu\rho)}\, U_m} > 1,$$

where U_m is the maximum velocity of the flow. He gave no physical explanation for his result.

Thus there are three new factors which arise on considering the stability of flows in the presence of magnetic fields:

(1) An anisotropic dissipative force acting on the disturbance alone.

(2) A new, long range, mechanism for the interaction of the disturbance and the mean flow.

(3) A mechanism for the propagation of the disturbance.

In general we expect the two latter effects to be unimportant when $R_m \ll 1$.

3. Stability of plane parallel flows with alined magnetic fields—low magnetic Reynolds number

3·1. *General equations*

Consider a steady flow whose velocity is $\mathbf{U}_0 = (U_0(y), 0, 0)$ and an infinitesimal disturbance velocity

$$\mathbf{u} = (u(y)\exp[\mathrm{i}(\alpha^* x + \gamma^* z - \beta t)],\quad v(y)\exp[\mathrm{i}(\alpha^* x + \gamma^* z - \beta t)],\quad w(y)\exp[\mathrm{i}(\alpha^* x + \gamma^* z - \beta t)]). \tag{3·1}$$

There is an alined magnetic field with flux density $\mathbf{B}_0 = (B_0, 0, 0)$ and an infinitesimal perturbation magnetic field,

$$\mathbf{b} = \{\phi(y)\exp[\mathrm{i}(\alpha^* x + \gamma^* z - \beta t)],\quad \psi(y)\exp[\mathrm{i}(\alpha^* x + \gamma^* z - \beta t)],\quad \chi(y)\exp[\mathrm{i}(a^* x + \gamma^* z - \beta t)]\}. \tag{3·2}$$

let
$$U(y) = \frac{U_0(y)}{\overline{U}},\quad c = c_r + \mathrm{i}c_i = \frac{\beta}{\alpha^* \overline{U}},\quad \alpha = \frac{\alpha^*}{l},$$
$$\gamma = \frac{\gamma^*}{l},\quad \lambda = \sqrt{(\alpha^2+\gamma^2)},\quad \frac{\overline{U}l}{\nu} = R,\quad \overline{U}l\mu\sigma = R_m,$$
$$y' = y/l,\quad \text{and}\quad \gamma^*/\alpha^* = \tan\theta,$$

re $\overline{U}$ is a characteristic velocity of the flow and l is a characteristic length.

If the above expressions for the velocity and magnetic field are inserted in the d. equations (2·1) to (2·6), and if differentiations are carried out with respect ', then Stuart (1954) has shown that the equations can be reduced to two ations in v and ψ, namely

$$(U-c)(v''-\lambda^2 v) - vU'' - \frac{B_0}{\mu\rho\overline{U}}(\psi''-\lambda^2\psi) = \frac{-\mathrm{i}}{\alpha R}(v^{\mathrm{iv}} - 2\lambda^2 v'' + \lambda^4 v), \tag{3·3}$$

$$(U-c)\psi - \frac{B_0 v}{\overline{U}} = \frac{-\mathrm{i}}{\alpha R_m}(\psi'' - \lambda^2\psi). \tag{3·4}$$

When $R_m \ll 1$ (3·4) reduces to

$$-\frac{B_0 v}{\overline{U}} = \frac{-\mathrm{i}}{\alpha R_m}(\psi'' - \lambda^2\psi).\dagger \tag{3·5}$$

This approximation is only valid for disturbances whose wavelength is $O[l]$ and quency $o[\overline{U}/l]$. These are not very restrictive conditions since they are usually isfied by the disturbances of interest, i.e. the most unstable. However, as pointed in § 2, this approximation should be justified, *a posteriori*, in any particular case ng the values of α and c found in the analysis.

Then from (3·5), (3·3) becomes

$$(U-c)(v''-\lambda^2 v) - vU'' + \frac{\mathrm{i}\sigma B_0^2 l\alpha v}{\rho\overline{U}} = \frac{-\mathrm{i}}{\alpha R}(v^{\mathrm{iv}} - 2\lambda^2 v'' + \lambda^4 v). \tag{3·6}$$

3·2. *Three-dimensional disturbances*

Equation (3·6) describes the motion of a disturbance travelling at an angle θ to and $\mathbf{B}_0$. Now the motion of such a disturbance can be described in terms of an uivalent one for which $\theta = 0$. Let $\alpha R = \lambda\bar{R}$ and $\bar{R} = R\cos\theta$ where $\bar{R}$ is the eynolds number for the equivalent disturbance.

Let
$$\frac{\sigma B_0^2 l}{\rho\overline{U}} = q_0 \quad \text{and} \quad \alpha q_0 = \lambda\bar{q},$$

here
$$\bar{q} = \frac{\sigma B_0^2 l}{\rho\overline{U}}\cos\theta.$$

hen (3·6) becomes

$$(U-c)(v''-\lambda^2 v) - vU'' + \mathrm{i}\lambda\bar{q}v = -(\mathrm{i}/\lambda\bar{R})(v^{\mathrm{iv}} - 2\lambda^2 v'' + \lambda^4 v). \tag{3·7}$$

† As pointed out by Hains (1965), (3·5) may not be the correct first order approximation hen $R_m \ll 1$ if the perturbed magnetic field is externally applied rather than induced by elocity perturbations. But for low frequency oscillations of interest, the currents due to ch a perturbation produce an irrotational $\mathbf{j}\times\mathbf{B}$ force and hence do not affect the velocity erturbations.

Assuming the existence of suitable boundary conditions for v which do not vary with the angle θ of the disturbance, we now have an eigenvalue relation between the parameters in (3·7) of the form

$$F(c, \lambda, \bar{q}, \bar{R}) = 0. \tag{3·8}$$

This relation is the same whatever the angle θ chosen for the disturbance. Equation (3·8) may be rewritten

$$G(c, \lambda, \theta, q_0, R) = 0. \tag{3·9}$$

The main information we want to derive from relations (3·8) and (3·9) is the velocity of the fluid at which the flow becomes unstable, given the value of the applied magnetic field and the values of the fluid properties. In terms of the mathematical problem we want to know, given q_0 or some other parameter involving B_0, what is the lowest value of $R, R_{\text{crit.}}$, for which the flow becomes unstable, i.e. when $c_i = 0$. To do this we calculate R for various values of c_r, λ and θ and look for its lowest value.

When $q_0 = 0$ Squire (1933) showed that disturbances for which $\theta > 0$ (three-dimensional disturbances) become unstable at higher values of R than those for which $\theta = 0$ (two-dimensional disturbances). If the lowest value of $\bar{R}$ for which $c_i = 0$ is $\bar{R}_{\text{crit.}}$, then for a disturbance at an angle θ,

$$R_{\text{crit.}} = \bar{R}_{\text{crit.}}/\cos\theta, \quad \text{which is greater than } \bar{R}_{\text{crit.}}.$$

The lowest value of $R_{\text{crit.}}$ occurs when $\theta = 0$ and $R_{\text{crit.}} = \bar{R}_{\text{crit.}}$. Hence the theorem is proved.

When $q_0 > 0$ if the lowest value of $\bar{R}$ at which $c_i = 0$ for some value of $\bar{q}$ is $\bar{R}_{\text{crit.}}$ then,

$$R_{\text{crit.}} = \frac{\bar{R}_{\text{crit.}}}{\cos\theta} \quad \text{and} \quad q_0 = \frac{\bar{q}}{\cos\theta}. \tag{3·10}$$

If
$$\theta = 0, \quad R_{\text{crit.}} = \bar{R}_{\text{crit.}} \quad \text{and} \quad q_0 = \bar{q}. \tag{3·11}$$

For the same value of $\bar{q}$, we have the same result as before that the most unstable disturbance occurs when $\theta = 0$. But for given q_0, i.e. a given flow and given magnetic field, as θ increases, $\bar{q}$ decreases and, depending on the value of θ and q_0, this may lead to an increase or decrease in $R_{\text{crit.}}$. Hence it is, in general, incorrect to conclude that the most unstable disturbances are those whose wavenumber vectors are parallel to the flow and magnetic field, i.e. those for which $\theta = 0$. Michael (1953) and Stuart (1954) did not appreciate that the magnetic interaction term $\bar{q}$ varied with θ for given B_0 and $\bar{U}$ and erroneously concluded that Squire's theorem could be extended to apply to flows with parallel magnetic fields.

Our result can easily be seen in physical terms. When there is no magnetic field there are two competing effects, the viscous damping of the disturbance, and the inertial interaction between the Reynolds stresses and the velocity gradient of the mean flow. The latter effect, which provides the mechanism for the mean flow to feed energy into the disturbance decreases as θ increases whereas the former is independent of θ. Hence the most unstable disturbances are those for which $\theta =$ When there is a magnetic field parallel to the flow, $\mathbf{B}_0$, and $R_m \ll 1$, there is a thir

ect due to the magnetic field acting on the induced currents, $\mathbf{j}_1$, as θ increases to $(\mathbf{B}_0 \cdot \nabla)\mathbf{u} \to 0$. It was shown in § 2 that when $R_m \ll 1$, $(\mathbf{B}_0 \cdot \nabla)\mathbf{u} = 0$ and there are applied currents on the boundaries, $\mathbf{j} = 0$ in the fluid. Hence as $\theta \to \frac{1}{2}\pi$, $\mathbf{j} \times \mathbf{B}_0$ creases. However, the inertial terms also decrease as θ increases. The reason why e ratio of electromagnetic to inertial forces for a disturbance with given wave-gth, λ, i.e. $\bar{q}$, decreases as θ increases, is because the electromagnetic forces $[\sigma B_0^2 |\mathbf{u}| \cos^2\theta])$ decrease proportionally to $\cos^2\theta$ and the inertial forces

$$(O[\rho |\mathbf{U}| \cos\theta |\mathbf{u}|/\lambda])$$

ly decrease proportionally to $\cos\theta$.

3·3. *General considerations for low R_m flows*

As a result of showing that Squire's theorem cannot be extended to plane parallel ws with a parallel magnetic field in § 3·2 we can draw some general conclusions out the stabilizing influence of a magnetic field.

From the relation (3·8) we can deduce a relation between $\bar{R}_{\text{crit.}}$ and $\bar{q}$ of the form

$$\bar{R}_{\text{crit.}} = f(\bar{q}). \tag{3·12}$$

uation (3·12) may be rewritten

$$R_{\text{crit.}} = f(q_0 \cos\theta)/\cos\theta \tag{3·13}$$

d for $\theta = 0$ becomes
$$R_{\text{crit.}} = f(q_0). \tag{3·14}$$

ossow (1959) and Stuart (1954) have obtained relations of the type (3·14) in amining the stabilizing influence of a parallel magnetic field on boundary layer ws and plane Poiseuille flow. They did not consider disturbances for $\theta > 0$. ypical $f(\bar{q})$ is shown in figure 2. Using this figure we show how to find the value of which gives the minimum value of $R_{\text{crit.}}$ for any given q_0. (We assume θ is positive, ough it could equally be negative.)

$OF'K'$ is a tangent drawn from the origin O to the curve of $f(x)$. $OP' = x'$ is the dinate of F'.

Let $q_0 = x_1 < x'$ and for some value of θ choose x_2 such that $x_2/x_1 = \cos\theta$. Therere $\bar{q} = q_0 \cos\theta = x_2$ and $\bar{R}_{\text{crit.}} = f(x_2) = P_2F_2$ on the diagram.

Since
$$R_{\text{crit.}} = \bar{R}_{\text{crit.}}/\cos\theta,$$
$$R_{\text{crit.}} = f(x_2)/\cos\theta = f(x_2) \times x_1/x_2 = P_1K_1$$

the diagram. But for $\theta = 0$, $R_{\text{crit.}} = P_1F_1$ and for any $\theta > 0$, $R_{\text{crit.}} > P_1F_1$. herefore $R_{\text{crit.}}$ is greater when $\theta < 0$ than when $\theta = 0$. Hence when $q_0 < x'$, $R_{\text{crit.}}$ a minimum when $\theta = 0$.

If now $q_0 = x_3 (> x')$ and we choose θ such that: $x_4/x_3 = \cos\theta$, then $\bar{q} = x_4$, and crit. $= f(x_4) = P_4F_4$ on the diagram. Then $R_{\text{crit.}} = P_3K_3$ on the diagram.

But $P_3K_3 < P_3F_3$ and hence $R_{\text{crit.}}$ is least for a value of $\theta > 0$. To find this value θ we choose θ such that P_3K_3 is least. P_3K_3 is least if $x_4 = x'$ and $K_3 = K'$. Then, general, for $q_0 > x'$, the minimum value of $R_{\text{crit.}}$ is given by

$$R_{\text{crit., min.}} = P_3K'. \tag{3·15}$$

The value of θ for which $R_{\text{crit.}}$ is a minimum is given by

$$\cos\theta = x'/x_3 = x'/q_0. \tag{3·16}$$

Note that, as $q_0 \to \infty$, $\theta \to \frac{1}{2}\pi$, since x' is fixed, and also $\theta = 0$ when $q_0 = x'$.

Thus any relation between $R_{\text{crit.}}$ and q_0 calculated by considering disturbances for which $\theta = 0$ can be converted to one giving the minimum value of $R_{\text{crit.}}$, $R_{\text{crit., min.}}$, for given q_0 by drawing a tangent from the origin to the $\theta = 0$ curve. Then the curve of $R_{\text{crit., min.}}$ against q_0 follows the $\theta = 0$ curve from F_0 to F' (see figure 3)

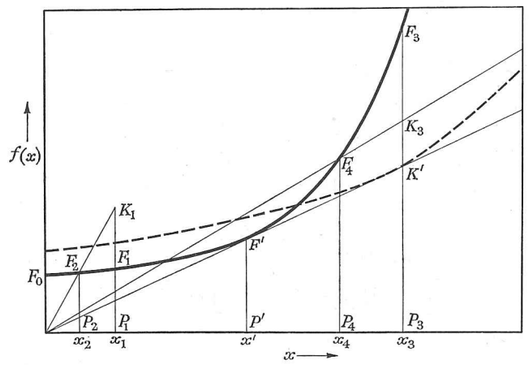

FIGURE 2. $F_0 F' F_3$ is a typical curve of $R_{\text{crit.}}$ against q_0 for two-dimensional disturbances. Here $q_0 = x$ and $f(x) = R_{\text{crit.}}$. The minimum value of $R_{\text{crit.}}$, taking into account three-dimensional disturbances, is shown to lie on the curve F_0F' and then the line $F'K'$. The dashed line is a typical $R_{\text{crit.}} - q_0$ curve at a constant value of $\theta > 0$.

and for $q_0 > x'$ it follows the tangent. The curve may also be described as the envelope of the curves of $R_{\text{crit.}}$ against q_0 at constant θ; a typical curve for $\theta > 0$ is shown in figure 2. Should it be possible to draw more than one tangent from the origin to the $\theta = 0$ curve, then the curve of $R_{\text{crit., min.}}$ against q_0 is a little more complicated to construct. Some general consequences follow from this method of constructing the curve.

First, we need only calculate the curve for $\theta = 0$ and for $q_0 \leqslant x'$ to know the value of $R_{\text{crit., min.}}$ at all values of q_0.

Secondly, we can now prove that, whatever the value of q_0, there is some finite value of R for which the flow is unstable, provided there is some finite value of R for which it is unstable when $q_0 = 0$. If there is any flow which is completely stable for all two-dimensional disturbances when $q_0 > Q$ then the curve of $R_{\text{crit.}}$ against q_0 for $\theta = 0$ will touch a line parallel to the ordinate and cutting the abscissa at $q_0 = Q$, e.g. the curve C in figure 3. Now it is possible to draw a tangent from the origin to any curve which cuts the ordinate and touches a line to the right of it and parallel to it. Then the curve of $R_{\text{crit., min.}}$ against q_0 becomes a straight line for some value of $q_0 > q'$, $(q' < Q)$, and hence for any value of q_0 there is some value of R for which the flow is unstable.

Thirdly if the curve of $R_{\text{crit.}}$ against q_0 for two-dimensional disturbances is of the form of curve C in figure 3, then the curves of λ against R for which q_0 is a constant, $c_i = 0$, and $\theta = 0$ are closed curves and when $q_0 = Q$, the closed curve degenerates to a point. It follows that similar curves of λ against R when $\theta > 0$ are also closed curves and that for a given value of θ, $= \theta_1$, there is some value of q_0, $= Q_1$, for which the curve of λ against R on which $q_0 = Q_1$, $c_i = 0$, and $\theta = \theta_1$, degenerates to a point. But, whatever the value of q_0, there is always some value of θ, $< \frac{1}{2}\pi$, for which the $\lambda - R$ curve has not degenerated to a point.

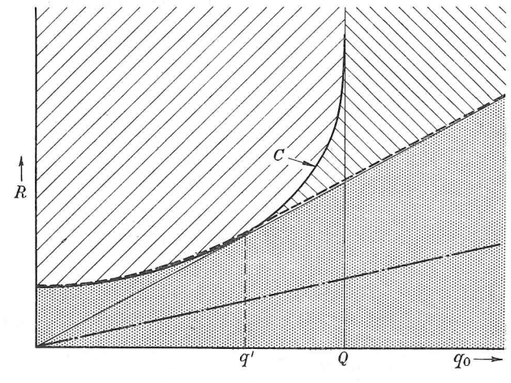

FIGURE 3. The effect of three-dimensional disturbances in a hypothetical flow for which all two-dimensional disturbances are stable when $q_0 > Q$. ▨, Unstable for all disturbances; ▧, stable for two-dimensional disturbances, unstable for three-dimensional disturbance; ▦, stable for all disturbances.

Fourthly, Drazin (1960) has shown that a sufficient condition for stability can be reduced for the flows we are considering. He only considered disturbances for which $\theta = 0$ and obtained the result that if

$$R < 8q_0/t^2, \tag{3·17}$$

where t is the maximum value of $\mathrm{d}u/\mathrm{d}y'$, then the flow is stable. Now the curve $R = 8q_0/t^2$ is a straight line and no tangent can be drawn to it from the origin. Hence this relation is equally valid for disturbances for which $\theta > 0$. See figure 3.

Thus we can state an upper limit and a lower limit to the extent that a magnetic field can *stabilize* a flow, but we still cannot say whether a parallel magnetic field can lower the critical Reynolds number of a flow or not, though no instance of this has yet been found.

4. Arbitrary magnetic Reynolds number

If R_m does not satisfy the condition that $R_m \ll 1$ we cannot simplify (3·4) to obtain an equation for v only, i.e. (3·6). From (3·4) we have

$$v = \frac{\overline{U}}{B_0}\left[(U-c)\,\psi + \frac{\mathrm{i}}{\alpha R_m}(\psi'' - \lambda^2\psi)\right].$$

Substituting this value of v into (3·3) we obtain an equation in ψ, which is proportional to the induced field in the y direction:

$$\left[(U-c)^2-A^2-\frac{\mathrm{i}U''}{\alpha R_m}\right](\psi''-\lambda^2\psi)+2U'(U-c)\psi'$$
$$=-\mathrm{i}\left[\frac{(\mathrm{D}^2-\lambda^2)^2}{\alpha R}(U-c)\psi+\frac{(U-c)(\mathrm{D}^2-\lambda^2)^2\psi}{\alpha R_m}\right]+\frac{1}{\alpha^2 R R_m}(\mathrm{D}^2-\lambda^2)^3\psi, \quad (4\cdot1)$$

where $\mathrm{D}=\mathrm{d}/\mathrm{d}y'$, and the Alfvén number $A=B_0/\sqrt{(\mu\rho)}\,\overline{U}$. This equation describes the motion of a disturbance travelling at an angle θ to $\mathbf{U}_0$ and $\mathbf{B}_0$; as in § 3 the motion of such a three-dimensional disturbance can be described in terms of an equivalent two-dimensional one.

Let $\alpha R=\lambda\bar{R}$ and $\alpha R_m=\lambda\bar{R}_m$, where $\bar{R}$ and $\bar{R}_m$ are the Reynolds number and magnetic Reynolds number for the equivalent disturbance.

Then
$$\bar{R}=R\cos\theta, \quad \bar{R}_m=R_m\cos\theta.$$

Equation (4·1) becomes

$$\left[(U-c)^2-A^2-\frac{\mathrm{i}U''}{\lambda\bar{R}_m}\right](\psi''-\lambda^2\psi)+2U'(U-c)\psi'$$
$$=-\mathrm{i}\left[\frac{(\mathrm{D}^2-\lambda^2)^2(U-c)\psi}{\lambda\bar{R}}+\frac{(U-c)(\mathrm{D}^2-\lambda^2)\psi}{\lambda\bar{R}_m}\right]+\frac{1(\mathrm{D}^2-\lambda^2)^3\psi}{\lambda^2\bar{R}\bar{R}_m}. \quad (4\cdot2)$$

Note that A is the same for any θ.

Assuming the existence of suitable boundary conditions for ψ which do not vary with the angle θ of the disturbance, we once more have an eigenvalue relation between the parameters in (4·2) of the form

$$F(c,\lambda,A,\bar{R}_m,\bar{R})=0. \quad (4\cdot3)$$

Note that we have one more parameter than in (3·8). This relation is the same for all values of θ. Equation (4·3) may be rewritten:

$$G(c,\lambda,\theta,A,R_m,R)=0. \quad (4\cdot4)$$

As in § 3, we are interested in finding the lowest value of R for which the flow becomes unstable, i.e. $c_i=0$. We examine the role of disturbances for which $\theta>0$.

For some value of $A>0$ and $R_m>0$, if the lowest value of $\bar{R}$ at which $c_i=0$ is $\bar{R}_{\text{crit.}}$, then

$$R_{\text{crit.}}=\frac{\bar{R}_{\text{crit.}}}{\cos\theta} \quad \text{and} \quad R_m=\frac{\bar{R}_m}{\cos\theta}, \quad (4\cdot5)$$

and if $\theta=0$, $R_{\text{crit.}}=\bar{R}_{\text{crit.}}$ and $R_m=\bar{R}_m$.

For a given flow and given magnetic field, i.e. a given value of A, as θ increases $\bar{R}_m$ decreases. It is generally found that the lower R_m the less the stabilizing effect of a magnetic field and so we expect that the most unstable disturbance occurs for some $\theta>0$. Anyway it is incorrect to conclude that the most unstable disturbances are those for which $\theta=0$, whatever the value of R_m.

This result may be seen in terms of the concepts of § 2. Consider a velocity disturbance, $\mathbf{u}$, which lies in the plane Oyk where Ok is the direction of propagation of the

disturbance. Then, provided the disturbance does not change its form as θ varies, as θ increases $\nabla\times(\mathbf{u}\times\mathbf{B}_0)$ and hence $\mathbf{j}_1$ and $\mathbf{b}_1$ decrease. Since $\mathbf{b}_1$ lies in the plane yk, $\nabla\times(\mathbf{U}\times\mathbf{b}_1)$ and hence $\mathbf{j}_2$ and $\mathbf{b}_2$ decrease as θ increases. Therefore the $\mathbf{j}_2\times\mathbf{B}_0$ as well as the $\mathbf{j}_1\times\mathbf{B}_0$ force decreases with θ. Thus, as well as in the inertial interaction, the electromagnetic interaction between the disturbance and the mean flow also decreases as θ increases.

We can draw some general conclusions about the stabilizing influence of a magnetic field at arbitrary R_m. From (4·3) we deduce a relation of the form

$$\bar{R}_{\text{crit.}}=f(\bar{R}_m,A),$$

which may be rewritten
$$R_{\text{crit.}}=\frac{f(R_m\cos\theta,\mathrm{A})}{\cos\theta}. \quad (4\cdot6)$$

For $\theta=0$, (4·6) becomes
$$R_{\text{crit.}}=f(R_m,A). \quad (4\cdot7)$$

Tarasov (1960) has examined the stabilizing influence of a parallel magnetic field in plane Poiseuille flow for arbitrary R_m by only considering disturbances for which $\theta=0$. He obtained results for $R_{\text{crit.}}$ at various values of A and R_m. The shape of a curve of $R_{\text{crit.}}$ against R_m for a constant value of A, plotted from Tarasov's results is similar to that of curve C in figure 3.

Since A does not vary with θ, we can apply the argument of § 3·3 to deduce the minimum value of $R_{\text{crit.}}$ when all values of θ are considered. Then we find as before that for R_m greater than some value, the $R_{\text{crit.}}$–R_m curve for constant A becomes a straight line, namely the tangent from the origin to the $\bar{R}_{\text{crit.}}$–$\bar{R}_m$ curve, i.e. the $R_{\text{crit.}}$–R_m curve for constant A for two-dimensional disturbances.

This will be the ultimate form of the $R_{\text{crit.}}$–R_m curve for constant A for all velocity profiles at all values of A. It follows, therefore, that there is no parallel magnetic field which will completely stabilize a flow for finite values of R_m. In other words, whatever the value of A or R_m, there is always some value of R for which the flow is unstable.

By only considering disturbances for which $\theta=0$, Tarasov erroneously concluded that there was always some value of A which could stabilize the flow.

Velikhov (1959) followed Michael (1953) in assuming that the most unstable disturbances occur for $\theta=0$ and thence deduced a sufficient condition for a parallel magnetic field to stabilize a flow when R and $R_m\to\infty$. If disturbances for which $\theta>0$ are considered, the basis of his arguments has to be changed, e.g. if

$$\theta=\tfrac{1}{2}\pi-O(R_m^{-1}], \quad \bar{R}_m=O[1],$$

and the dissipative terms in (4·2) could not be ignored. The dissipative terms can only be ignored if $\bar{R}_m\to\infty$ and $\bar{R}\to\infty$. Then Velikhov's result, that if $A>1$, all flows are stabilized, is correct. In general, therefore, a careful examination is needed of the limiting processes $R\to\infty$ or $R_m\to\infty$ when three-dimensional disturbances are considered.

Conclusion

It was stated in § 3 that the main purpose of the stability analysis was to find the lowest velocity at which the flow becomes unstable, given the value of the applied magnetic field and the values of the fluid properties. It is not very instructive,

physically, to consider $R_{\text{crit.}}$ as a function of $q_0 = \sigma B_0^2 l/\rho\overline{U}$ as we did in § 3 or as a function of A and R_m as in § 4 since q_0, A, and R_m are not independent variables if one considers B_0 and $\overline{U}$ as the parameters to be varied in an experiment. We considered these particular non-dimensional parameters since they appear in the stability equations. From the graphs already shown one could plot other graphs of $R_{\text{crit.}}$ against $M = B_0 l(\sigma/\eta)^{\frac{1}{2}}$ for values of constant P, $= \nu\mu\sigma$, say. This would be a simple operation since

$$M = \sqrt{(Rq_0)} = \sqrt{(A^2 R R_m)}.$$

Replotting Stuart's results in this way indicates that the form of the $R_{\text{crit.}}$–M curve $P \ll 1$ is similar to that of the $R_{\text{crit.}}$–q_0 curve for $R_m \ll 1$. (See figure 4.) It is easily proved that for sufficiently high values of M the $R_{\text{crit.}}$–M curve becomes a straight line, which is a tangent from the origin to the curve for a two-dimensional disturbance. It is interesting to note that when $M = 50$ the angle at which the most unstable disturbance travels to the direction of flow is 60°. Thus in an experiment with mercury the effect of three-dimensional disturbances will become apparent at values of the magnetic field of about 2000 G in a duct whose width is about 1 cm.

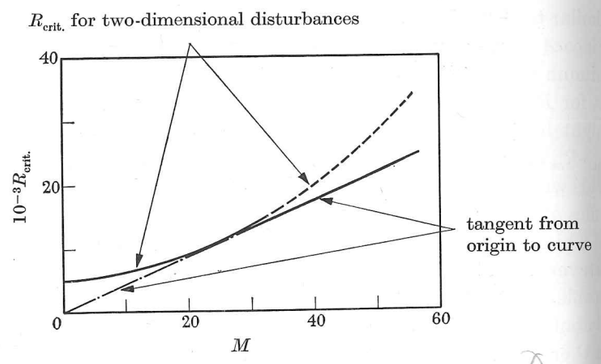

FIGURE 4. $R_{\text{crit.}}$ against $M(= B_0 l(\sigma/\eta)^{\frac{1}{2}})$ for plane Poiseuille flow when $\mu\sigma\nu \ll 1$, based on the theory of Stuart (1954).

The only experimental work done on the stability of parallel flows with parallel magnetic fields has been done with flows in *circular* tubes (Globe 1961). There is no satisfactory theory for the onset of instability of such a flow with or without a magnetic field.

In experiments on the stability of plane Poiseuille flows with no magnetic fields it has not proved possible to obtain a critical Reynolds number in agreement with that predicted by linearized theory. It is likely to be equally difficult in experiments with a parallel magnetic field. There is more likelihood of success with experiments on the stability of boundary layers with parallel magnetic fields.

Though we have only discussed neutrally stable disturbances ($c_i = 0$), growing disturbances also become three-dimensional as the magnetic field increases. The rate of growth of a disturbance depends on the dimensionless 'amplification

xponent' $\beta = \overline{U}\alpha c_i$. Michael (1961) showed that, if we regard $\overline{U}$ as the parameter to e varied so that $R \propto \overline{U}$, then

$$\beta = \frac{\nu}{L^2}\alpha c_i R = \frac{\nu}{L^2}\lambda\bar{R}c_i \propto \lambda\bar{R}c_i.$$

ote that the value of this expression is independent of θ.

Consider the case of $R_m \ll 1$; then a curve of α against R, at constant values of Rc_i and q_0, is the same as that of an equivalent two-dimensional disturbance for hich λ is plotted against $\bar{R}$ at constant values of $\lambda\bar{R}c_i$ and $\bar{q}$. If $\bar{R}_{\text{crit.}}$ is the lowest alue of $\bar{R}$ for a given $\bar{q}$ and $\lambda\bar{R}c_i$, and we then plot $\bar{R}_{\text{crit.}}$ against $\bar{q}$ for constant $\bar{R}c_i$, we can calculate the minimum value of $R_{\text{crit.}}$ for given q_0 and $\lambda\bar{R}c_i$, using the onstruction of § 3. Thus, as with the case of $c_i = 0$, when q_0 becomes sufficiently reat the curves become straight lines. In experimental terms this means that we an calculate the minimum velocity of the mean flow for a given amplification rate f the disturbance and given magnetic field.

Though we have only examined the stability of fluids with uniform properties nder the action of a uniform magnetic field, by virtue of the physical reasons given n § 2 it is likely that, in general, three-dimensional disturbances will be the most nstable in practical situations, m.h.d. generators for instance, where magnetic elds are applied to the flow of fluids with non-uniform properties. For an example f some of the other interesting kinds of instability which can occur under such ircumstances see McCune (1965).

I should like to thank Dr J. A. Shercliff for the helpful advice he has given me in he preparation of this paper. This work is published by permission of the Central lectricity Generating Board.

REFERENCES

handrasekhar, S. 1961 *Hydrodynamic and hydromagnetic stability*. Oxford University Press.
razin, P. G. 1960 Stability of parallel flow in a parallel magnetic field at small magnetic Reynolds numbers. *J. Fluid Mech.* **8**, 130.
lobe, S. 1961 The effect of a longitudinal magnetic field on pipe flow of mercury. *Trans. Amer. Soc. Mech. Engrs.* **83**, (C), 445.
lains, F. D. 1965 Stability diagrams for magnetogasdynamic channel flow. *Phys. Fluids*, 8, 2014.
lichael, D. H. 1953 The stability of plane parallel flows of electrically conducting fluids. *Proc. Camb. Phil. Soc.* **49**, 166.
lichael, D. H. 1961 Note on the stability of plane parallel flows. *J. Fluid Mech.* **10**, 525.
lcCune, J. E. 1965 Non-linear effects of fluctuations on MHD performance. *Sixth Symp. on Eng. Aspects of Magnetohydrodynamics*. Pittsburgh, 1965.
ossow, V. J. 1959 Boundary-layer stability diagrams for electrically conducting fluids in the presence of a magnetic field. *N.A.S.A. Tech. Rep.* R-37.
quire, H. B. 1933 On the stability for three-dimensional disturbances of viscous fluid flow between parallel walls. *Proc. Roy. Soc.* A, **142**, 621.
hercliff, J. A. 1965 *A textbook of magnetohydrodynamics*. Pergamon.
tuart, J. T. 1954 On the stability of viscous flow between parallel planes in the presence of a coplanar magnetic field. *Proc. Roy. Soc.* A, **221**, 189.
arasov, Yu. A. 1960 Stability of plane Poiseuille flow of a plasma with finite conductivity in a magnetic field. *Soviet. Phys. JETP*, **10**, 1209 (in English).
elikhov, E. P. 1959 The stability of a plane Poiseuille flow of an ideally conducting fluid in a longitudinal magnetic field. *Soviet Phys. JEPT*, **9**, 848 (in English).
ooler, P. T. 1961 Instability of flow between parallel planes with a co-planar magnetic field. *Phys. Fluids*, **4**, 24.

INTERNATIONAL ATOMIC ENERGY AGENCY
EUROPEAN NUCLEAR ENERGY AGENCY

INTERNATIONAL SYMPOSIUM ON
MAGNETOHYDRODYNAMIC ELECTRICAL POWER GENERATION

Salzburg, Austria, 4-8 July 1966

SM-74/13

REVISED ABSTRACT

ON SOME FLUID DYNAMIC EFFECTS IN LARGE SCALE M. H. D. GENERATORS

J. C. R. HUNT - UNIVERSITY OF WARWICK, COVENTRY

At the present time we are unable to carry out a complete analysis of the fluid dynamics and electrodynamics of an M. H. D. generator. However, various aspects of the behaviour of an M. H. D. generator may be examined by the use of simplified models e.g.

(i) One-dimensional gas dynamics. (e.g. Louis et al, 1964).

(ii) The current distribution can be found if the velocity is assumed constant across the duct. (e.g. Witalis, 1965).

(iii) The skin friction and heat transfer to the walls can be calculated by boundary layer analysis if the flow is assumed to be laminar. (Kerrebrock, 1961).

(iv) A complete description of the velocity and current distribution across the duct can be given if the flow is assumed to be uniform, laminar, incompressible and not-varying in the flow direction. (Hunt & Stewartson, 1965).

Taken together, these and other models will enable us to describe most of the effects in an M. H. D. generator.

In this paper another simplification is considered in which the electromagnetic forces are assumed to be much larger than the inertial forces. The ratio of these two forces is measured by the parameter, $S = \sigma B_0^2 d / \rho \bar{U}$, where σ is the conductivity, Bo the magnetic field, d the width of hhe duct, ρ the density and $\bar{U}$ the mean velocity. Thus $S \gg 1$. We also assume that the magnetic Reynolds number is very much less than one. In the largest experimental generators now being built $S \sim 2$. Thus, though the results of this model are not immediately applicable, they should indicate the effects of increasing the magnetic field strength and the size of M. H. D. generators.

When S >> 1, one can consider the duct to be divided into 2 regions:

(i) A core region where electromagnetic forces are balanced by the pressure gradient and where inertial as well as viscous forces are negligible.

(ii) Boundary layers on the walls where again inertial forces are negligible but where the viscous, electromagnetic and pressure forces are of the same order.

We show how it is then possible to calculate the core flow in diverging ducts and in ducts with non-uniform magnetic fields, with the Hall effect and compressibility included, and obtain approximate answers for these otherwise very difficult problems. We also demonstrate the simplifications in the analysis of the boundary layers which result from this approximation.

3

ON SOME FLUID DYNAMIC EFFECTS IN LARGE SCALE M. H. D. GENERATORS

J. C. R. HUNT - UNIVERSITY OF WARWICK, COVENTRY, ENGLAND

1. INTRODUCTION

At the present time we are unable to carry out a complete analysis of the fluid dynamics and electrodynamics of an M. H. D. Generator. However various aspects of the behaviour of an M. H. D. Generator may be examined by the use of simplified models: the greater the simplification the more complete the description.

Laminar incompressible flow in a rectangular duct has been examined in [1] and laminar compressible boundary layer flows in [2] and [3] but most generator calculations use the method of one-dimensional gas dynamics, [4] and [5], which is based upon the assumptions that the variations of flow and fluid properties are small across the generator duct and that transverse velocities are small. Calculations based on this approximation have proved satisfactory for inviscid flow regions outside boundary layers, e.g. in the entrance region of a duct or for fully developed turbulent flow in a duct. In the former case the effects of heat transfer and viscous friction are mainly felt in the boundary layers; they only affect the flow outside the boundary layers by varying the thickness of the boundary layers. In the latter case, though there are large velocity gradients at the wall, the wall effects are diffused right across the duct. The electromagnetic effects are considered by adding the electromagnetic $\vec{J} \times \vec{B}$ body force to the momentum equation and the work done by the electric field, $\vec{E} \cdot \vec{J}$, to the energy equation. When the Hall effect and the problem of segmented electrodes are considered it is found that the current varies across the duct. In that case the current distribution is usually calculated by assuming the velocity is constant across the duct, e.g. [9] but ignoring the effects on the flow of J x B varying across the duct. Thus these calculations are valid for highly turbulent flows in ducts with small changes in cross-sectional area and where the electromagnetic forces are small compared to the inertial forces.

In this paper we consider another model for flow in a M. H. D. generator duct in which we assume the electromagnetic body forces are very much larger than the inertial forces. ~~thus~~ The ratio of these two forces is measured by the parameter $S = \sigma B_0^2 d / \rho U$, where σ is the conductivity, B_0 the magnetic flux density, d a characteristic duct width, ρ the density and U a characteristic velocity, the value of σ being assumed to be typical for the central regions of the duct. We also assume the magnetic Reynolds number, Rm, is very much less than one. Hence

$H^2/Re = S \gg 1$; $Rm \ll 1$, where Re is the Reynolds number and H ($= B_0 d (\sigma/\eta)^{\frac{1}{2}}$, where η is the viscosity) is the Hartmann number. In the largest experimental generators now being built:

$$H \simeq 10^3, \quad Re \simeq 5 \times 10^5 \text{ and hence } S \simeq 2.$$

The most important physical effect of raising S is the damping of the turbulence in the flow. Murgatroyd [6] showed that when $Re/H < 225$ the turbulence in a flat channel is damped out. However, for values of Re/H greater than 225 the turbulence is damped in the centre of the duct where the velocity gradients are small and as the magnetic field is further increased the last remaining turbulence is damped from the boundary layers. Thus, since in existing generators the turbulence is highly damped and the electromagnetic forces are of the same order or greater than the inertial forces, the basic assumptions of most existing generator calculations are not satisfied. Therefore, though the results of this model are not immediately applicable, they should indicate the effects of increasing the magnetic field strength and the size of M. H. D. generators, as well as demonstrating some of the defects of existing models.

When $S \gg 1$, one can consider the duct to be divided into 2 regions.

(i) A core region where electromagnetic forces are balanced by the pressure gradient and where inertial as well as viscous forces are negligible.

(ii) Boundary layers on the walls where again inertial forces are negligible but where the viscous, electromagnetic and pressure forces are of the same order. The thickness of the layers is assumed to be very much smaller than the duct width.

In many existing M. H. D. generators, the generator ducts have large changes in their cross-sectional area, but because the calculations are based on one-dimensional gas dynamics the effects of large transverse velocities caused by the area change are not considered. We show how flow in such ducts can be calculated exactly when $S \gg 1$. Another problem not suitable for solving by one-dimensional gas dynamics is that of calculating the effect of variations in the magnetic field both along and across the duct, whereas in our approximation a fairly simple method exists for this calculation.

By means of our boundary layer approximations we examine the effects of viscous friction and heat transfer at the wall when S increases. We conclude that owing to the damping of the turbulence which occurs when $S \gg 1$ and the formation of slowly growing boundary layers the effects on the core flow of the wall shear stress and heat transfer become progressively less as S increases.

2. CORE FLOW

In this section we consider the flow in the core and therefore we will ignore viscous forces. The governing equations for the steady flow of a conducting gas are taken to be:

Momentum : $$\rho(\vec{u}.\nabla)\vec{u} = -\nabla p + \vec{J}\times\vec{B}, \qquad (2.1)$$

Continuity: $$(\rho.\nabla)\vec{u} + (\vec{u}.\nabla)\rho = 0, \qquad (2.2)$$

Energy: $$\rho(\vec{u}.\nabla)\left(h+\frac{|\vec{u}|^2}{2}\right) = \vec{E}.\vec{J} + \nabla.(k\nabla T), \qquad (2.3)$$

Ohm's Law: $$\vec{J} = \sigma(\vec{E}+\vec{u}\times\vec{B}) - (\omega\tau/|B|)(\vec{J}\times\vec{B}) \qquad (2.4)$$

Maxwell's Equations: $$\nabla.\vec{B} = 0, \qquad (2.5)$$

$$\nabla\times\vec{E} = 0, \qquad (2.6)$$

$$\nabla\times\vec{B} = \mu\vec{J}. \qquad (2.7)$$

Where the symbols have their usual meaning. In this paper we consider the magnetic field to be produced by external coils and we assume that the magnetic Reynolds number, Rm is sufficiently small for us to ignore the field produced by the induced currents, $\vec{j}$. Let the imposed field be $\vec{B}_0$, then in the generator duct

$$\nabla.\vec{B}_0 = \nabla\times\vec{B}_0 = 0. \qquad (2.8)$$

We now consider the equations when the magnetic field is uniform and $S \gg 1$. Then, using the co-ordinate system of Fig.1, equations (2.2) and (2.3) become:

$$\left.\begin{aligned} 0 &= -\partial p/\partial x - j_z B_0, && \text{a}\\ 0 &= -\partial p/\partial y, && \text{b}\\ 0 &= -\partial p/\partial z + J_x B_0, && \text{c} \end{aligned}\right\} \qquad (2.9)$$

$$\rho\left(u_x\frac{\partial h}{\partial x} + u_y\frac{\partial h}{\partial y} + u_z\frac{\partial h}{\partial z}\right) = E_x J_x + E_y J_y + E_z J_z + \nabla.(k\nabla T) \qquad (2.10)$$

As is to be expected this approximation leads to our neglecting the inertial terms in (2.9) and (2.10). Hence taking the curl of (2.9) we have:

$$\frac{\partial J_x}{\partial y} = \frac{\partial J_y}{\partial y} = \frac{\partial J_z}{\partial y} = 0. \qquad (2.11)$$

We now show by an order of magnitude argument that when $S \gg 1$ and the flow is compressible we can ignore the heat conduction terms in 2.10. From (2.9) we see that the characteristic distance in which ρ changes in the x - direction is $0(S^{-1})$ and hence T changes in a similar distance. Then

$$\partial/\partial x(k\,\partial T/\partial x) = O\left[\frac{c_p\,\eta}{P_r} \times \frac{\bar{u}^2 S^2}{\gamma R M^2 d^2}\right] = O\left[\frac{S^2}{R_e P_r M^2} \times \frac{\rho\,\bar{u}^3}{d}\right],$$

where P_r is the Prandtl number and M ($\simeq \bar{u}/\sqrt{\gamma RT}$) a typical value of the Mach Number. Also

$$\rho u_x c_p\,\partial T/\partial x = O\left[\frac{\rho\,\bar{u}^3 c_p S}{\gamma R M^2 d}\right] = O\left[\frac{S}{M^2} \times \frac{\rho\,\bar{u}^3}{d}\right].$$

Hence $$\partial/\partial x\,(k\,\partial T/\partial x)\,/\,(\rho u_x c_p\,\partial T/\partial x) = O[S/R_e P_r],$$

and, since in most cases $Re \gg S$ and $Pr = 0(1)$, we can ignore the heat conduction terms. Physically this means that in the core the heat generated by ohmic dissipation is convected rather than conducted away.

For the symmetrical generator shown in Fig.(1), $J_y = 0$ on the centre line and hence from (2.11),

$$j_y = E_y = 0$$

throughout the duct. Thence, from (2.7),

$$\frac{\partial E_x}{\partial y} = \frac{\partial E_z}{\partial y} = 0, \qquad (2.7)$$

and Ex, E_z, j_x, j_z are all functions of x and z only. Then, since we can ignore the conduction terms in (2.10) we have:

$$\frac{\partial}{\partial y}\left\{\rho\left(u_x \frac{\partial h}{\partial x} + u_y \frac{\partial h}{\partial y} + u_z \frac{\partial h}{\partial z}\right)\right\} = 0. \qquad (2.12)$$

Since $\partial T/\partial x = 0(S) \gg \partial T/\partial y$ and by considering $\partial \vec{J}/\partial y$ we can formally show that the solution:

$$\partial T/\partial y = \partial u_x/\partial y = \partial u_z/\partial y = \partial \rho/\partial y = 0 \qquad (2.13)$$

satisfies all the equations including (2.12). Also we can construct a solution to fit the boundary conditions which satisfies (2.13).

The consequence of the limiting solution (2.13) is that all fluid properties as well as the velocity, current and electric field become functions of x and z only. In an incompressible flow this would not occur whatever the value of S, because there is no coupling between the velocity and temperature, but in a compressible flow the velocity and fluid properties are coupled so that when $S \gg 1$ and $\frac{\partial p}{\partial y} = \partial \vec{J}/\partial y = 0$ the coupling necessitates that all the other properties are also uniform in the y- direction.

If now we consider the flow in a segmented M. H. D. generator in which the electrodes are connected so that $J_x = 0$, then $\partial p/\partial z = 0$ and we can show by an order of magnitude argument in considering the boundary layers (see 3) that, if the duct width in the z- direction is constant, $u_z \ll u_x$ in the core. Then $\partial T/\partial z = 0$ and equations (2.9) - (2.10) may be written:

$$\partial p/\partial x = -\sigma u_x B_o^2 (1-K), \qquad (2.14)$$

$$\rho u_x\,\partial h/\partial x = -\sigma u_x^2 B_o^2 K(1-K), \qquad (2.15)$$

where K = (- Ez/Ux B_o). Since U_x and ϱ do not vary in the y or z-direction. Ux ϱ A = constant. (2.16)

where A (x) is the cross-sectional area. Thus we have arrived at a set of equations with a one-dimensional form, yet we can satisfy the boundary conditions on Uy in a duct with large variation of the duct width, for Uy may be calculated from (2.2) once U_x and ϱ are found from (2.14) - 2.16). Since U_x satisfies (2.16), it is easily seen that Uy satisfies the condition that:

$$U_y / U_x = df/dx \quad \text{when } y = f(x) \text{ . (See fig. 1).}$$

The properties of this set of equations has not yet been studied but some observations can be made at this time.†

Firstly, if U_x is constant across the duct, the total velocity, $(U_x^2 + U_y^2)^{\frac{1}{2}}$ is clearly greatest near the walls in a diverging duct. This implies an increased drag on the walls and reduced tendency to separate.

Secondly, these equations become invalid where large gradients of velocity occur such as near shocks or near the exit of a duct.

Thirdly, if $j_x \neq 0$, large transverse pressure gradients exist and hence large changes in fluid properties across the duct. Then it is not possible to calculate the current distribution near segmented electrodes in the manner of Witalis [9] without considering the changes in velocity, conductivity and Hall effect across the duct. To illustrate this, let us write $j_x = \partial\psi/\partial y$, $j_y = 0$, $j_z = -\partial\psi/\partial x$. Then there is a simple integral to equations (2.9 a and 2.9 c), i.e. p-$D_o\psi$ = constant. Thus the pressure is constant along the current lines and large changes in fluid properties across the duct will occur.

Fourthly, the variables in these equations* only depend on boundary conditions at values of x [redacted]. The conditions in the walls at $y = \pm f(x)$ affect the current in the boundary layers which in turn affects the current in the core. Thus we do not have a direct interaction between the walls and the core flow as in ordinary one-dimensional gas dynamics but an indirect electromagnetic interaction.

Fifthly, we can consider all the variables in the equations as the first term of an expansion in decreasing powers of S_1 where S_1 is the value of S at the entrance, e.g.

$$U_x = Ux_o + S_1^{-1} Ux_1 + S^{-2} Ux_2 + \ldots .$$

Knowing Ux_o from our zeroth approximation we can calculate the first approximation and thus we can see the effect of the inertial terms. This approach has been used by Hunt and Leibovitch [8] to examine incompressible flow and found to be much simpler than expanding in ascending powers of S.

* i.e. (2.14 - 2.16).

† The main limitation of this analysis, as pointed out by Baylis, is that it is only valid when $M^2 \ll 1$.

Lastly, it is of interest to note that equations (2.14 - 2.16) are exactly the same as those for a frictionless constant velocity duct [7]. The differences in this approach and that of one-dimensional gas dynamics will appear most marked when the higher order approximations, as discussed in the preceding paragraph, are considered

3. BOUNDARY LAYERS

As explained in § 1, our aim in this section is to consider the boundary layers on the walls perpendicular to the magnetic fields when $S \gg 1$. We assume the walls to be electrically insulating and then the approximate equations written in terms of the boundary layer co-ordinates s, n and z are:

$$\partial/\partial s\,(\rho u_s) + \partial/\partial n\,(\rho u_n) + \partial/\partial z\,(\rho u_z) = 0 \quad , \tag{3.1}$$

$$\left.\begin{aligned} 0 &= -\partial p/\partial s - J_z B_0 \cos\alpha + \partial/\partial n\,(\eta\,\partial u_s/\partial n), && \text{a)}\\ 0 &= -\partial p/\partial n + J_z B_0 \sin\alpha \quad , && \text{b)}\\ 0 &= -\partial p/\partial z + J_s B_0 \cos\alpha + \partial/\partial n\,(\eta\,\partial u_z/\partial n), && \text{c)} \end{aligned}\right\} \tag{3.2}$$

$$\rho\left(u_s\,\partial h/\partial s + u_n\,\partial h/\partial n + u_z\,\partial h/\partial z\right) = \partial/\partial n\,(k\,\partial T/\partial n) + \partial/\partial n\left(\eta\,\partial/\partial n\left(u_s^2+u_n^2+u_z^2\right)/2\right) + J_s E_s + J_z E_z \quad , \tag{3.3}$$

$$J_s = \frac{\sigma}{1+(\omega\tau\cos\alpha)^2}\left\{E_s + \omega\tau\cos\alpha\,E_z + B_0\cos\alpha\left(-u_z + \omega\tau\cos\alpha\,u_s\right)\right\}, \tag{3.4}$$

$$J_z = \frac{\sigma}{1+(\omega\tau\cos\alpha)^2}\left\{E_z - \omega\tau\cos\alpha\,E_s + B_0\cos\alpha\left(u_s + \omega\tau\cos\alpha\,u_z\right)\right\}, \tag{3.5}$$

where $\tan^{-1}\alpha = df/d\alpha$. (fig. 1).

For typical generator loading conditions $K = -E_z/UB \sim 3/4$, and then the current density in these layers is very much greater than that in the core. However, the conductivity is usually low near the wall and since the velocity gradients there are large the level of turbulence will be greater in these layers than in the core and our approximation less valid. When $H \gg 1$ and $S \gg 1$ the boundary layer thickness, δ, is $0\,(H^{-1})$ as may be seen in (3.2 a). For the reasons discussed in § 2 the velocity and temperature variations are coupled and consequently the velocity and temperature boundary layer are identical.

If the wall is kept at a constant temperature while the core is at Tc we can show that in (3.3) the convective terms are very much smaller than the conducting terms particularly when $(1 - K) \ll 1$. In the core the convective terms are of the same order as the $\vec{J}.\vec{E}$ term and much greater than the conduction terms, but in the boundary layers $\vec{J}.\vec{E}$ is $0(K(K-1))$ times its value in the core and the viscous dissipation term is $0\,(\eta\,u_{s(\text{core})}\,H^2/a^2)$ which is $0\,(1/K(K-1)$ times the value of $\vec{J}.\vec{E}$ in the core. Thus in the boundary layers, since the convective terms are of the same order as in the core, most of the extra heat dissipation is too great for convection and is conducted away through the walls.

If there is no heat loss through the walls, the gas in the boundary layer heats up as it progresses, the heat being convected along. Clearly in this case our approximation is invalid.

The approximate equations may now be written in the following way, using the values of pressure gradient in the core and ignoring terms of $0(\delta)$.

$$\partial/\partial s\,(\varrho u_s) + \partial/\partial n(\varrho u_n) + \partial/\partial z(\varrho u_z) = 0, \qquad (3.1)$$

$$\partial/\partial n(\eta\,\partial u_s/\partial n) - (j_z - j_{z\,core})B_0 = 0, \qquad (3.6)$$

$$\partial/\partial n(\eta\,\partial u_z/\partial n) + (j_s - j_{s\,core})B_0 = 0, \qquad (3.7)$$

$$j_s E_s + j_z E_z + \partial/\partial n\left(\eta\frac{\partial}{\partial n}(u_w^2 + u_z^2)/2\right) + \partial/\partial n(k\,\partial T/\partial n) = 0 \qquad (3.8)$$

$$\partial E_s/\partial n = \partial E_z/\partial n = 0, \qquad (3.9)$$

where the suffix 'core' refers to the value of the variable in the core. We can deduce simple results by integrating (3.6) and (3.7) with respect to n from n = 0 to n = δ. We obtain

$$\left.\begin{aligned} B_0\int_0^\delta (j_z - j_{z\,core})\,dn &= -|\eta\,\partial u_s/\partial n|_{n=0} = -\tau_s, \\ B_0\int_0^\delta (j_s - j_{s\,core})\,dn &= |\eta\,\partial u_z/\partial n|_{n=0} = \tau_z \end{aligned}\right\} \qquad (3.10)$$

where τ_s, τ_z are the components of skin friction in s and z directions. When $K \to 1$, j_z and j_s become very much greater than their value in the core. In this special case

$$E_s\int_0^\delta j_s\,dn + E_z\int_0^\delta j_z\,dn = \left|k\,\frac{\partial T}{\partial n}\right|_{n=0} = Q,$$

where Q is the heat leaving the walls. From (3.10),

$$(E_s\tau_z - E_z\tau_s)/B_0 = Q.$$

Thus we have a relation between τ and Q which is independent of the fluid properties but which is only valid when the generator is almost on open circuit.

Let us now consider the special case of $J_z \simeq 0$ in the core in order to find the order of magnitude of the swirl velocity, U_z, induced by the Hall effect. We assume $U_s \gg U_z$ in the core and then show that this is true. From (3.4), in the core:

$$E_s \simeq -\omega\tau\cos\alpha\,(E_{\phi z} + B_0 U_s\cos\alpha) \simeq -\omega\tau\cos^2\alpha\,U_s B_0(1-K).$$

Hence in the boundary layer, where U_s is small near the wall:

$$j_s \simeq \frac{\sigma}{1+(\omega\tau\cos\alpha)^2}\left(-U_{s\,core}B_0\,\omega\tau\cos^2\alpha - U_z B_0\cos\alpha\right).$$

Substituting this approximate value for j_s in (3.7) we have:

$$U_z = -O\left[\frac{\sigma U_{s\,core} B_o^2 \omega\tau \cos^2\alpha\, \delta^2}{1+(\omega\tau\cos\alpha)^2}\right] = -O\left[U_{s\,core}\right],$$

since δ is 0 (H^{-1}) and $w\tau$ is assumed to be 0 (1).

Thus the swirl velocity is of the same order as the core velocity in the boundary layer. But an equal quantity of gas must return in the opposite direction in the core and since the flow properties do not vary in the y - direction, we have:

$$U_{z\,core} = -O\left[\frac{\delta}{a} U_{z\,boundary\ layer}\right] = -O\left[H^{-1} U_{s\,core}\right]$$

Thus we can say that the swirl velocity U_z is small in the core when $j_x = 0$. Since $U_z = -O(U_s)$ in the boundary layer it means that in this case $\tau_z = -O(\tau_s)$.

We now estimate the order of magnitude of τ_s and thence examine the effect on the core flow of the boundary layers.

$$\tau_s = O\left[\eta_w U_{s\,core}/\delta\right] < O\left[\eta_{core} \frac{U_{s\,core}}{\delta}\right],$$

where η_w is the value of viscosity at the wall and if the wall is cooled $\eta_w < \eta_{core}$. Hence

$$\tau_s \lesssim O\left[U_{x\,core} B_o (\sigma\eta)^{1/2}\right],$$

where σ and η are taken at their core values. Then if the total current leaving the generator is I, by adding the current in the boundary layers to that in the core we have:

$$I = \sigma U_{x\,core} B_o (1-K) - \tau_s/B_o \simeq \sigma U_{x\,core} B_o\left[1-K-O(H^{-1})\right]$$

Thus it is only when $(1-K) \simeq (H^{-1})$ that the effect of the walls on the core flow is appreciable. Therefore, whatever the roughness or the heat withdrawn from the walls perpendicular to the field when $(1-K) \gg H^{-1}$ the core flow is unaffected. This is an important result as it shows that even if the walls are very rough*, as is often the case in M. H. D. generators, the flow in the core will not be greatly affected. Thus the situation is very different from a normal compressible duct flow where turbulence distributes the shear stresses and the heat input at the wall over the duct and these effects have to be considered in the core.

4. NON-UNIFORM MAGNETIC FIELDS

As a simple example of the method for examining the effect of non-uniform magnetic fields we consider the flow in the core of a constant area duct when there is no Hall effect and the magnetic

* provided the size of the roughness elements is less than the thickness of the boundary layer.

field, $\vec{B}_o$, only varies in the y and z directions. Since $\vec{B}_o$ satisfies (2.9) when Rm≫1, we can write the components of $\vec{B}_o$ as:

$$B_x = 0, \quad B_y = -\frac{\partial A}{\partial z}, \quad B_z = \frac{\partial A}{\partial y}. \tag{4.1}$$

where A satisfies, $\nabla^2 A = 0$. (4.2)

and the momentum equations for our special case as:

$$0 = -\partial p/\partial x - (J_z B_y - J_y B_z), \tag{4.3}$$

$$0 = -\partial p/\partial z = -\partial p/\partial y. \tag{4.4}$$

Thence (3.3) becomes:

$$\partial\psi/\partial y \cdot \partial A/\partial z - \partial\psi/\partial z \cdot \partial A/\partial y = P, \tag{4.5}$$

where $J_x = 0$, $J_y = -\partial\psi/\partial z$, $J_z = \partial\psi/\partial y$, and $P = \partial p/\partial x$.

The general solution to (3.5) may be written as

$$\psi = f(A) + P\int_A \frac{dy}{(\partial A/\partial z)}, \tag{4.6}$$

where the integral is a line integral taken along a line of constant A, i.e. a field line. In the case of a rectangular duct in which the magnetic field is symmetric about the centre line in both directions, the current distribution is symmetric and $\psi = 0$ at $y = 0$. Then (3.6) becomes:

$$\psi = P\int_0^y (A \text{ constant}) \frac{dy}{(\partial A/\partial z)}. \tag{4.7}$$

As a very simple example consider a mainly uniform magnetic field in the y direction which has a small parabolic variation in the y and z directions. Then:

$$A = -\left[b_0 z + \frac{b_1 z^3}{3} - b_1 z y^2\right],$$

where $b_0 \gg b_1$. The solution for ψ to first order in b_1/b_0 is:

$$\psi = -\frac{P y}{b_0}\left[1 - \frac{b_1 z^2}{b_0} + \frac{b_1 y^2}{3 b_0}\right].$$

Thence $$J_z = -\frac{P}{b_0}\left[1 - \frac{b_1 z^2}{b_0} + \frac{b_1 y^2}{b_0}\right],$$

and $$J_y = -\frac{2 P b z y}{b_0^2}.$$

This method can be extended to more complicated situations. Also it enables us to find the velocity distribution in the core, though the boundary layer structure then has to be taken into account.

REFERENCES

(1) Hunt, J. C. R. & Stewartson, K. 1965. J. Fluid Mech. 23, 563

(2) Kerrebrock, J. L. 1961. J. Aero/Space Sci. 28, 631

(3) Hale, F. J. & Kerrebrock J. L. 1964. AIAA 2, 461

(4) Swift-Hook, D. T. & Wright. J. K. 1963. J. Fluid Mech. 15, 97

(5) Louis, J. F. Etal. 1964. Phys. Fluids 7, 362

(6) Murgatroyd, W. 1953. Phil. Mag. 44, 1348

(7) Carter, C. etal, 1964. MHD Conference, Paris. Paper 85

(8) Hunt, J. C. R. & Leibovitch, S. 1966
submitted for publication to J. Fluid Mech.

(9) Witalis, E.A. 1965. J. Nuc. Energy. C. 7, 235.

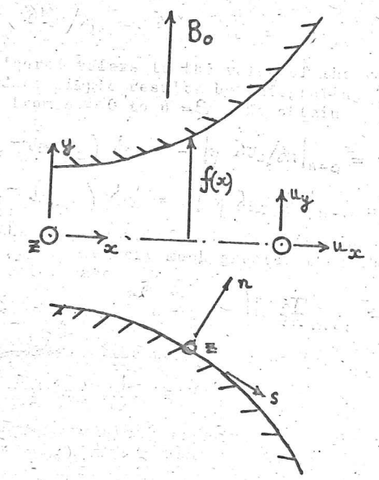

Fig. 1. Notation for the analysis of the core and boundary layer flows.